Axial stereogenicity for designing inherently chiral organic semiconductors

PhD in Chemical and Environmental Sciences – XXX Cycle

Dipartimento di Scienza e Alta Tecnologia

Università degli Studi dell'Insubria

PhD dissertation:

Giulio APPOLONI

Supervisor: Prof. Tiziana BENINCORI

2016/2017

Acknowledgement

I would like to thank all the people involved in this project, without them this thesis would not has been possible:

Prof. Tiziana Benincori

Prof. Andrea Penoni

Prof. Sabine Ludwigs for the support during my abroad period and for the possibility to meet a different culture.

Dr. Klaus Dirnberger

Dr. Beatrice Omiecienski

And all the people from IPOC group

Prof. Francesco Sannicolò

Prof. Patrizia Romana Mussini

Dr. Serena Arnaboldi

Dr. Monica Panigati

Dr. Elsa Quartapelle Procopio

Prof. Rocco Martinazzo

Dr. Roberto Cirilli

Prof. Sergio Abbate

Prof. Giovanna Longhi,

Dr. Giuseppe Mazzeo

In the present thesis the following analysis were carried out by co-workers:

- Electrochemical monomer characterization and enantiorecognition tests by dr. Serena Arnaboldi and prof. Patrizia Romana Mussini of Università degli Studi di Milano
- Racemate resolution through HPLC on a chiral stationary phase by dr. Roberto Cirilli of Istituto Superiore di Sanità di Roma
- Optical characterization by dr. Monica Panigati and dr. Elsa Quartapelle Procopio of Università degli Studi di Milano
- Chiroptical characterization by prof. Sergio Abbate, prof. Giovanna Longhi and dr. Giuseppe Mazzeo of Università degli Studi di Brescia.

1. Foreword

Chirality is an intriguing molecular property occurring in different chemical fields: organic chemistry, bioorganic chemistry, biochemistry, medicinal chemistry are just few examples of areas where chirality has a dominant role.

However, chirality is not just a concept confined to chemistry but it is hidden in everyday life on Earth.

The word "chirality" derives from ancient Greek χείρ, "hand", and it is a property of an object not to be superimposable to its mirror image. From this definition it appears immediately clear the origin of the word "chirality": chiral molecules are not superimposable to their mirror image, just like hands or feet. In such a case, there are two possible forms of the same object, which are called *enantiomers*, again from Greek: ἐναντίος meaning "opposite" and μέρος meaning "part".

Condition for chirality is the absence of second order symmetry elements. A chiral object of whatsoever nature does not possess any symmetry plane (σ), nor inversion centre (*i*), nor roto-reflexion axes (S_n).

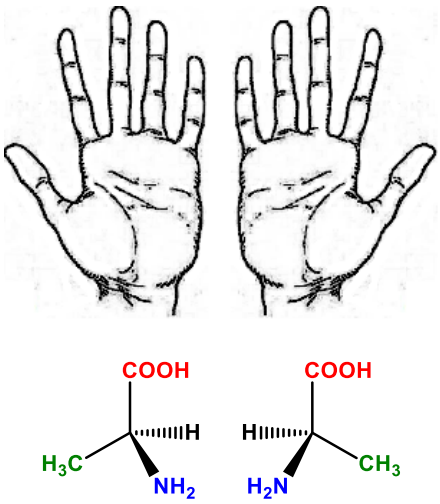

Figure 1: Left and right hand, *L*- and *D*-alanine.

Chirality, however, extends to less intuitive situations: chirality properties characterize the mathematical and geometric world. For example, helices are chiral objects: indeed, helices (like screws and propellers) exist in a clockwise and an anti-clockwise shape which are not superimposable mirror-images. From the helix concept comes also the "right-hand rule", a wide-spread easy way to understand vectors, a cornerstone in mathematics and physics.

Furthermore, chirality is not only a theoretical trick to explain mathematical concepts: chirality is fundamental in Nature, from inorganic materials to animals and humans. Crystals, for example,

can be chiral, as Louis Pasteur first noticed and explained: in 1848 he could manually separate crystals of (2*R*, 3*R*)- and (2*S*, 3*S*)-tartaric acid, demonstrating also that solutions of the two acids had opposite optical rotation. After this historical example, chirality was found a frequently occurring phenomenon in crystals: in Figure 2 it is possible to observe two couples of enantiomeric quartz crystals; in this case, chirality in quartz is related to the nature of bonding between tetrahedral silicate groups, which results in either right- or left-handed helixes running through these network-covalent solids.[1]

Figure 2: Two couples of enantiomeric quartz crystals.[1]

In living organisms, chirality is more frequent and much more important than in minerals: gastropod shells, produced by mollusks, show an elliptical chiral structure. In Figure 3 pictures of two shells are reported, both from *Neptunea* genus, with opposite helix configuration. Anyhow it is funny to notice that Nature clearly selected a preferential structure: the 90% of gastropod shells, indeed, are dextral (or right-handed) ones.

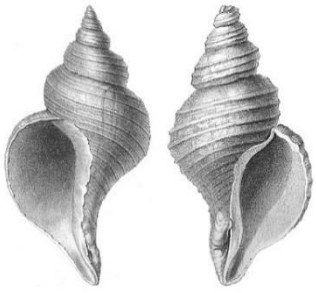

Figure 3: *Neptunea angulate* shell (left) and *Neptunea despecta* shell (right).[2]

The biological examples of chirality are countless: tree logs, vines, roots or leaves in some plants are some of the macroscopic right- or left-handed biological structures.

The examples of chirality reported so far underline how this concept is widespread but, back to the issue, chirality involves fundamental consequences especially in chemistry.

The presence of chirality in molecules is strictly related to the presence of at least one stereogenic element: stereogenic elements associated to chirality are generally rigid tridimensional elemental structures, constituted either by a single atom or by a group of atoms, characterized by directional ligands. The permutation of two ligands produces a stereoisomer of the original molecule.[3]

Chemists have individuated the most commonly occurring elemental structures, which are responsible, when present, for the existence of stereoisomers, enantiomers and diastereoisomers, in order to facilitate the description of how the atoms of each stereoisomer are distributed in the space. Sufficient, but not necessary, condition to produce stereoisomers is the presence in the molecule of at least one stereogenic element.

In fact, some organic molecules exist as different stereoisomeric species even though devoid of classical rigid stereogenic elements, like topological stereoisomers[4], and the so called "residual" stereoisomers.[5] Topological stereoisomers, like three-foil knots, oriented catenanes and Moebius strips are characterized by "mechanical" bonds.

The most popular tridimensional stereogenic elements, then capable of generating chirality in a molecule, are the stereogenic center, or stereocenter, the stereogenic axis, the stereogenic plane and the helix.

The enantiomers display identical scalar physical properties (properties devoid of sign), like melting point, boiling point, solubility, n_D and UV, IR and NMR spectra. They are characterized by identical energies, at least at a macroscopic level.

Two enantiomers display opposite pseudo-scalar physical properties (properties endowed with opposite sign), like optical rotatory power (α_D), and circular dichroism (electronic CD and vibrational CD). Most importantly, they exhibit different reactivity towards chiral reagents.[6] Although characterized by the same chemical-physical properties, two enantiomers are not interchangeable when they interact with a chiral environment.

For example, (*R*)-carvone smells of spearmint oil while (*S*)-carvone smells of caraway oil; 2-(4-isobutylphenyl)propanoic acid (Figure 4 A), better known as the painkiller ibuprofen, has the desired pharmacological effect in its (*S*)-configuration, while the (*R*)-form is nearly inactive.

(*R*)-Thalidomide is an effective sedative, which has a soothing effect that relieves anxiety and makes the patient drowsy, while the (*S*)-enantiomer is known to cause teratogenic birth defects called phocomelia, a congenital disorder involving malformation of the limbs (Figure 4 B). In 1960s in Germany, thalidomide could be bought without a prescription and shortly after the drug was sold, 5,000-7,000 infants were born with phocomelia. It was further proposed that the

thalidomide tragedy could have been avoided if the single (*R*)-enantiomer had been used, but humans interconvert (*S*)- and (*R*)-thalidomide enantiomers rapidly by both oral and intravenous assumption.[7]

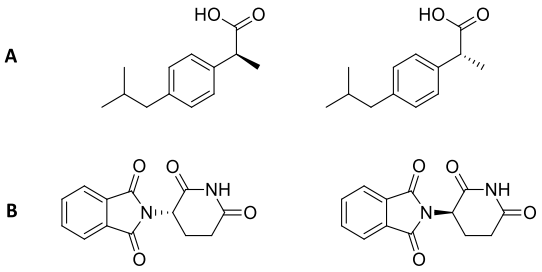

Figure 4: A) *S*- and *R*-ibuprofen. B) *S*- and *R*-thalidomide.

It appears clearly why the choice of the right enantiomer and the evaluation of a possible interconversion between enantiomers are so crucial, especially for drugs: enantiomers are involved in a stereoselective recognition by biological receptors inside and outside cells. The two enantiomers of the same molecules differ in their interactions with targets (generally enzymes, proteins or other chiral molecules) and these differences in interactions lead to differences in the biological activities of the two enantiomers, such as their pharmacology, pharmacokinetics, metabolism, toxicity or immune response.

The aim of this PhD work was to exploit the properties of a class of molecules endowed with axial stereogenicity, and to use them to obtain innovative structures suitable for the realization of enantioselective sensors.

We are aware that the potential inherent to chiral molecules is almost unlimited and that this work represents just a little, but carefully investigated and hopefully innovative step toward a better knowledge of stereoselective phenomena.

"You, Enantiomer
Dual but the same

Wrap the taste of the essence
Meaning of twin existence
Two forms, one path, one soul"

Chirality, Chaos Plague

2. Introduction: electroactive polymers and the "inherent chirality" concept

2.1. Organic semiconductors

Since the discovery of the photoelectric effect by the Italian Pochettino,[8] consisting in the emission of electrons from a material when light is shone over the material, many organic compounds have been studied as multi-functional materials due to their capability of showing different and remarkable properties such as charge transport, light absorption/emission, photoconductivity or electroluminescence.

All the above-mentioned peculiar properties of these materials are certainly related to their chemical structure and can be strictly correlated to the presence of sequences of π-conjugated double bonds along the backbone of the molecule. The π-conjugated orbitals, highly delocalized over the carbons of the backbone, can create the electronic mobility suitable for giving origin to semiconducting properties. Organic semiconductors (OSCs), *single-molecule* or polymeric semiconductors, show peculiar optical and electronic properties which make them suitable candidates, as the traditional inorganic counterpart, for the preparation of optoelectronic devices. However, the critical and the most widely explored features in OSCs are the HOMO/LUMO energy gap and the possibility of performing chemical or electrochemical doping. The oxidative (*p* doping) or reductive doping (*n* doping), which converts OSCs from insulators into reliable conductors, is a key point in the preparation of materials suitable for the above-mentioned applications.

Furthermore, the main advantage of the OSCs is a better processability compared to their inorganic counterparts. In addition, it is possible to customize the chemical structure in order to modify the chemical-physical properties, tuning some characteristics of the material for a specific purpose. A further interesting feature of the OSCs relies on the possibility of casting films at room temperature and on flexible, transparent and cheap substrates.

The potential applications of OSCs were realized and described for the first time in 1976 by Shirakawa, Heeger and MacDiarmid, when a redox potential was applied to an intrinsically insulating organic polymer, the polyacetylene, for the first time.[9] The polyacetylene, considerable as the prototype of polymeric OSCs and the simplest member of the family, is an insulator at the fundamental state (with a conductivity lower than 10^{-5} $\Omega^{-1}cm^{-1}$ but was turned

into a strong charge conductor when it was oxidized by exposure to iodine vapors, acquiring a 10^8 times greater conductivity, thus attaining values close to those exhibited by silver.

This behavior is due to the small ionization potential of the conjugated chain, since the π electrons can be relatively easily removed to form a polymeric cation without substantial disruption of the σ bonds which are responsible for maintaining the connectivity of the polymeric backbone, as shown in Figure 5.

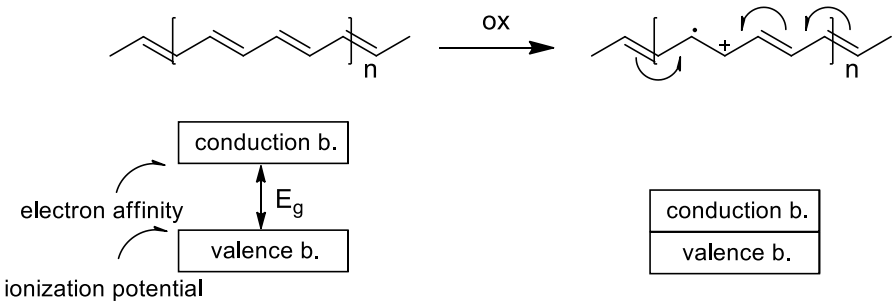

Figure 5: Chemical *p* doping of polyacetylene.

The origin of the finite energy gap in conjugated systems lies in the alternation of single and double bonds. In the hypothetical case of complete electron delocalization, all the C–C bonds should have an equal length and the extension of the conjugated chain would produce a progressive closure of the energy gap.

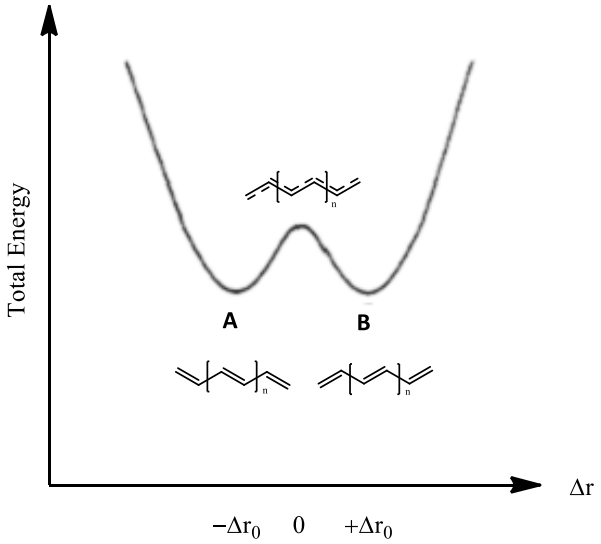

Scheme 1: BLA and lowering of band gap in polyacetylene.

Theoretical and experimental work, however, has shown that one-dimensional conjugated systems are unstable;[10] the combined effects of electron-phonon coupling and electron-

electron correlation lead to the localization of π-electrons with the aperture of a gap of at least ≈ 1.50 eV in the case of a simple polyenic system. Thus, bond length alternation (BLA) represents the major contribution to the magnitude of the energy gap (Scheme 1). Consequently, synthetic approaches leading to structural modifications resulting in a reduced BLA can be expected to produce a decrease in the HOMO-LUMO gap.[11]

The second generation of OSCs was characterized by peculiar structural and chemical modification of the backbone, consisting in the substitution of the all-trans double bond conjugated chain with carbocyclic or heterocyclic aromatic rings. This approach maintained an efficient conjugation in the system and produced a greatly improved stability of the material, making also much more feasible its functionalization.[12] Moreover, the introduction of hetero-aromatic systems into the conjugated chain hugely enlarged the panorama of synthetically accessible compounds, allowing an even finer tuning of the optical and of the electronic properties.

The second generation OSCs, which attracted greatest attention by the scientific community, are based on poly-*para*-phenylene (PPP), polyphenylenevinylene (PPV), poly-aniline (PANI) and poly-2,5- thiophene (PT) (Figure 6).

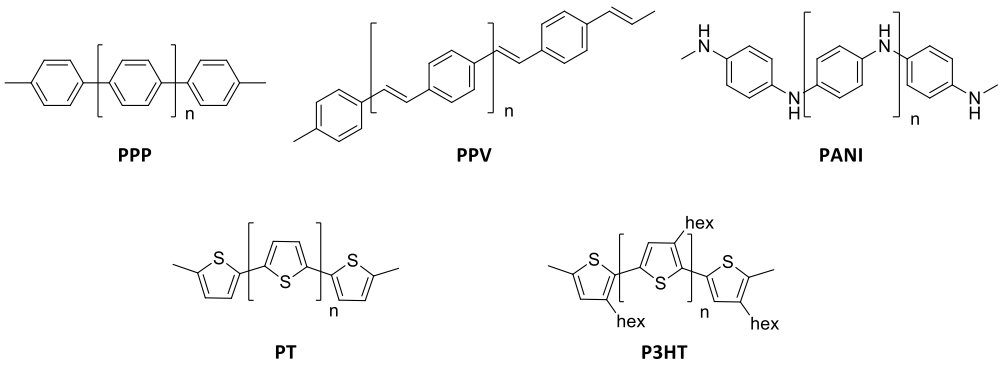

Figure 6: PPP, PPV, PANI, PT and P3HT general structures.

Unlike polyenes, poly-aromatic systems have a non-degenerate ground state. Thus, contrary to polyenic systems, the two limiting mesomeric forms obtained by the flip of the double bonds are not energetically equivalent (Scheme 2). While the aromatic form is energetically more stable, the quinoid form has a higher energy and a lower energy gap.[13] Obviously, the energy needed to switch from the aromatic to the quinoid form directly depends on the aromatic stabilization resonance energy of the aromatic unit.

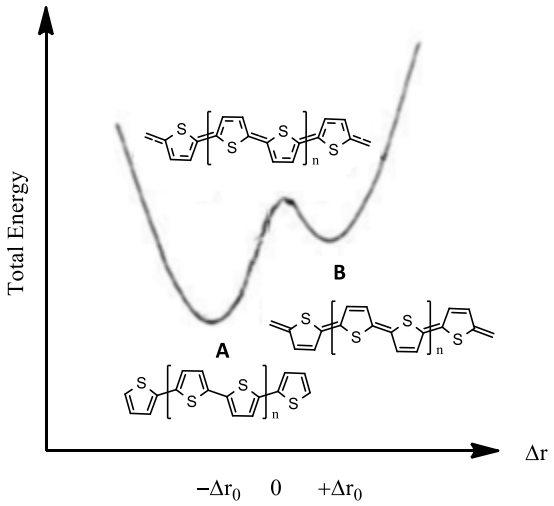

Scheme 2: BLA and lowering of band gap in PT, aromatic and quinoid form.

This resonance effect tends to confine the π-electrons within the aromatic ring and hence to prevent their delocalization along the whole conjugated chain. Despite the extremely interesting optoelectronic and charge-conduction properties, these polymers generally show a dramatic insolubility in organic solvents, even in the case of low molecular weight oligomers, such as the sexiphenylene and sexithiophene systems.

The aromatic backbone has been functionalized with alkyl chains, ether functions, aromatic rings or polar groups to enhance the solubility and to improve the performances of the final material. Unlike the polyacetylene, the introduction of substituents does not compromise the electric properties of the polymer. In Figure 6 the regioregular poly(3-hexylthiophene) (P3HT) is reported, one of the most popular polymeric OSCs employed as donor materials in bulk-heterojunction solar cells. P3HT represent an example of functionalized polymer, based on the simpler PT, properly modified to improve solubility without modification of the conductive backbone.[14]

Also those materials, like polyacetylene, are insulator in their fundamental state but become conductors as a result of a doping process: like anticipated, it can be oxidative, the most commonly used process for polythiophene materials, or reductive. The *p*- and the *n*-doping process consists respectively in removal or injection of one or two electrons occurring on every three heterocyclic units. In the case of *p*-doping, oxidation develops through the subsequent formation of species defined respectively polaron and bipolaron, as schematized in Scheme 3 for the case of PT *p*-doping.

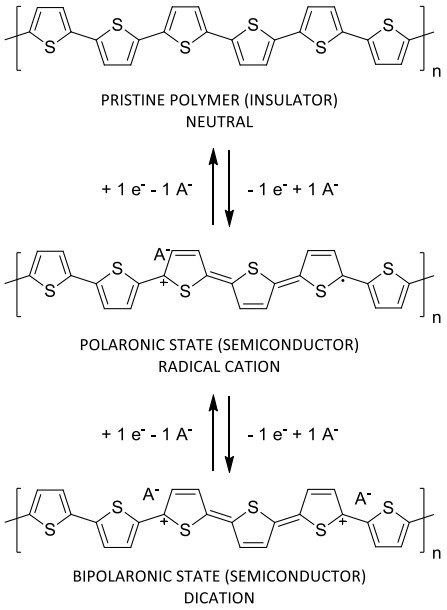

Scheme 3: Insulator and semiconductor state for PT polymer.

The most common polymerization method, used for the preparation of polythiophenes, consists on an oxidative treatment that can be performed by chemical or electrochemical processes.

The application of an oxidative process with a chemical oxidant, such as $FeCl_3$ or $(NH_4)_2S_2O_8$, leads to the formation of powders with polymeric structure, which behave as current conductors but are, unfortunately, insoluble in most organic solvents. The counteranions A^- (Scheme 3) coming from the oxidizing agent (eg. Cl^- and HSO_4^-/SO_4^{2-} respectively from $FeCl_3$ and $(NH_4)_2S_2O_8$) is incorporated in the material to compensate for the "holes" (electronic deficiencies) due to the electronic removal.

As for the preparation of electroactive polymers by electrochemical oxo-reduction processes, the imposition of an oxidative potential sufficient to induce the oxidation of a monomer leads to the deposition of the polymer on the surface of the working electrode. Electrochemically oxidized monomers can be deposited on different electrodes surfaces: Gold, Indium-Tin oxide (ITO), Platinum, glassy carbon (GC) electrodes are suitable for the deposition of electroactive polymeric materials and the choice of different substrates corresponds, often, to very different investigation techniques.

However, in any case, the initial polymerization steps, corresponding to the oxidation of the monomer and to the formation of oligomers, may occur in solution rather than on the electrode surface. Moreover, in the electrochemical synthesis, the ions A^-, which compensate the charge of the holes induced by oxidative doping, are extracted by the supporting electrolyte during the deposition process.

2.2. Chiral electroactive materials

Chiral electroactive materials were investigated with the aim of combining in the same material the conduction properties typical for OSCs polymers with the ability to discriminate between the two enantiomers of an analyte.

Chirality is generally introduced in the polyconjugated semiconductors by attaching chiral pendants to the electroactive backbone and the presence of carbon stereocenters invariably characterizes the chiral substituents.

A wide variety of examples that exploit this general approach are known in literature; many natural chiral substituents were selected for the side-chains functionalization and, in particular, sugars, amino acids or artificially synthesized structures designed for this specific application. The most studied chiral polymers were the thiophene-based ones, derived from the chemical or electrochemical oxidation of thiophene monomers functionalized in position 3[15][16] or 3,4.[17]

This approach, however, is not limited to the design of chiral oligo- and poly-thiophenes only (some examples are reported in Figure 7), but other examples concern the possibility of using poly-pyrrole[18] derivatives (some examples are reported in Figure 8).

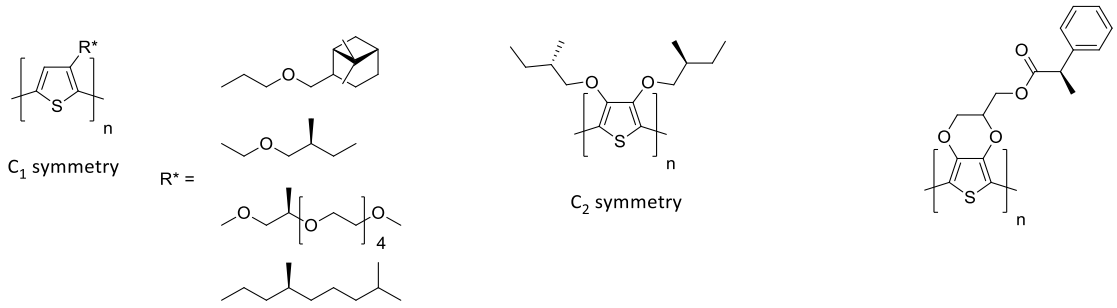

Figure 7: Literature examples [15][16][17] of chiral side-chain functionalization for thiophene-based polymers.

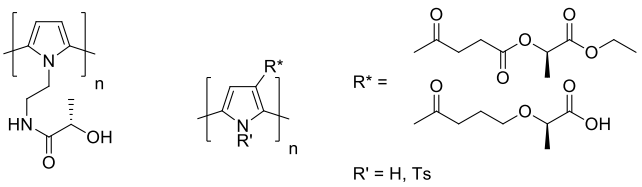

Figure 8: Literature examples [18] of chiral side-chain functionalization for pyrrole-based polymers.

A general drawback of this kind of chiral electroactive materials is that they give relevant chirality manifestations only under particular experimental conditions. For example, in the case reported in Figure 9, no CD signal is detectable in $CHCl_3$ solution, while a progressive signal

increase is observed by subsequent additions of aggregating protic solvents, like methanol, which induce a helical arrangement in a chain aggregation process.[17]

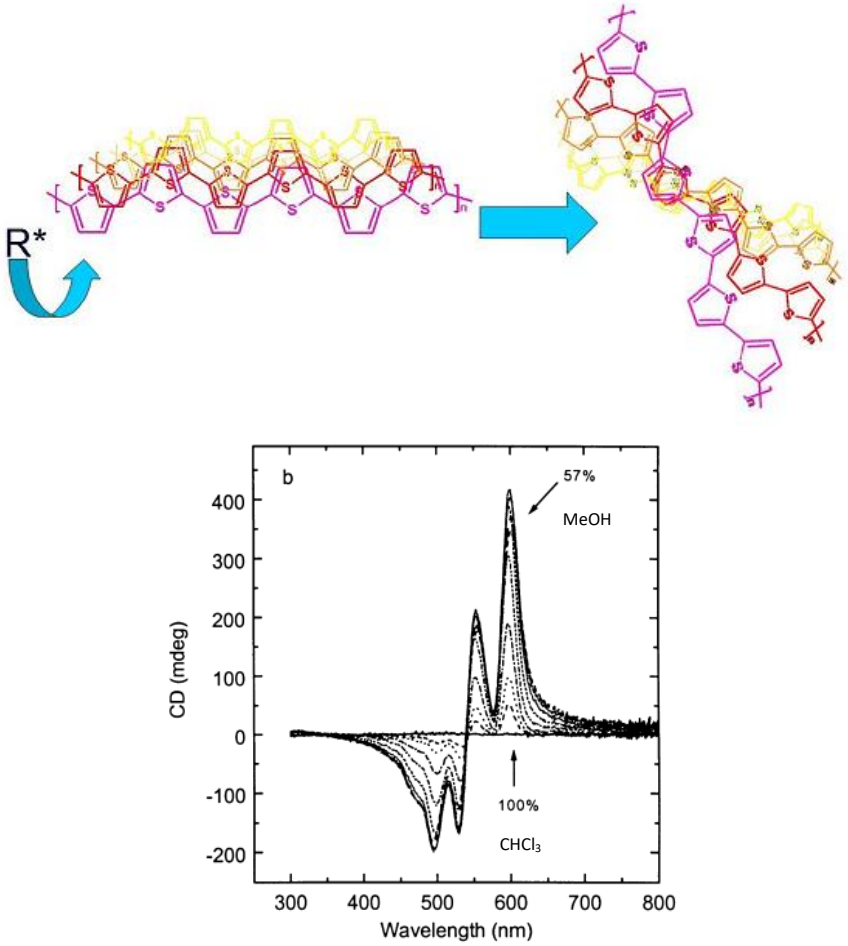

Figure 9: Helical arrangement (top) and CD profile with increasing amounts of MeOH, aggregating protic solvent (bottom).[17]

In addition, a further aspect to be considered is the fact that the alpha positions of the 3-functionalized monomers are constitutionally heterotopic due to the C_1-symmetry. By consequence the polymers resulting from oxidation of this kind of monomers are not constitutionally regular being constituted by a mixture of different regioisomers, as reported in Figure 10.

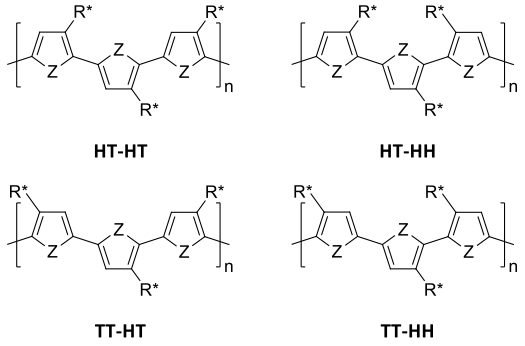

Figure 10: Different regioisomeric trimeric units resulting from a C_1-symmetric monomer.

In order to obtain ordered materials, it is necessary to perform a regioselective chemical polymerization, generally quite laborious, as reported by Kane-Maguire and co-workers.[15]

One of the most attractive application for this kind of materials is in the field of enantioselective sensors,[19] being well documented that the electrically conductive polymers are able to modify their electrical properties in the presence of organic substances. By consequence, if the conductive material, a film over the sensors surface in this case, is chiral, it may behave differently in the presence of one or of the other enantiomer of a chiral analyte and, possibly giving well-defined different responses.

However, few examples are reported in literature. Outstanding results were obtained when a chiral electroactive compound was employed in the realization of an Organic Field-Effect Transistor (OFET)[20] shown in Scheme 4. The device is characterized by a double layer able of combine field effects and chiral enantiorecognition. The two layers are constituted by two alkoxyphenylthiophene-based oligomers which differ only in the structure of the side-chains.

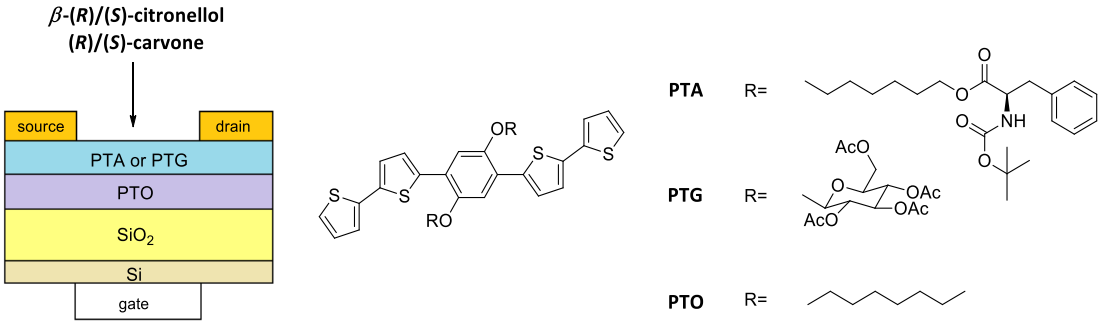

Scheme 4: OFET general structure and side-chain moieties.[20]

The amino acid *L*-phenylalanine *N*-BOC and β-*D*-glucose tetraacetate, responsible for chiral recognition, respectively in PTA and PTG, were chosen as examples of chiral substituents, easily available from natural sources and inexpensive.

It was found to be essential to combine the two layers because, when only one was used, it was not possible to observe the so-called amplified current field effects, probably due to the steric hindrance of the substituents on the side-chains.

The response of a transistor based on PTA / PTO structure exposed to vapors of (*R*)-, (*S*)-citronellol and their corresponding racemates is reported in Figure 11. It is immediately clear that the response of the two enantiomers is different and, in particular, the *S* enantiomer shows a higher current intensity than the *R* one.

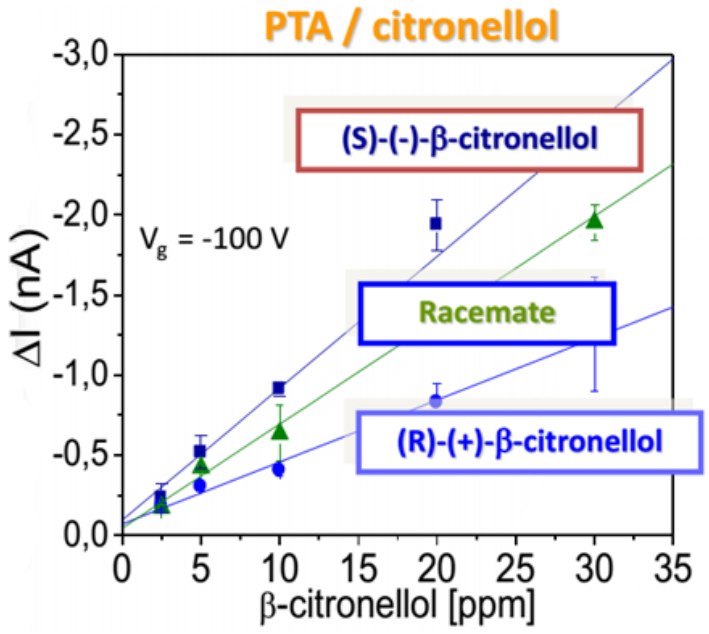

Figure 11: Typical current intensity vs. concentration curve showing the response as current increment of an electrolyte-gated OFET biosensor to the two enantiomers of β-citronellol and its racemate.[20]

Moreover, the response of the transistor (expressed in current intensity ΔI/nA) appears to be linearly correlated with the concentration of the vapors and the racemate shows an intermediate behaviour, as expected, between the two enantiopure profiles. Last but not least, the sensitivity of this technique is remarkable, allowing to measure vapors concentration of 5 ppm and even below. The sensitivity is, of course, crucial for the reliability and the feasibility of the devices and their possible applications.

Another use of these materials, particularly interesting in our research perspectives, is the possibility of preparing modified electrodes. Few examples are known and the results obtained are partially satisfying because, the modified electrodes reported in literature exhibit weak responses towards the enantiomers of the same analyte.

Dong and co-workers,[21] for example, reported the preparation of a chiral electrode obtained coating a GCEs with a film of the modified poly-EDOT reported in Figure 7. The chiral EDOT, nicknamed as (*R*)- or (*S*)-PEDTM-PP was electropolymerized in CH_2Cl_2. In Figure 12 it is possible to observe the response of the electrodes during cyclic voltammetry analysis. As previously mentioned, a small difference, expressed in mV, between the CV profile of the two enantiomers of DOPA could be measured and the CV patterns resulted to be almost superimposable.

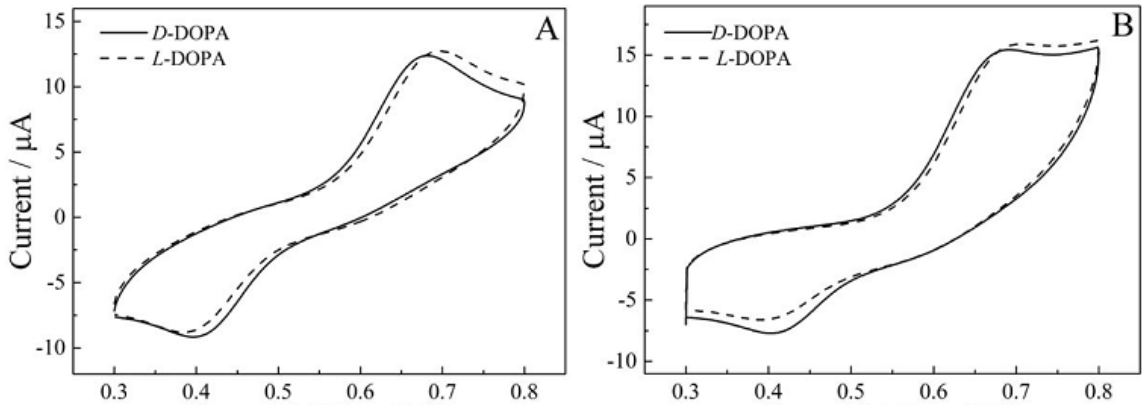

Figure 12: Enantioselective properties of modified electrodes (coated with pEDOT functionalized with chiral pendants). A) (*R*)-PEDTM-PP B) (*S*)-PEDTM-PP. CV condition: 0.25 M H_2SO_4 containing 0.5 mM *L*-DOPA (dashed line) or *D*-DOPA (solid line), 50 mV s^{-1} scan rate.[21]

Another drawback of those kind of modified electrodes is that the response towards the enantiomers is generally expressed through the current intensity and not through the absolute potential required for the oxidation of the analyte. This is the case reported by Pleus and Schwientek[18] who electrodeposited on platinum electrodes the chiral pyrrole monomers reported in Figure 8. Different pyrrole 1- or 3-substituted with chiral pendants were employed as starting material for the preparation of chiral sensors that were tested in the presence of the two enantiomers of camphosulfonic acid (CSA) as supporting electrolyte and doping agent. The results obtained are reported in Figure 13 showing that the observed differences in current densities are rather small (below 70 µA).

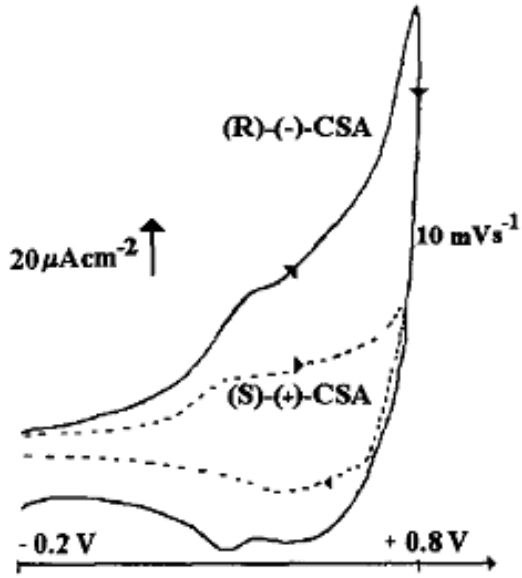

Figure 13: Enantioselective properties of modified electrodes (coated with polypyrrole functionalized with chiral pendants). CV condition: ACN containing (*R*)-(-)-CSA or (*S*)-(+)-CSA (0.1 M) as doping agent, 10 mV s^{-1} scan rate.[18]

2.2.1. Chiral electrodes and chiral sensors

Many different approaches were reported in literature to realize chiral electrodes not involving the electrodeposition of chiral monomers.

The first approach, suggested first by Muskal and co-workers[22] in 1995, then by Nakanishi[23] and Fu,[24] involves the preparation of sensors modified with chiral Self-Assembled Monolayers (SAMs): different selected monolayers (ω-mercaptocarboxylic acid, homocysteine or *N*-isobutyryl-*L*-(*D*)-cysteine) were employed to functionalize electrodes (Hg or Au), leading to remarkable results in terms of enantioselectivity. Furthermore, it was highlighted that nanosized chiral spaces are fundamental as enantioselection sites, suggesting that a strong correlation between structure and organization in the monolayer should be involved.

Specifically, Muskal reported the preparation of a SAM obtained with a carbomethoxy phenylalanine derivative of 6-mercaptohexanoic acid and the properties of a hanging mercury drop electrode (HMDE) modified with *D-, L-,* and the *DL*-monolayer were evaluated.

In Figure 14 it is possible to observe the cyclic voltammograms of $Ru(NH_3)_6^{3+}$ on a modified electrode with the enantiopure SAMs and racemic SAM versus the unmodified electrode: it is evident that the rate of electron transfer of the redox couple is substantially decreased by the presence of a monolayer and, specifically, the electron transfer resulted to be less intense on HMDE modified with heterochiral monolayer with respect to homochiral monolayer.

This behaviour was considered attributable to the organization of the layers on the electrode surfaces.

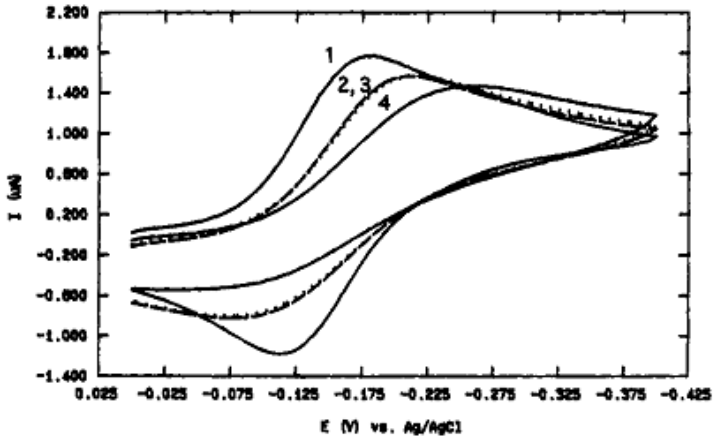

Figure 14: Cyclic voltammetry of 1 mM $Ru(NH_3)_6^{3+}$ in 0.1 M acetate buffer (pH 6.0) on a bare HMDE (1) and on mercury drops modified with pure enantiomers: *D* (2), *L* (3), and racemic mixture (4), 100 mV s^{-1} scan rate.[22]

On the other hand, Nakanishi’s group tested the enantioselectivity of SAMs obtained from homocysteine (Hcy) deposited on the (111)-oriented gold surface, and they tested, after the chiral SAMs deposition, the redox behavior of 3,4-dihydroxyphenylalanine (DOPA) in acidic solution. The shape of the voltammograms, reported in Figure 15 was found to depend upon the combination of the chirality of *L*- and *D*-Hcy and that of *L*- and *D*-DOPA: it is possible to observe that the difference between the oxidation and reduction potential for the DOPA enantiomers on the different SAMs reach values between 50 and 100 mV.

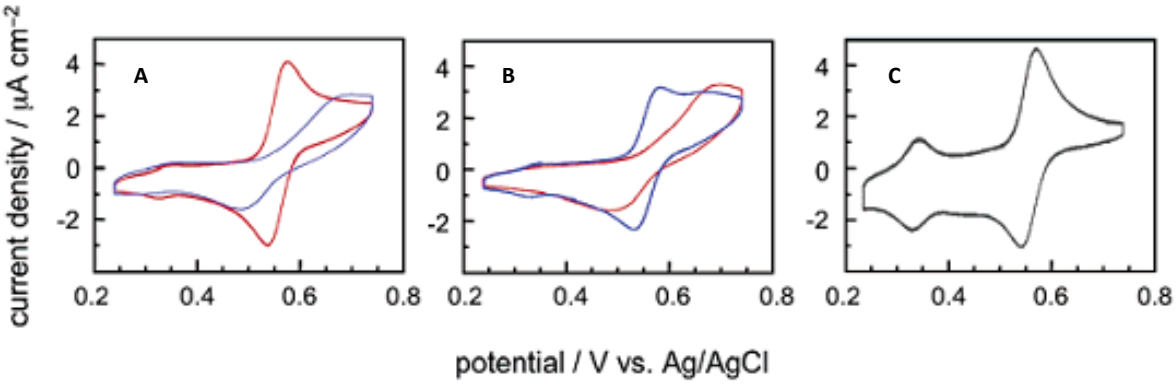

Figure 15: A) Cyclic voltammograms for redox reactions of DOPA at gold electrodes modified with *L*-Hcy; B) Cyclic voltammograms for redox reactions of DOPA at gold electrodes modified with *D*-Hcy; both in aqueous 0.25 M H_2SO_4. Red and blue curves represent the voltammograms for *D*- and *L*-DOPA, respectively. C) CV profile obtained with bare gold electrode for *L*-DOPA. 5 mV s^{-1} scan rate.[23]

A third example considering the use of SAM for the enantiorecognition of chiral analytes comes from the research of Fu: a sensor, obtained from *N*-isobutyryl-*L*-(*D*)-cysteine (NIBC) enantiomers self-assembled monolayer was tested for recognizing the enantiomers of DOPA. In Figure 16 it is reported that *L*- and *D*-DOPA display identical CV profiles on a bare gold electrode, while there is a variation in the current intensity when a chiral SAM electrode is employed. The effect of some interferences was also investigated and the enantiorecognition ability was tested also in the presence of ascorbic acid or tyrosine, since electrochemically closely related to DOPA. The tests performed with interferences give satisfying results.

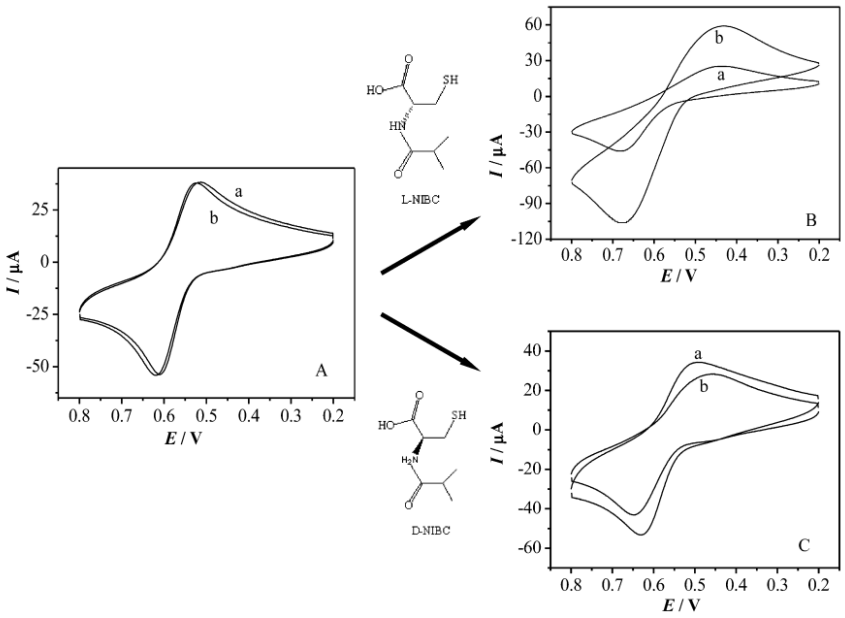

Figure 16: Cyclic voltammetries for redox reactions of 5 mM *L*-DOPA (a) and *D*-DOPA (b) in 0.25 M H_2SO_4, 100 mV s^{-1} scan rate. A) Bare gold electrode, B) *L*-NIBC-Au functionalized, C) *D*-NIBC-Au functionalized.[24]

Chiral electrodes can be also prepared by functionalization with chiral molecular layers: Nie[25] and co-workers prepared a chiral electrochemical sensor via cysteic acid modified glassy carbon electrode that resulted to be suitable for discriminating tyrosine enantiomers. While previous research was focused on the evaluation of different peak current density between two enantiomers, the Authors suggested a new method the main goal of which consisted in the fact that enantioselection evaluation is based on the difference between the oxidation potential peaks. In Figure 17 different voltammograms are reported: on CyA-GC modified electrodes, the oxidative potential of the enantiomers of tyrosine shifted negatively, and the peak current increased; in particular, the difference of the peak potential [$\Delta E_p(E_D - E_L)$] was found to be 40 mV.

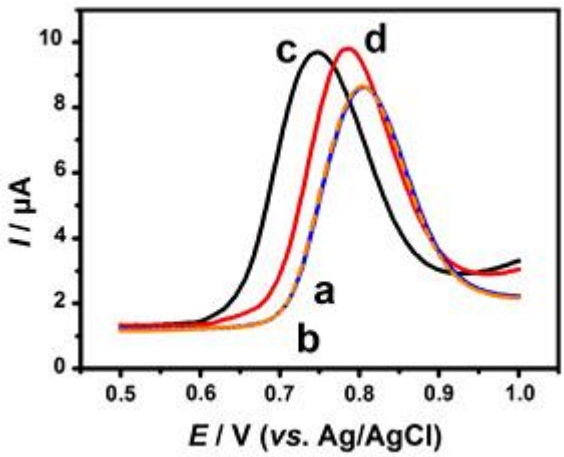

Figure 17: Different potential voltammograms of (a) *D*-Tyr on GC electrode (orange dashed line), (b) *L*-Tyr on GC electrode (blue solid line), (c) *D*-Tyr on CyA-GC electrode and (d) *L*-Tyr on CyA-GC electrode.[25]

Another approach, elaborated by Kuhn[26][27] and co-workers, consists in the preparation of molecularly imprinted chiral mesoporous metal surfaces; these materials were obtained by electrochemical reduction of platinum salts in the presence of a liquid crystal phase and chiral molecules (*L*- and *D*-DOPA or *R*- and *S*-mandelic acid): the matrix obtained through this procedure showed outstanding enantiodiscrimination ability between the enantiomers of the imprinted molecules and it was used as chiral electrode. The general structure of the chiral-imprinted mesoporous platinum film is depicted in Figure 18 A: Pt is deposited on an Au electrode surface in the presence of a liquid crystal and the chiral template; surfactant and DOPA are then removed by accurate washing with large amounts of water, leading to an alignment of the mesopores in a hexagonal lattice. The electrodes were studied by differential pulse voltammetry (DPV) and the profile obtained with chiral electrode imprinted with *L*-DOPA is shown in Figure 18 B.

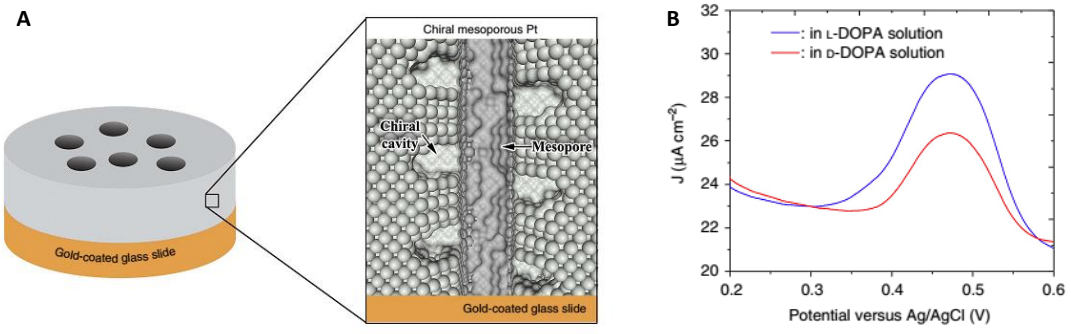

Figure 18: A) Mesoporous chiral matrix structure. B) DPV of chiral mesoporous platinum electrode imprinted with *L*-DOPA using a *L*-DOPA/$PtCl_6^{2-}$ ratio of 1/25. CV conditions: 50 mM HCl containing 4 mM using L- or D- DOPA as probes.[26]

A high difference between the electro-oxidation current densities was observed due to the different interaction between the enantiomers of DOPA with the chiral mesoporous surface.

The apparent drawback of this approach is that this kind of electrodes are able to discriminate, at least in theory, only the enantiomers employed to imprint them.

2.3. “Inherently chiral” electroactive materials

In the research group where the present PhD thesis was developed, a new and original design of chiral electroactive materials was developed a few years ago. A new class of chiral oligo- and poly-heterocycles, completely different from those reported in the literature, was designed: they are prepared by oxidation of monomers displaying the general structure shown in Figure 19.

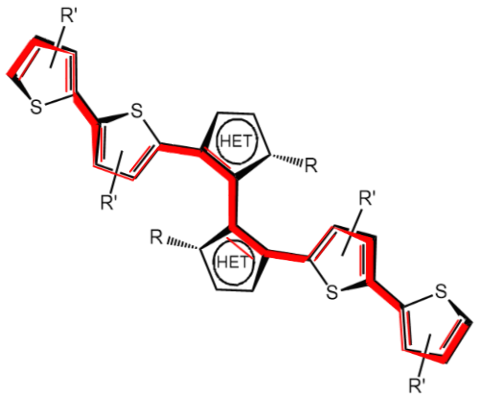

Figure 19: General structure of the class of inherently chiral OSCs monomers.

The guidelines followed for designing this kind of monomers are based on the following rationale:

- Chirality results from a tailored torsion internally generated along the conducting oligothiophene backbone. From here comes the appellative of inherently chiral monomers, since the stereogenic element, namely the stereogenic axis, is not external to the conjugated chain, like in the previously mentioned literature examples, but it is part of it. Thus, the same conjugated system responsible for the optical and electrochemical properties of the materials is also responsible for molecular chirality and, by consequence, the chiroptical and enantiorecognition properties of the material are strictly correlated to the electrochemical ones.

- The stereogenic core responsible for chirality (a stereogenic axis) is an atropisomeric bithiophene or bipyrrole system. Both sub-classes have been deeply investigated and many new members of both of them have been prepared in our laboratories.
- The stereogenic unit is tailored to conjugatively interconnect the two bithienyl termini, as indicated by the red conjugated sequence in the formula reported above.
- A node is located on the interanular bond: conjugative transmission between the two halves is not precluded, while polymeric network tridimensionality is important for amplifying the electro-optical performances.
- The symmetry of the monomers is C_2. Thus, the thiophene α–positions involved in the oxidative polymerization are homotopic and full regioregularity of the polymers is guaranteed.

The first intrinsically non-planar, dissymmetrical multithiophene-based monomer, the 2,2'-bis(2,2’-bithiophene-5-yl)-3,3'-bithianaphthene, nicknamed BT_2T_4, was synthesized few years ago.[28] Its general structure is reported in Figure 20: the red circle represents the central node associated to a calculated torsional angle of 70°, proving the non-planarity of the structure. The green small squares represent the two terminal α-position, the only suitable positions for chemical or electrochemical oxidation. Their homotopism guarantees full regioregularity of the oxidation products.

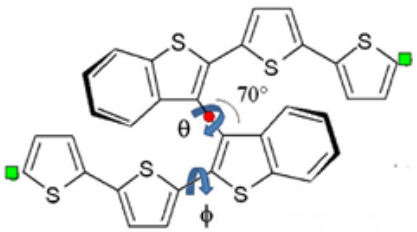

Figure 20: Structural formula of BT_2T_4 and dihedral angle between the two halves.[28]

The stereogenic axis coincides with the 3,3’ interanular bond; the hindered rotation along this axis produces a couple of atropisomeric enantiomers (Figure 21). Discrete Fourier Transform (DFT) calculations suggested a racemization barrier value of 43 kcal mol^{-1}, confirming that the interconversion of the antipodes can develop at very high temperature, higher than 100 °C.

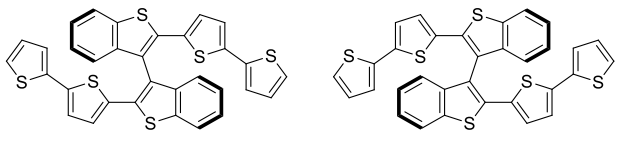

1

Figure 21: Structural formulas of (*R*)- and (*S*)-BT_2T_4 enantiomers.

BT_2T_4 was prepared starting from the commercially available thianaphthene, according to the strategy reported in Scheme 5. The thianaphthene was brominated in 3-position with liquid bromine in a chloroform solution and in the presence of sodium acetate; the 3-bromothianaphtene (**2**) was then converted into the 3,3’-bithianaphthene (**3**) through a copper dichloride mediated anion coupling performed at -90°C. The 2,2’-dibromo-3,3’-bithianaphthene (**4**), which is the key intermediate, was obtained through a bromination reaction in the presence of potassium acetate in a 55% yield.

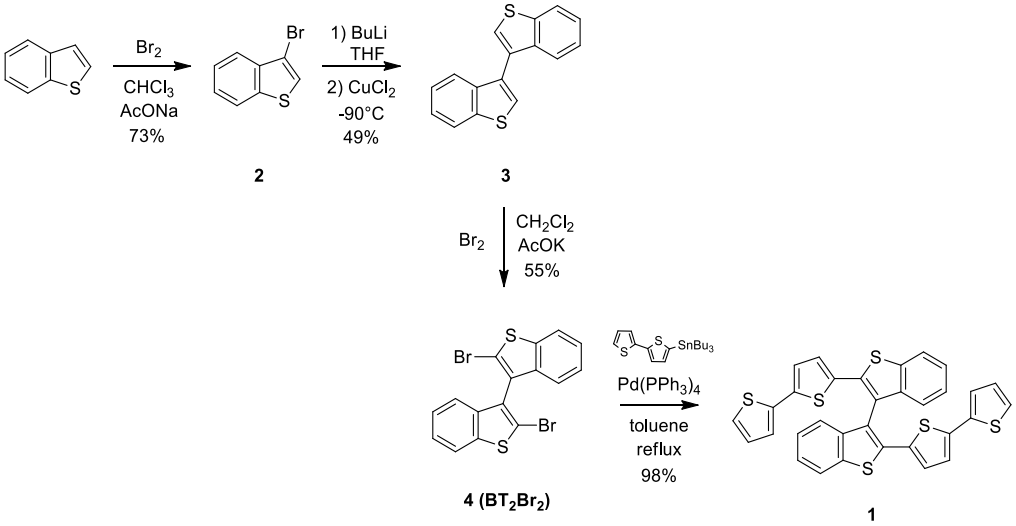

Scheme 5: Synthesis of racemic BT_2T_4.

The final step is the palladium (0) catalyzed Stille-reaction between the 2,2’-dibromo derivative **4** and the 5-tributylstannyl-2,2’-bithiophene (**5**), obtained, in turn, by reaction of the anion of the 2,2’-bithiophene with tributylstannyl chloride (Scheme 6)**.**

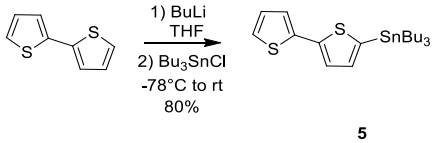

Scheme 6: Synthesis of 5-tributylstannyl-2,2’-bithiophene.

Thanks to this rather simple reaction scheme, BT_2T_4 could be obtained in satisfactory overall yields and its properties deeply investigated.

The monomer was electrochemical and spectroelectrochemical characterized: the material resulting from the electro-polymerization of **1** as racemate revealed very interesting properties. For example, it worked excellently as an efficient cross-linker and three-dimensional promoter when used as a co-monomer in an electropolymerization processes, essential step for the preparation of a Molecularly Imprinted Polymer (MIP), or even exceptionally performing as an element of recognition in a piezomicrogravimetric chemosensor, highly selective for the melamine and its derivatives.[28]

After complete characterization of the racemate, compound **1**, was resolved into antipodes by semi-preparative HPLC on a chiral stationary phase and the enantiopure monomers were characterized from a chiroptical point of view. In Figure 22 it is possible to observe the chiral HPLC chromatogram simultaneously monitored by UV and CD detectors: the two peaks, corresponding to the two enantiomers are perfectly separated (about 4 minutes difference in the retention times).

After the separation of the two enantiomers, their CD spectra were recorded and correlated to the one calculated for the *S*-enantiomer in order to assign the absolute configuration of the stereogenic axis (Figure 22 B). The first eluted monomer resulted to be the (*S*)-(+)-**1**.

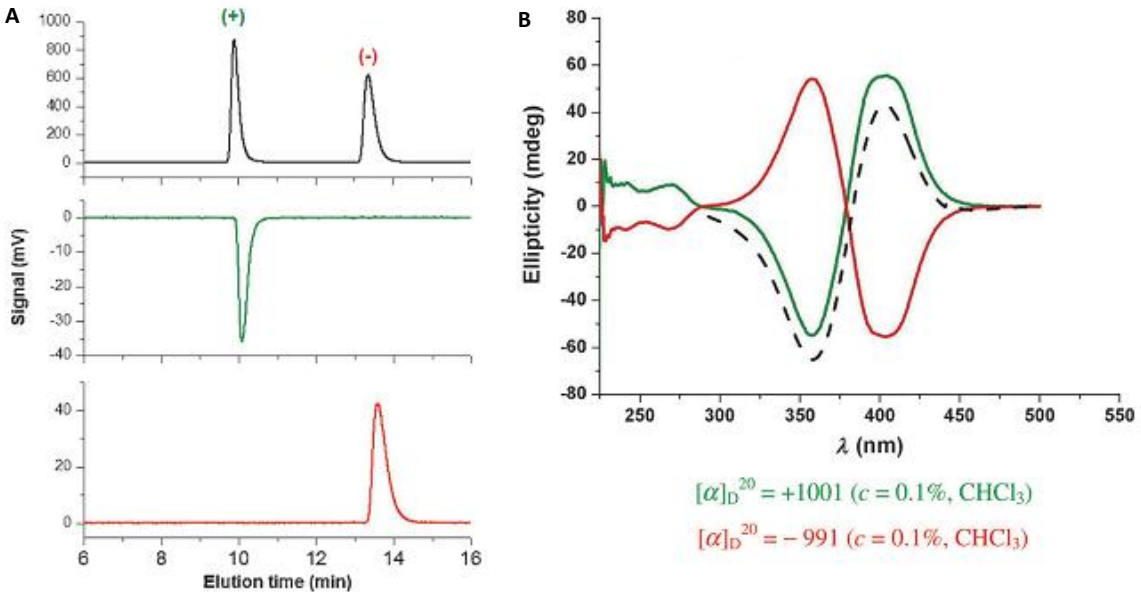

Figure 22: A) Analytical resolution of racemate of BT_2T_4 through HPLC on a chiral stationary phase. CPS: Chiralpak IB-3 (250 x 4.6 mm I.D.), eluent: n-hexane : CH_2Cl_2 : EtOH= 100 : 5 : 0.2, T= 25 °C, detector UV (black) and CD at 360 nm. B) CD spectra or (*S*)-BT_2T_4 (green), (*R*)-BT_2T_4 (red) and calculated CD for (*S*)-BT_2T_4 (dotted black).[29]

Last but not least, the very high values of the specific rotatory power of the antipodes, about 1000, demonstrate the importance of the presence of the inherently dissymmetric chromophore.[29]

The *R* enantiomer of the BT_2T_4 was, chemically oxidized with $FeCl_3$ in order to have larger quantities of material available for the complete characterization and applicative experimentation of the enantiopure oligomers.[30] The standard procedure involved the addition of a diluted solution of enantiopure **1** in chloroform to a slurry of the oxidant and the subsequent reduction of the oxidized material with hydrazine hydrate. The obtained material was then extracted with a Soxhlet apparatus and analyzed through MALDI spectrometry (Figure 23). In the spectrum, the presence of the dimer, as the main product, of the trimer in relevant amounts and of superior oligomers is evident.
However, a surprising result was found when the oligomeric mixture was submitted to a high-resolution LDI analysis: all the oligomers were found to be cyclic and not open structures.

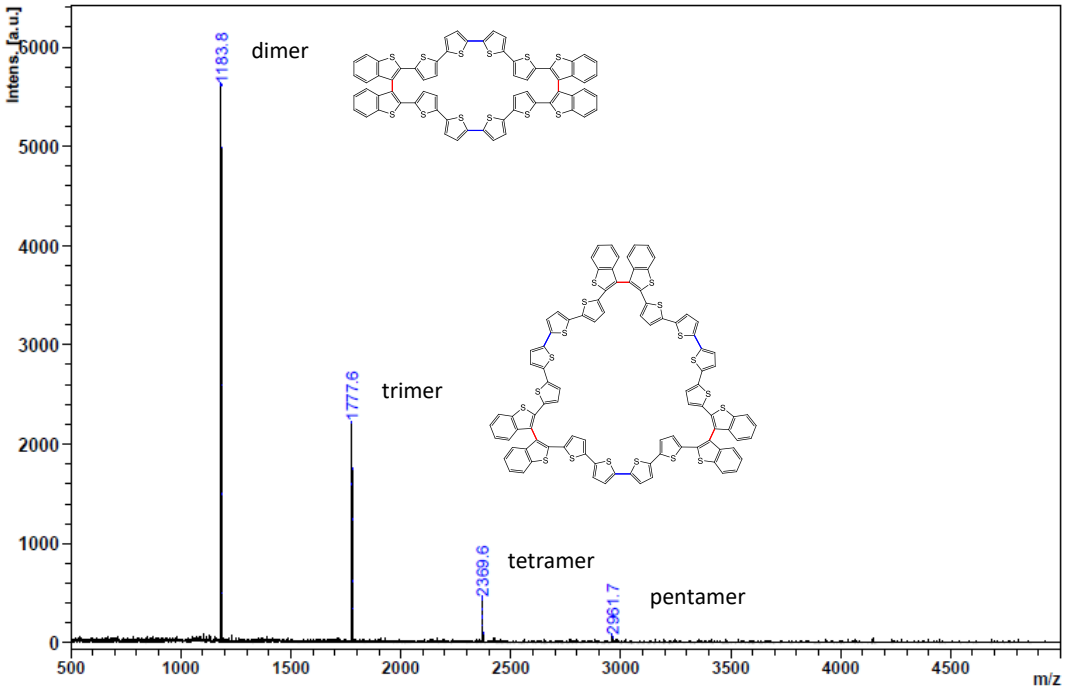

Figure 23: MALDI analysis of chemically oxidized BT_2T_4.[30]

In Figure 24 is also possible to observe the structures, obtained by DFT calculation in the general gradient approximation, of two and three-member rings formed by oxidation of the *R* enantiomer. In both cases the symmetry is D_n: the dimer appears as an ellipse with a 6 Å minor axis length, while the trimer is an equilateral triangle with an 18 Å geometrical height.

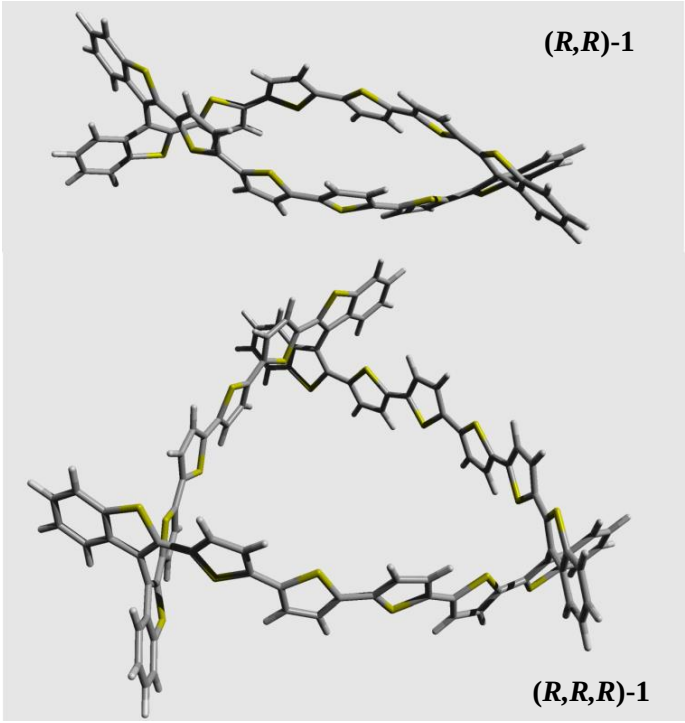

Figure 24: Calculated structures for cyclic dimer (*R,R*)-**1** and cyclic trimer (*R,R,R*)-**1**.

The symmetry of these structures was confirmed by ^{1}H-NMR analysis (Figure 25) of pure (*R,R*)-**1** and (*R,R,R*)-**1**, isolated in a pure state after an accurate column chromatography. In fact, the spectra of both oligomers show only four coupled signals for the benzothiophene ring and four doublet related to the protons in β position of the two thiophene units connected to the thianaphtene ring.

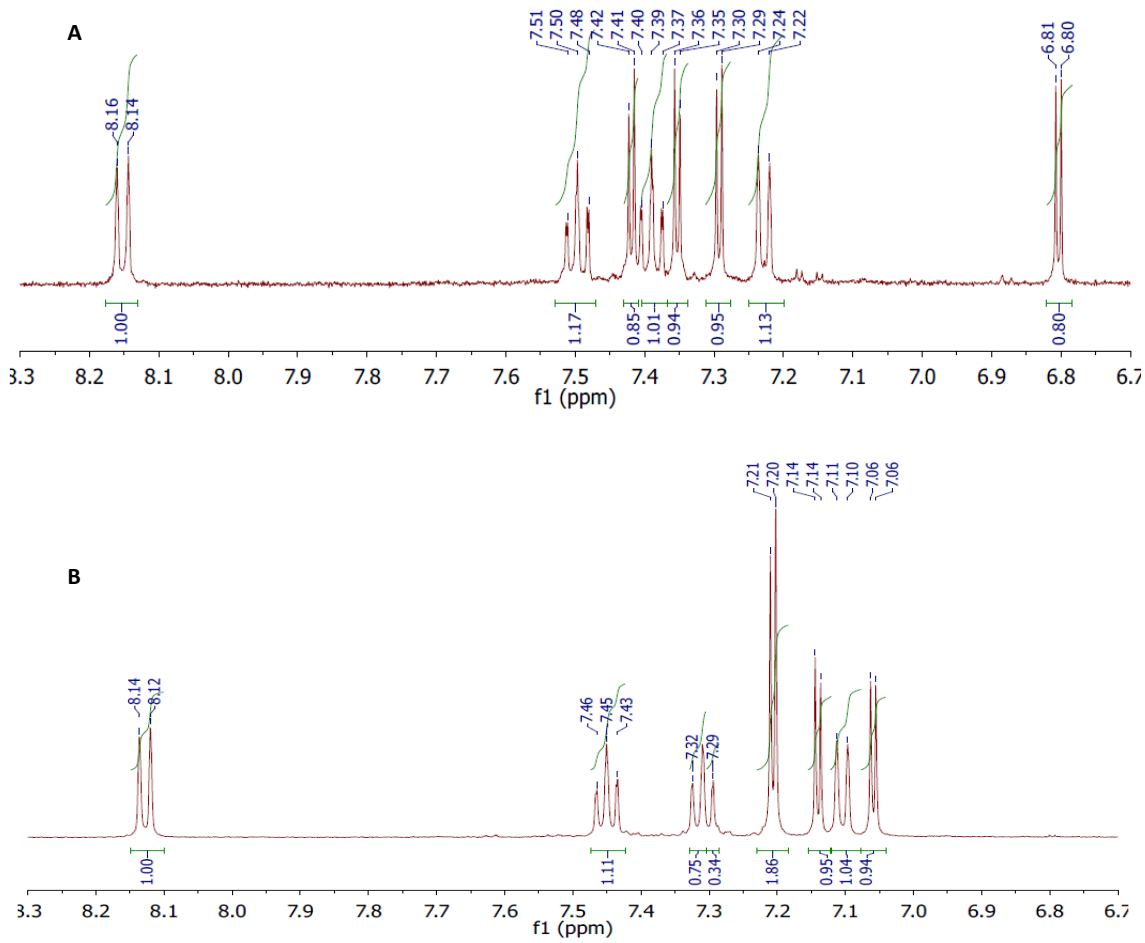

Figure 25: ^{1}H-NMR of cyclic dimers (A) and cyclic trimers (B) of monomer **1**.

The enantiopure oligomers obtained from the chemical oxidation were isolated and characterized by a chiroptical point of view. Remarkable, in the chiral photoluminescence spectra, are the high values of g comparable to those of helicenes.

Prompted from the outstanding features of compound **1**, the enantiopure monomers were electropolymerized on electrode surfaces in order to produce chiral electrodes and the enantiorecognition ability of electrodes coated with the enantiopure films were tested. In Figure 26 it is possible to observe the results obtained with gold electrodes coated with thin films of oligo-(*S*)-**1** or oligo-(*R*)-**1**: the tests were performed using commercially available (*R*)-(+)- and (*S*)-(-)-*N,N*-dimethyl-1-ferrocenylethylamine as chiral probes.

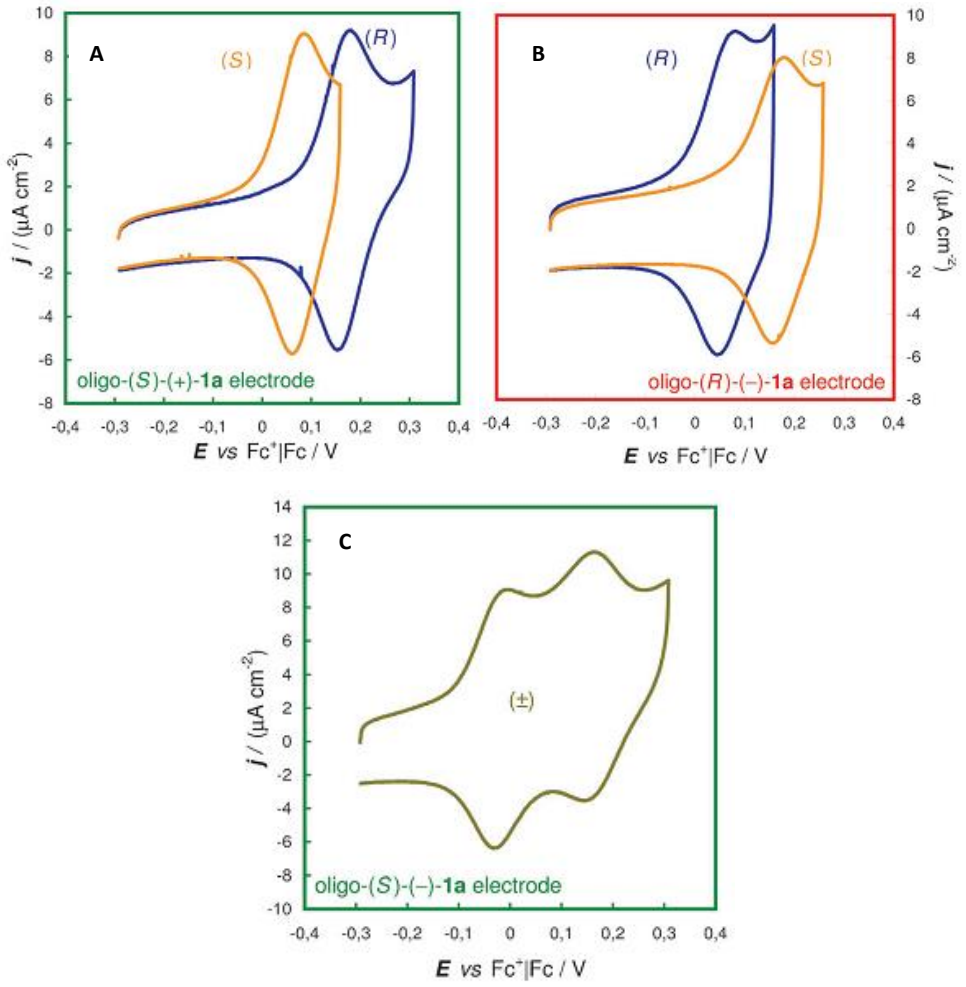

Figure 26: A) Enantiorecognition tests on enantiopure oligo-(*S*)-**1** (deposited form thirty-six cycles, 0.5 mM monomer solution in CH_2Cl_2 + $TBAPF_6$, 200 mV s^{-1} scan rate) with the enantiopure probes (8 Mm *N,N*-dimethyl-1-ferrocenylethylamine in $BMIMPF_6$). B) Enantiorecognition tests on enantiopure oligo-(*R*)-**1** (deposited form thirty-six cycles, 0.5 mM monomer solution in CH_2Cl_2 + $TBAPF_6$, 200 mV s^{-1} scan rate) with the enantiopure probes (8 Mm *N,N*-dimethyl-1-ferrocenylethylamine in $BMIMPF_6$). C) Enantiorecognition tests with enantiopure oligo-(*S*)-**1** and the racemic probe. [31]

It is easy to observe that the electrodes coated with the enantiomeric oligo-(*R*)-**1** and oligo-(*S*)-**1** films display an outstanding, perfectly specular, enantiodiscrimination ability towards the probes, with a formal oxidative potential difference of about 100 mV.

Furthermore, the probe showing the lower oxidative potential on the (*S*)-film was oxidized at a higher potential on the (*R*)-film and vice versa. The same tests were performed on dopamine, MeDOPA and ofloxacin and the enantiopure films equally gave impressive enantiorecognition responses for all the compounds used as chiral probes.[31]

The wide-range enantioselectivity of the inherently chiral electrode surfaces was fully confirmed also in aqueous media since large peak potential differences were obtained for a series of chiral DOPA-related molecules (Figure 27). Moreover, interesting modulating effects on enantiodiscrimination can be observed as a function of both molecular structure and pH.[32]

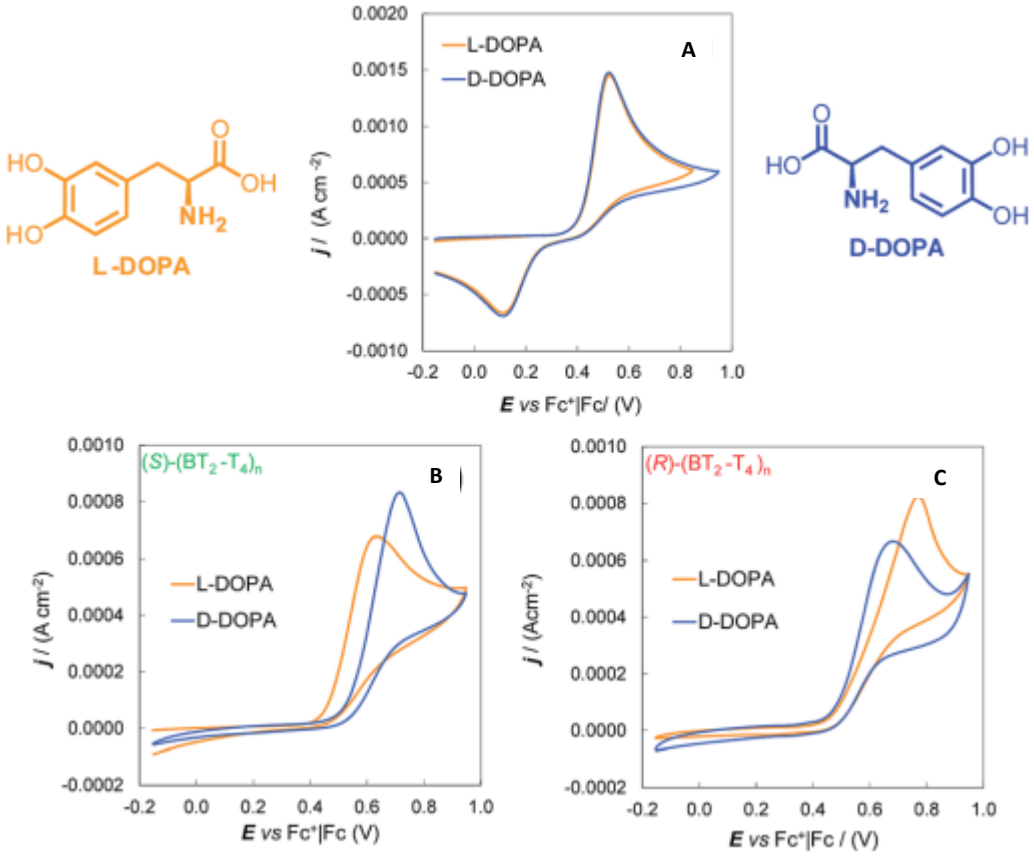

Figure 27: Cyclic voltammetry characteristics of DOPA enantiomers (4 mM in H_2O + 50 mM HCl). (a) Bare GC electrode. (b) and (c) GC electrode coated with (*S*)-(BT_2T_4) and (*R*)-(BT_2-T_4) film, respectively. [31]

3. Research subject

The present PhD research was focused on the following topics:

- Application of the racemic oligomers derived from the oxidation of BT_2T_4 as donor materials in bulk-heterojunction solar cells.
- Design of new inherently chiral compounds based on the modification of the structure of BT_2T_4. Three different modification strategies were carried out starting from the general structure of compound **1**:
    1. side chains elongation, in order to achieve, after a chemical or electrochemical oxidation, cyclic oligomers with bigger cavity;
    2. side chains planarization by blocking the two thiophene moieties in a rigid fused heterocyclic system, in order to achieve compounds where the rigidity and higher conjugation extent should improve optoelectronic properties;
    3. side chain modification by introducing different substituents on the bithiophene units, in order to tune electronic and steric properties.
- Design of new inherently chiral compounds based on the modification of the structure of 2,2'-biindole atropisomeric scaffold.
- Design of enantiopure inherently chiral monomers accessible through a stereoselective strategy.
- Design of inherently chiral monomers based on the spider-like oligothiophene structures.

4. Electroactive materials based on 3,3'-bithianaphthene scaffold

4.1. A family of solution-processable macrocyclic and open-chain oligothiophenes with atropoisomeric scaffolds: structural and electronic features for potential energy applications

Conjugated oligothiophene macrocycles are interesting objects especially because they idealize conducting polymers without ends; in addition, they are more soluble in organic solvents compared to their linear counterparts offering electrosensitive cavities of different sizes for selective inclusion of guest molecules.[33]

A preliminary investigation on the possible application as donors of the cyclic oligomers derived from chemical oxidation of racemic BT_2T_4 in bulk-heterojunction solar cells was carried out in order to verify if they were suitable to interact with fullerene derivatives as electron-acceptor counterparts.

The whole racemic materials and the stereoisomers distribution for the different macrocycles resulting from the $FeCl_3$ chemical oxidation of racemic **1** were preliminarily investigated.[34] Careful column chromatography of the crude orange-red solid obtained after Soxhlet extraction allowed to isolate cyclic dimers and trimers in a pure state. The fractions were analyzed by HPLC on a chiral stationary phase and the corresponding chromatograms are reported in Figure 28.

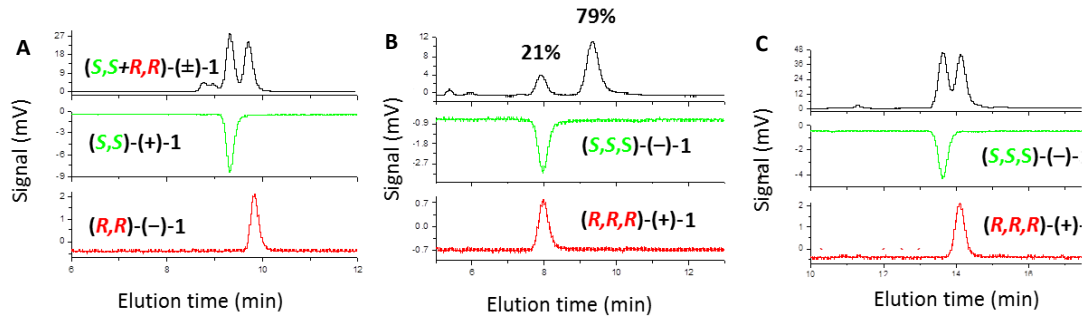

Figure 28: A) Analytical resolution of the racemate of cyclodimers of **1** through HPLC on a CSP in comparison with enantiopure samples of (*S,S*)-**1** (green) and (*R,R*)-**1** (red). B) Analytical HPLC separation on an achiral SP of the two racemic diastereoisomers of cyclotrimer and confirmation that the first eluted product is the homochiral racemate by comparison with authentic enantiopure samples. C) Analytical resolution of the racemate of the cyclotrimer of **1** by HPLC on a CSP in comparison with enantiopure samples of (*S,S,S*)-**1** (green) and (*R,R,R*)-**1** (red).[34]

The cyclodimeric compound **1** is exclusively constituted by the racemate and unexpectedly, no evidence of the formation of the *meso* diastereoisomer was observed. At the same time, analysis of the cyclotrimer on an achiral stationary phase demonstrated that it is constituted by a 4:1 mixture of the two expected diastereoisomeric racemates.

In order to rationalize the observed behaviour during the formation of cyclic dimers and trimers, the preferred conformation of the radical cations of the open chains dimer and trimer was calculated. The dimeric (*R*,*R*)-**1** and (*S*,*S*)-**1** stereoisomers display the two bithiophene terminals oriented on the same side, thus prone to undergo the intramolecular oxidative coupling while, for the (*R*,*S*)-*meso* the two bithiophene units extend along opposite directions penalizing the intramolecular coupling affording the *meso* cyclodimer. The (*R*,*S*)-*meso*, for this reason, is more prone to give a further coupling with monomer of **1** than to close to give the *meso* macrocycle. An open-chain trimer is formed in which the bithiophene extremities are again oriented in a favorable conformation for undergoing ring closure.

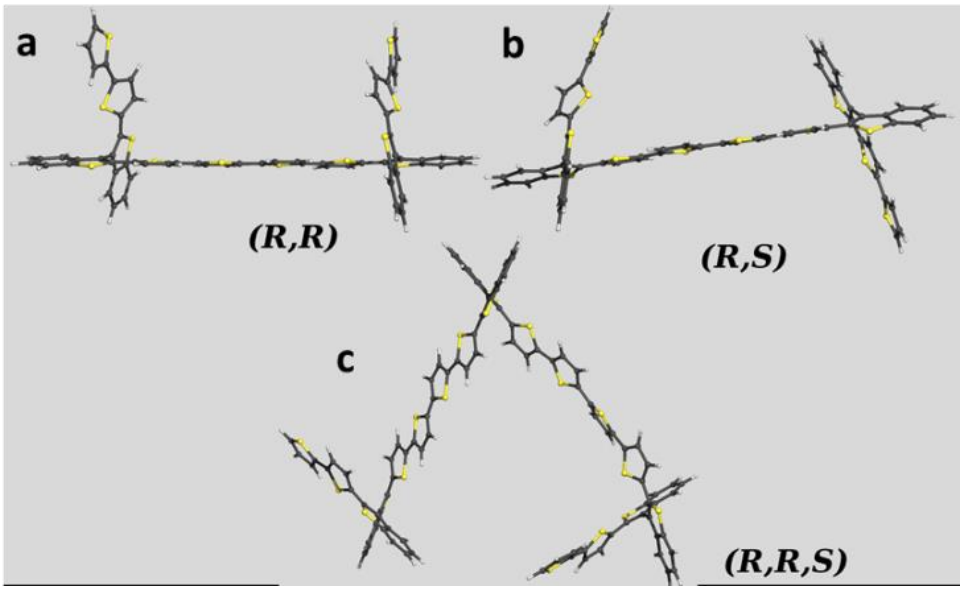

Figure 29: Preferred calculated conformation for the radical cation of (*R*,*R*)-dimer (a), of (*R*,*S*)-dimer (b) and (*R*,*R*,*S*)-trimer (c). [34]

Furthermore, the synthesis of an open-chain dimer was planned, in order to compare the properties of closed and open structures as donors towards fullerene derivatives in bulk heterojunction solar cells.

Compound **6** was obtained through a $CuCl_2$ promoted oxidative coupling of the anion of compound **1** generated, in turn, by treatment of the latter with *n*-BuLi.

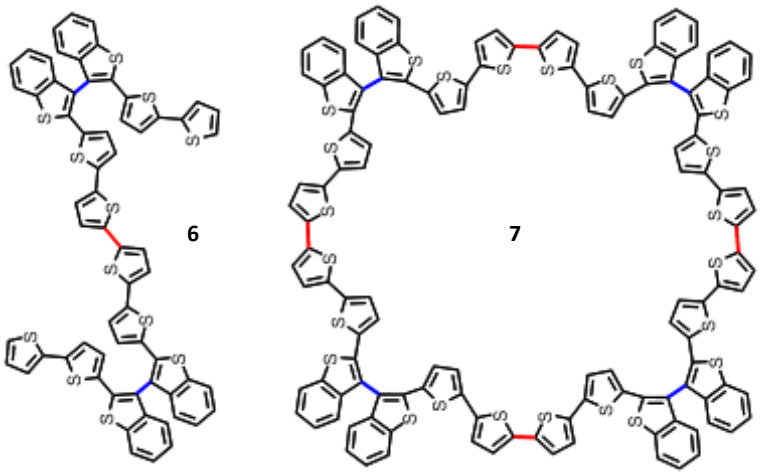

Figure 30: Open-chain dimer **6,** macrocyclic square-shaped tetramer **7**. Blue bonds represent the stereogenic axes; red bonds are the connections between monomer **1** units.[34]

The HPLC analysis of **6** on a chiral stationary phase, reported in Figure 31, shows that the open-chain dimeric product is constituted by a mixture of the two enantiomers and the *meso* stereoisomer in a statistical 1:2:1 ratio (undetected by the circular dichroism detector).

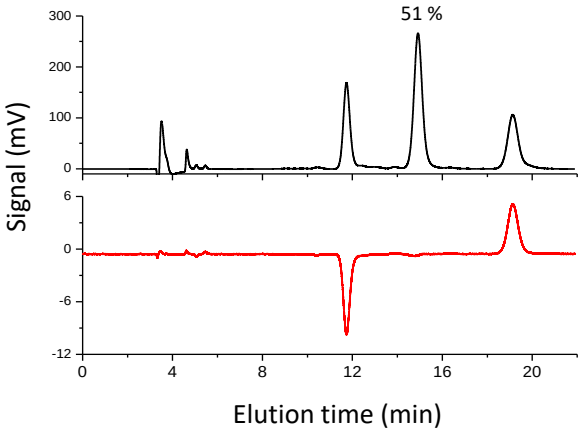

Figure 31: Analytical resolution of the racemate of **6** through HPLC on a chiral stationary phase. CSP: Chiralpak IB 250 mm x 4.6 mm I.D, eluent: *n*-hexane : CH_2Cl_2 : ethanol 100 : 10 : 2, flow rate: 1 mL/min, temperature: 25°C, detector: UV (black) and CD (red) at 360 nm.[34]

The availability of open dimers allowed us to accede to the macrocyclic tetramer **7**, that was synthesized through a $FeCl_3$-promoted cyclodimerization process of compound **6**. The process implies coupling between the α position of the terminal thiophenes and, as expected, it produced oligomers with an even number of BT_2T_4 subunits: the undesired oligomers were removed by several cycles of selective precipitation in *n*-hexane. A mixture of stereoisomeric macrocyclic tetramers was obtained, in this way, in a good purity state.

Compounds **6** and **7** were analytically and chemically characterized and the observed properties were compared with those of cyclic dimers and trimers: photophysical and electrochemical characterization were also performed.

The stereoisomeric mixtures of open chain **6** and cyclic dimers and trimers have been tested separately as donors in bulk-heterojunction solar cells in combination with commonly used acceptors, namely C_{60} and PCBM.

The results of the preliminary experiments gave very interesting indications on the more promising strategies to adopt in the design of these kind of materials.

Firstly, a preliminary theoretical investigation was performed in order to acquire elements useful to rationalize the experimental results: The C_{60} and PCBM fullerenes and the stereoisomers of **6**, cyclodimer and cyclotrimer oligothiophenes have been separately modeled. Calculations showed that both C_{60} and PCBM fit in cyclodimer and cyclotrimer and **6** cavities giving stable dyads.

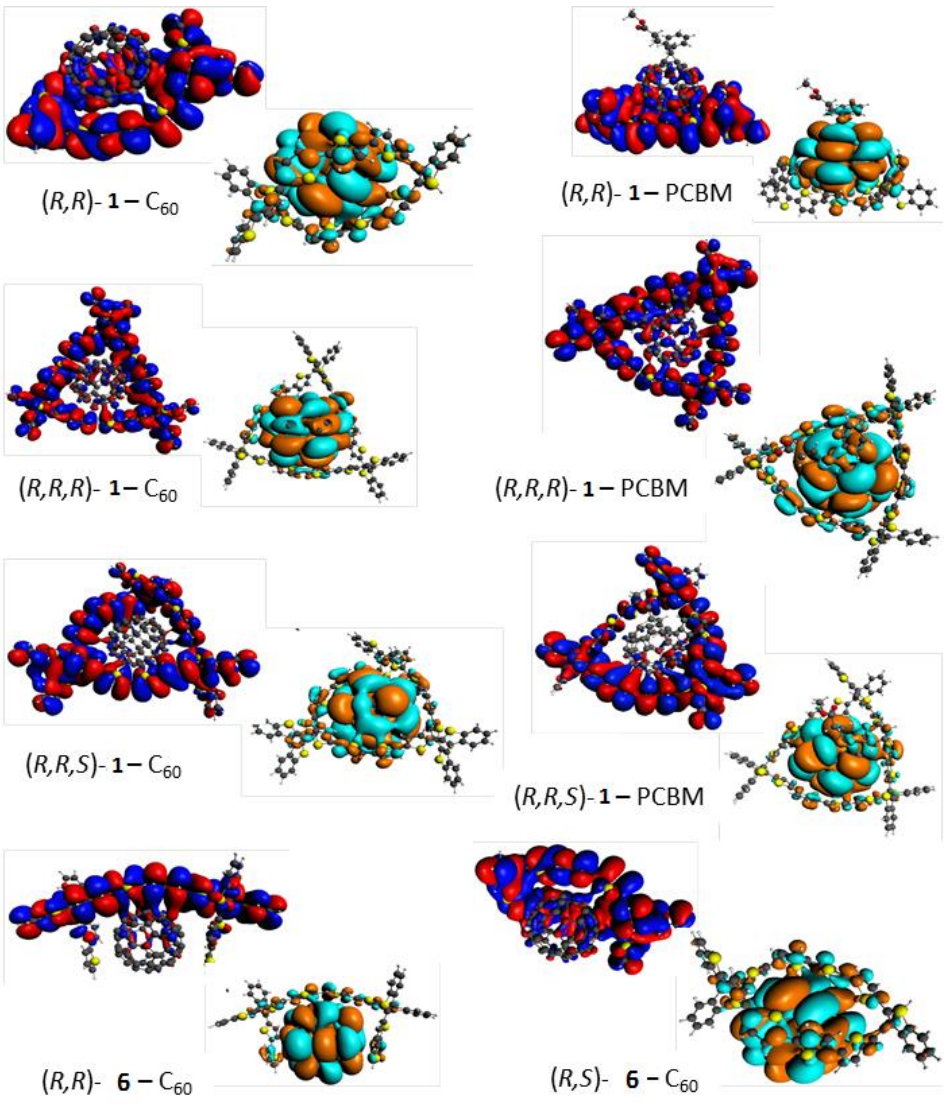

Figure 32: Molecular orbitals (red-blue: HOMO; orange-cyan: LUMO) of oligothiophene : fullerene adducts.[34]

The interaction mainly involves the HOMO and the LUMO of each couple (

Figure 32) and the coordination enthalpy of the dyad increases with the number of thiophenes facing the fullerene surface. Due to their lower rigidity, the open homologues **6** seem to embrace more effectively the C_{60}/PCBM molecule resulting in a stronger stabilization of the dyad with respect to the cyclic dimer.

Photovoltaic properties of cyclic oligothiophene: PCBM and cyclic oligothiophene: C_{60}, in solution-deposited by spin coating inverted solar cells, were investigated. The best PCEs (Power Conversion Efficiency) were obtained from inverted solar cells fabricated by first spin-coating at a spinning speed of 1000 rpm. The active layer (~ 40 nm) was spin-coated at 1000 rpm for 90 s on top of ZnO from solution in o-dichlorobenzene heated at 60 °C. The total concentration of the active components was 20 mg mL^{-1}. 10 nm of MoO_3 buffer layer anode was deposited in a thermal evaporator in a vacuum of 106 mbar and the devices were completed by the deposition of 100 nm of silver. Each substrate contained three cells, with a nominal active area of 25 mm^2 each Thermal annealing (150°C, 30 min) was found to be ineffective on the PCBM-based device performances and it has not been tested on C_{60}-based devices. The thicknesses of the active layer were generally around 40 nm, although its high roughness makes them difficult to measure. The J–V curves of the polymer solar cells under AM 1.5 illumination at 100 mW cm2 are shown in Figure 33.

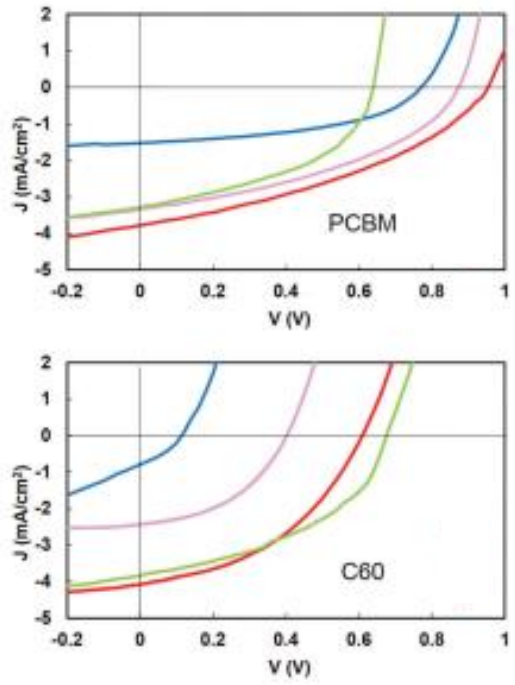

Figure 33: J–V curves of oligothiophene:fullerene blends. Top: PCBM; bottom: C_{60}. Profiles for: cyclodimers (blue line), cyclotrimers (red line), open-chain dimers (green line) and mixture (purple line).[34]

Among the oligomers, the mixture of stereoisomeric trimers exhibits the highest PCE (about 1.1%), while that of cyclic dimers leads to a PCE of about 0.3%. The PCE value of the oligomer mixture is in between. EQE (External Quantum Efficiency) curves substantially confirm the trend.
Interestingly, the devices based on the open-chain dimer **6** demonstrated both PCE and EQE greater than those shown by cyclic dimer.
However, cyclic trimers, that can allocate fullerenes without fully incorporating them, gave interesting results in terms of PCE, while promising results in terms of efficiencies have been achieved in the case of the tweeze-shape dimeric system, although composed 50% by the meso form displaying the zig-zag geometry mentioned above.
Even though the conclusive performances could not be compared with those reported in the specialized literature, this work gave useful indications for the design of promising architectures of thiophene-based cyclic and open-chain macromolecules employable as active layers in solar cell devices.[34]

4.2. 3,3'-Bithianaphthene derivatives based on the bithiophene pendant elongation strategy

4.2.1. 2,2'-Bis(2,2':5',2''-terthiophen-5-yl)-3,3'-bithianaphthene (BT_2T_6)

As anticipated, the first strategy planned to modify the general structure of compound **1** was to extend the bithiophene side chains in order to obtain cyclic oligomers of different size.
The simplest structural change was to add a thiophene unit to the bithiophene pendant and the synthesis of compound **10**, nicknamed BT_2T_6, was planned according to the strategy followed for the preparation of BT_2T_4.
The terthiophene **8**, the key intermediate to accede to the corresponding stannyl derivative **9**, was obtained in good yields through a Pd(0) catalyzed Stille reaction between two equivalents of 5-tributylstannyl-thiophene and one equivalent of 2,5-dibromo-thiophene, both commercially available.
Compound **8** was then treated with *n*-BuLi and the generated anion was reacted with trimethyl-stannyl chloride to give the (2,2':5',2''-terthiophen-5-yl)trimethylstannane **9**, which was coupled with the 2,2'-dibromo-3,3'-bithianaphthene **4** through a palladium(0) mediated Stille coupling, in refluxing toluene solution.

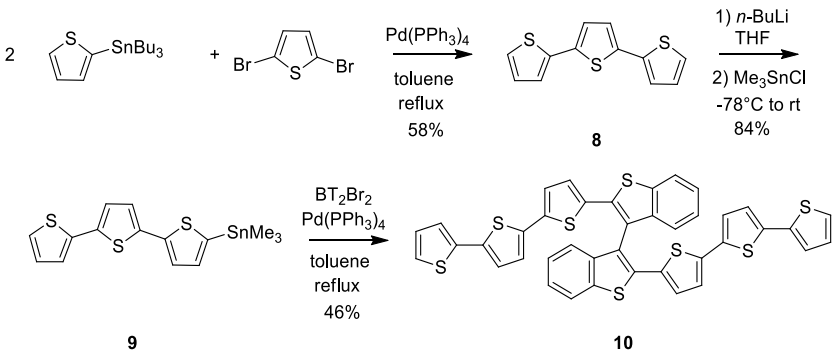

Scheme 7: Synthesis of 2,2'-bis(2,2':5',2''-terthiophen-5-yl)-3,3'-bithianaphthene (BT_2T_6) **10**.

The racemate was oxidized in dry $CHCl_3$ by adding the monomer to a $FeCl_3$ slurry, according to the procedure described in Chapter 2 for BT_2T_4. The residue, obtained after Soxhlet extraction with THF, was analyzed by HR-MALDI and the corresponding spectrum is reported in Figure 34. It is evident that the residue was constituted exclusively by dimers and trimers.

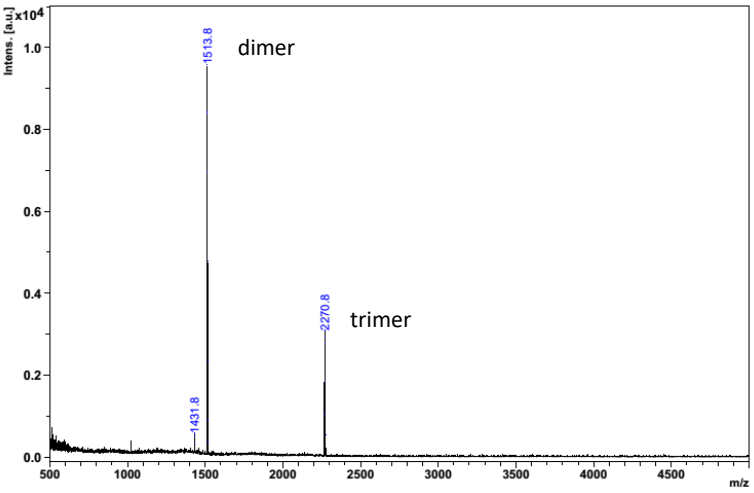

Figure 34: MALDI analysis of chemically oxidized BT_2T_6. Oligomers extracted by THF.

However, to better investigate the expected formation of superior oligomers, the residue obtained after THF extraction was further extracted with chlorobenzene in the Soxhlet apparatus and the soluble portion was submitted again to HR-LDI analysis. The spectrum demonstrated the presence of higher molecular weight oligomers insoluble in THF, such as cyclic tetramers and pentamers.

In Figure 35, the experimental (A) and the theoretical (B) patterns of the peaks corresponding to cyclic dimers and trimers are reported. It is evident that fitting is very good. In addition, the absence of linear oligomers was demonstrated.

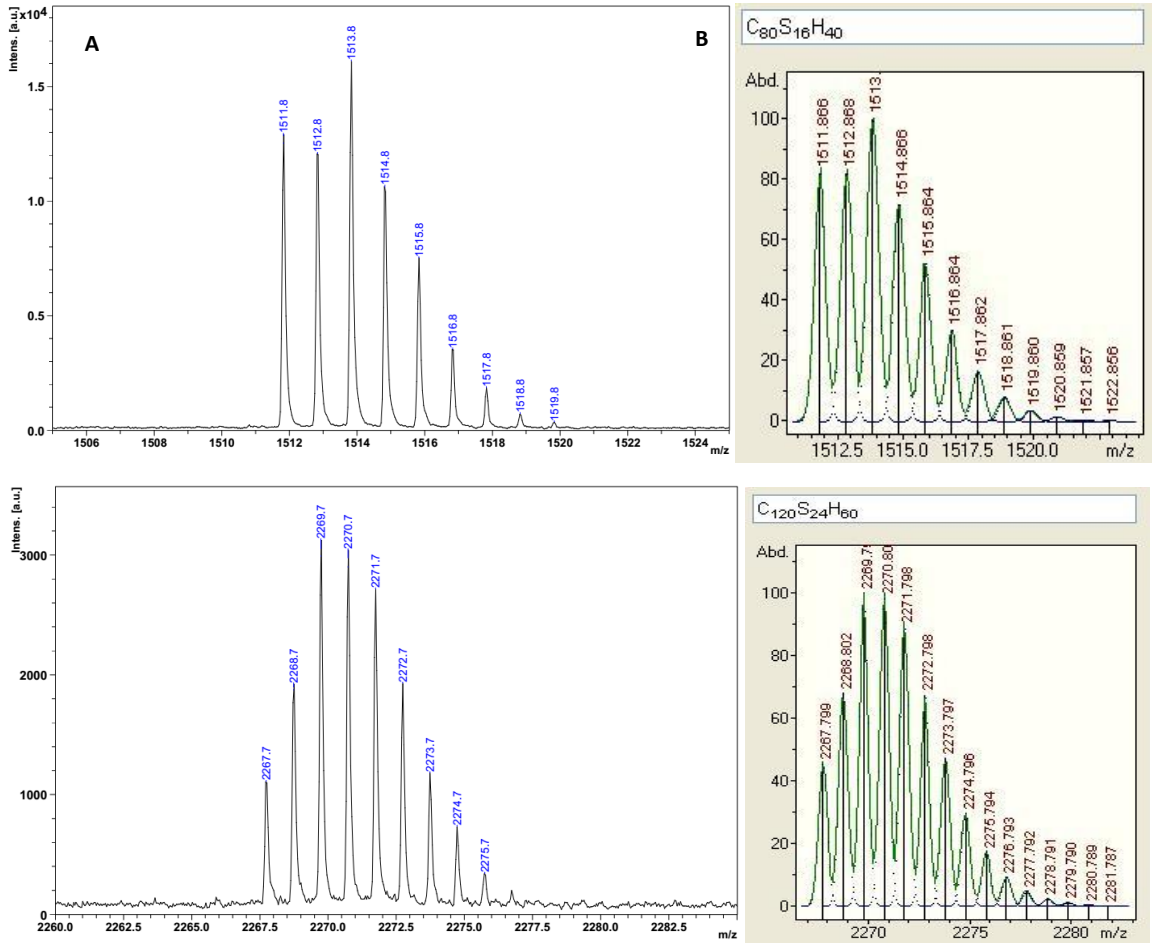

Figure 35: HR-MALDI analysis of the oligomers resulting from the $FeCl_3$ oxidation of BT_2T_6 and extracted with THF. Experimental (A) and theoretical (B) pattern of the peaks corresponding to the cyclic dimers and trimers.

The electrochemical characterization of BT_2T_6 shows a narrower HOMO-LUMO gap than BT_2T_4, with both first oxidation and first reduction processes taking place at more advantageous potentials compared with BT_2T_4 behaviour, so that the reduction process becomes visible even in CH_2Cl_2 on account of the improved conjugation. In addition to the first oxidation peak, which, according to its broad shape, could correspond to the merging oxidation peaks of the two slightly interacting homotopic moieties, a second oxidation process can be observed, which could be consistent with the longer conjugated chains in the two moieties.

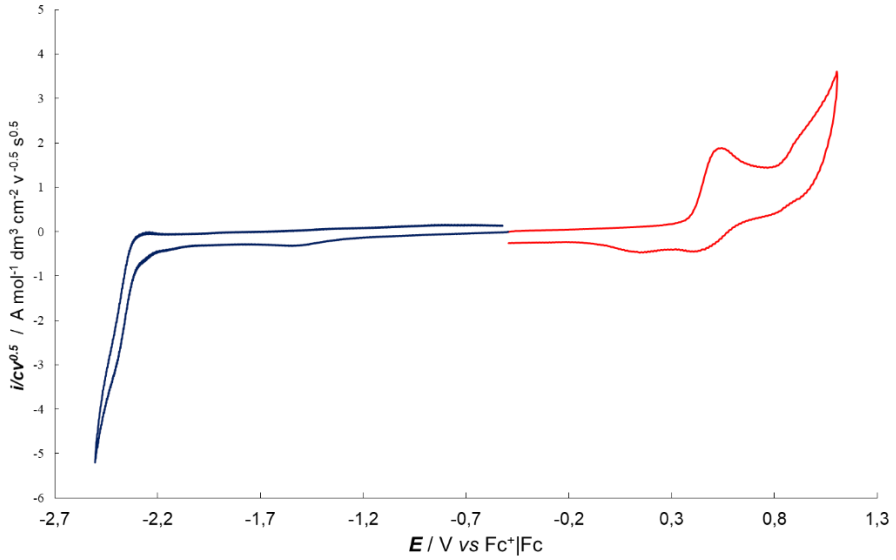

Figure 36: Complete CV patterns of BT_2T_6 monomer (0.5 mM), scan rate: 200 mV s^{-1}, solvent: CH_2Cl_2 + 0.1 M $TBAPF_6$.

Several experiments have been carried out in order to electrochemically oligomerize monomer **10** and to investigate the properties of the resulting conductive film (ec-p(BT_2T_6)). The electrodeposition of monomer **10** was performed under potentiodynamic (Figure 37 A and B) conditions, using a 1 mM solution of the monomer in CH_2Cl_2 + 0.1 M $TBAPF_6$, scan rate = 50 mVs^{-1}, on gold electrode (for CV analysis), ITO electrode (for CV and spectroelectrochemical analysis) and 10 µm interdigitated platinum electrodes (for *in-situ* conductance analysis). The growth of the oligomeric films on the electrodes was very regular, especially on the gold electrode, due to the high affinity of the sulfur atoms for the electrode surface.

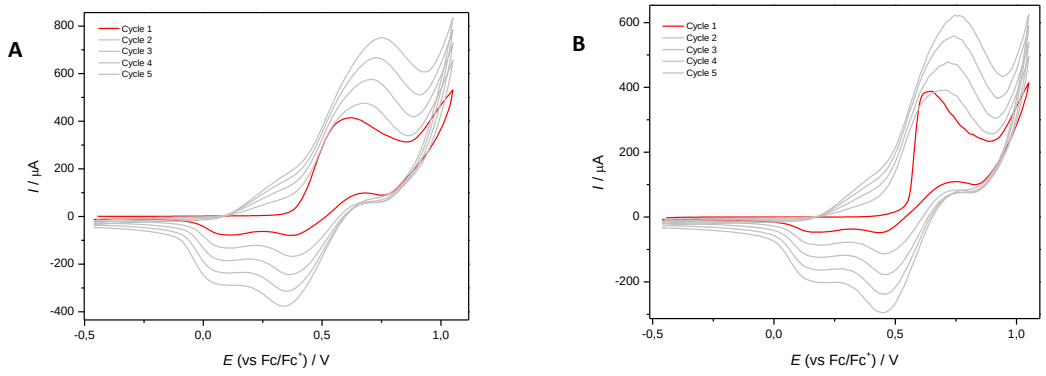

Figure 37: Potentiodynamic electrooxidation of BT_2T_6 on gold (A) and ITO (B) electrodes. Five consecutive cycles, 50 mV s^{-1} scan rate, 1 mM solution of BT_2T_6in CH_2Cl_2 + 0.1 M $TBAPF_6$.

Taking advantage of the equipment available in the laboratories of prof. Ludwigs at the Universität zu Stuttgart, the oligomeric films were characterized not only by voltammetry, but

also through spectroelectrochemical and *in-situ* Conductance (ISC) analysis. In Figure 38 A and B the anodic cyclovoltammetry and the related UV spectrometric analysis are reported.

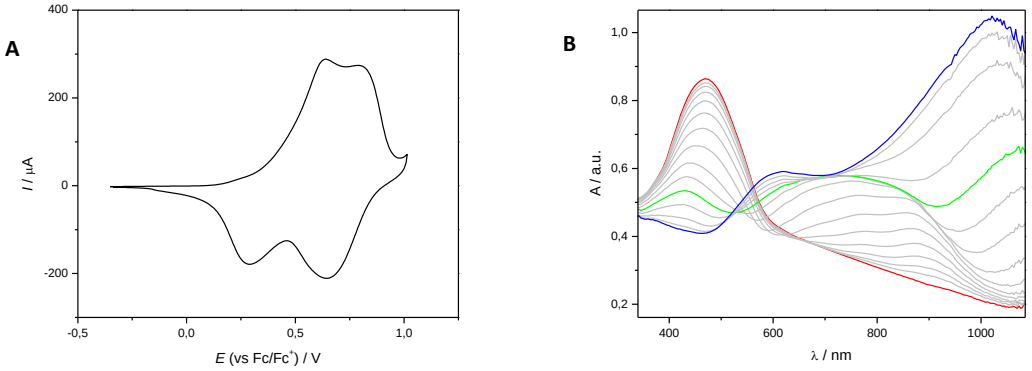

Figure 38: *In-situ* spectroelectrochemistry of ec-p(BT_2T_6): A) Cyclic voltammogram of the reversible p-doping of ec-p(BT_2T_6) (deposited on ITO electrode from five cycles, 1 mM monomer solution in CH_2Cl_2 + $TBAPF_6$, 50 mV s^{-1} scan rate), ACN + 0.1 M $TBAPF_6$ solution, 20 mV s^{-1} scan rate. B) Vis/NIR spectra of ec-p(BT_2T_6) recorded during the forward scan (oxidation) in the p-doping process: profiles for neutral (red), radical cation (green) and dication species (blue) are highlighted.

Spectroelectrochemical analysis is extremely useful to investigate the UV behaviour of an oligothiophene oligomeric film while a cyclic potential is applied to it. According to this technique, the different UV profiles corresponding to the different species formed during the oxidation process can be highlighted. The neutral film absorption band is characterized by a λ_{max} of 468 nm, whereas the radical cation, transient and ephemeral species, exhibited a λ_{max} at 761 nm, that shifts to 1021 nm in the transition between radical cation and dication. From both the CV profile and the spectroelectrochemical data it was possible to deduce that the radical cation is prompt to be further oxidized to dication: on one hand, the distance between the two peaks (of about 150 mV) and, on the other hand, the height of the band at 761 nm and the contemporary presence of the band at 1021 nm are clear evidence of the formation of the dicationic species.

In-situ conductance measurements confirmed the conductivity of the charged species, both dication and anion, but also the instability of the radical cation.

As for the anion generated on the same film, it was found to be more conductive than the dication but the most interesting behaviour can be observed in the anodic window. A very low conductivity was observed for the radical cation, as highlighted by the small shoulder observable in the backward scan (proved by a sudden change in the slope of the conductivity profile).

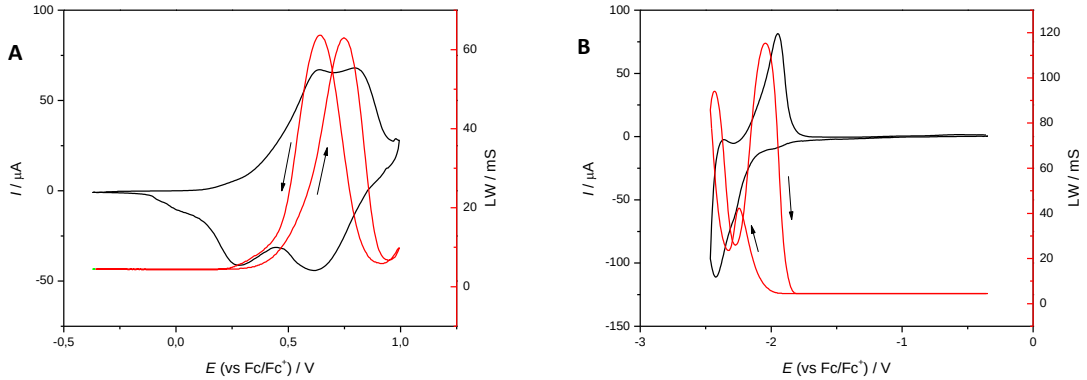

Figure 39: *In-situ* conductance analysis of ec-p(BT_2T_6) (deposited on 10 µm interdigitated Pt electrode, 1 mM monomer solution in CH_2Cl_2 + $TBAPF_6$, 50 mV s^{-1} scan rate) recorded in ACN + 0.1 M $TBAPF_6$ solution, 20 mV s^{-1} scan rate. A) Anodic scan. B) cathodic scan.

After the characterization of the racemate, compound **10** was resolved through HPLC on a chiral stationary phase. The chromatogram corresponding to the analytical separation of the enantiomers of **10** is reported in Figure 40.

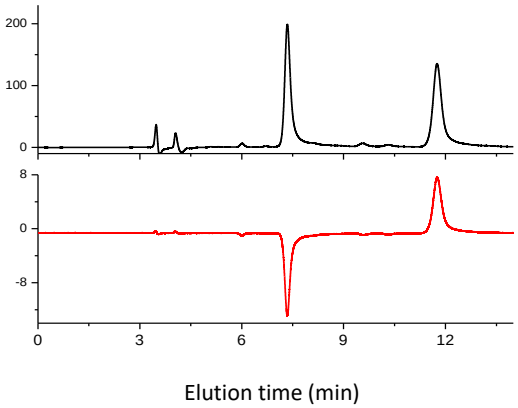

Figure 40: Analytical resolution of the racemate of BT_2T_6 through HPLC on a chiral stationary phase. CSP: Chiralpak IB 250 mm x 4.6 mm I.D. Eluent: *n*-hexane : CH_2Cl_2 : ethanol-100 : 10 : 2, flow rate: 1 mL/min, temperature: 25°C, detector: UV (black) and CD (red) at 360 nm.

Even though the analytical separation was very good, some scale-up difficulties were found moving from analytic to semi-preparative scale. Scaling up the conditions employed for the analytical resolution, the formation of an unknown peak with lower elution time was observed; reinjection of the material corresponding to the unknown peak, the unexpected correspondence with the racemate of BT_2T_6 was found (Figure 41 A). This behaviour was ascribed to the formation of aggregates due to the high amount of material injected in the semi-preparative resolution process. The problem was solved by modifying the ratio of the solvents constituting the eluent without changing the immobilized phase: the amount of CH_2Cl_2 was reduced and the

ethanol percentage was increased. Under these experimental conditions, the separation was satisfactory and the resolution could be scaled up to semi-preparative level (Figure 41 B).

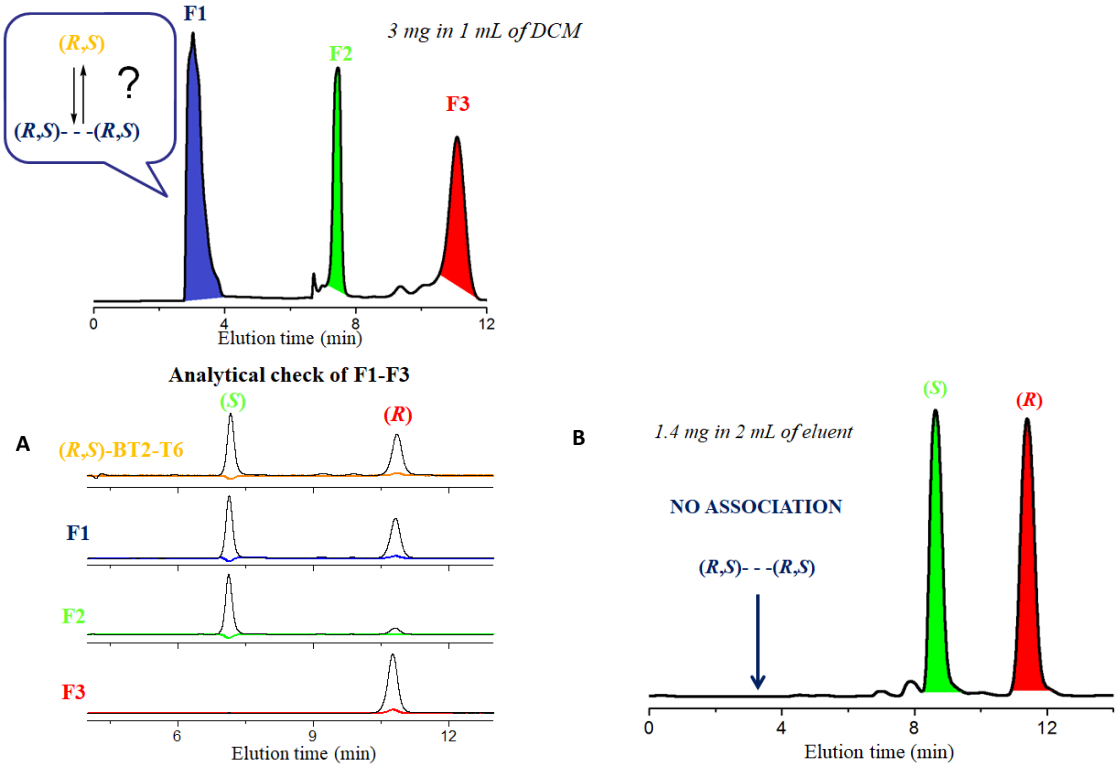

Figure 41: Semi-preparative resolution of the racemate of BT_2T_6 through HPLC on a chiral stationary phase. CSP: Chiralpak IB 250 mm x 4.6 mm I.D. A), eluent: *n*-hexane : CH_2Cl_2 : ethanol 90.5 : 8 : 1.5, flow rate: 1 mL/min, temperature: 25°C, detector: UV (black) and CD (red) at 360 nm. B) Eluent: *n*-hexane : CH_2Cl_2 : ethanol 90 : 1 : 10, flow rate: 1 mL/min, temperature: 25°C.

The absolute configuration of the stereogenic axis was assigned by comparison of the Electronic Circular Dichroism (ECD) spectra, reported in Figure 42, with those recorded for BT_2T_4, attributing to the first eluted enantiomer, exhibiting positive Cotton effect, the *S* configuration. The $[\alpha]_D^{20}$ of the latter, measured in chloroform, was found to be +1368°, and -1582° for the second eluted (*R*) antipode.

The chiroptical characterization of the enantiomers of BT_2T_6 was completed by recording the Chiral PhotoLuminescence (CPL) spectra: CPL is a luminescence phenomenon that provides the dissymmetric emission of right and left circularly polarized light, thereby providing information on the excited state chiroptical properties of the systems. This technique recently became a widely applied tool for the investigation of organic molecules and not only for lanthanide complexes, as formerly.[35][36] It is common to report the degree of CPL in terms of luminescence dissymmetry factor g_{lum}, which represents the ratio of the difference in intensity of left-circularly polarized light (I_L) versus right-polarized light (I_R) divided by the average total luminescence

intensity. For organic luminescent molecules (generally polyconjugated molecules endowed with axial or helical stereogenicity) this value range between 10^{-2} to 10^{-4}.

For BT_2T_6 the CPL band is positive for the first eluted enantiomer (as already observed for BT_2T_4)[37] and the g_{lum} was found to be 3.3×10^{-3}, surprisingly lower than that exhibited by BT_2T_4, that was 9.0×10^{-3}.

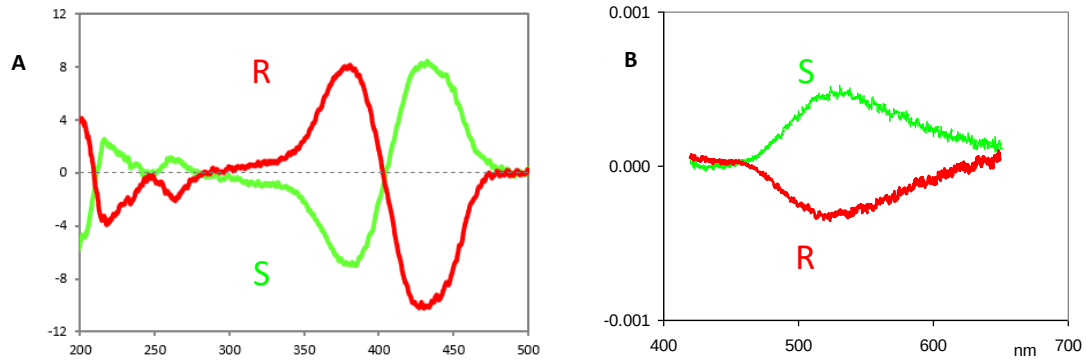

Figure 42: A) CD profiles of (*S*)-(+)-**10** (green) and (*R*)-(-)-**10** (red). B) CPL of (*S*)-(+)-**10** (green) and (*R*)-(-)-**10** (red).

Analogously to the experiments carried out on BT_2T_4, enantiopure (*S*)-BT_2T_6 was electroligomerized on a glassy carbon electrode and the chiral surface was used for enantiorecognition tests with chiral probes. The enantiorecognition test where the two enantiomers of DOPA are used as chiral probes is reported in Figure 43. The results were outstanding since a difference of ≅ 200 mV was found between the oxidative potentials of the two enantiomers of DOPA. The values found for the enantiorecognition of DOPA on (*S*)-ec-p(BT_2T_6) enantiopure film are two times higher than those shown by ec-p(BT_2T_4). The wider cavities characterizing the cyclic compounds resulting from BT_2T_6 oligomerization look more suitable for accommodating the analyte, as indicated by the electronic transfer occurring at lower oxidative potentials, in comparison with the case of BT_2T_4.[31]

BT_2T_6 showed, however, some processability issues due to its low solubility, that is remarkably lower than that shown by BT_2T_4. For that reason, it was planned to synthesize compound **15** in which the same backbone was functionalized with lipophilic chains that should have improved monomer solubility.

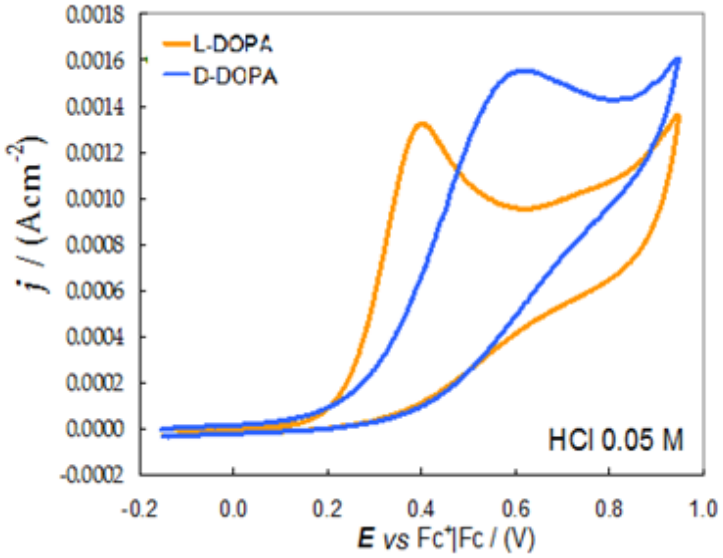

Figure 43: Enantiorecognition tests on enantiopure oligomeric (*S*)-ec-p(BT_2T_6) (deposited form thirty-six cycles, 0.5 mM monomer solution in CH_2Cl_2 + $TBAPF_6$, 200 mV s^{-1} scan rate) in the presence of enantiopure probes *L*- and *D*-DOPA (4 mM in 50 mM HCl).

4.2.2. 2,2'-Bis[3',4'-di-*n*-butyl-(2,2':5',2''-terthiophen)-5-yl]-3,3'-bithianaphthene (BT_2T_6Bu)

The synthesis of compound **15**, reported in Scheme 2, required the achievement of the functionalized terthiophene derivative **13** that was obtained in two steps starting from commercially available 3,4-dibromothiophene. The latter was converted in high yields into the corresponding 3,4-di-*n*-butylthiophene (**11**)**,** through a nickel catalyzed Kumada reaction with butylmagnesium bromide in diethyl ether. Compound **11** was then dibrominated with bromine in a chloroform and acetic acid solution to give the corresponding 2,5-dibromo-3,4-di-*n*-butylthiophene (**12**); the dibromo derivate is a suitable substrate for a double Stille reaction with 2-tributyl-stannylthiophene to give the 3',4'-di-*n*-butyl-2,2':5',2''-terthiophene (**13**) in moderate yields.

Compound **13** was then reacted with *n*-BuLi to give the corresponding anion, that was treated with trimethyltin chloride to afford the stannyl derivative **14** that was coupled, in turn, following a Stille procedure, with BT_2Br_2 affording the final target **15**, even if in low yields.

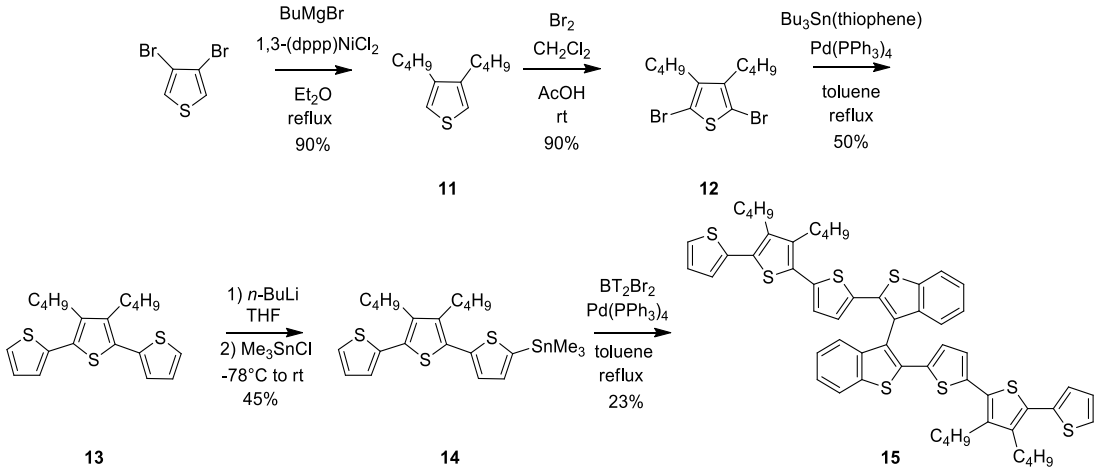

Scheme 8: Synthesis of 2,2'-bis(3',4'-di-*n*-butyl-(2,2':5',2''-terthiophen-5-yl)-3,3'-bithianaphthene (BT_2T_6Bu) **15**.

The cathodic and anodic cyclic voltammetric pattern for BT_2T_6Bu monomer in ACN + 0.1 M $TBAPF_6$ at 200 mV s^{-1} scan rate is reported in Figure 44 A.

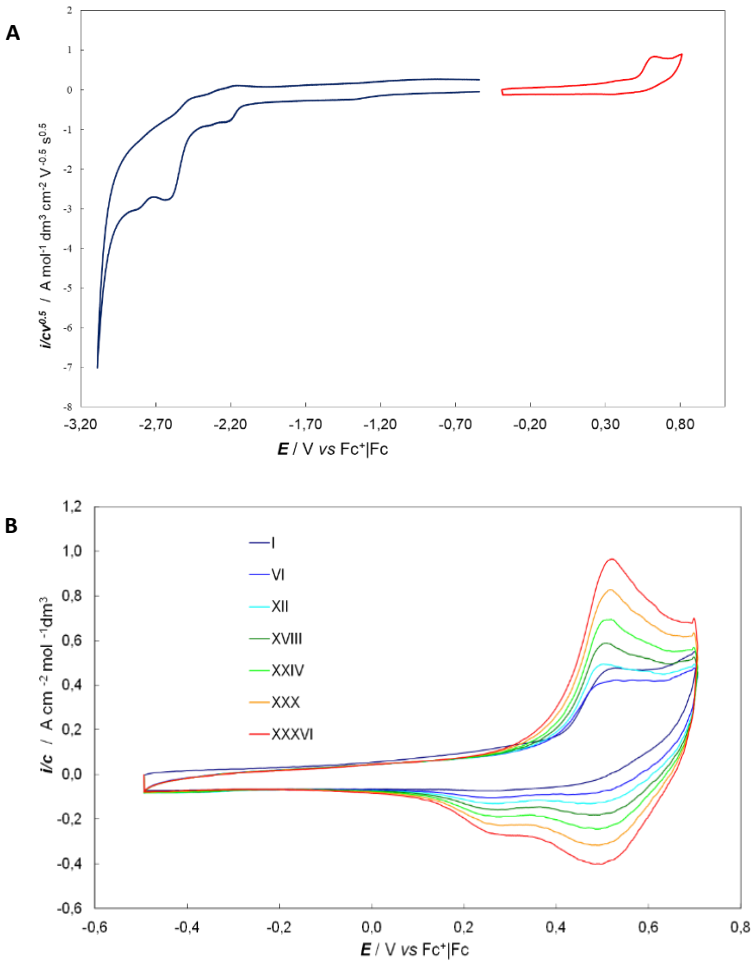

Figure 44: A) Complete CV patterns of BT_2T_6Bu, 200 mV s^{-1} scan rate, solvent: ACN + 0.1 M $TBAPF_6$. B) Potentiodynamic electrooxidation of BT_2T_6Bu on glassy carbon electrode. Thirty-six consecutive cycles at 200 mV s^{-1} scan rate, 0.5 mM of BT_2T_6Bu in ACN + 0.1 M $TBAPF_6$.

The electrochemical CV pattern shows a HOMO-LUMO gap narrower than BT_2T_4, with both first oxidation and first reduction processes taking place at more advantageous potentials, on account of the improved conjugation due to the addition of the two thiophene moieties.
Besides the first oxidation peak a second oxidation process can be observed, which would be consistent with the longer conjugated chains in the two moieties.
The deposition of the oligomeric films (reported in Figure 44 B) was performed using a 0.5 mM solution of the monomer, in acetonitrile + 0.1 M $TBAPF_6$, on glassy carbon electrode. The resulted oligomeric film of BT_2T_6Bu gave a fast, regular and virtually unlimited electroligomerization process; additionally, the films are very stable upon repeated potential scans in a monomer-free solution.

Also in this case, the resolution of the racemate at analytical level through chiral HPLC was not trivial, since several chiral columns were tested and good separation was observed only when chiral stationary phase based on an uncommon cellulose derivative, the cellulose tris(3-chloro-4-methyl-phenyl)carbamate, was employed. The chromatogram, reported in Figure 45 shows well separated signals of the antipodes. Unfortunately, the resolution at a semi-preparative level could not be performed due to the long elution times required for the two antipodes, namely 20 and 30 minutes.

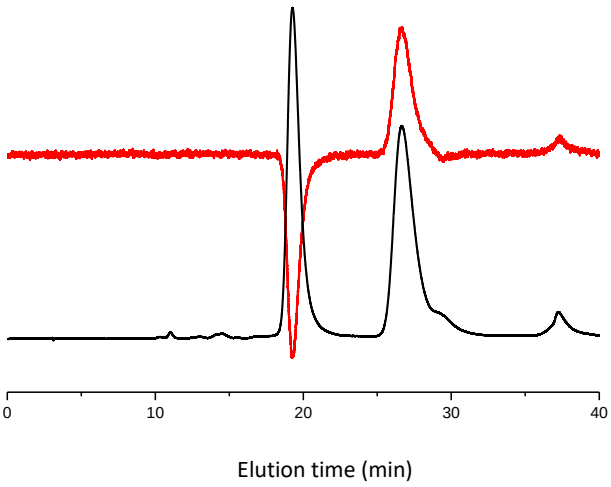

Figure 45: Analytical resolution of the racemate of BT_2T_6Bu through HPLC on a chiral stationary phase. CSP: Lux-cellulose 2 (250 mm x 4.6 mm I.D.), eluent: *n*-hexane : IPA 100 : 0.25, flow rate: 1 mL/min, temperature: 35°C, detector: UV (black) and CD (red) at 350 nm.

4.3. 3,3'-Bithianaphthene derivatives based on the bithiophene pendant planarization strategy

As mentioned in Chapter 3, the modification strategy of the BT_2T_4 structure implies a planarization of 2,2'-bithiophene pendants that were substituted by fused ring heterocycles.
In particular, the scaffold of 3,3'-bithianaphthene was functionalized with 4,4-di-*n*-hexyl-4*H*-cyclopenta[1,2-b:5,4-b']dithiophene (CPDT) and *N*-*n*-octyl-dithieno[3,2-*b*:2',3'-*d*]pyrrole (DTP) pendants where the 2,2'-bithiophene units are forced to be coplanar by a methylene unit or a nitrogen atom, respectively.
An important advantage of these scaffolds was their easy functionalization by introduction of suitable substituents on the methylene groups or on the nitrogen atoms, leading to more soluble and more easily processable materials.
On the other hand, a breakdown was related to the fact that these bithiophene pendants required a specific, not trivial syntheses. These heteroaromatic compounds, however, are today very popular building blocks, since they are known to lead to materials with very favorable properties, like a decrease in the HOMO-LUMO separation and an increase in charge mobility[38][39][40][41] due to the extended conjugation in the ground state, to the planar molecular geometry and to their quite rigid structure.
We considered that these systems should confer some peculiar properties to our inherently chiral materials.

4.3.1. 2,2'-Bis(*N*-*n*-octyl-dithieno[3,2-*b*:2',3'-*d*]pyrrol-2-yl)-3,3'-bithianaphthene (BT_2DTP_2)

The synthesis of the 2,2'-bis(*N*-*n*-octyl-dithieno[3,2-*b*:2',3'-*d*]pyrrol-2-yl)-3,3'- bithianaphthene (**18**), nicknamed BT_2DTP_2, (Scheme 9) requires the preparation of *N*-*n*-octyl-DTP (**16**) as the key intermediate, that was easily obtained in high yields following the well-known Buchwald protocol, starting from commercially available 3,3'-dibromo-2,2'-bithiophene and *n*-octylamine. Compound **16** was then treated with *n*-BuLi and the resulting anion reacted with tributyl-stannylchloride to give the stannyl derivative **17** which was used, in turn, in a Pd(0) catalyzed Stille coupling reaction with the dibromo derivative BT_2Br_2 **4**, in DMF solution, to give the final product **18** in good yields.

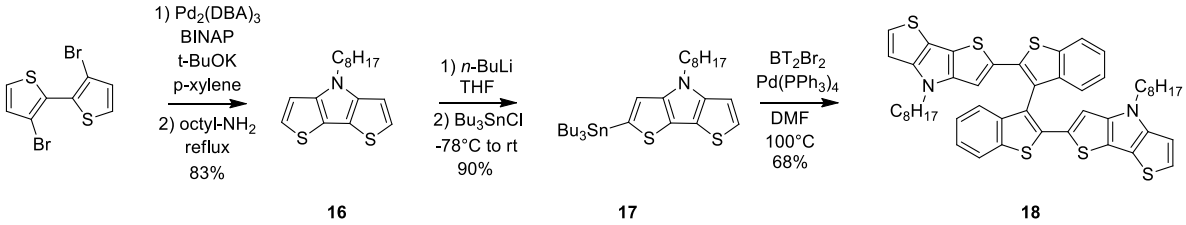

Scheme 9: Synthesis of 2,2'-bis(*N*-*n*-octyl-dithieno[3,2-*b*:2',3'-*d*]pyrrol-2-yl)-3,3'-bithianaphthene (BT_2DTP_2) **18**.

BT_2DTP_2 **18** was oxidized with $FeCl_3$ in dry chloroform solution to lead to a much more complex oligomeric mixture than those obtained with the previously synthesized inherently chiral monomers. Indeed, in addition to large amounts of dimers and trimers (Figure 46), a remarkable series of superior oligomers was found in the material extracted with a soxhlet apparatus using THF as solvent. The presence of the *n*-octyl chains strongly increases the solubility of the reaction products, making possible their extraction and identification at least at a qualitative analytical level. Also in this case HR MALDI spectrum demonstrated that the oligomers are cyclic and not linear structures by comparison of the experimental with the calculated patterns of the single peaks.

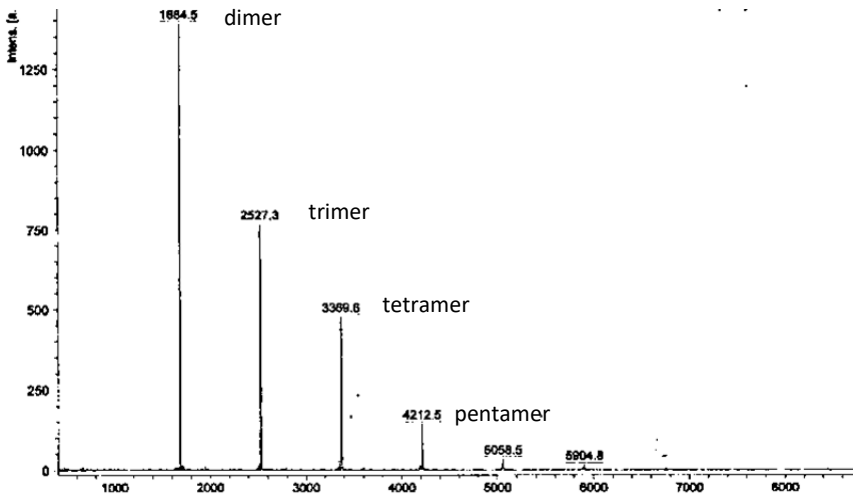

Figure 46: Maldi analysis of chemically oxidized BT_2DTP_2. Oligomers extracted by THF.

Monomer **18** was also electrochemically characterized and electro-oligomerized to give ec-p(BT_2DTP_2).

The complete cyclic voltammetric pattern of monomeric BT_2DTP_2 is reported in Figure 47 A : two nearly equivalent peaks are present, corresponding to the two active terminal units involved in

the electrooxidation process, separated by the central node but still communicating through the conjugated system.

The electrodeposition of the monomer (0.5 mM) on a glassy carbon electrode was performed at 200 mV s^{-1} scan rate, in acetonitrile + 0.1 M $TBAPF_6$ solution (Figure 47 B): electrode coating took place fast and regularly and the resulting films were stable when tested in a monomer free solution. In addition, a large radical cation stabilization was observed from the deposition profile of the oligomeric film, as demonstrated by neat separation and large distance between the peaks.

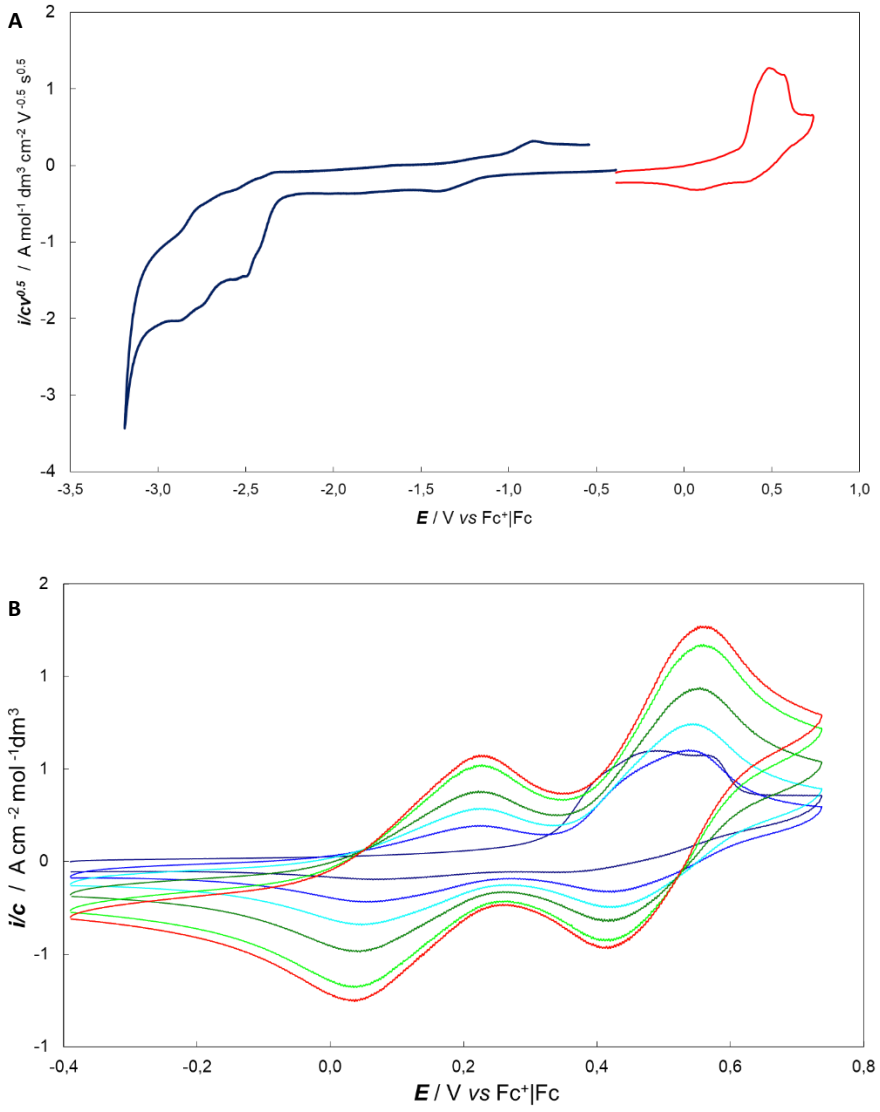

Figure 47: A) Complete CV patterns of BT_2DTP_2 monomer (0.5 mM); 200 mV s^{-1} scan rate; solvent: ACN + 0.1 M $TBAPF_6$. B) Potentiodynamic electrooxidation of BT_2DTP_2 on GC electrode. Thirty-six consecutive cycles at 200 mV s^{-1} scan rate, 0.5 mM of BT_2DTP_2 in ACN + 0.1 M $TBAPF_6$.

The racemate was resolved into antipodes by HPLC at a semi-preparative level and the CD detected chromatograms (Figure 48) demonstrated a perfect separation of the enantiomers.

Furthermore, the specific rotatory powers are impressive, in accordance with the presence of an inherently dissymmetrical chromophore in the molecule. The first eluted BT_2DTP_2 enantiomer exhibited $[\alpha]_D^{25}$= +928° while the second one displayed $[\alpha]_D^{25}$ = -1042°, in chloroform solution.

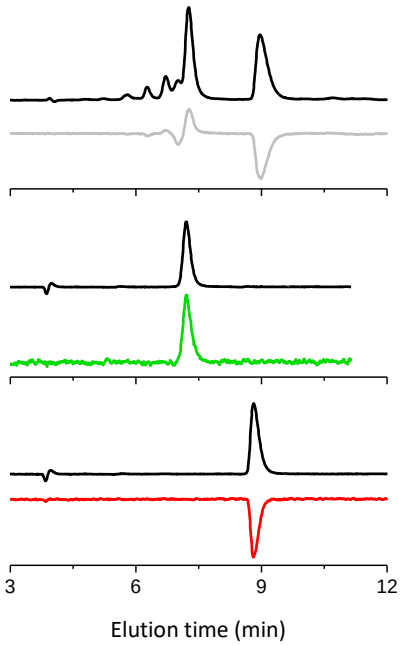

Figure 48: Analytical resolution of the racemate of BT_2DTP_2 through HPLC on a chiral stationary phase. CSP: Chiralpak IA (250 mm 4.6 mm I.D.), eluent: *n*-hexane : CH_2Cl_2 : ethanol 100 : 2 : 1, flow rate: 1 mL/min, temperature: 40°C, detector: UV and CD at 254 nm.

The ECD and CPL spectra of monomer **18** are reported in Figure 49. The green-trace spectra correspond to the first eluted enantiomer, while the red ones correspond to the second eluted one.

All the ECD spectra are dominated by exciton-type features[42] centred at 400 nm.

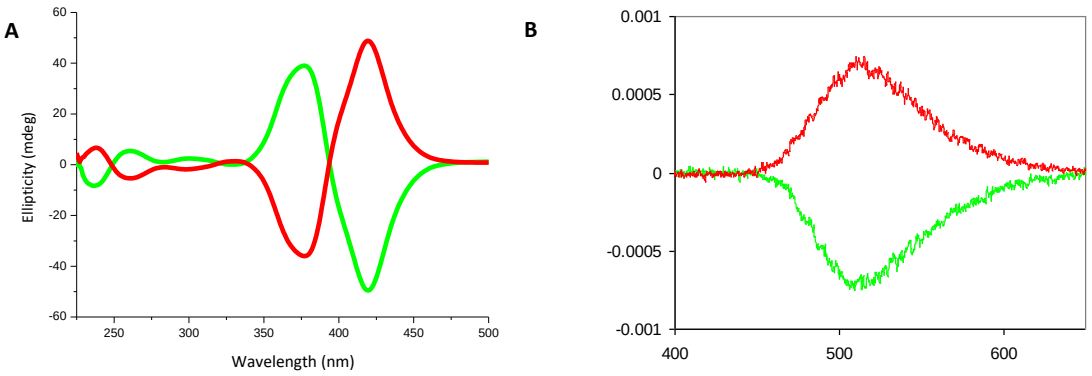

Figure 49: A) CD profiles of (*R*)-(+)-**18** (red) and (*S*)-(-)-**18** (green). B) CPL of (R)-(+)-**18** (green) and (*S*)-(-)-**18** (red).

The second eluted enantiomer, under these experimental conditions, showed a positive Cotton effect and, in analogy with other inherently chiral monomers based on the same atropisomeric scaffold, the *S* configuration can be attributed to the levorotatory antipode.

The monomer exhibited lower luminescent properties with respect to the BT_2T_4: CPL spectra, indeed, showed g_{lum} values equal to 5.0×10^{-3}, while BT_2T_4 enantiomers exhibited a 9×10^{-3} value, as reported above.

The enantioselection capability of BT_2DTP_2 films was tested electrodepositing the enantiopure monomers from ACN solutions, due to the scarce aptitude of these materials to electroligomerize in ionic liquid media, like $BMIMPF_6$.

The results obtained with films of (*R*)-ec-p(BT_2DTP_2) or (*S*)-ec-p(BT_2DTP_2) are depicted in Figure 50 , using commercially available (*R*)-(+)- and (*S*)-(–)-*N,N*-dimethyl-1-ferrocenylethylamine as chiral probes.

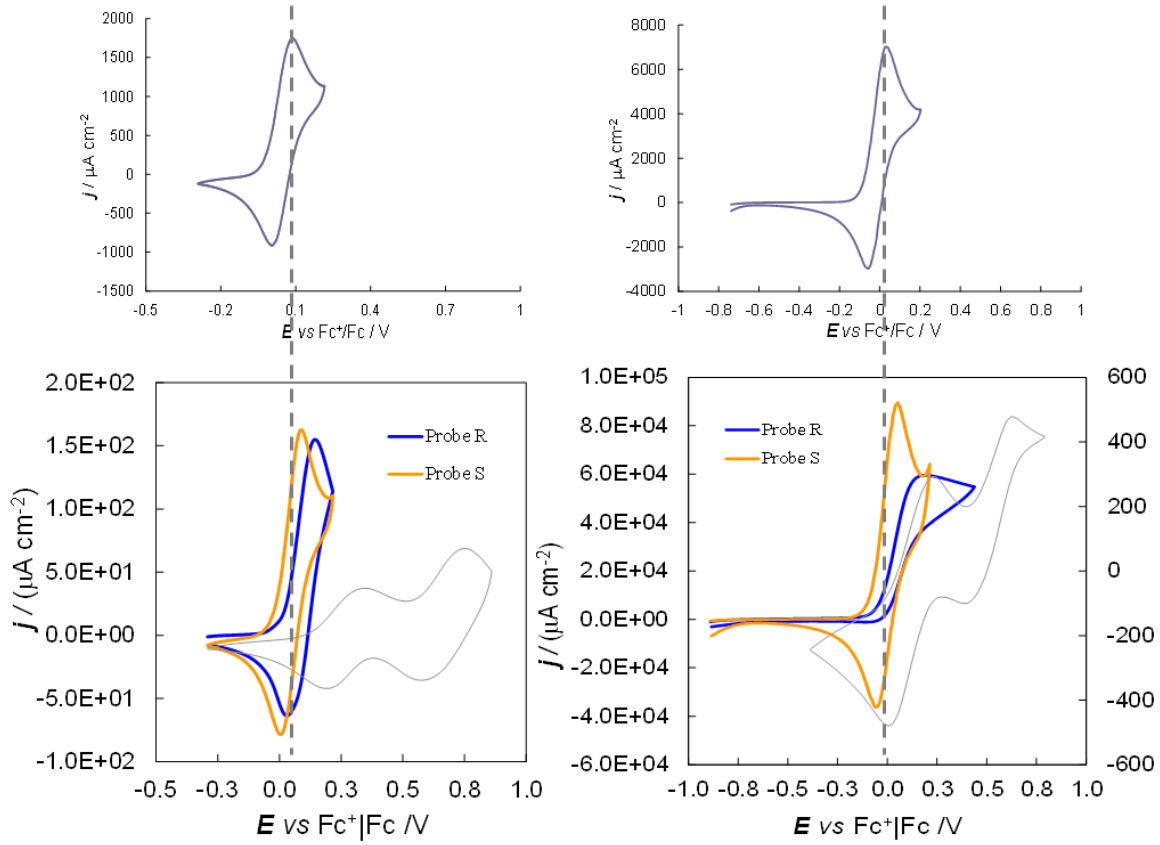

Figure 50: Top: CV patterns of (*R*)-(+)- and (*S*)-(–)-*N,N*-dimethyl-1-ferrocenylethylamine recorded on GC bare electrode in $BMIMPF_6$ (on the left) and in ACN + $TBAPF_6$ 0.1 M (on the right). Bottom: Enantiorecognition tests on ec-p(*R*)-(BT_2DTP_2) in presence of the ferrocene based chiral probes on GC electrode. On the left: tests in $BMIMPF_6$, on the right: tests in ACN + $TBAPF_6$ 0.1 M. CV pattern of the stabilized oligomer film is reported for comparison (grey line).

The BT_2DTP_2 chiral surfaces displayed very good enantiorecognition capability, especially when enantiopure films were tested in ACN + $TBAPF_6$ 0.1 M solution, with a peak separation between the chiral probes of about 160 mV.

Interestingly, the voltammetric signal is not characterized by a fully canonic shape in the case of probe with *R* configuration, probably due to a partial superimposition of the probe signal with the signal of the film (grey line in Figure 50). In the case of ionic liquid, however, the peak separation is about 0.049 V.

4.3.2. 2,2'-Bis(4,4'-di-*n*-hexyl-4*H*-cyclopenta[1,2-b:5,4-b']dithiophen-2-yl)-3,3'-bithianaphthene (BT_2CPDT_2)

The preparation of CPDT, which is the key intermediate necessary for coupling with BT_2Br_2 in the synthesis of BT_2CPDT_2, requires several steps which had been studied in the laboratories where the present thesis project was developed many years ago (Scheme 10).

The first step is a benzoin-type condensation of 3-thiophenecarboxyaldehyde, mediated by thiamine hydrochloride, in ethanol, at pH 9, to give the 3,3'-thienoin (**19**). The latter was easily and quantitatively oxidized with copper sulfate to give the 3,3'-dithienoyl (**20**), which, in the presence of KOH, undergoes a very fast rearrangement affording the 3,3'-thienylic acid (**21**). This reaction step is crucial and reaction times and temperature must be strictly controlled.

The aluminum trichloride promoted pentadienyl cation-type electrocyclization of **21** in benzene solution (we did not find alternative solvents) gave the CPDT-4-carboxylic acid (**22**), that gave the CPDT (**23**) by a copper-mediated decarboxylation in quinoline solution at 100 °C.

The dialkylated derivative **24** was obtained in high yields by exhaustive CPDT alkylation, performed with *n*-hexyliodide generated *in situ* by reaction of the corresponding bromide with KI, in the presence of KOH as a base, in DMSO solution.

The stannylderivative **25** was obtained, as usual, by reaction of the lithium derivative of dihexyl-CPDT with tributyl-stannylchloride. The final step is the reaction between the 2,2'-dibromo-3,3'-bithianaphthene BT_2Br_2 **4** and the 2-tributylstannylderivative **25**, in the presence of palladium tetrakis(triphenylphosphine), according to Stille's procedure.

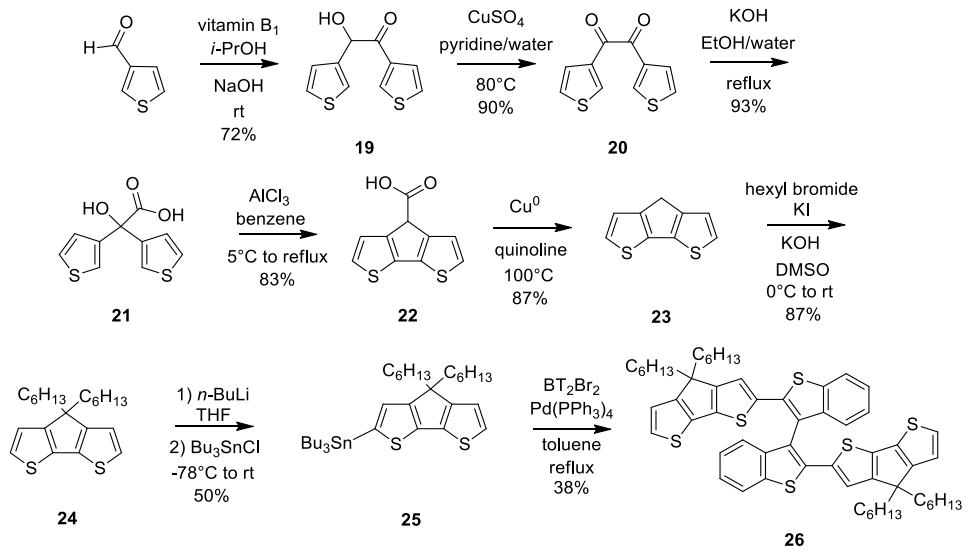

Scheme 10: Synthesis of 2,2'-bis(4,4'-di-*n*-hexyl-4*H*-cyclopenta[1,2-b:5,4-b']dithiophen-2-yl)-3,3'-bithianaphthene (BT_2CPDT_2) **26**.

The racemate was resolved into antipodes by HPLC at a semi-preparative level and the CD detected chromatograms (Figure 51) demonstrated a perfect separation of the enantiomers: in the BT_2CPDT_2 case, the elution times were highly satisfying. The measured specific rotatory powers resulted to be very high: $[\alpha]_D^{25}$= +883° ad $[\alpha]_D^{25}$ = -878°, respectively.

The ECD spectra are reported in Figure 52. The green-trace spectrum corresponds to the first eluted enantiomer, while the red one corresponds to the second eluted one.

All the ECD spectra are dominated by exciton-type features[42] centred at 400 nm like it was observed for the BT_2DTP_2. The first eluted enantiomer, in these experimental conditions, showed a positive Cotton effect similarly to BT_2T_4, for which the *S* configuration was attributed to the first eluted enantiomer on the basis of a comparison with the *S* calculated CD curve.

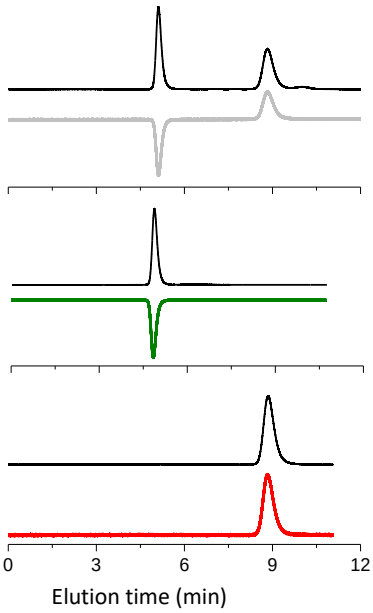

Figure 51: Analytical resolution of the racemate of BT_2CPDT_2 through HPLC on a chiral stationary phase. CSP: Chiralpak IB-3 (250 mm 4.6 mm I.D.), eluent: *n*-hexane : CH_2Cl_2 100 : 2, flow rate: 1 mL/min, temperature: 25°C, detector: UV and CD at 254 nm.

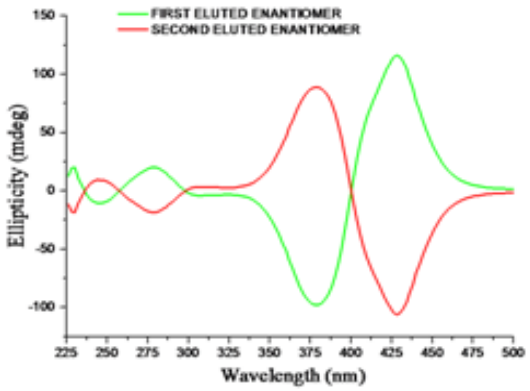

Figure 52: A) CD profiles of (*S*)-(+)-**26** (green) and (*R*)-(-)-**26** (red).

The complete cyclic voltammetric pattern of BT_2CPDT_2 monomer, recorded at 200 mV s^{-1} scan rate, in ACN + 0.1 M $TBAPF_6$ solution is reported in Figure 53. In this case, it is possible to observe, as previously reported for the BT_2DTP_2 monomer, two nearly equivalent oxidation peaks, corresponding to the oxidation of the two homotopic terminal thiophene units, which are not independent but slightly communicating through the central node of the stereogenic axis.

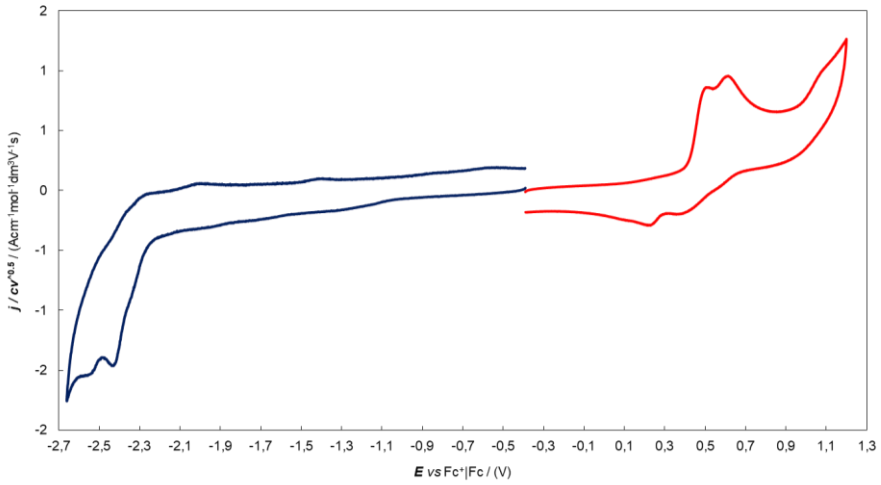

Figure 53: Complete CV patterns of BT_2CPDT_2 monomer (0.5 mM), 200 mV s^{-1} scan rate, solvent: ACN + 0.1 M $TBAPF_6$.

Oligomerization attempts were unsuccessful both in CH_2Cl_2 and acetonitrile solution, due to the high solubility of the oligomerized products in these solvents.

Electrodeposition experiments were carried out in pure ionic liquid (BMIM TFSI, Figure 54) but the solubility of the monomer in this medium was unsatisfactory.

Oligomerization of BT_2CPDT_2 was successfully performed in a 1:1 mixture of CH_2Cl_2 and the BMIM TFSI ionic liquid, on a screen-printed gold electrode (Figure 55, grey line).

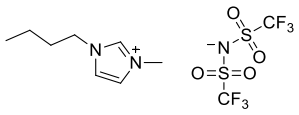

Figure 54: BMIM TFSI, 1-butyl-3-methylimidaziolium bis(trifluoromethylsulfonyl)imide.

After electrodeposition of enantiopure (*S*)-ec-p(BT_2CPDT_2), the enantiorecognition ability of the chiral film was tested, employing, as usual, the (*R*)-(+)- and (*S*)-(–)-*N,N*-dimethyl-1-ferrocenylethylamine ferrocene, dissolved in pure ionic liquid.

The enantiodiscrimination results for the two probes are quite satisfactory, the difference between the oxidative potential of the two enantiomers being about 100 mV, as reported in Figure 55.

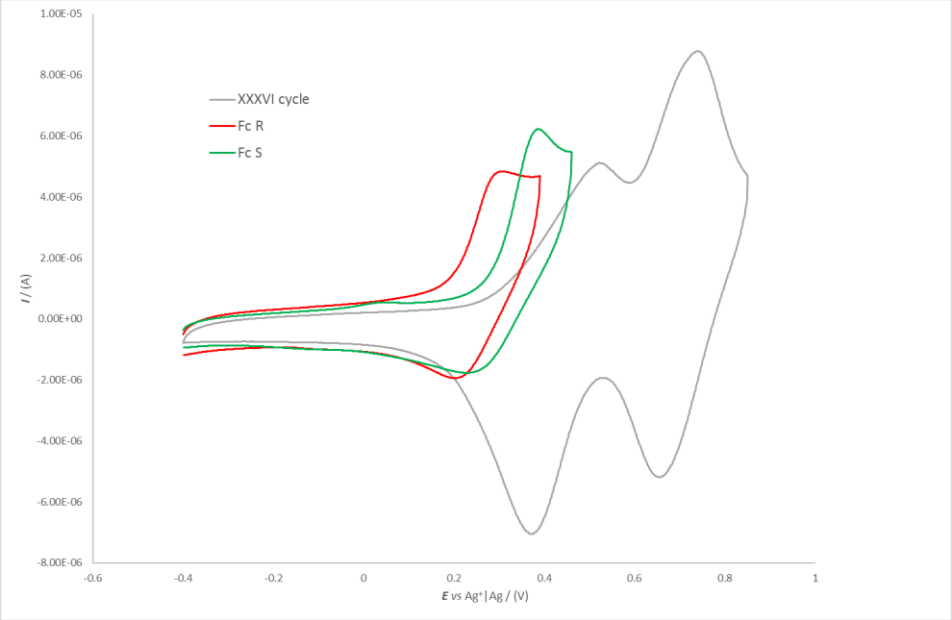

Figure 55: Enantiorecognition tests on enantiopure oligomeric (*S*)-ec-p(BT_2CPDT_2) (deposited form thirty-six cycles on SPE gold electrode, 0.5 mM monomer solution in in 1:1 ionic liquid : CH_2Cl_2, 200 mV s^{-1} scan rate) (grey line) in the presence of enantiopure probes *(R)*-(+)- and (*S*)-(−)-*N*,N-dimethyl-1-ferrocenylethylamine (red and green line, respectively).

4.4. 3,3'-Bithianaphthene derivatives based on the bithiophene pendant modification strategy

4.4.1. 2,2'-Bis(2,2':3',2''-terthiophen-5'-yl)-3,3'-bithianaphthene ($BT_2(T_3)_2$)

The synthesis of a monomer endowed with intermediate characteristics between BT_2T_4 and BT_2T_6 appeared an interesting target for studying the effects of an additional thiophene unit not involved in the conjugative delocalization along the main backbone, but crucial for determining its conformational characteristics. In collaboration with the University of Stuttgart, we planned the synthesis of a new inherently chiral monomer, endowed with six thiophene units but characterized by a branched terthiophene structure, supported in this project by the expertise in this field of prof. Ludwigs' group.[43][44][45]

The synthesis started from commercially available 2-bromothiophene that was treated with *n*-BuLi, diisopropylamine and trimethylsilyl chloride in order to protect the position 5 with the trimethylsilyl group. Compound **27** was obtained in quantitative yields. Two equivalents of compound **27** were then treated with magnesium turnings to give the corresponding Grignard reagent, that was employed in a Kumada coupling reaction, catalyzed by 1,2-(dppe)$NiCl_2$, with

2,3-dibromothiophene, to give the protected 2,2':3',2''-terthiophene **28**. The anion of the latter, generated with *n*-BuLi, was converted into the stannyl derivative **29**, that was used in the palladium catalyzed Stille-reaction with the 2,2'-dibromo derivative BT_2Br_2 **4** to give the new compound **30**. The final deprotection reaction of **30**, effected with tetrabutylammonium fluoride (TBAF) in THF solution, allowed to accede to the 2,2'-bis(2,2':3',2''-terthiophen-5'-yl)-3,3'-bithianaphthene $BT_2(T_3)_2$ (**31**) in quantitative yields.

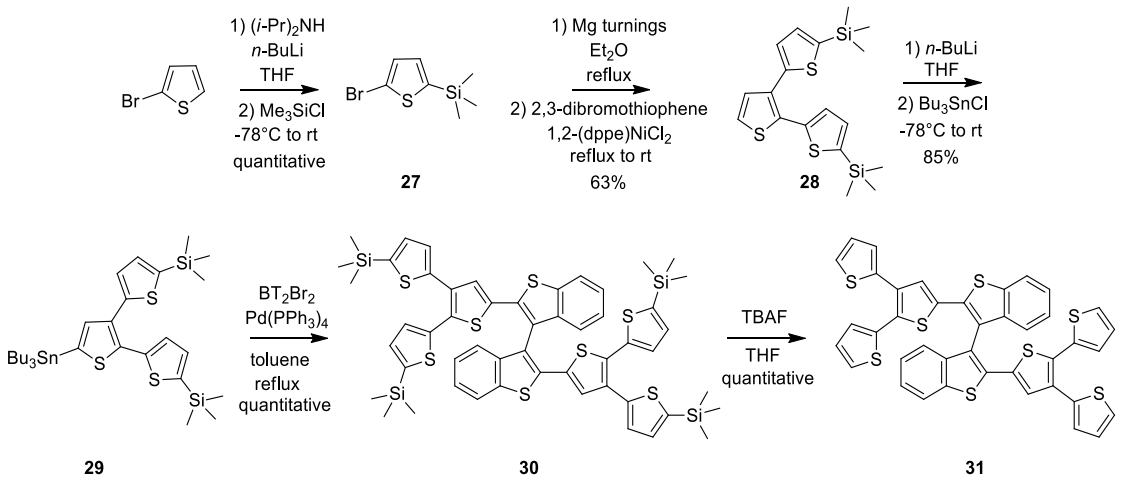

Scheme 11: Synthesis of 2,2'-bis(2,2':3',2''-terthiophen-5'-yl)-3,3'-bithianaphthene ($BT_2(T_3)_2$) **31**.

The chemical oxidation of compound **31** was performed by reaction with iron trichloride, in dry chloroform solution, in order to investigate if also branched monomers were able to produce cyclic oligomers. The thiophene in β position, indeed, could complicate the reaction trend due to the possible formation of branched oligothiophenes, sterically hindering the formation of cyclic structures.

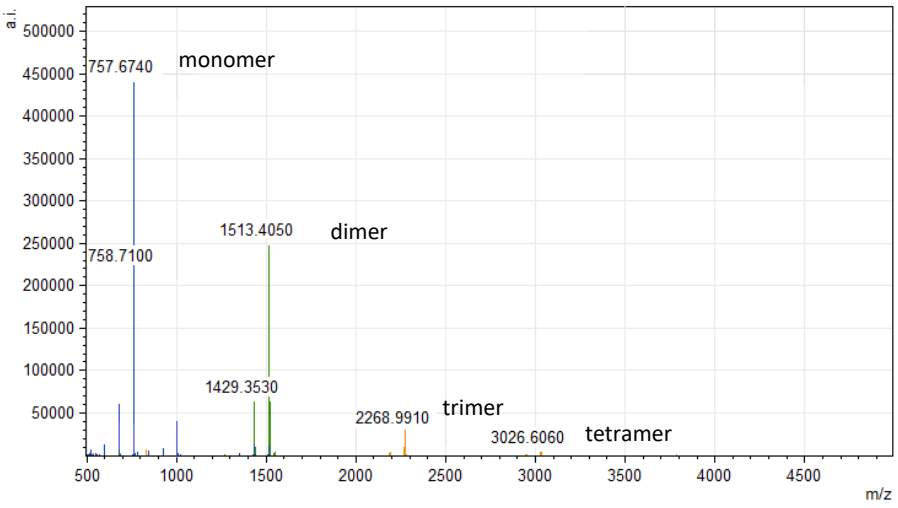

Figure 56: MALDI analysis of chemically oxidized $BT_2(T_3)_2$. Oligomers extracted by THF.

The MALDI spectrum, reported in Figure 56, demonstrated that the oxidation trend was analogous to that exhibited by the previously investigated monomers: indeed, a regular decreasing distribution between cyclic dimers, trimers and small amounts of tetramers was observed.

The formation of cyclic compounds was proved by comparing the isotopic distribution of the peaks present in the HR MALDI spectrum with the calculated one.

$BT_2(T_3)_2$ was also electrochemically oxidized in the laboratories of prof. Ludwigs and the properties of the resulting films investigated with different techniques, such as cyclic voltammetry, spectroelectrochemistry and *in-situ* conductance.

The deposition of the oligomeric films was performed under potentiodynamic conditions (reported in Figure 57 A and B), using a 1 mM solution of the monomer in acetonitrile + 0.1 M $TBAPF_6$ (scan rate = 50 mV s^{-1}), on 10 µm interdigitated platinum and ITO electrodes.

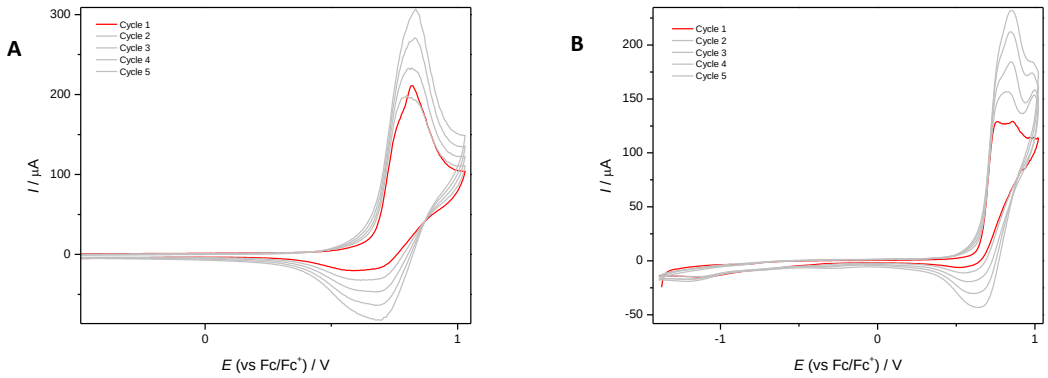

Figure 57: Potentiodynamic electro-oxidation of $BT_2(T_3)_2$ on platinum (A) and ITO (B). Five consecutive cycles at 50 mV s^{-1} scan rate; 1 mM of compound $BT_2(T_3)_2$ in ACN + 0.1 M $TBAPF_6$.

Cyclovoltammetric analysis and spectroelectrochemical investigation (Figure 58 E and F) revealed an interesting behavior, highlighted by comparison of these results with those collected for BT_2T_4 (Figure 58 A and B) and BT_2T_6 (Figure 58 C and D) under analogous experimental conditions.

A progressive lower stabilization of the radical cation was observed moving from BT_2T_4 (**1**) to BT_2T_6 (**10**) to $BT_2(T_3)_2$ (**31**).

BT_2T_4, indeed, showed the more pronounced stabilization, since two peaks are well detectable in the CV, the first one corresponding to the radical cation and the second one to the dication. The same mentioned stabilization can be also observed from the UV spectrum where the bands

corresponding to these species can be clearly individuated and the transient species, namely the radical cation, can be separated from the neutral and the double charged ones.

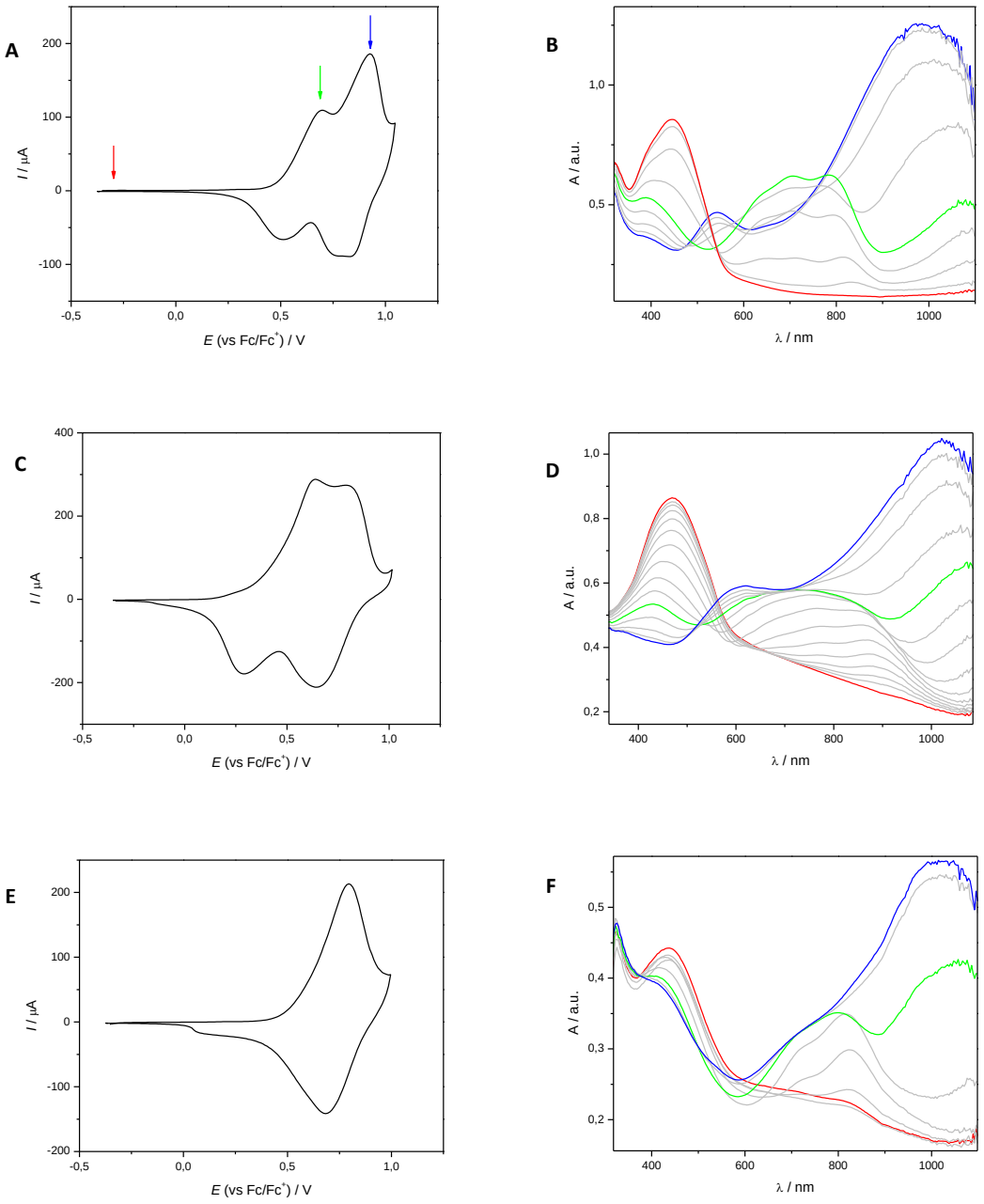

Figure 58: *In-situ* spectroelectrochemistry of ec-p($BT_2(T_3)_2$)**:** A) Cyclic voltammogram of the reversible p-doping of ec-p(BT_2T_4) (deposited on ITO electrode from five cycles, 1 mM monomer solution in ACN + 0.1 M $TBAPF_6$ at 50 mV s^{-1} scan rate). B) Vis/NIR spectra of ec-p(BT_2T_4) recorded during the forward scan (oxidation) in the p-doping process: profiles for neutral (red), radical cation (green) and dication species (blue) are highlighted. C) Cyclic voltammogram of the reversible p-doping of ec-p(BT_2T_6) (deposited on ITO electrode from five cycles, 1 mM monomer solution in ACN + 0.1 M $TBAPF_6$ at 50 mV s^{-1} scan rate). D) Vis/NIR spectra of ec-p(BT_2T_6) recorded during the forward scan (oxidation) in the p-doping process: profiles for neutral (red), radical cation (green) and dication species (blue) are highlighted. E) Cyclic voltammogram of the reversible p-doping of ec-p($BT_2(T_3)_2$) (deposited on ITO electrode from five cycles, 1 mM monomer solution in ACN + 0.1 M $TBAPF_6$ at 50 mV s^{-1} scan rate). F) Vis/NIR spectra of ec-p($BT_2(T_3)_2$) recorded during the forward scan (oxidation) in the p-doping process.

BT_2T_6 showed a similar behaviour, even if the peaks are less pronounced: the radical cation resulted to be a transient and less defined species.

This trend is even more evident for $BT_2(T_3)_2$: in the CV, only one oxidation peak can be observed and, from the spectroelectrochemical analysis, the radical cation (λ_{max} at 798 nm) resulted to be an extremely evanescent species. This trend can be summarized considering the delocalization of the charged species that appears to be more extended in a more conjugated system (BT_2T_6) and even more in a branched structure ($BT_2(T_3)_2$) with respect to the parent monomer BT_2T_4.

In-situ conductance analysis confirmed the behaviour observed in spectroelectrochemical experiments. Comparisons of the results obtained for BT_2T_6 (Figure 39), with those achieved for $BT_2(T_3)_2$ (Figure 59), allowed to deduce that the branched structure of the terthiophene in $BT_2(T_3)_2$ greatly destabilizes the radical cation species. Radical cation stabilization, therefore, resulted to be dependent not only on the size of the side chain in the monomer and in the oligomeric structures, but also on the spatial 3D arrangement.

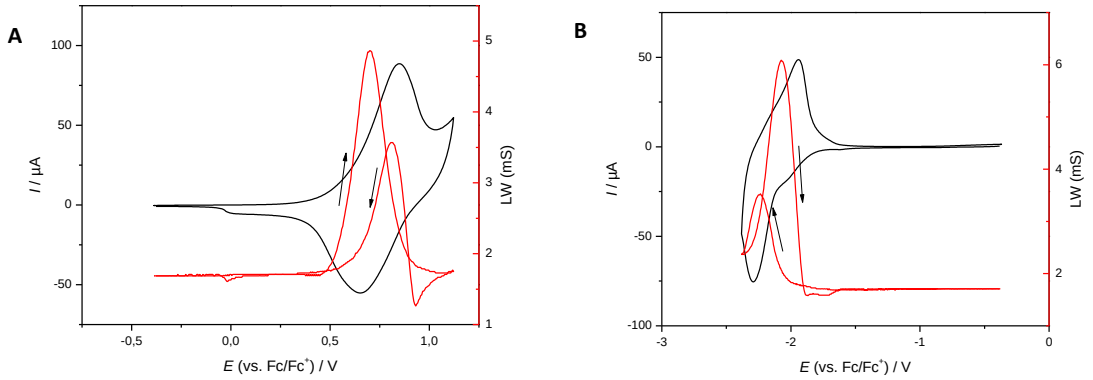

Figure 59: *In-situ* conductance analysis of ec-p($BT_2(T_3)_2$) (deposited on 10 µm interdigitated Pt electrode, 1 mM monomer solution in ACN + $TBAPF_6$, 50 mV s^{-1} scan rate) recorded in ACN + 0.1 M $TBAPF_6$ solution, 20 mV s^{-1} scan rate. A) Anodic scan. B) cathodic scan.

4.4.2. 2,2'-Bis{bi[2,2'-(3,4-ethylenedioxy)thiophen-5-yl]}-3,3'-bithianaphthene (BT_2E_4)

Monomer **34**, in which the atropisomeric core of the 3,3'-bithianaphthene is decorated with four 3,4-ethylenedioxythiophene (EDOT) units, was designed in order to obtain a compound interesting not only for its stereochemical properties but also for its intrinsic conductive behaviour.

Poly-(3,4-ethylenedioxythiophene), better known as pEDOT (commercially, as Baytron®), represents a smart material in the field of conductive polymers due to its peculiar properties. It plays a relevant role in electronic, antistatic and electric applications.[46][47] It is generally used as homopolymeric layer or in association with polystyrene sulfonic acid (PSS) that allows the formation of the pEDOT-PSS complex, widely used as conductive layer in electroluminescent devices and OFETs. Furthermore, pEDOT is an electrically-conducting conjugated polymer that shows remarkable conductivity, relatively stable in its oxidized form, endowed with a quite low redox potential, a moderate band gap and, last but not least, can form nearly transparent thin films.[48]

By consequence, the possibility to prepare a material that combines the concept of inherent chirality with remarkable characteristics of EDOT appeared very attractive.

The synthesis of BT_2E_4 was planned according to the general strategy applied for the preparation of all the other monomers based on the 3,3'-bithianaphthene scaffold, which required, in this case, the availability of the stannyl derivative **33**. The bis-EDOT **32** was obtained in good yields starting from commercially available EDOT, which was treated with *n*-BuLi and the resulting anion submitted to oxidative coupling effected by $CuCl_2$.[49]

The bis-EDOT was then stannylated to give compound **33**, suitable precursor for the Pd-catalyzed Stille reaction with BT_2Br_2 **4**; monomer **34** was obtained in high yields, after overnight refluxing in toluene, and it was fully characterized from an analytical and spectroscopic point of view.

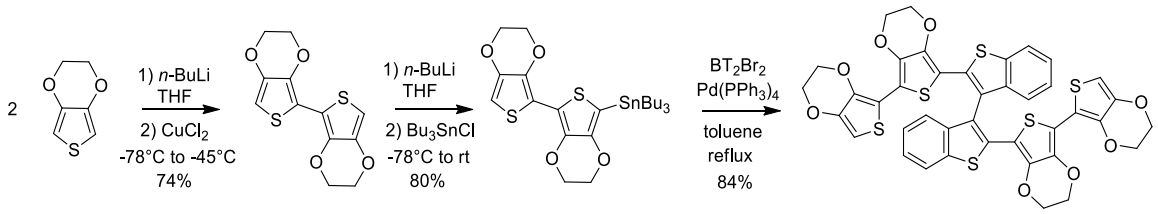

32 **33** **34**

Scheme 12: Synthesis of 2,2'-bis{bi[2,2'-(3,4-ethylenedioxy)thiophen-5-yl]}-3,3'-bithianaphthene (BT_2E_4) **34**.

TD-DFT calculation were performed by dr. Carmen Ruiz Delgado at the Universidad de Málaga and the lateral views of the optimized geometries for BT_2E_4 and BT_2T_4 are reported in Figure 60. As we can observe, similar distortions between the two thianaphthene units are found upon EDOT substitution, whereas the external thiophene units become almost coplanar when going from BT_2T_4 to BT_2E_4 due to the benefits of electron rigidification through inter-ring S-O interactions.

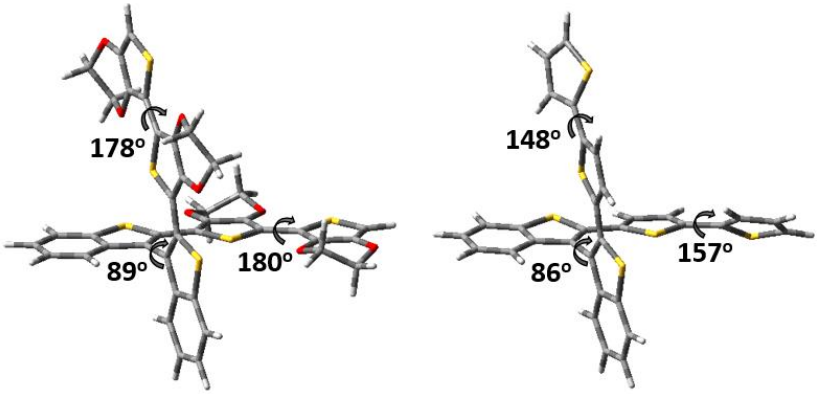

Figure 60: Lateral views of the CAM-B3LYP/6-31G**-optimized geometries of BT_2E_4 (left) and BT_2T_4 (right).

In Figure 61 the voltammetric patterns of BT_2E_4 (light grey) and BT_2T_4 (grey), for sake of comparison, are reported. The anodic CV patterns for both monomers consist of two equal nearly merging peaks pointing to two equal, slightly interacting conjugated systems.

Actually, in CH_2Cl_2 these two peaks exhibit a 1:1 current ratio especially at higher scan rates, while in more polar acetonitrile they merge (in fact unlike the former case the following shoulder decreases with increasing scan rate and should therefore correspond to an electron transfer product).

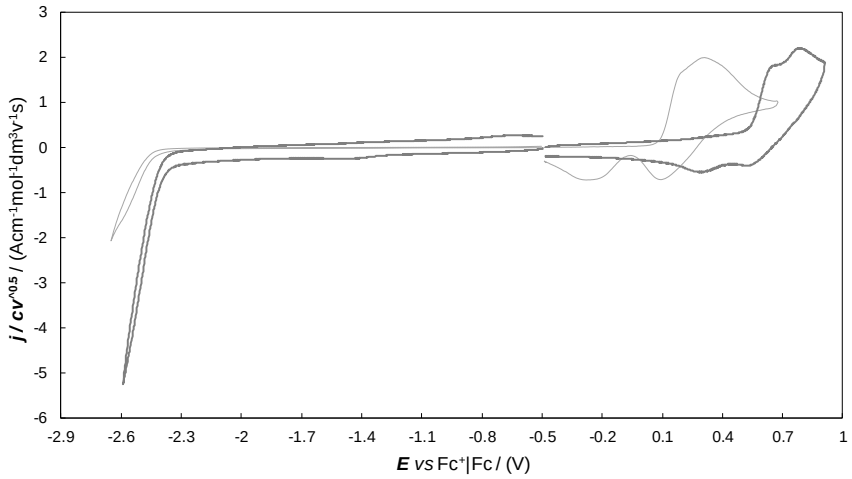

Figure 61: Electrochemical characterization of BT_2E_4 (light grey) and BT_2T_4 (grey) monomer at 200 mVs^{-1}, on GC electrode in CH_2Cl_2 + $TBAPF_6$ 0.1.

The residual interaction between the two half moieties (constituted by three thiophene rings) through the interanular bond causes a negative shift of the oxidation potentials with respect to α-terthiophene ($E_{ox,I}$ BT_2E_4 = 0.19 V and $E_{ox,I}$ = 0.64 V BT_2T_4 *vs* $E_{ox,I}$ α-terthiophene = 1.53 V).[50]

In addition, electron-richness of EDOT rings and the increase of planarity of each bis-EDOT wings (suggested by theoretical data) make the BT_2E_4 monomer a better reductant.

Cathodic peaks in Figure 61 are not visible as a consequence of the narrower potential window of CH_2Cl_2 respect to acetonitrile.

Consistently with their intrinsic 3D structures, BT_2E_4 and BT_2T_4 electrooligomerize very rapidly and regularly, a behavior steadily maintained even after several consecutive CV cycles (Figure 62 A). The inductive effect of four EDOT moieties is transferred from monomer to oligomer films ec-p(BT_2E_4) with a strong decrease of the oxidation onset potential, E^{ox}_{onset}, of about 0.85 V. The anodic cycle clearly shows two well-separated oxidation waves with maxima at 0.05 and 0.33 V *vs* $Fc^+|Fc$. Concerning first reduction a value of -1.89 V for E_{onset} can only be provided, whereas the E_{onset} for first oxidation is -0.39 V, resulting in a ΔE_{onset} = 1.5 V.

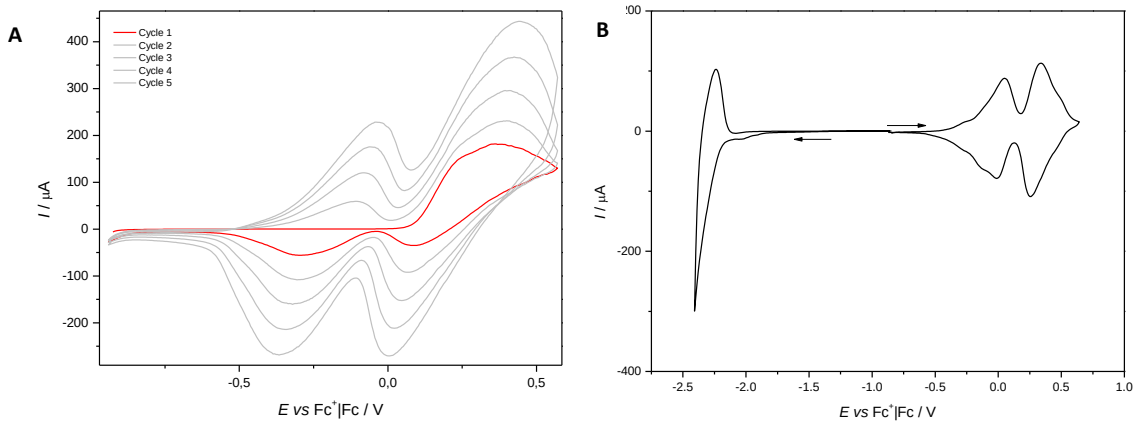

Figure 62: A) Electrooligomerization of BT_2E_4 (1 mM) in a 0.1 M $TBAPF_6$ CH_2Cl_2 solution on ITO electrode, scan rate 50 mV s^{-1}. B) CV profile of ec-oligo(BT_2E_4) in a 0.1 M $TBAPF_6$ acetonitrile monomer free solution on ITO electrode, scan rate 20 mV s^{-1}.

	λ_{max}/nm (eV)										
oligomer	**neutral state**	**radical cation**		**dication**		$E^{1/2}_{ox,I}$ /V[b]	$E^{1/2}_{ox,II}$/V[b]	$E^{1/2}_{red,I}$/V[b]	E^{ox}_{onset}/V[b] (HOMO/eV)	E^{red}_{onset}/V[b] (LUMO/eV)	**E band gap/eV**
ec-oligo(BT_2E_4)	516	700	798	1005		0.03	0.29		-0.39 (-4.71)	-1.70 / -1.89 (-3.40 / -3.21)	1.31 / 1.5
ec-oligo(BT_2T_4)	449	714	791	543	986	0.60	0.86	-1.76	0.44 (-5.54)	-1.60 / -1.75 (-3.50 / -3.35)	2.04 / 2.19

Table 1: Optical and electrochemical characteristics of BT_2E_4 and BT_2T_4 in comparison with ec-p(EDOT)[56] recorded in CH_2Cl_2 + $TBAPF_6$.

In-situ spectroelectrochemical measurements were performed in order to study absorption profiles as a function of the electrode potential with the aim of correlating redox waves in the cyclic voltammograms with relative abundance of the neutral and charged species involved in the process. In Figure 63 A and C the cyclic voltammograms of ec-oligo(BT_2E_4) and ec-oligo(BT_2T_4) deposited on ITO electrodes are shown. The corresponding absorption spectra during the

forward anodic scans are shown in Figure 63 B and D. Backward scans, not reported here, point to reversible charge/discharge processes for both oligomeric films with a small hysteresis.

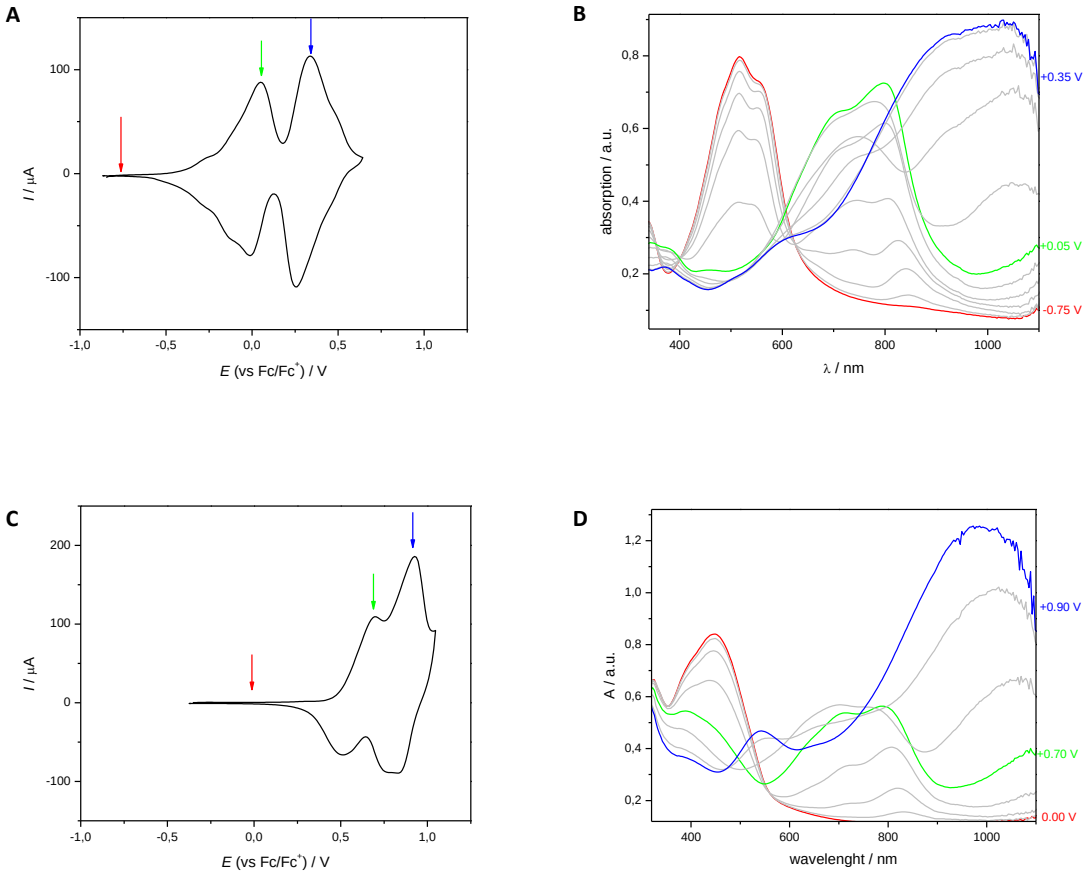

Figure 63: *In-situ* spectroelectrochemistry of ec-p(BT_2E_4): A) Cyclic voltammogram of the reversible p-doping of ec-p(BT_2E_4) (deposited on ITO electrode from five cycles, 1 mM monomer solution in CH_2Cl_2 + $TBAPF_6$, 50 mV s^{-1} scan rate) ACN + 0.1 M $TBAPF_6$ solution, 20 mV s^{-1} scan rate. B) Vis/NIR spectra of ec-p(BT_2E_4) recorded during the forward scan (oxidation) in the p-doping process: profiles for neutral (red), radical cation (green) and dication species (blue) are highlighted.

From the absorption spectra, the p-doping of both oligomeric films reveals three different species. In the neutral state ec-oligo(BT_2E_4) has an absorption maximum at 516 nm with a slightly visible vibronic structure. The first band at shorter wavelengths corresponds to the neutral state, attributed to the π–π* transition; Upon the anodic voltammetric scan the absorption band of the neutral species (red curve in Figure 63 B at E = -0.75 V) decreases while a new absorption band with a peak maximum of 798 nm (green curve in Figure 63 B at E = 0.05 V) arises. The gradual conversion of the neutral species into the radical cation one also results in an isosbestic point at about 600 nm. At more positive potentials, the absorption band of the radical cation in turn decreases with concurrent increase of a third characteristic absorption band at around

1000 nm (blue curve in Figure 63 B at $E = 0.35$ V), indicating the formation of the dication species.[51]

In Figure 64, the absorptogram of the ec-p(BT_2E_4) is reported: particularly remarkable is the perfectly reversible profiles for the wavelengths associated to the neutral, radical cation and dication species; furthermore, no hysteresis was observed for the λ_{max} of neutral and dication species.

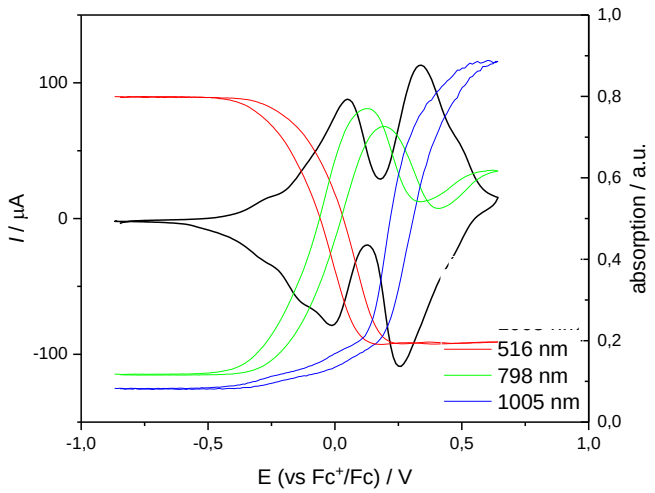

Figure 64: Absorptogram of BT_2E_4. Absorption as function of polarization potential at constant wavelengths, corresponding to maximum absorbance for the neutral film (516 nm), radical cation (798 nm) and dication (1005 nm). ITO in ACN + 0.1 M $TBAPF_6$; scan rate: 20 mV s^{-1}.

The conductance of the oligomeric films was finally investigated by electrodepositing the two monomers on 10 µm Pt interdigitated electrodes (Figure 65). At lower oxidation levels conductivity is supported by polarons (relative maximum at 0.1 V *vs* $Fc^+|Fc$ and about 0.5 V *vs* $Fc^+|Fc$ for ec-p(BT_2E_4) and ec-p(BT_2T_4) respectively).

At more positive potentials, where bipolarons become the dominant charge carriers (Figure 63), a second peak signal is observed, with the films reaching their maximum conductivity around 0.4 V *vs* $Fc^+|Fc$ and 0.8 V *vs* $Fc^+|Fc$ for ec-oligo(BT_2E_4) and ec-p(BT_2T_4) respectively. At the conductivity maximum both polarons and bipolarons are present, allowing an electron hopping mechanism of bipolarons from polaron or neutral states according to a "mixed valence" conductivity that disappears when there are no unoxidized or polaron sites, explaining our observed conductivity decrease with further positive polarization.[52][53][54] Hysteresis is observed from the direct to the reverse potential sweep, with the maximum of conductance being shifted at higher values for the charge process respect to the discharge one according to previous data on polythiophene films.[55] In Figure 65 B and D films are polarized in the cathodic direction, and

the conductance signal possibly correspond to radical anion and dianion states. The overall pattern is rather similar to the one observed for p-doping, with maxima at slightly higher λ_{max} values respect to the p-doping case.

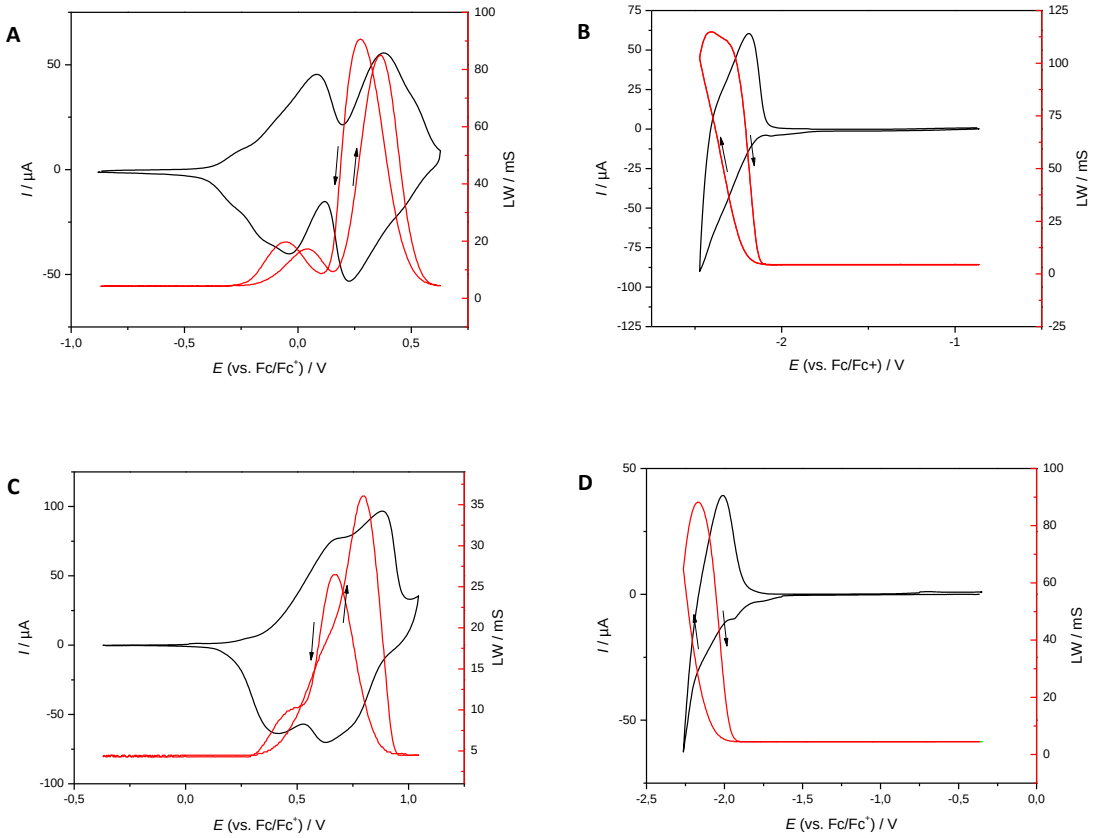

Figure 65: *In-situ* conductance analysis of ec-p(BT_2E_4) (deposited on 10 µm interdigitated Pt electrode, 1 mM monomer solution in CH_2Cl_2 + $TBAPF_6$, 50 mV s^{-1} scan rate) ACN + 0.1 M $TBAPF_6$ solution, 20 mV s^{-1} scan rate. A) Anodic scan. B) cathodic scan. *In-situ* conductance analysis of ec-p(BT_2T_4) (deposited on 10 µm interdigitated Pt electrode, 1 mM monomer solution in ACN + $TBAPF_6$, 50 mV s^{-1} scan rate) ACN + 0.1 M $TBAPF_6$ solution, 20 mV s^{-1} scan rate. C) Anodic scan. D) cathodic scan.

Monomer **34** was also chemically oxidized in order to evaluate the formation of macrocyclic oligomers; unfortunately, the presence of the EDOT units leads to oligomers which are much less soluble than those obtained from the oxidation of BT_2T_4. For this reason, we found impossible to extract significant amounts of material with the Soxhlet apparatus. However, a MALDI spectrum was recorded on the oligomeric mixture recovered from the electrodes surface after electrodeposition. The analysis of the spectrum (Figure 66) showed that the film was constituted by a mixture of oligomers, even if, due to the low resolution, it was not possible to understand whether they were cyclic or open-chain structures.

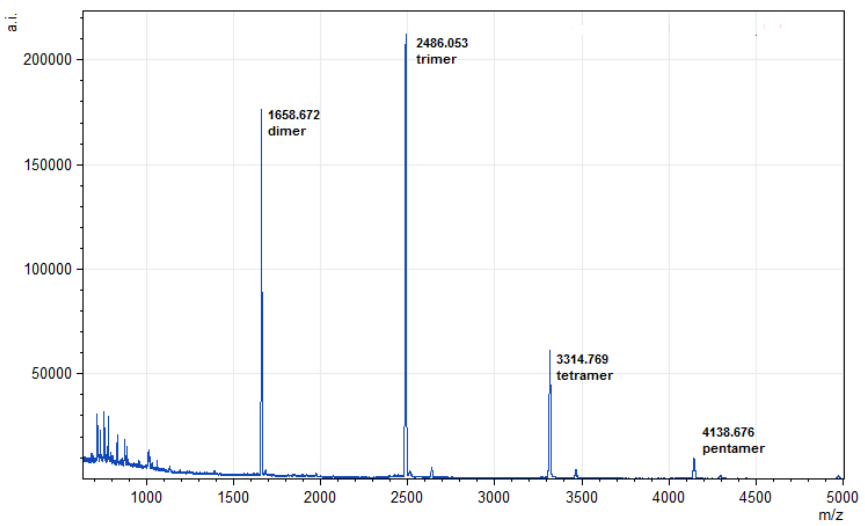

Figure 66: MALDI analysis of electrochemically oxidized BT_2E_4. Oligomeric material analyzed through solid-phase method.

After the characterization described above, the racemate of BT_2E_4 was submitted to HPLC analysis on a chiral stationary phase in order to resolve it into antipodes. Unfortunately, we did not succeed in resolving it into antipodes even at analytical level.

The best results we obtained are reported in Figure 67. The peaks characterized by an elution time of 29 and 33 minutes, respectively, correspond to the two antipodes, as confirmed by the CD detector, but the separation was partial and required long elution times. Furthermore, a broad peak with elution time in the range of 15-25 minutes was present in the chromatogram, probably due to the formation of aggregates, since the presence of by-products could be excluded on the basis of the ^{1}H-NMR spectrum.

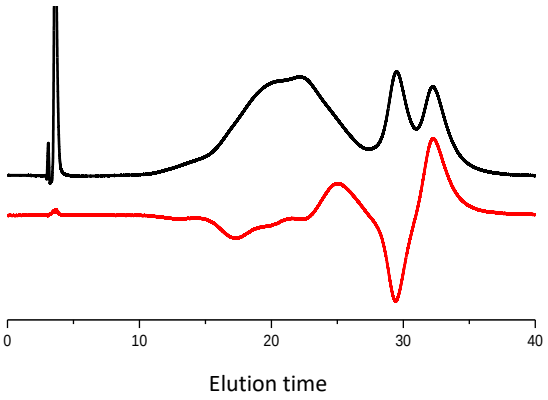

Figure 67: Analytical resolution attempts of racemate of BT_2E_4 through HPLC on a chiral stationary phase. CSP: Chiralpak IB (250 mm x 4.6 mm I.D.), eluent: *n*-hexane : IPA-70 : 30, flow rate: 1 mL/min, temperature: 25°C, detector: UV (black) and CD (red) at 360 nm.

4.4.3. 2,2'-Bis{2-[7-(thiophen-2-yl)-2,1,3-benzothiadiazol-4-yl]thiophen-5-yl}-3,3'-bithianaphthene (BT_2BTD_2)

The last monomer synthesized, with the aim to confer special properties to the material by functionalizing the bithiophene chains connected to the bithianaphthene atropisomeric scaffold, was characterized by the introduction of a 2,1,3-benzothiadiazole (BTD) ring between the thiophene units of BT_2T_4. BTD is one of the most important heterocyclic ring used in the chemistry of photoluminescent compounds and widely employed in light technology.[57][58] The derivatives of BTD (beside fungicides, herbicides and antibacterial applications) normally possess several favorable characteristics for electronics: indeed, they exhibit strong electron-withdrawing nature, they are efficient fluorophores, afford well-ordered crystal structures as a result of their highly polarized properties and are suitable to be used as electron acceptors units for devices based on donor-acceptor (D-A) interactions.

Consequently, the introduction of the BTD system in inherently chiral structure appeared to be particularly appealing in the light of obtaining compounds with bigger cavities and, at the same time, endowed with different, and hopefully better, optical and optoelectronic properties.

The synthesis of the new monomer **38**, showed in Scheme 13, started from commercially available benzo[c][1,2,5]thiadiazole, which afforded the corresponding dibromo derivative **35** in good yields by reaction with bromine in refluxing hydrobromic acid solution. The presence of the two bromine atoms was the key for the subsequent introduction of the two thiophene moieties through a Stille coupling.

The 4,7-di(thiophen-2-yl)benzothiadiazole (**36**) was obtained in satisfactory yields and converted into the corresponding mono-anion by regioselective lithiation with *n*-BuLi in the presence of 2,2,6,6-tetramethylpiperidine in THF solution. The anion was quenched with trimethylstannyl chloride to give the corresponding stannyl derivative **37**, which was used without further purification in a new Pd-catalyzed Stille coupling with BT_2Br_2 **4** using DMF as solvent.

The expected 2,2'-bis{2-[7-(thiophen-2-yl)-2,1,3-benzothiadiazol-4-yl]thiophen-5-yl}-3,3'-bithianaphthene (**38**), nicknamed with acronym BT_2BTD_2, was obtained in moderate yields and fully characterized from an analytical and spectroscopic point of view.

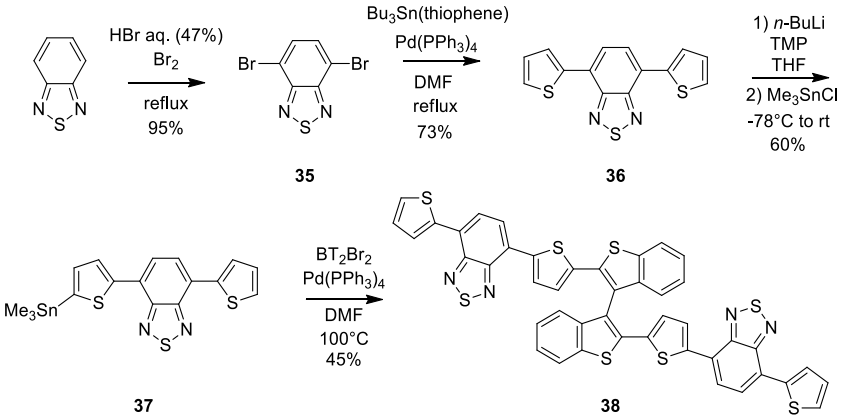

Scheme 13 : Synthesis of 2,2'-bis{2-[7-(thiophen-2-yl)-2,1,3-benzothiadiazol-4-yl]thiophen-5-yl}-3,3'-bithianaphthenee (BT_2BTD_2) **38**.

BT_2BTD_2 appeared, at first sight, to be optically different from the other inherently chiral monomers synthesized so far that display a yellowish color, the introduction of the benzothiadiazole confers a deep red color to BT_2BTD_2.

A detailed discussion of the optoelectronic properties of this compound is reported in paragraph 4.5.1.

BT_2BTD_2 was chemically oxidized with iron trichloride following the standard procedure and the MALDI spectrum of the material collected by Soxhlet extraction is reported in Figure 68. The spectrum shows the presence of some unreacted material and of the dimeric compound only. This unexpected result could be ascribed to the low solubility of the starting monomer, and by consequence of the oligomers, rather than to the inability of BT_2BTD_2 to form higher molecular weight oligomers.

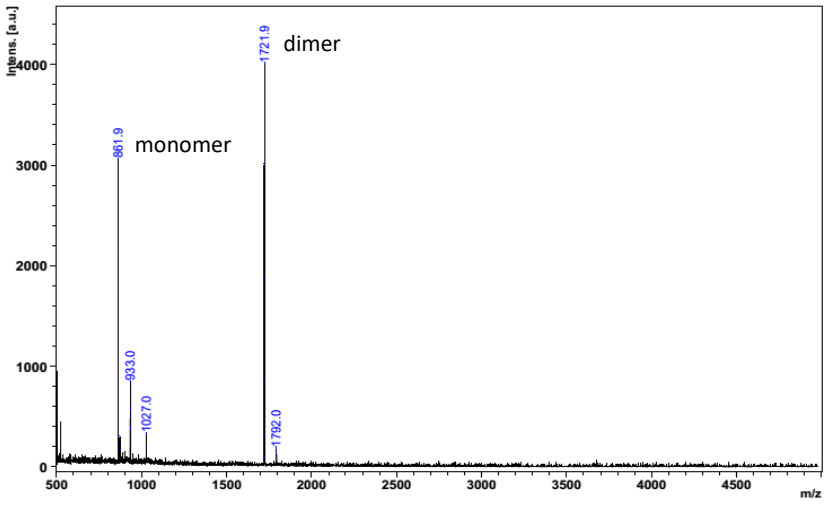

Figure 68: MALDI analysis of chemically oxidized BT_2BTD_2. Oligomers extracted by THF.

BT_2BTD_2 was electrochemically characterized on a GC electrode both as monomer and as oligomeric film.

The oligomeric film was deposited from a 0.5 mM solution of BT_2BTD_2 in CH_2Cl_2 + 0.1 M $TBAPF_6$, at 200 mV s^{-1} scan rate and the voltammogram is reported in Figure 69 B. The reduction potential resulted to be expectedly high due to the presence of the benzothiadiazole system: the energy gap of monomer **38** was 0.6 V less than that found for BT_2T_4.

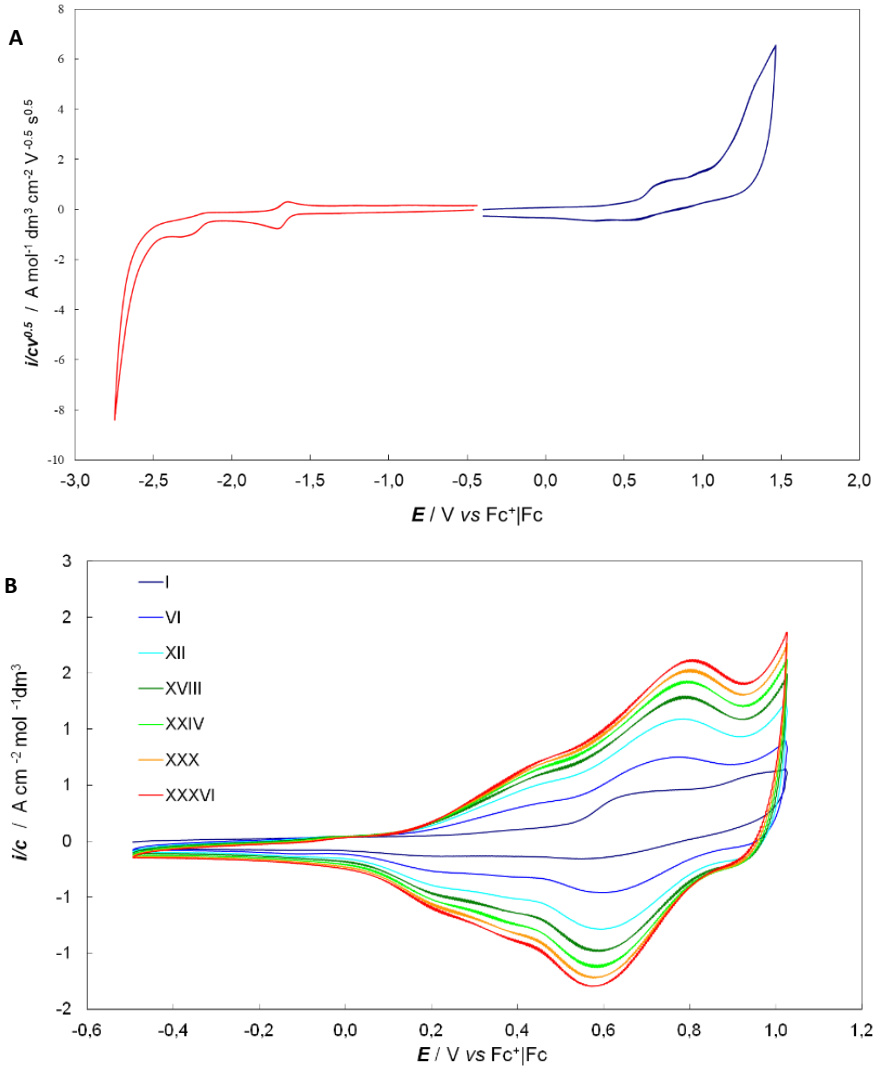

Figure 69: A) Complete CV patterns of BT_2BTD_2 monomer (0.5 mM), 200 mV s^{-1} scan rate, solvent: ACN + 0.1 M $TBAPF_6$. B) Potentiodynamic electro-oxidation of BT_2BTD_2 on GC electrode. Thirty-six consecutive cycles at 200 mV s^{-1} scan rate, 0.5 mM of BT_2BTD_2 in CH_2Cl_2 + 0.1 M $TBAPF_6$.

Despite the interesting properties of this new inherently chiral compound, the low solubility of BT_2BTD_2 was found an unsurmountable problem in the attempts of racemate resolution by HPLC on a chiral stationary phase.

4.5. Summary of 3,3'-bithianaphtene compounds

4.5.1. Photophysical 3,3'-bithianaphtene monomers comparisons

The absorption and the emission spectra of all the new chiral monomers based on 3,3'-bithianaphthene scaffold, recorded in diluted, air-equilibrated dichloromethane solution, at room temperature are summarized in a sequence of Figures, from Figure 70 to Figure 73, while the photophysical data are given in Table 2.

	λ_{abs} (solution) (nm)	λ_{em} (solution) (nm)	Lifetime τ (ns)	Quantum yield Φ (solution)	λ_{em} (solid) (nm)	Quantum yield Φ solid	ε [M^{-1} cm^{-1}]
BT_2T_4	398	535	1.95	21%	509	13%	48000
BT_2T_6	408	521	0.7	13%	557	2%	56700
BT_2T_6Bu	395	534	0.7	12%	554	11%	56000
BT_2DTP_2	391	523	1.16	12%	540	3%	59000
BT_2CPDT_2	398	535	1.95	21%	540	3%	58000
$BT_2(T_3)_2$	305; 369	508	0.9	8.5%	538	7%	36000
BT_2E_4	401	536	1.8	14%	560	17%	57500
BT_2BTD_2	358; 485	633	6.3	51%	672	5%	38500

Table 2: Optical characterization of 3,3'-bithianaphthene monomers. Values were recorded in CH_2Cl_2 deaerated solution.

Compared to the parent monomer BT_2T_4, the absorption maxima of BT_2T_6, BT_2T_6Bu, BT_2DTP_2, BT_2CPDT_2 and BT_2E_4 are red-shifted of more than 19 nm. This red-shift is presumably due to the wider π-conjugation afforded by the elongation of the α-oligothiophene chain in the case of BT_2T_6 and BT_2T_6Bu. On the other hand, in the case of BT_2DTP_2 and BT_2CPDT_2, the bathochromic effect is attributable to the central fused-ring units, which increases the planarity of the system, allowing a more extended π-conjugated ground state than in the more flexible α-oligothiophene chain of BT_2T_4.

Quite different is the case of BT_2E_4, in which the red-shifted absorption band is probably due to the increased planarization of the bithiophene lateral edge imposed by the steric hindrance of the EDOT substituents. This hypothesis is further supported by the observed increased extinction coefficients (ranging from 5.6×10^4 and 5.9×10^4 M^{-1} cm^{-1} for the different oligothiophenes, in comparison with 4.8×10^4 M^{-1} cm^{-1} for BT_2T_4) and by the slight vibronic structure observed in the spectra of BT_2DTP_2 and BT_2CPDT_2, as expected for a more planar and more rigid conformation.

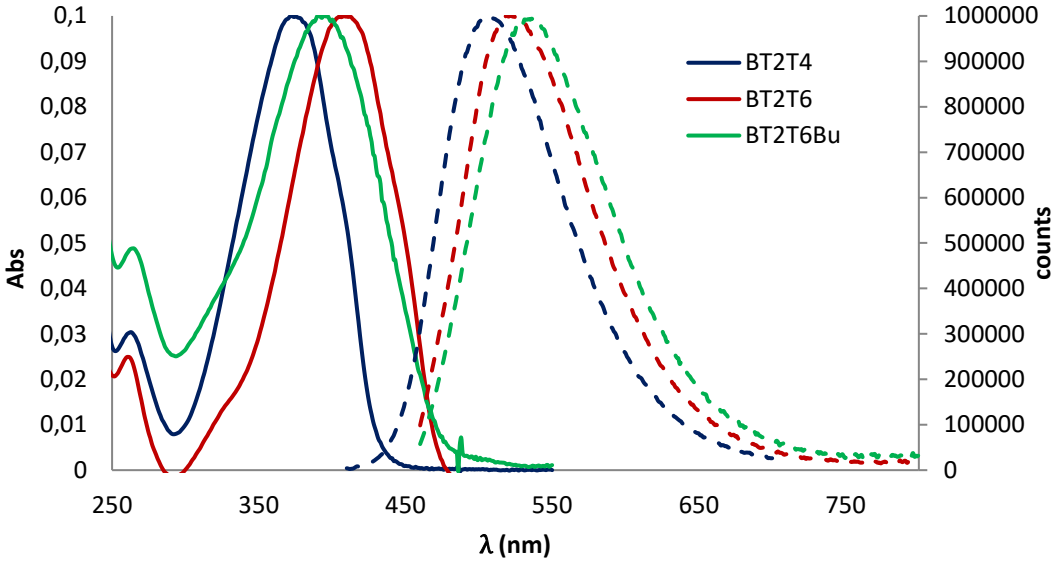

Figure 70: UV profile (solid lines) and fluorescence profile (dashed line) of BT_2T_4, BT_2T_6 and BT_2T_6Bu. Profiles were recorded in CH_2Cl_2 deaerated solution.

All the observed absorption maxima correspond to the $\pi \rightarrow \pi^*$ transition, also in the case of the BT_2DTP_2, since the nitrogen lone-pair is involved in the aromatic π-system of the pyrrole fused ring and, therefore, the $n \rightarrow \pi^*$ transition would not be expected. The presence of nitrogen atom has a slight influence on the frontier orbitals, acting as electron withdrawing with π-orbitals and destabilizing mainly the HOMO level.

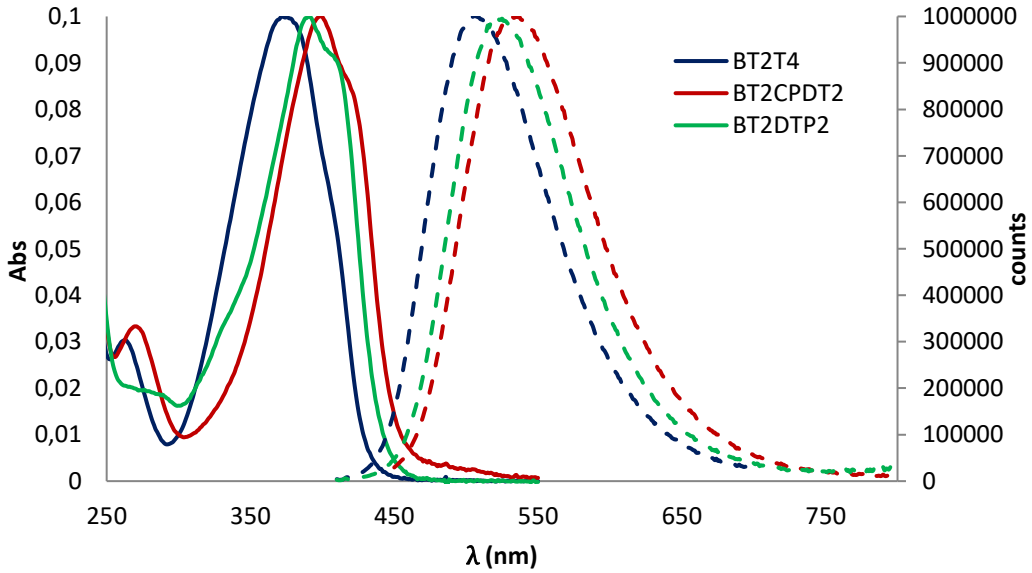

Figure 71: UV profile (solid lines) and fluorescence profile (dashed line) of BT_2T_4, BT_2CPDT_2 and BT_2DTP_2. Profiles were recorded in CH_2Cl_2 deaerated solution.

However, the electrochemical data (Table 3) indicate that both the HOMO and the LUMO levels are equally affected (being the LUMO level stabilized), and consequently the transition energy is

not affected by the presence of the pyrrole unit as it might be expected.[59][60] Indeed, a red shift of the absorption is observed even if it is the smallest one in the series.

A completely different behavior was observed for $BT_2(T_3)_2$ and for BT_2BTD_2. In both cases two different absorption bands were observed, with a strong reduction of the molar extinction coefficients. In the case of the $BT_2(T_3)_2$ the higher energy absorption band, at 305 nm, is attributable to the $\pi \rightarrow \pi^*$ transition localized on the lateral, non-conjugated thiophene ring, while the lower energy band at 369 nm is due to the $\pi \rightarrow \pi^*$ transition involving the atropoisomeric scaffold. Both of them result blue-shifted with respect to the BT_2T_4, in agreement with the reduced coplanarity afforded by the thiophene substituent in β position on the thiophene ring of the lateral chain.

In the case of BT_2BTD_2, the high energy absorption band at 358 nm, is assigned as a $\pi \rightarrow \pi^*$ transition, while the low energy band, at 485 nm and strongly red-shifted with respect to the band of BT_2T_4, is most probably due to the intramolecular charge transfer (ICT) transition between the donor benzothiophene moiety and the benzothiadiazole acceptor unit where the LUMO is localized.[61][62] The nature of the LUMO is confirmed also by the electrochemical data; indeed, BT_2BTD_2 displays the lowest reduction potential of the whole series and, consequently, the lowest band-gap.

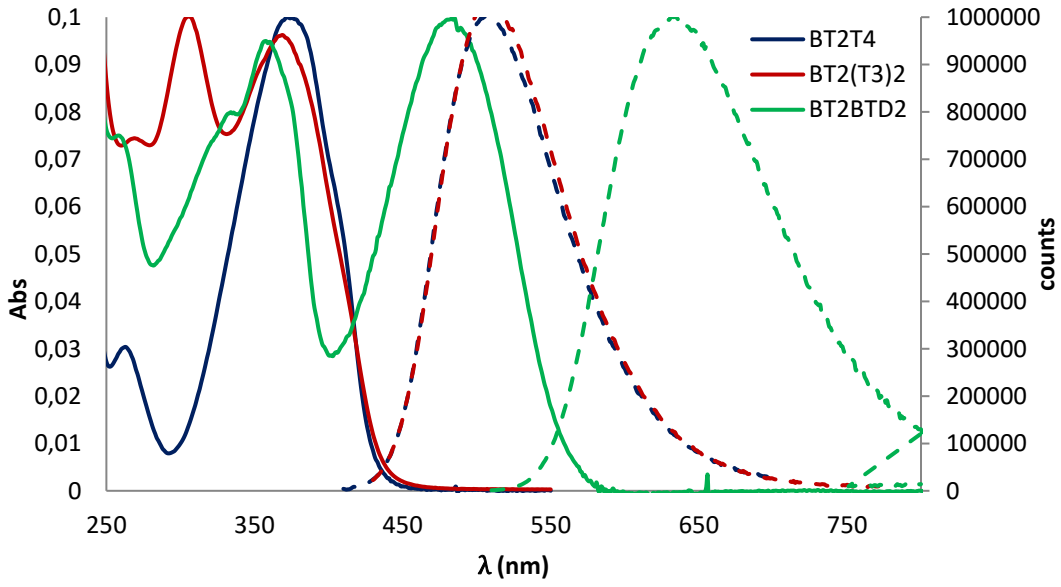

Figure 72: UV profile (solid lines) and fluorescence profile (dashed line) of BT_2T_4, $BT_2(T_3)_2$ and BT_2BTD_2. Profiles were recorded in CH_2Cl_2 deaerated solution.

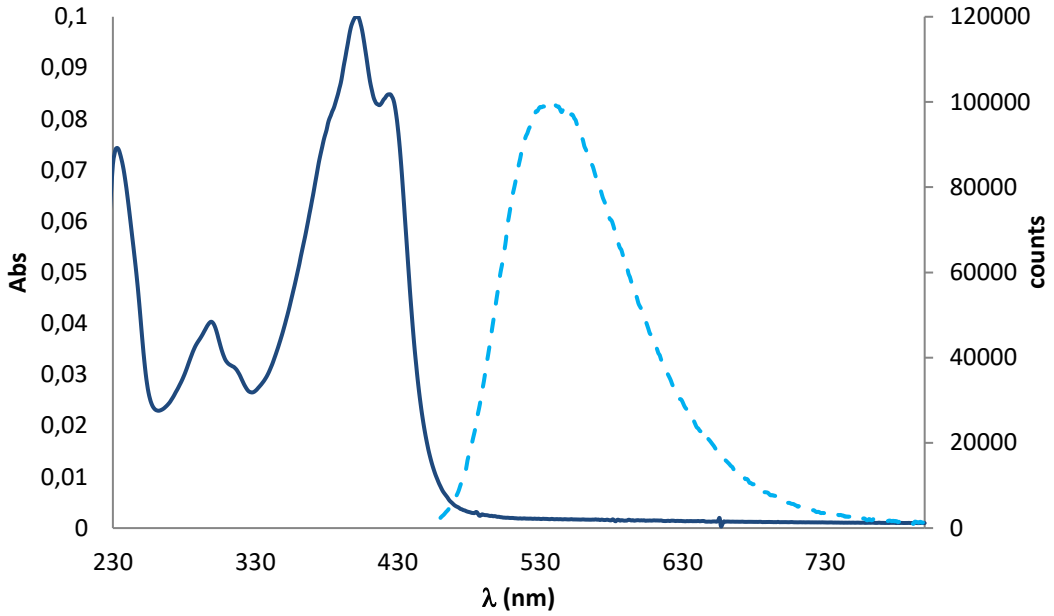

Figure 73: UV profile (dashed line) and fluorescence profile (solid line) of BT_2E_4. Profiles were recorded in CH_2Cl_2 deaerated solution.

Structural factors have significant effects also on the emission properties of these oligothiophenes. In particular, the increased conjugation among the thiophene rings affords a red shifted emission maximum. Only the $BT_2(T_3)_2$ monomer displays the same emission energy of the parent compound BT_2T_4, thus confirming again the lack of conjugation between the three lateral thiophene rings. While the introduction of the fused-ring units, as in BT_2CPDT_2 and BT_2E_4, allowing an extension of the π-conjugation, affords an important red shift of the emission band. As already observed in the absorption spectrum, the emission of BT_2BTD_2 results strongly red-shifted. This monomer displays also the longest emission lifetime and the highest photoluminescence quantum yield within the series, in agreement with the ICT character of the emission transition.

Backbone structure and rigidity, can have a significant effect on the photoluminescence quantum yield Φ of this kind of oligothiophenes. Indeed, the presence of the chemical bridge reduces the occurring of the interanular torsional vibrations, thus resulting in increased fluorescence. This effect is particularly evident for BT_2CPDT_2 and $BT_2(T_3)_2$, showing the highest and the lowest Φ values respectively (Φ = 21% for BT_2CPDT_2 and Φ = 8% for $BT_2(T_3)_2$). All the other monomers display Φ values which are intermediate with respect these two values. In particular it is interesting to note that the emission intensities of BT_2T_6 and of the analogous buthyl derivative BT_2T_6Bu, are lower than the emission of the parent compound BT_2T_4. Indeed,

the third thiophene ring provides an increase of the torsional and vibrational modes thus resulting in decreased emission intensities.

Moreover, the presence of the node, even if it should not preclude conjugative interaction, affords a distortion from the coplanarity of the two halves thus hampering the formation of an extended conjugated planar structure. The lack of vibrational structure in the emission spectra is in agreement with this hypothesis. Actually, the ground state of these oligothiophenes barely match the planar quinoid-like structure proposed for the excited states, thus requiring a greater conformational reorganization energy.

Ongoing from emission in solution to the solid state, the panorama is completely different. The more planar oligothiophenes display the lowest emission quantum yields. This is most probably due to the formation of π-π staking interactions between the molecules which leads to the formation of weakly emissive aggregated species predominantly in the solid state. In agreement with this hypothesis the emissions intensities of BT_2T_6Bu and of BT_2E_4, both containing substituents on the β positions on the lateral thiophenes having an important steric demand, result the highest ones within the series and, for BT_2E_4, even higher than the solution emission intensity.

On the other hand, the strong quenching of the emission observed for BT_2BTD_2 on passing from solution to solid state is correlated to the ICT nature of the transition which, in the solid state, could occur in intermolecular way, instead of in intramolecular one, affording a separation of charge and a quenching of the emission.

4.5.2. Electrochemical 3,3'-bithianaphthene monomer comparisons

Table 3 summarizes the electrochemical characteristics of the 3,3'-bithianaphthene monomers. Generally, all the monomers resulted to have similar electrochemical properties, with oxidation E_{onset} between 0.32 and 0.49 V *vs* $Fc|Fc^+$ redox couple and reduction E_{onset} between -2.21 and -2.43 V *vs* $Fc|Fc^+$.

BT_2DTP_2 showed slightly different electrochemical properties: the introduction of the dithienopirrole unit leads to an energy band gap of 2.65 V, similar to those found for the other analyzed monomers. However, both the oxidation and reduction onset potentials resulted to be at higher potential.

The properties of BT_2BTD_2 were found to be particularly remarkable: the introduction of the benzothiadiazole, indeed, led to strong increase of the reduction potential and, consequently, to

a decrease of the energy band gap. Additionally, HOMO and LUMO energies resulted to be particularly low.

	E^{ox}_{onset}/V *vs* Fc+|Fc	E^{red}_{onset}/V *vs* Fc+|Fc	Electrochemical band gap/eV	HOMO (eV)	LUMO (eV)
BT_2T_4	0.49	-2.43	2.92	-5.29	-2.37
BT_2T_6	0.32	-2.30	2.62	-5.12	-2.50
BT_2T_6Bu	0.35	-2.12	2.47	-5.15	-2.33
BT_2DTP_2	0.71	-1.94	2.65	-5.12	-2.47
BT_2CPDT_2	0.41	-2.21	2.62	-5.21	-2.59
BT_2E_4	0.05	-2.37	2.42	-4.75	-2.43
BT_2BTD_2	0.53	-1.72	2.25	-5.85	-3.62

Table 3: Electrochemical characterization of 3,3'-bithianaphthene monomers. Analysis were carried out in ACN + 0.1 M $TBAPF_6$, 200 mV s^{-1}.

5. Electroactive materials based on 2,2’-biindole scaffold

In order to expand the investigation on inherently chiral materials, in parallel to the monomers characterized by a 3,3’-bithianaphthene atropisomeric scaffold, a different class of inherently chiral compounds, based on the 2,2-biindolic core, was investigated. The first member of this family, namely the *N*-methyl derivative (3,3'-bis(2,2'-bithiophen-5-yl)-1,1'-bismethyl-1*H*,1'*H*-2,2'-biindole) **39a** (reported in Figure 74), had been synthesized some years ago and the choice of this atropisomeric core was based both on electronic and steric considerations.

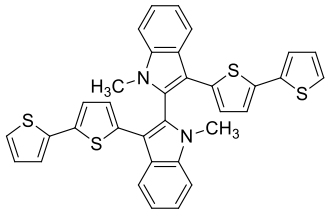

39a

Figure 74: Structural formula of IND_2T_4Me **39a**.

As for the electronic properties, the oxidative potential of the biindole core, much electron richer than the bithianaphthene scaffold, results to be very low, allowing to perform the enantiorecognition tests in a hitherto unexplored potential region.

By means of DFT calculations the structure of the more stable conformers of BT_2T_4 and IND_2T_4Me was determined: the dihedral angles of the biheteroaromatic scaffolds resulted to be very different, moving from 82° for BT_2T_4 to 115° for IND_2T_4Me (Figure 75).

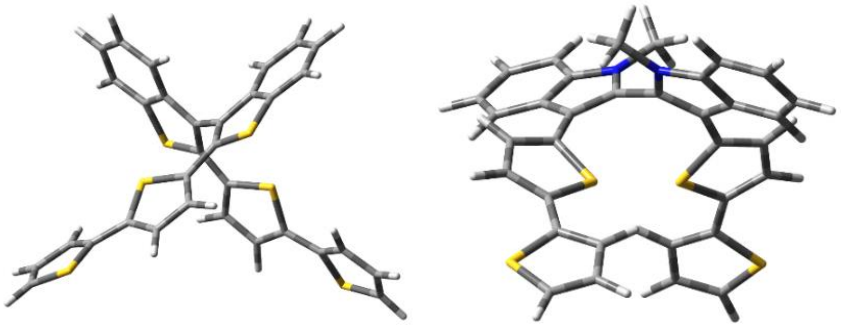

Figure 75: Geometry of the most stable conformers of BT_2T_4 (left) and IND_2T_4Me (right). DFT calculations at B3LYP/TZVP level of theory.

Furthermore, the biindole core can be easily functionalized at the nitrogen atoms allowing a simple tuning of some properties of the final material important for applicative purposes, such as solubility and processability.

Racemic IND_2T_4Me was electrochemically characterized. The complete CV pattern of monomer **39a**, recorded at 200 mV s^{-1} scan rate, in CH_2Cl_2 + 0.1 M $TBAPF_6$ solution, is reported in Figure 76 A. It is characterized by numerous oxidation peaks: the first couple of reversible oxidation peaks corresponds to the oxidation of the biindolic core, while the second pair of peaks corresponds to the oxidation of the bithiophene moieties.

The electrodeposition of IND_2T_4Me on GC electrode over thirty-six consecutive potentiodynamic cycles is reported in Figure 76 B: the growth of the oligomeric film is smooth and regular and the electrodeposited film was found highly stable under repeated oxidative cycles.

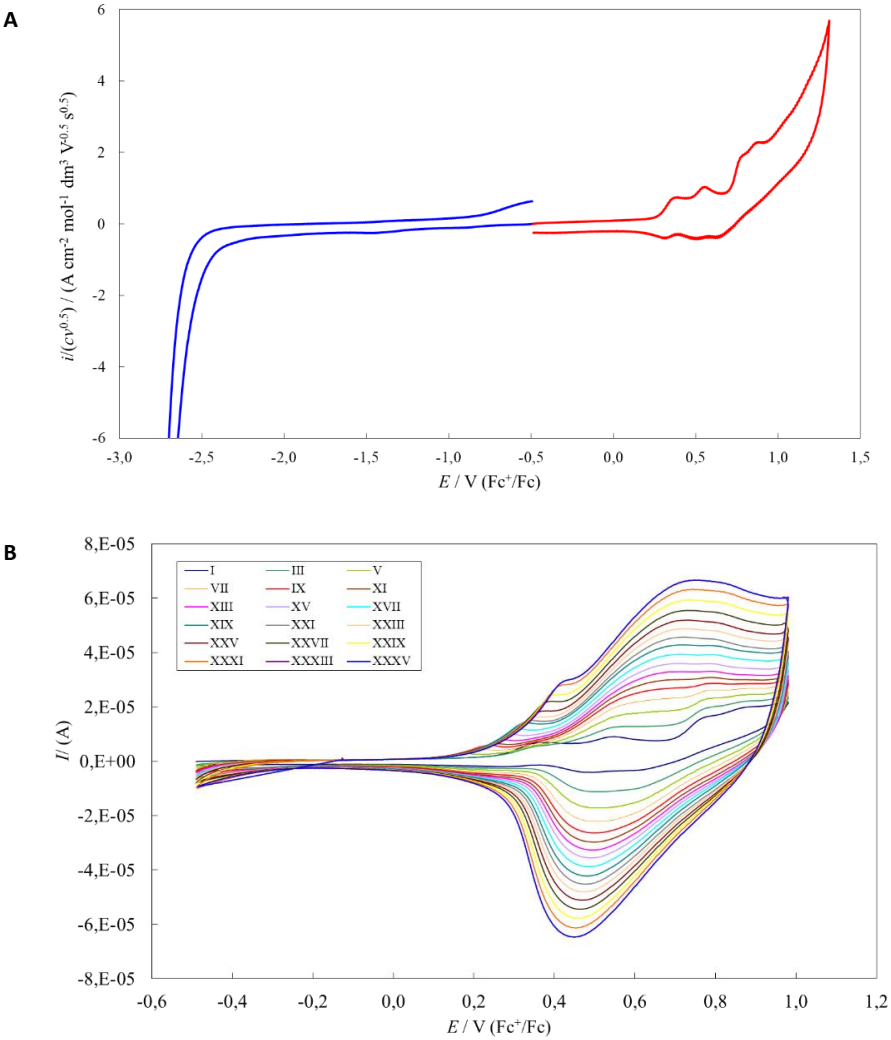

Figure 76: A) Complete CV pattern of IND_2T_4Me monomer (0.5 mM), 200 mV s^{-1} scan rate, solvent: CH_2Cl_2 + 0.1 M $TBAPF_6$. B) Potentiodynamic electro-oxidation of IND_2T_4Me on GC electrode. Thirty-six consecutive cycles at 200 mV s^{-1} scan rate, 0.5 mM of IND_2T_4Me in CH_2Cl_2 + 0.1 M $TBAPF_6$.

The racemate was resolved into antipodes through semi-preparative HPLC on a chiral stationary phase. The HPLC chromatograms, CD detected, of the racemate and of pure enantiomers are reported in Figure 77.

The $[\alpha]_D^{20}$ values are +808° and -818° (0.1 M in $CHCl_3$) for the first and the second eluted enantiomer respectively.

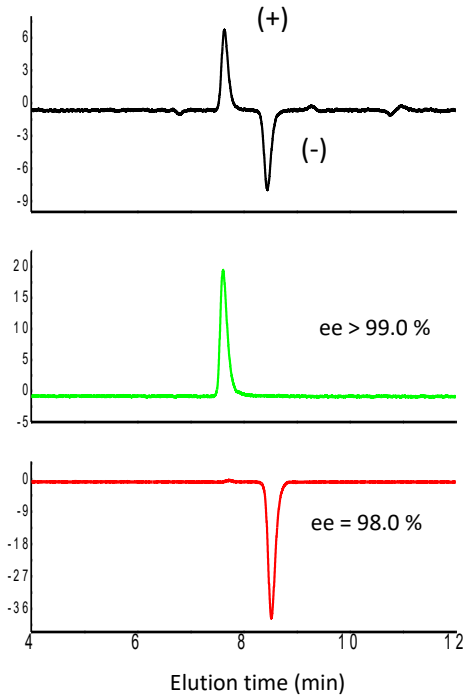

Figure 77: Analytical esolution of the racemate of IND_2T_4Me through HPLC on a chiral stationary phase. CSP: Chiralpak IB-3 (250 mm x 4.6 mm I.D.), eluent: *n*-hexane : CH_2Cl_2 : ethanol 100 : 5 : 1, flow rate: 1 mL/min, temperature: 25°C, detector: UV and CD at 380 nm.

The enantiopure antipodes of IND_2T_4Me were fully characterized from a chiroptical point of view. The ECD and the CPL spectra are reported in Figure 78.

The antipodes exhibited remarkable g_{lum} values (3.0×10^{-3}) similar to that showed by BT_2T_4 enantiomers. The absolute axial configuration was assigned by comparison of the ECD profile of the first eluted monomer with the calculated ECD profile for the (*S*) enantiomer (Figure 78 B).

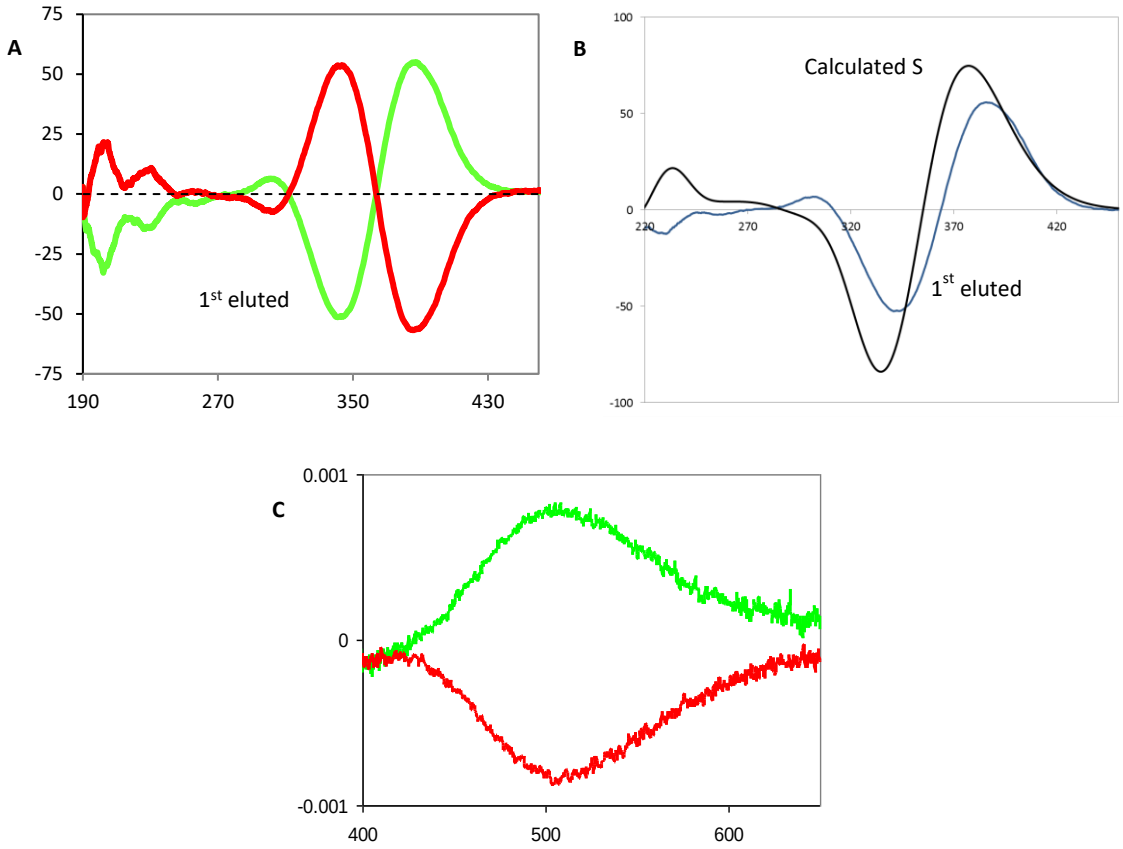

Figure 78: A) CD profiles of (+)-**39** (green) and (-)-**39** (red). B) Experimental and calculated ECD and absorption spectra for the first eluted monomer (*S*). C) CPL of (+)-**39** (green) and (-)-**39** (red).

Prompted by the preliminary interesting results obtained for the IND_2T_4Me, a deeper investigation on this monomer was carried out under different perspectives during the present PhD research project: in particular, the chemical oxidation was studied for the first time and some interesting enantiorecognition experiments were performed.

5.1. The family of the *N*-alkylderivatives of the 3,3'-bis(2,2'-bithiophen-5-yl)-1*H*,1'*H*-2,2'-biindole

The general synthetic pathway, reported in Scheme 15, of the 2,2'-biindole based monomers is a variant of the Larock reaction, that is particularly advantageous since it allows the formation of the interanular bond between the two indole units and their functionalization with the heteroarylic substituents in a single step.[63]

The classical Larock reaction was reported for the first time in 1991 and found wide application for the preparation of a wide variety of indoles with different substituents.[64] Larock heteroannulation is a palladium-catalyzed chemoselective and "ligandless" heteroannulation

between *ortho*-iodoanilines and disubstituted alkynes to form substituted indole derivatives: the catalytic cycle is reported in Scheme 14.

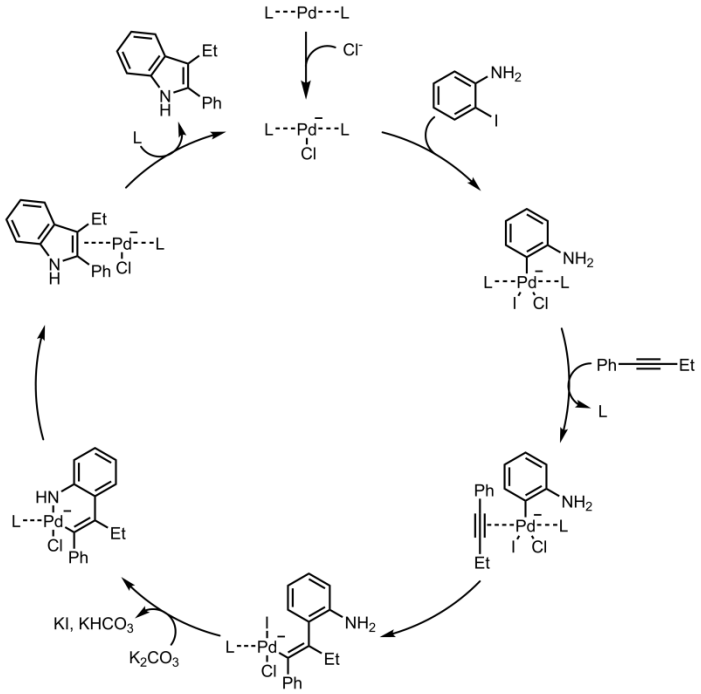

Scheme 14: Catalytic cycle of the classic Larock Pd-catalyzed heteroannulation.

As anticipated, we used an interesting variant of the Larock reaction presented by Abbiati[63] for the preparation of 2,2'-biindole derivatives functionalized in position 3 with different aryl substituents.

The reaction requires a double alkyne derivative, namely the 2,2,2-trifluoro-*N*-(2-(4-[2,2,2-trifluoro-acetylamino-phenyl]-buta-1,3-diynyl)-phenyl)-acetamide **41** and a suitable aromatic haloderivative. We exploited this strategy using heteroaromatic iododerivatives and, for the synthesis of this family, we employed the 5-iodobithiophene **42**, obtained by direct iodination with *N*-iodosuccinimide in 1 : 1 $CHCl_3$: acetic acid solution.

Compound **40** was synthesized, according to the literature procedure, from commercially available 2-iodoaniline that underwent a Sonogashira palladium-catalyzed reaction in the presence of ethynyltrimethylsilane (TSA) and copper(I) iodide in triethylamine as a solvent. The 2-alkynyl aniline was not isolated and, after deprotection of the trimethylsilyl group by means of KF, underwent a Glaser coupling in the presence of oxygen as oxidant with copper (I) as a catalyst.[65] Product **41** was then obtained in good yields by acylation of **40** with trifluoracetic anhydride in a pyridine and CH_2Cl_2 solution The trifluoroacetyl group is crucial for the subsequent Larock coupling reaction, since it reduces the nucleophilicity of the nitrogen atoms and directs the catalyst to selectively bind to the alkyne to promote the closure of the indole

ring. The last step was the above mentioned palladium mediated Larock coupling that gave the 3,3'-bis(2,2'-bithiophen-5-yl)-1*H*,1*H*'-2,2'-biindole (**43**) in acceptable yields.

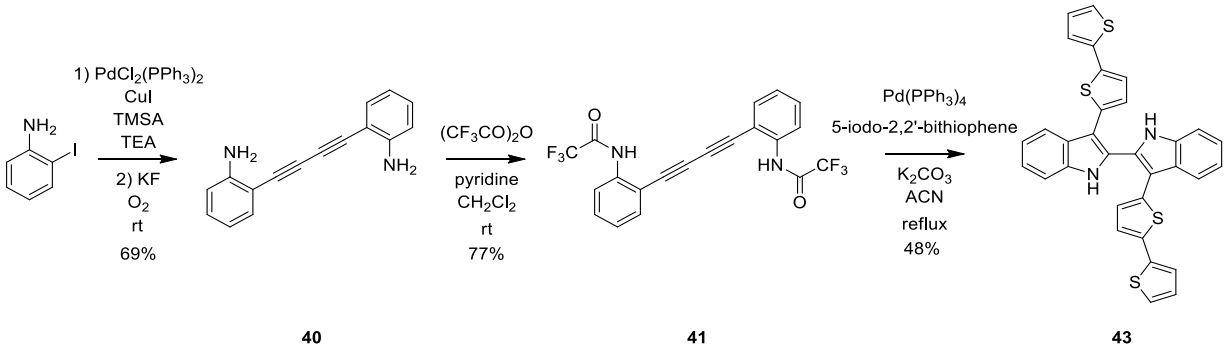

Scheme 15: Synthesis of the 3,3'-bis(2,2'-bithiophen-5-yl)-1*H*,1'*H*-2,2'-biindole (IND_2T_4H) **43**.

The 2,2'-biindole derivatives **43** was used as the key intermediate for access all the alkylated derivatives **39a-d**. The final step consists in the reaction of the appropriate alkyl iodine with the dianion generated by using KOH in *N,N*-dimethylformamide at 0 °C.

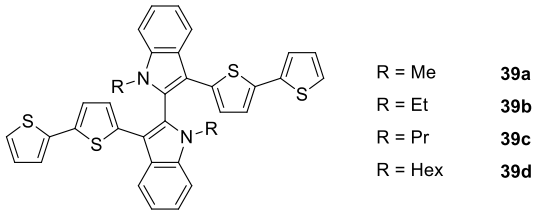

Figure 79: Structural formula of IND_2T_4 derivatives with differen *N*-*n*-alkylic chains.

The racemates of all the mentioned *N*-alkylated compounds were resolved into antipodes at analytical level by HPLC on CSP (chiral stationary phase). The HPLC chromatograms are reported in Figure 80. It is interesting to observe that, as the length of the alkylic chains increases, the separation of the two antipodes is easier. In particular, a very good resolution was obtained when the biindole scaffold was functionalized with propyl and hexyl groups.

Additionally, it was observed an inversion of the absolute configuration of the first eluted enantiomer by moving from the *N*-methyl to the *N*-ethyl derivatives.[66]

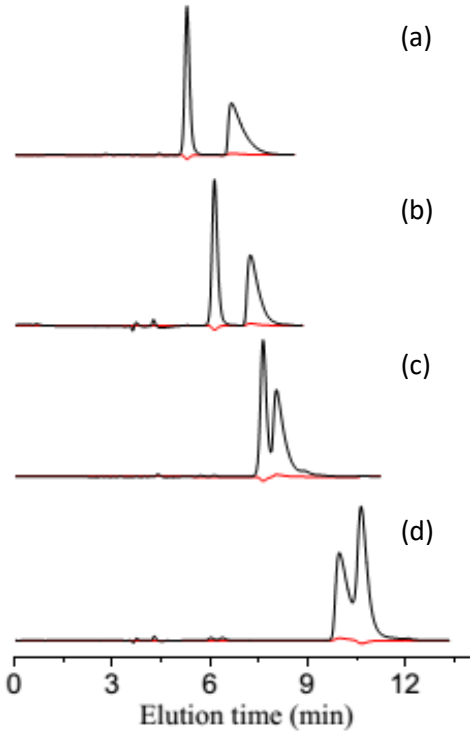

Figure 80: Analytical resolution of the racemate of A) IND_2T_4Hex B) IND_2T_4Pr C) IND_2T_4Et D) IND_2T_4Me through HPLC on a chiral stationary phase. CSP: Chiralpak IB-3 (250 mm x 4.6 mm I.D.), eluent: *n*-hexane : ethanol 100 : 10, flow rate: 1 mL/min, temperature: 25°C.

Unfortunately, the monomer functionalized with hexyl groups was found to be too soluble for electrochemical purposes and, consequently, its use for the preparation of chiral surfaces was limited, despite the easy racemate resolution process.

The monomer functionalized with methyl groups gives very stable oligomeric films, but the resolution process is long and tedious due to the small difference between the retention times of the antipodes. A good compromise between electrochemical feasibility and racemate resolution was found in IND_2T_4Pr.

The electrochemical characterization of IND_2T_4Pr and subsequent potentiodynamic film deposition are reported in Figure 81.

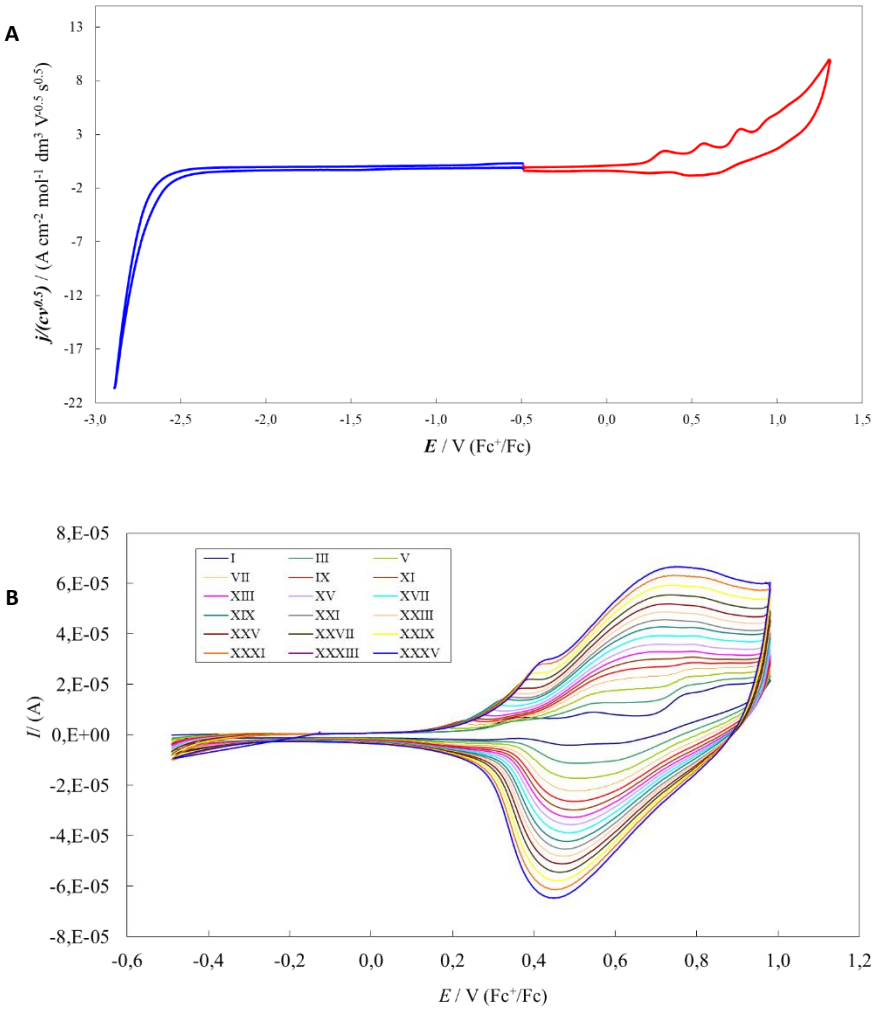

Figure 81: A) Complete CV pattern of IND_2T_4Pr monomer (0.5 mM), 200 mV s^{-1} scan rate, solvent: CH_2Cl_2 + 0.1 M $TBAPF_6$. B) Potentiodynamic electro-oxidation of IND_2T_4Pr on GC electrode. Thirty-six consecutive cycles at 200 mV s^{-1} scan rate, 0.5 mM of IND_2T_4Pr in CH_2Cl_2 + 0.1 M $TBAPF_6$.

A preliminary enantiorecognition test was carried out on the enantiopure oligomeric films of (*S*)-IND_2T_4Me and (*R*)-IND_2T_4Pr, which are the first eluted monomers in the resolution process. The enantiomers of the *N,N*-dimethyl-1-ferrocenylethylamine were used as probes, which provided an electrochemical and chemically reversible peak in a region where the conjugated film is still neutral (Figure 83 A). The results were really outstanding: the separation between the oxidative peaks of the two enantiomers was found 270 mV.

Furthermore, the oxidation potential value of the *S* probe resulted to be the lower on the film derived from the electrooxidation of the first eluted enantiomer of IND_2T_4Me (Figure 82 A), while it showed the higher oxidative potential value on the film derived from the electrooxidation of the first eluted enantiomer of IND_2T_4Pr. This was a proof of the inversion of the configuration of the eluted enantiomers during the racemate resolution processes.

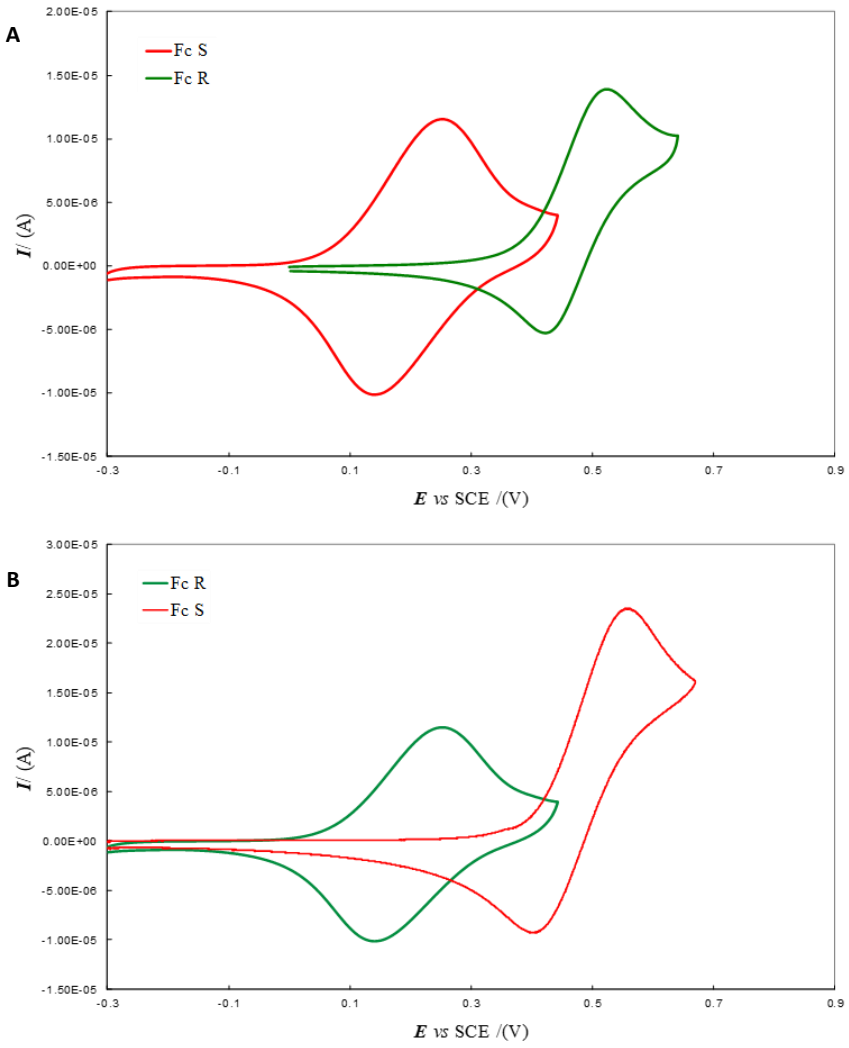

Figure 82: Enantiorecognition tests on enantiopure ec-p(IND_2T_4Me). A) (*S*)-ec-p(IND_2T_4Me) (deposited from thirty-six cycles 0.5 mM monomer solution in CH_2Cl_2 + $TBAPF_6$, 200 mV s^{-1} scan rate on GC electrode) in the presence of (*R*)- and (*S*)-enantiopure *N,N*-dimethyl-1-ferrocenylethylamine (2 mM) in CH_2Cl_2+ 0.1 M $TBAClO_4$ solution, 50 mV s^{-1} scan rate. B) A) (*R*)-ec-p(IND_2T_4Pr) (deposited from thirty-six cycles 0.5 mM monomer solution in CH_2Cl_2 + $TBAPF_6$, 200 mV s^{-1} scan rate on GC electrode) in the presence of enantiopure (*R*)- and (*S*)- *N,N*-dimethyl-1-ferrocenylethylamine (2 mM) in CH_2Cl_2 + 0.1 M $TBAClO_4$ solution, 50 mV s^{-1} scan rate.

Additional enantiorecognition experiments were carried out on the films derived from the electrooxidation of both the enantiomers of IND_2T_4Me.

Madopar®, a drug used for the treatment of Parkinson disease, which consists in a 4:1 mixture of L-DOPA and benserazide, was used as probe: it is. A single oxidation peak was observed. Also in this case the enantiodiscrimination was very high: the difference between the oxidation potential values is 140 mV.

The third test (Figure 83 B) was carried out with Ketoprofen, a very popular non-steroidal anti-inflammatory drug (NSAID), in CH_2Cl_2 solution + $TBAPF_6$ as a support electrolyte. The electrochemical reduction of the ketonic function is involved in this test. Great enantiodiscrimination (about 330 mV) was observed also in this case, which deserves special

attention since it is one of the rare examples of enantioselection observed in the cathodic region.

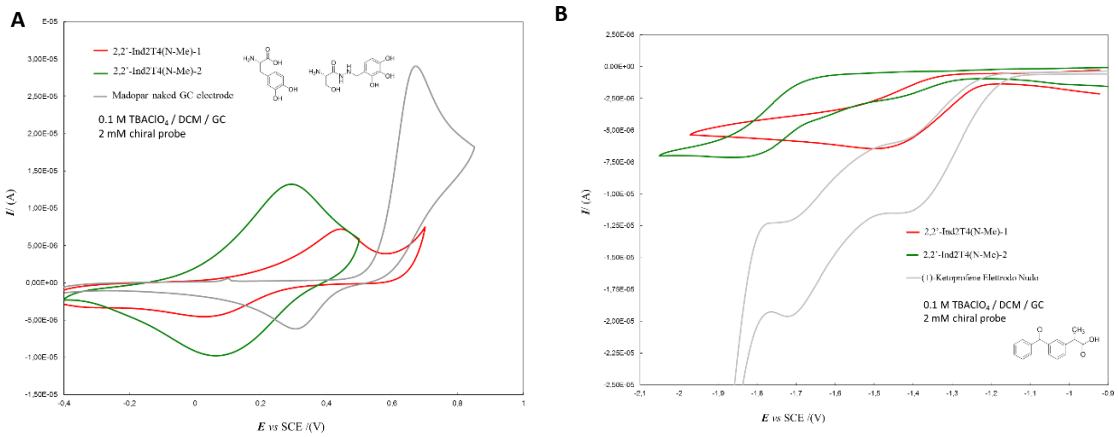

Figure 83: Enantiorecognition tests on enantiopure ec-p(IND_2T_4Me). A) (*S*)-ec-p(IND_2T_4Me) (red) and (*R*)-ec-p(IND_2T_4Me) (green) (deposited from thirty-six cycles 0.5 mM monomer solution in CH_2Cl_2 + $TBAPF_6$, 200 mV s^{-1} scan rate on GC electrode) in the presence of Madopar drug (2 mM), in HCl + water at pH 2, 50 mV s^{-1} scan rate. B) (*S*)-ec-p(IND_2T_4Me) (red) and (*R*)- ec-p(IND_2T_4Me) (green) (deposited from thirty-six cycles 0.5 mM monomer solution in CH_2Cl_2 + $TBAPF_6$, 200 mV s^{-1} scan rate on GC electrode) in the presence of Ketoprofen drug (2 mM), in CH_2Cl_2 solution + 1 M $TBAClO_4$, 50 mV s^{-1} scan rate.

Racemate IND_2T_4Me was chemically oxidized by adding the monomer to a $FeCl_3$ slurry in dry $CHCl_3$. The residue, obtained after Soxhlet extraction with THF, was submitted to a purification process by gravimetric column chromatography, in order to isolate each single oligomer. Each fraction was analyzed by HR-MALDI and in Figure 84 the spectra of the two main fractions collected during the chromatographic process are reported.

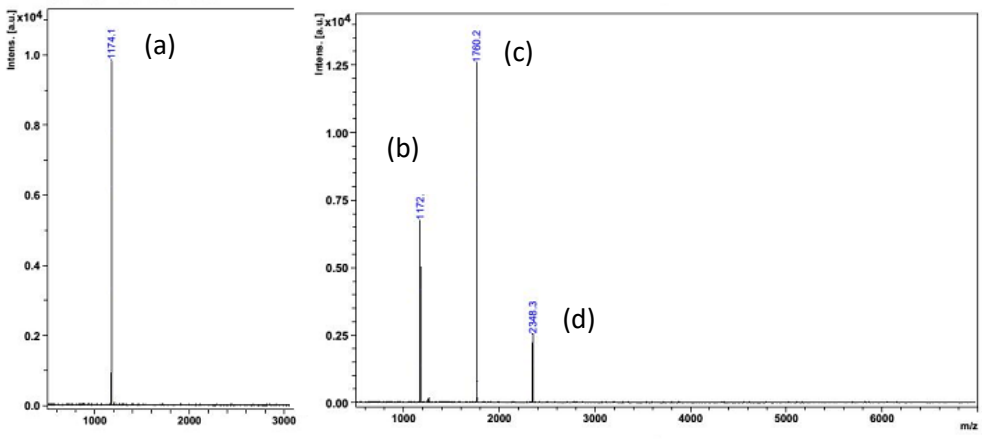

Figure 84: MALDI analysis of the $FeCl_3$ oxidation products of IND_2T_4Me separated by column chromatography, after extraction with THF. Mass spectrum corresponding to linear dimers (a), left. Mass spectrum corresponding to a mixture of cyclic dimers (b), cyclic trimers (c) and cyclic tetramers (d), right.

The first fraction was constituted by the linear dimer while, the second fraction, was constituted exclusively by cyclic oligomers, namely dimers, trimers and tetramers according to what previously observed for the $FeCl_3$ oxidation of the analogous monomer based on the 3,3'-bithianaphthene scaffold.

5.2. Synthesis of 2,2'-bis{2-[7-(thiophen-2-yl)-2,1,3-benzothiadiazol-4-yl]thiophen-5-yl}-*N*,*N*'-dihexyl-1*H*,1'*H*-2,2'-biindole, IND_2BTD_2Hex

As shown in the previous chapter, monomer BT_2BTD_2, characterized by the presence of the benzothiadiazole system, is endowed by some peculiar opto-electronic features. The λ_{max} in the emission and absorption spectra are red-shifted by 100 nm compared to the values measured for other monomers. In addition, the half-life time of the charged species is from 5 to 10 times higher, while the quantum yield in solution, which is around the 12% for the other monomers, reaches the 50%.

Unfortunately, the scarce solubility of the compound, and the even lower solubility of the oligomers resulting from its oxidation, makes BT_2BTD_2 difficult to employ for applicative purposes. For this reason, the synthesis of a new monomer, based on the structure of 2,2'-biindole was planned, in the perspective of obtaining a derivative with similar optoelectronic properties, but more soluble and, therefore, more easily processable.

Furthermore, the new monomer would be the first example of the 2,2'-biindole series in which the atropisomeric system is functionalized with a sequence of three heteroaromatic units which could produce, after oxidation, cyclic oligomers quite larger than those obtained from all the other members of this family investigated so far.

The synthesis of this new monomer, nicknamed IND_2BTD_2Hex, was planned according to the strategy developed for the other monomers of this class, that requires the availability of a suitable haloderivative as intermediate.

The synthesis of the iododerivative **44a** was carried out with NIS in a 2:1 mixture of $CHCl_3$ and acetic acid, as described in literature[67]

Unfortunately, the monoiododerivative was obtained together with considerable amounts of the diiododerivative which was found difficult to remove. Obviously, the presence of the latter would have strongly complicated the subsequent reaction due to the formation of oligomers derived from its coupling with butadiine **40**.

In order to plan a clean reaction, we resorted to the preparation of the bromoderivative **44b**, which was affected by reaction of compound **36** with NBS in a 1:1 mixture of CH_2Cl_2 and acetic acid. The formation of the dibromoderivative was surprisingly not observed under these experimental conditions and the bromoderivative **44b** was isolated in a pure state in 95% yields.
The palladium mediated Larock coupling was carried out in DMF solution, instead that in acetonitrile, in order to grant both the solubilization of compound **44b** and a higher reaction temperature, given the expected lower reactivity of the bromoderivative in comparison with the corresponding iodocompound. Unfortunately, the Larock coupling took place in very low yields and a further optimization of the reaction conditions is certainly required.
The last step of the sequence was the introduction of two *n*-hexyl groups, which was carried out with sodium hydride as deprotonating agent in DMF at room temperature. Compound **46** was isolated in moderate yields, together with some amount of the monosubstituted product.

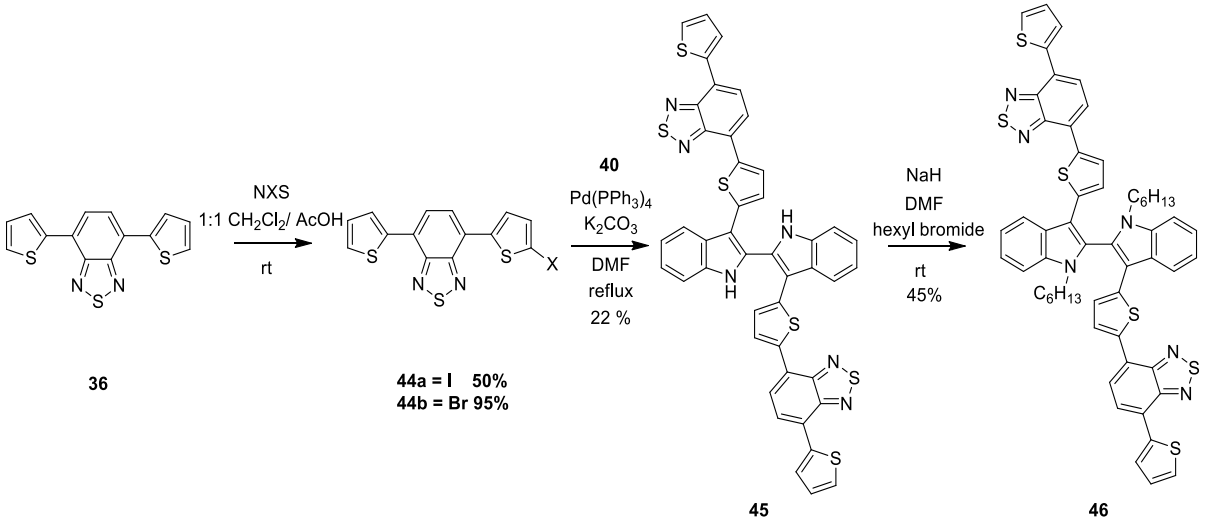

Scheme 16: Synthesis of 2,2'-bis{2-[7-(thiophen-2-yl)-2,1,3-benzothiadiazol-4-yl]thiophen-5-yl}-*N*,*N*'-dihexyl-1*H*,1'*H*-2,2'-biindole, IND_2BTD_2Hex **46**.

Compound IND_2BTD_2Hex was electrochemically characterized both as monomer and as oligomeric film (Figure 85 A and B). The oxidative pattern was found to be very similar to the above-mentioned IND_2T_4Me and IND_2T_4Pr while the reductive pattern resulted to be characterized by the presence of two consecutive electrochemically and chemically reversible peaks related to the presence of the benzothiadiazole units. The deposition proceeded regularly in CH_2Cl_2 and the pattern resembles that of IND_2T_4Me.

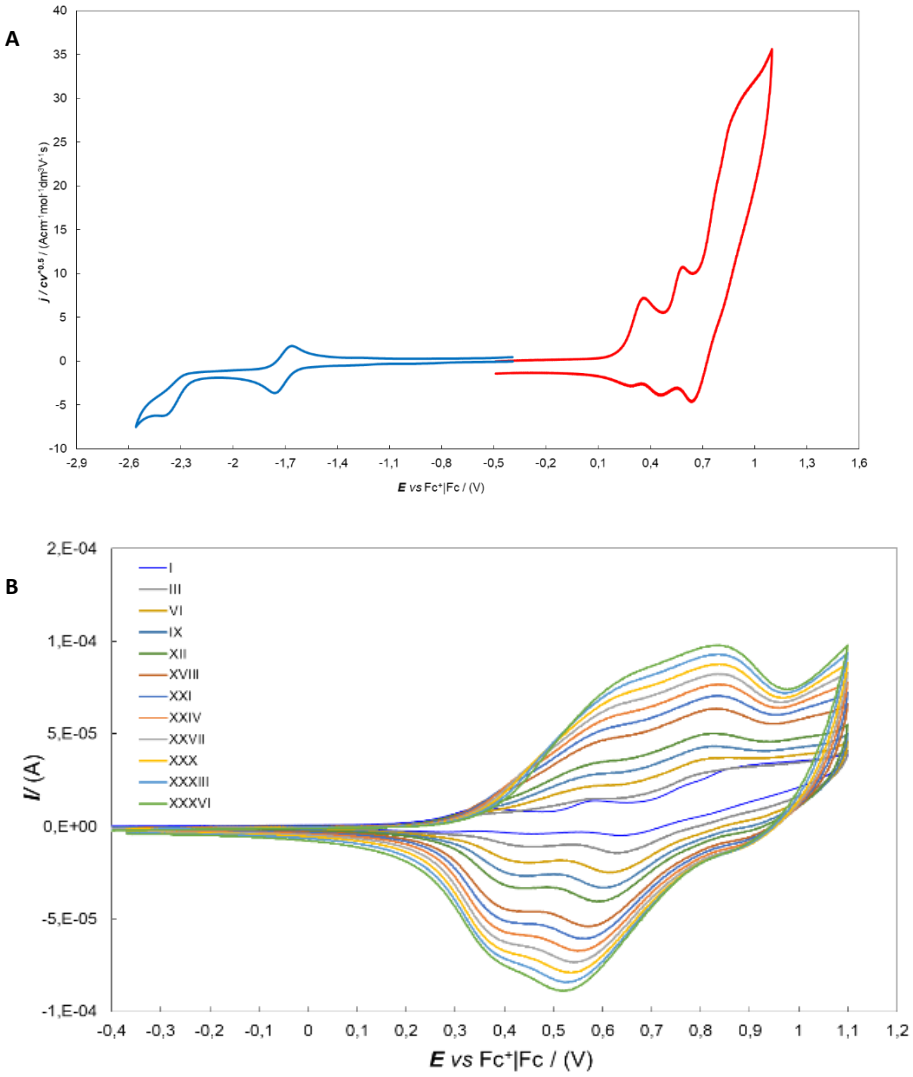

Figure 85: A) Complete CV pattern of IND_2BTD_2Hex monomer, 200 mV s^{-1} scan rate, solvent: CH_2Cl_2 + 0.1 M $TBAPF_6$. B) Potentiodynamic electro-oxidation of IND_2BTD_2Hex on GC electrode. Thirty-six consecutive cycles at 200 mV s^{-1} scan rate, 0.5 mM of IND_2BTD_2Hex in CH_2Cl_2 + 0.1 M $TBAPF_6$.

After the analysis performed on the racemate, compound **46** was resolved into antipodes at analytical level by HPLC on a chiral stationary phase.

Figure 86 reports the chromatogram corresponding to the separation of the two enantiomers that resulted to be well defined.

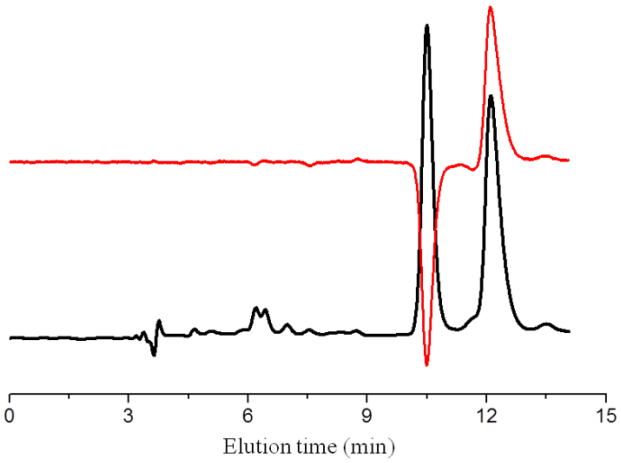

Figure 86: Analytical resolution of the racemate of IND_2BTD_2 through HPLC on a chiral stationary phase. CSP: Chiralpak IB (250 mm x 4.6 mm I.D.), eluent: *n*-hexane : IPA : CH_2Cl_2 100 : 5 : 2, flow rate: 1 mL/min, temperature: 40°C, detector: UV (black) and CD (red) at 380 nm.

5.3. Photophysical 2,2'-biindole monomers comparisons

The photophysical data of the absorption and of the emission spectra of the 2,2'-biindole based monomers, recorded in diluted, air-equilibrated dichloromethane solution at room temperature, are reported in Table 4.

	λ_{abs} (solution) (nm)	λ_{em} (solution) (nm)	Lifetime τ (ns)	Quantum yield Φ (solution)	ε [M^{-1} cm^{-1}]
BT_2T_4	398	535	1.95	21%	48000
IND_2T_4H	324	523	1.26	20.5%	35000
IND_2T_4Me	364	503	1.12	15%	31000
IND_2T_4Et	363	502	1.01	12%	37000
IND_2T_4Pr	363	499	0.99	11.5%	34000
IND_2BTD_2Hex	325; 503	695	-	31%	-
BT_2BTD_2	358; 485	633	6.3	51%	38500

Table 4: Optical characterization of 2,2'-biindole monomers. Values were recorded in CH_2Cl_2 deaerated solution.

As the analogous benzothiophene derivatives, all these new chiral monomers upon optical excitation display an intense emission in the yellow region of the visible spectrum. However, the absorption maxima of the chiral monomers based on 2,2'-biindole scaffold resulted blue-shifted with respect to the parent monomer BT_2T_4. This blue shift is presumably due to the different electron density of the indole ring which is higher than that of the benzo-thiophene system.

The electrochemical data, reported in paragraph 4.5.2, confirmed this hypothesis; indeed, in comparison with the HOMO and LUMO levels of BT_2T_4, the LUMO and, with less extent also the HOMO levels of the IND_2Me result destabilized.

However, as expected, the substitution at the nitrogen atoms does not affect the photophysical properties of the molecules (Figure 87). Indeed, as reported in Table 4, no differences of the maxima of the absorption and emission bands were observed moving from the methyl to the propyl derivative, together with the same molar extinction coefficients and photoluminescence quantum yields.

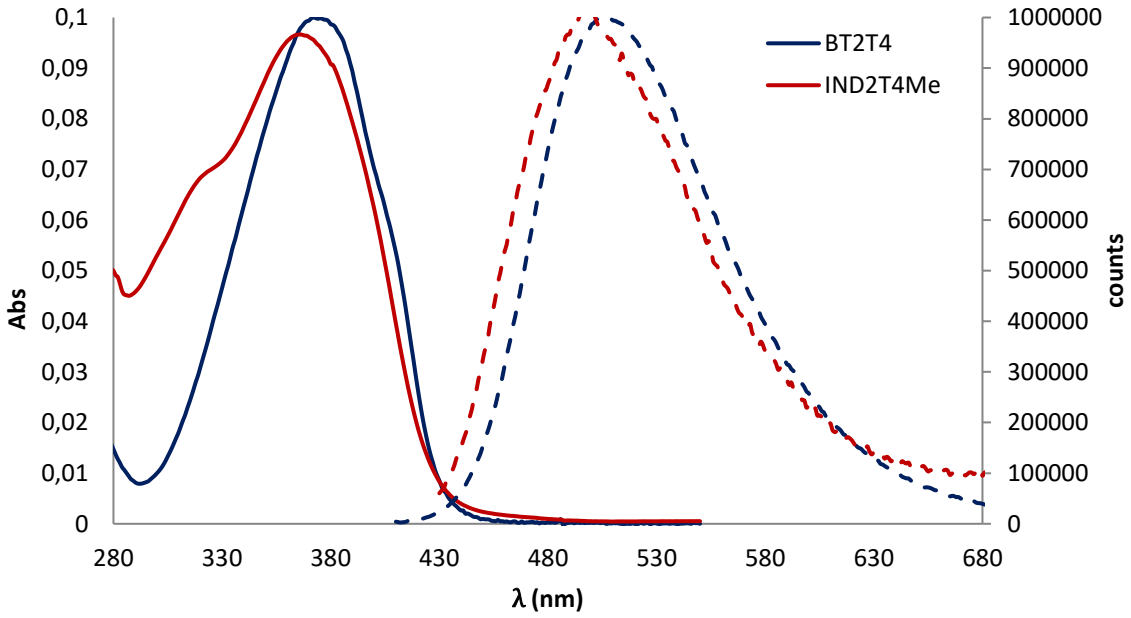

Figure 87: UV profile (solid lines) and fluorescence profile (dashed line) of BT_2T_4 and IND_2T_4Me. Profiles were recorded in CH_2Cl_2 deaerated solution.

As already reported for the benzothiophene derivative BT_2BTD_2, also in this case a special behavior were shown by the biindolic derivative functionalized with the benzothiadiazole moiety as lateral substituents of the atropoisomeric scaffold (Figure 88). Two different absorption bands were observed, the higher energy band attributable to the π-π^* transition, while the lower energy band is due to the ITC transition between the electron donor biindolic moiety and the benzothiadiazole acceptor unit.

If compared with the absorption spectrum of the analogous BT_2BTD_2, the higher energy band is strongly blue-shifted, while the lower energy band resulted moderately red-shifted (only 10 nm vs a blue shift of about 50 nm for the higher energy band).

This behavior is in agreement with the electrochemical data underlying again that the electronic structure of the biindolic system mainly affect the LUMO level, destabilizing it and therefore increasing the π-π* energy gap. On the contrary to the HOMO level, involved in the ICT transition, is only slightly destabilized with respect the HOMO level of BT_2BTD_2 and, therefore, the position of the ICT band is only 10 nm red shifted. Finally, the emission maximum resulted red-shifted (695 nm vs 633 nm) and partially quenched in agreement with the low energy gap value.

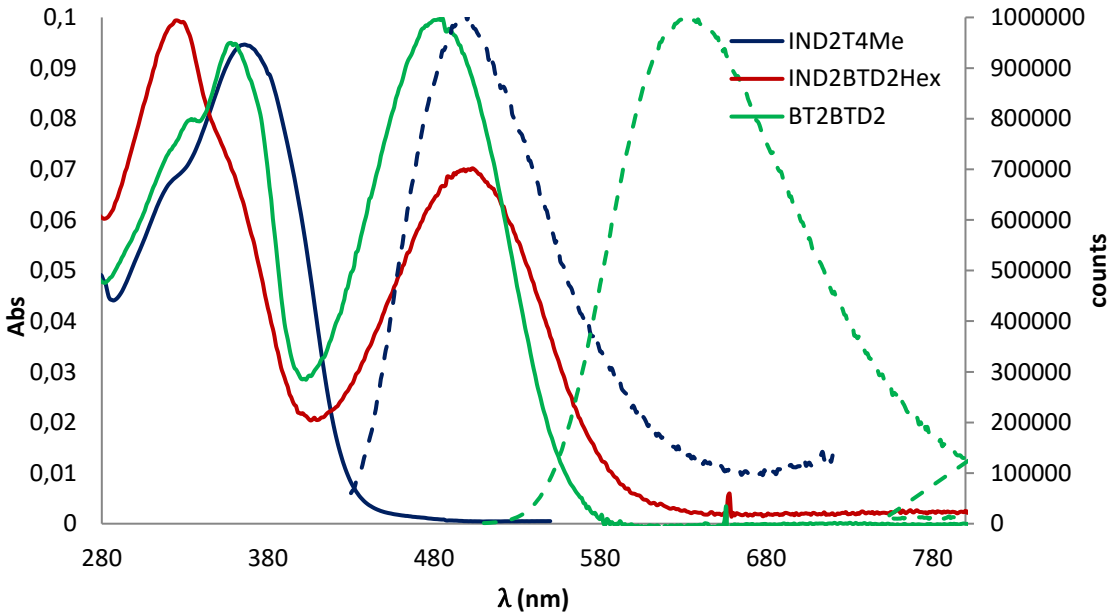

Figure 88: UV profile (solid lines) and fluorescence profile (dashed line) of IND_2T_4Me, IND_2BTD_2Hex and BT_2BTD_2. Profiles were recorded in CH_2Cl_2 deaerated solution.

6. Approaches to large scale resolution of racemates

All the monomers investigated so far present a drawback for their application on a large-scale level in the enantiopure form, namely the resolution into antipodes, which is achieved by HPLC on a chiral stationary phase at a semi-preparative level. This is a very powerful method even if expensive for the large consumption of solvents, tedious and time-consuming. We considered the resolution of the racemates into antipodes by HPLC on CSP a so critical bottleneck that we felt mandatory to find an alternative resolution method. We envisaged two different strategies as the most promising ones to reach this goal: the introduction into the molecule of two new identical homotopic stereogenic elements and the synthesis starting from enantiopure scaffolds. The results we obtained in experimentally testing the feasibility of these approaches are reported in the following paragraphs.

6.1. Introduction of new stereogenic elements

The first monomer synthesized according to the above-mentioned strategy was designed by exploiting a cornerstone concept: the introduction of an additional stereogenic element on a couple of enantiomers leads to the formation of diastereoisomers that, by definition, have different chemical-physical properties and, in principle, are separable through classic methodologies, such as fractional crystallization or chromatography on an achiral stationary phase.

The presence of two functionalizable nitrogen atoms in the 2,2'-bindole scaffold was considered very useful for the introduction of two homomorphic chiral pendants characterized by a carbon stereocenter.

The selected pendant was the 1-phenylethyl, group which was introduced using both the enantiomers of the 1-bromo-ethylbenzene as alkylating agent.

The enantiopure antipodes of 1-bromoethylbenzene, unfortunately, are not commercially available and they were synthesized starting from enantiopure (*R*)- and (*S*)-phenylethanol. They were converted into the corresponding bromoderivative with phosphorus oxybromide in dry pentane solution, in the presence of pyridine. The substitution reaction does not proceed through a pure $S_{N}2$ mechanism, as reported in the Scheme 17, since partial racemization was

observed, as demonstrated by the enantiomeric excesses of the resulting bromoderivatives which were found to range from 76 to 86%.

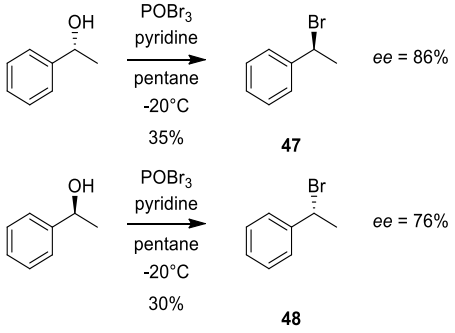

Scheme 17: Synthesis of (*S*)-1-bromoethylbenzene **47** and (*R*)-1-bromoethylbenzene **48**.

Biindole alkylation was carried out in DMF using KOH as a base; the theoretical stereochemical outcome of the alkylation reaction is reported in Scheme 18.

Obviously, the incomplete enantiomeric purity of the alkylating reagents complicates the stereochemical outcome of the *N*-alkylation; indeed, eight possible stereoisomers could be formed in the reaction, even if in different ratios. As expected, the most abundant stereoisomers should be those characterized by identical configuration of the stereogenic carbons.

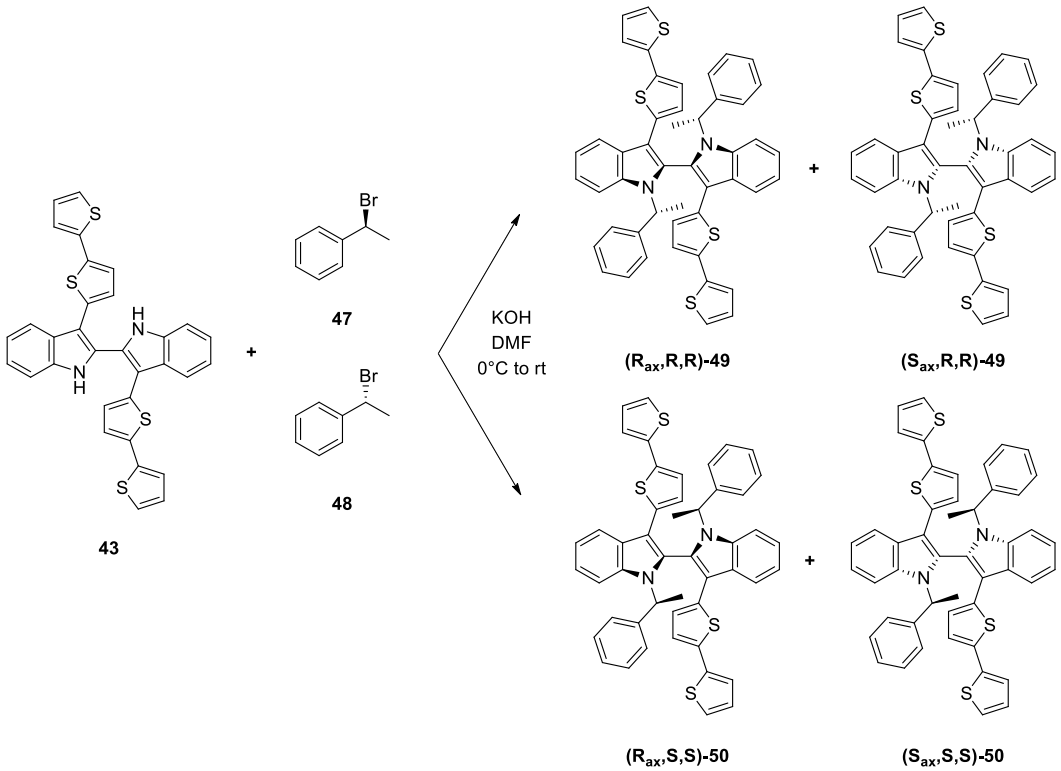

Scheme 18: Synthesis of 3,3'-bis(2,2'-bithiophen-5-yl)-1,1'-bis((*R*)-1-phenylethyl) -1*H*,1'*H*-2,2'-biindole IND_2T_4(*R*)Ph **49** and 3,3'-bis(2,2'-bithiophen]-5-yl)-1,1'-bis((*S*)-1-phenylethyl)-1*H*,1'*H*-2,2'-biindole IND_2T_4(*S*)Ph **50**.

Several stereoisomers were clearly distinguishable in the ^{1}H-NMR spectra. Their isolation by column chromatography was, however, difficult since they exhibited quite similar R_f values, exception made for the most retained one, which was obtained in an about 15% yield.

According to the previous observation, these stereoisomers should be characterized by the presence of pendants with the identical configuration at the stereogenic center but with undetermined configuration of the stereogenic axis. Furthermore, the inversion of the configuration of the stereogenic center of the alkylating reagent was assumed, with consequent formation of the (*R*,*R*) diastereoisomers from the (*S*)-bromoderivative and of the (*S*,*S*)-ones from the (*R*)-bromoderivative.

Furthermore, a sample of the stereoisomer obtained from (*R*)-1-bromoethylbenzene was analyzed by HPLC on a chiral stationary phase. The chromatogram, reported in Figure 89, showed the presence of a main peak with an area of ~ 92.5%. Furthermore, two other stereoisomers with shorter retention times are distinguishable, the first eluted one in a 7.5% percentage, and the second one in traces.

Considering that the stereogenic axis is expected to give a much greater contribution to the chiroptical properties of these compounds than the stereocenters, the minor components of the mixture should be related to stereoisomers with opposite configuration of the stereogenic axis. One with opposite CD profile should be the related enantiomer.

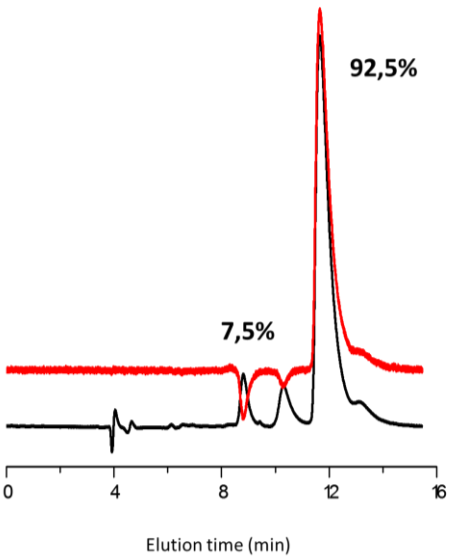

Figure 89: Stereoisomeric purity control of IND_2T_4(*S*)Ph through HPLC on a chiral stationary phase. CSP: Chiralpak IB-3 (250 mm x 4.6 mm I.D.), eluent: *n*-hexane : IPA : CH_2Cl_2 : DEA 100 : 1 : 1 : 0.1, flow rate: 1 mL/min, temperature: 25°C, detector: UV (black) and CD (red) at 360 nm.

Interestingly, the HPLC analysis showed that the stereoisomeric purity of the isolated diastereoisomer was about 85%, reflecting the enantiomeric purity of the starting alkylating reagent.

However, in order to complete the stereochemical characterization of the main stereoisomer, it will be necessary to establish the absolute configuration of the stereogenic axis which, in the case of other inherently chiral monomers, was assigned on the basis of the comparison of the experimental circular dichroism curves of the two antipodes with that calculated for one enantiomer, generally the one having (S_{ax}) configuration.

Calculations are currently under way.

The IND_2T_4(*S*)Ph stereoisomer isolated in an acceptable stereoisomeric purity level was then electrochemically characterized and the cyclic voltammograms are depicted in Figure 90.

The CV profiles, recorded in two solvents, CH_2Cl_2 and acetonitrile, on the same electrode surface (glassy graphite) and at the same scan rate (0.2 V / s^{-1}) are reported in Figure 90. The comparison between the data obtained in the two solvents was possible because the electrode potential values were referred to the same Fe / Fe^+ redox couple.

The tendency of the monomer for oxidative electro-oligomerization was verified in both solvents, but, in both cases, no film deposition was observed on the electrode surface, probably due to the steric hindrance of the bulky substituents at the indole nitrogen. Overcrowding probably prevents deposition.

In order to overtake this problem, we tried to perform the chemical oligomerization with different reagents, but all the attempts were found unsuccessful.

Oxidation attempts with $FeCl_3$ in dry chloroform led to a degradation product, probably involving indole ring overoxidation.

A second method was based on the $CuCl_2$ promoted coupling of the bisanion of IND_2T_4(*S*)Ph, generated with *n*-butyllithium on the terminal alpha positions of the 2,2'-bithiophenes units.

In this case, no reaction took place and the starting material was completely recovered. It is not clear whether deprotonation does not occur or if the bulky phenylethyl groups sterically interfere with the correct approach of the anions.

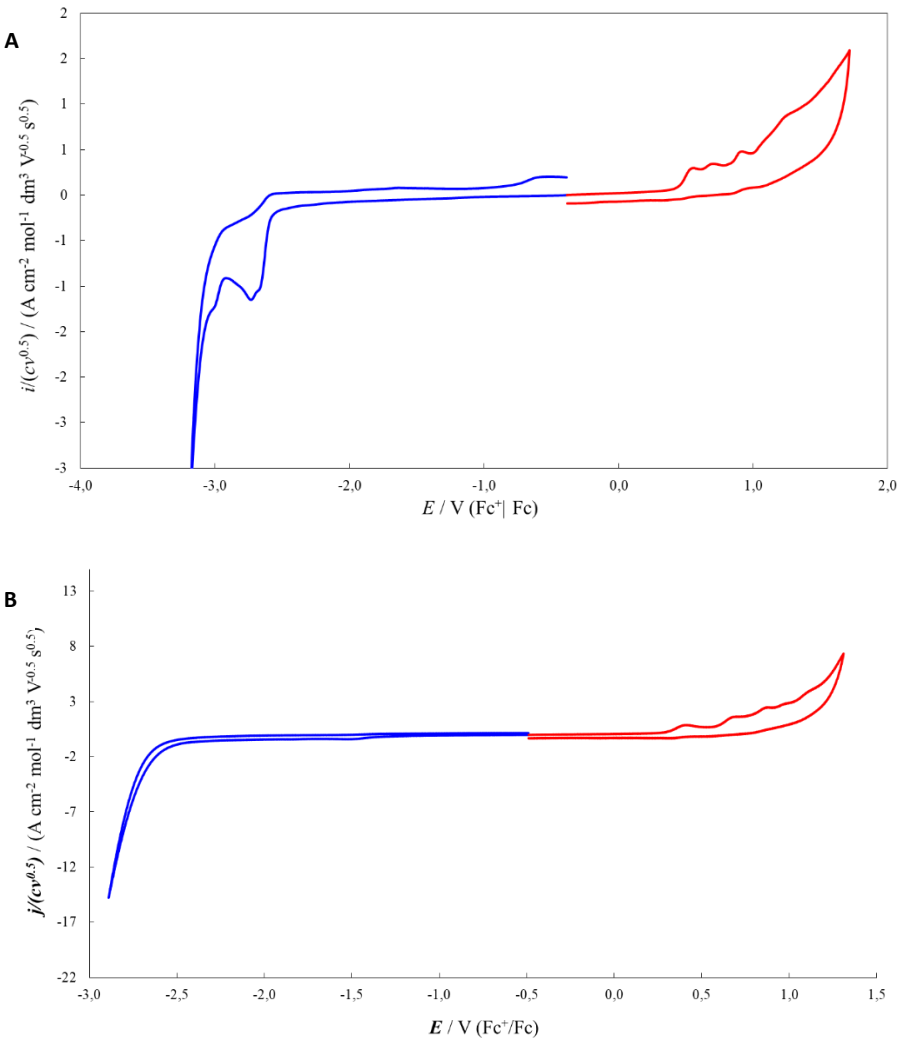

Figure 90: A) Complete CV pattern of IND_2T_4(*S*)Ph monomer (0.5 mM), 200 mV s^{-1} scan rate, solvent: ACN + 0.1 M $TBAPF_6$. B) Complete CV pattern of IND_2T_4(*S*)Ph monomer (0.5 mM), 200 mV s^{-1} scan rate, solvent: CH_2Cl_2 + 0.1 M $TBAPF_6$.

6.2. Synthesis from enantiopure precursors: 2,2'-bis(2,2'-bithiophen-5-yl)-1,1'-binaphthalene, BN_2T_4

The second strategy we adopted to accede to enantiopure monomers at a preparative level was a synthesis involving an easily accessible enantiopure scaffold.

We considered as a good candidate the 1,1'-binaphthalene system, since a careful analysis of the literature demonstrated the good accessibility of enantiopure 2,2'-dibromo-1,1-binaphthalene, [68][69], which could be used as the intermediate of choice in the final Pd-mediated Stille coupling reaction with the 5-tributhylstannyl-2,2'-bithiophene.

The synthesis, depicted in Scheme 21, started from commercially available β-naphthol which was converted into β-naphthylamine **53** through a Bucherer reaction. This reaction was carried out at a multi-gram scale in a stainless steel autoclave in the presence of ammonium sulfite, in aqueous ammonia at 145°C.

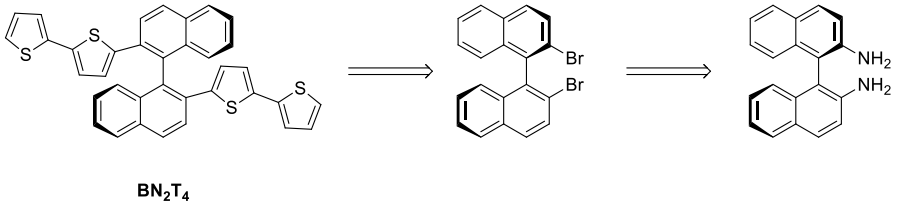

Scheme 19: Retrosynthetic pathway for the preparation of BN_2T_4.

β-Naphthylamine was then converted into 1,1'-binaphthalene-2,2'-diamine **52** through an unusual copper mediated oxidative coupling reaction. The copper reagent was an adduct of copper dichloride with two molecules of benzylamine and was easily prepared by reaction of $CuCl_2$ with benzylamine in methanol solution.

Racemic binaphthyldiamine **52** was then resolved into antipodes by selective precipitation of the diastereoisomeric salts with the two enantiomers of the camphosulfonic acid from a mixture of CH_2Cl_2, water and methanol. The enantiomeric excess was evaluated by HPLC on a chiral stationary phase and by specific optical rotation power: the *ee* found were 98% for the (*R*)-binaphthylamine and 99% for the (*S*)-binaphthylamine **53**.

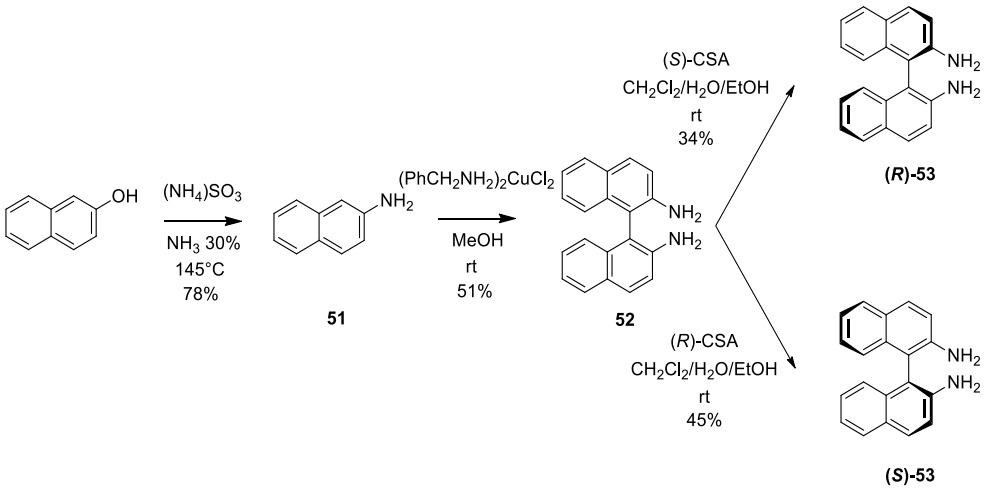

Scheme 20: Synthesis of (*R*)-binaphthylamine **(*R*)-53** and (*S*)-binaphthylamine **(*S*)-53**.

The two binaphthyldiamine enantiomers were then converted into the double diazonium salts that was reacted, according to a Sandmeyer-type reaction effected with KBr and HgBr, into the

(*R*)- and (*S*)-2,2'-dibromo-1,1'-binaphthalene **54**. The diazonium salts were prepared by reaction of the bisamine with sodium nitrite in sulfuric acid and pyridine, keeping the temperature under -5°C; a solution of urea was added to the reaction mixture in order to remove nitrous acid excess before the addition of the metal bromide salts. The yields varied between 45 and 60%, and the enantiomeric excesses, checked by chiral HPLC on CSP, were found to be 96% for the (*R*)-2,2'-dibromo-1,1'-binaphthalene **(*R*)-55** and 98% for the (*S*)-2,2'-dibromo-1,1'-binaphthalene **(*S*)-55**.

The functionalization of the binaphthalenic scaffold was first carried out by applying the classical Stille procedure, successfully employed for the synthesis of the 3,3'-bithianaphtene-based derivatives, but, in this case, the synthesis unexpectedly failed.

The Suzuki reaction was then selected as an alternative approach and the (*R*)-dibromoderivative was reacted with 5-(4,4,5,5-tetramethyl-1,3,2-dioxaborolan-2-yl)-2,2'-bithiophene in a 3:1:1 mixture of toluene, water and ethanol, in the presence of sodium carbonate as base and Pd-tetrakis as catalyst.

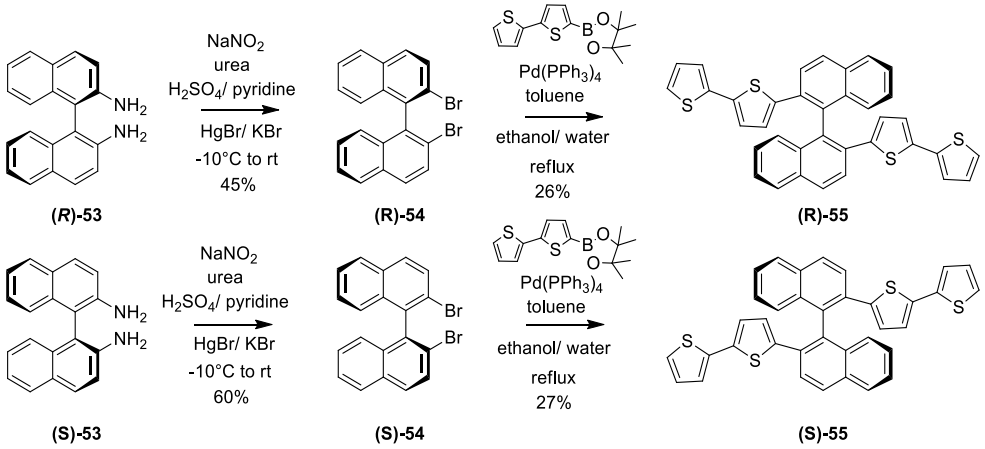

Scheme 21: Synthesis of (*R*)-2,2'-bis(2,2'-bithiophen-5-yl)-1,1'-binaphthalene ((*R*)-BN_2T_4) **(*R*)-55** and (*S*)-2,2'-bis(2,2'-bithiophen-5-yl)-1,1'-binaphthalene ((*S*)-BN_2T_4) **(*S*)-55**.

Under these experimental conditions the (*R*)-2,2'-bis(2,2'-bithiophen-5-yl)-1,1'-binaphthalene **(*R*)-55** was obtained in 26% yields after careful chromatographic purification together with large amounts of 3-(2,2'-bithiophen-5-yl)-1,1'-binaphthalene **56**.

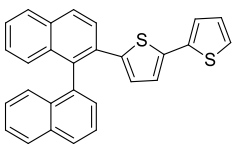

56

Figure 91: 2-(1,1'-binaphthalen-2-yl)-2,2'-bithiophene, Suzuki's reaction by-product.

Some attempts of modify the base involved were performed in order to improve the yields of the Suzuki coupling reaction by extensively changing the experimental conditions, but no significant results were achieved. [68][69]

Despite the low yields, however, a very encouraging enantiomeric excess of 96% was obtained, evaluated by HPLC on CSP (Figure 92 A).

The same procedure was then applied to the preparation of the *S* enantiomer which was obtained with identical results (Scheme 21) in terms both of yields and enantiomeric excess.

Specific optical rotation power values were found to be +207° for the *R* enantiomer and -206° for the *S* antipode.

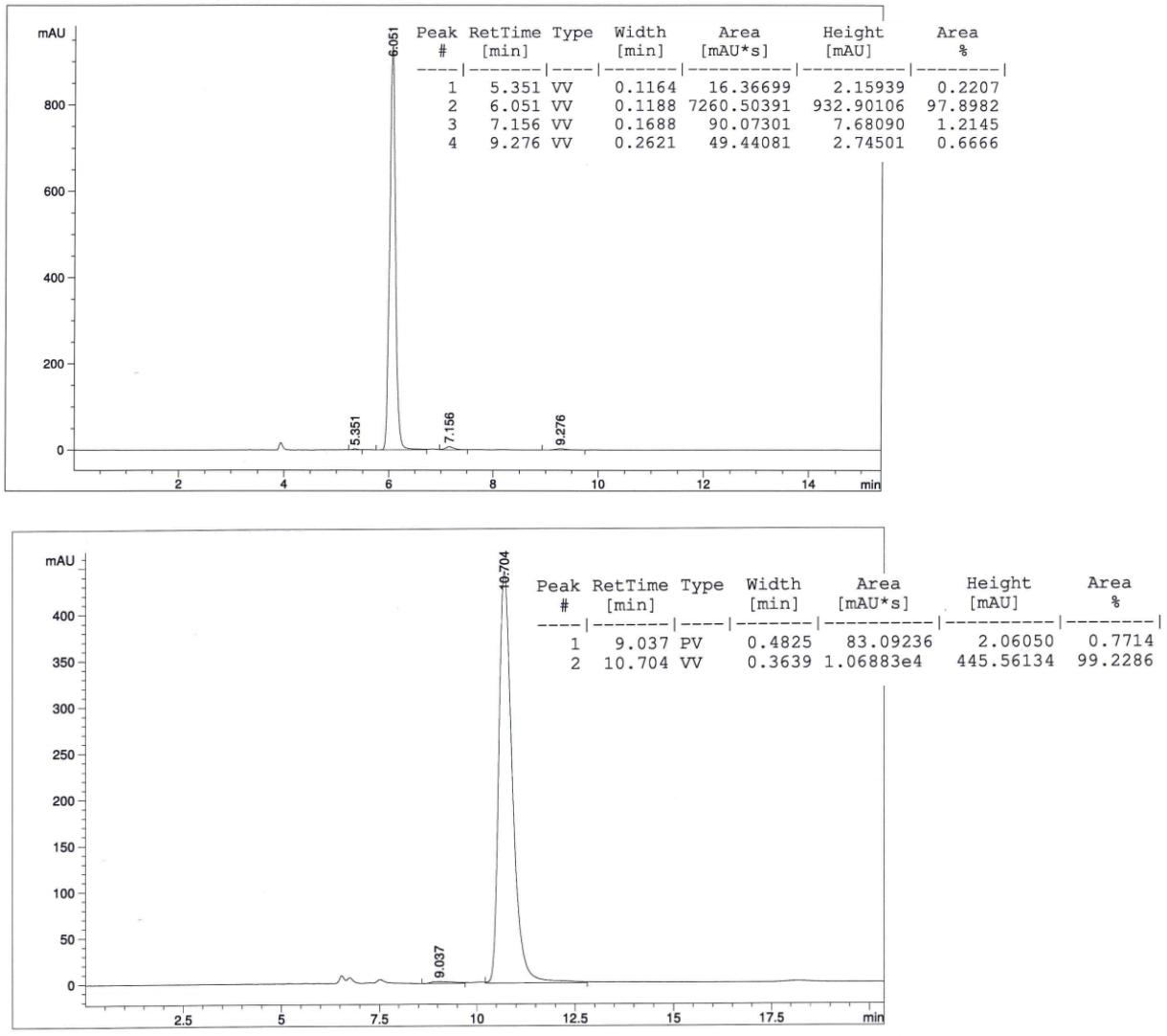

Figure 92: A) Enantiomeric purity control of ((*R*)-BN_2T_4) **61** through HPLC on a chiral stationary phase**.** B) Enantiomeric purity control of ((*S*)-BN_2T_4) **62** through HPLC on a chiral stationary phase.

Despite the numbers of steps involved, we considered this synthetic strategy as extremely interesting under multiple points of view: first of all, all the reactions can be carried out on large

scale and do not require expensive chiral reagents. The second important point is that the conversion of the diamine into the dibromo-binaphthalene and the Suzuki coupling do not influence the configurational stability of the stereogenic axis, keeping the enantiomeric purity substantially unchanged.

In Figure 93 A, the complete cyclic voltammetric pattern of monomeric BN_2T_4, recorded at 200 mV s^{-1} potential scan rate in CH_2Cl_2 + 0.1 M $TBAPF_6$ is reported: the peaks in the cathodic region were not observable because of the use of CH_2Cl_2 that narrow the potential window.

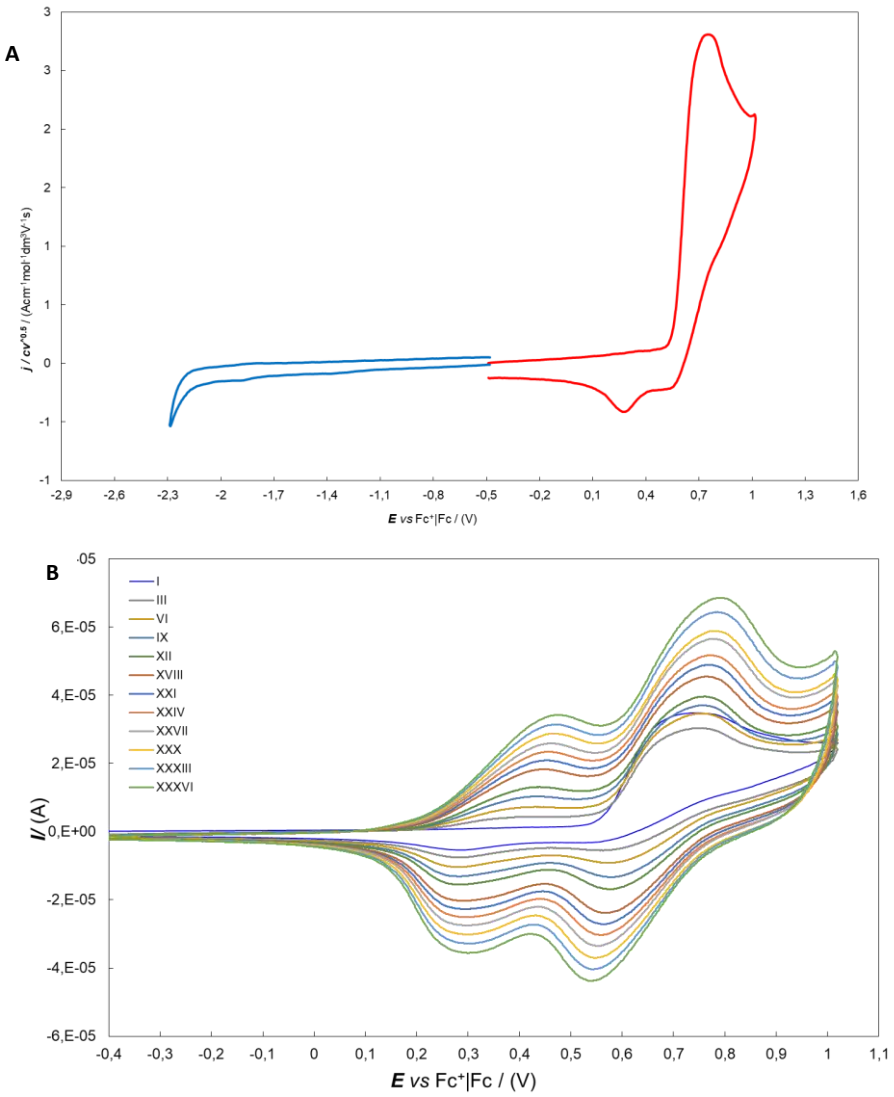

Figure 93: A) Complete CV pattern BN_2T_4 monomer, 200 mV s^{-1} scan rate, solvent: CH_2Cl_2 + 0.1 M $TBAPF_6$. B) Potentiodynamic electro-oxidation of (*S*)-BN_2T_4 on GC electrode. Thirty-six consecutive cycles at 50 mV s^{-1} scan rate, 0.5 mM of BN_2T_4 in CH_2Cl_2 + 0.1 M $TBAPF_6$.

From electrochemical analysis, BN_2T_4 appeared relatively similar to its bithianaphthene counterpart: oxidation potentials, however, were shifted to more positive values in respect to

BT_2T_4 because of the worse conjugation in the naphthalene compared to thianaphthene. Additionally, the oxidation peak was a merge of two oxidation electron transfer located on the two α homotopic positions: this means that the two halves of the monomer are barely interacting (less then for BT_2T_4).
BN_2T_4 was able to oligomerize on electrode surface (Figure 93 B) giving a stable oligomeric film, suitable for enantiorecognition tests.

Our research group is performing some profilometry experiments in order to correlate the morphology and homogeneity of the films with enantiorecognition capability: it was observed, indeed, that some variables (like deposition scan rate, number of deposition cycles and concentration of the starting monomer) deeply influence the quality of the final film. Electrooligomerization was performed in this case at 50 mV s^{-1} for the above-mentioned reasons because no enantiodiscrimination was observed on the films obtained applying a 200 mV s^{-1} scan rate.
Enantiorecognition tests were carried out on enantiopure oligomeric (*S*)-ec-p(BN_2T_4) in the presence of (*R*)- and (*S*)-enantiopure *N,N*-dimethyl-1-ferrocenylethylamine as chiral probes. The cyclic voltammogram depicted in Figure 94 displayed the presence of two oxidative peaks for each enantiomer. The first peak did not display any enantiodiscrimination and was related to the oxidation of the chiral probes on the bare glassy carbon electrode; on the other hand, the second oxidation peak was related to the oxidation of the probes on the chiral oligomeric network surface and displayed a difference of 80 mV between the two enantiopure probes. This behaviour can be ascribed to the irregularity of the film surface: the presence of a nanoporous structure allowed the interaction of the probes both with the film surface and the unfunctionalized electrode. An additional proof of this trend was observed for the achiral ferrocene probe (grey line in Figure 94): also in this case, two oxidation peaks can be observed due to the two surfaces where the oxidation processes can take place.

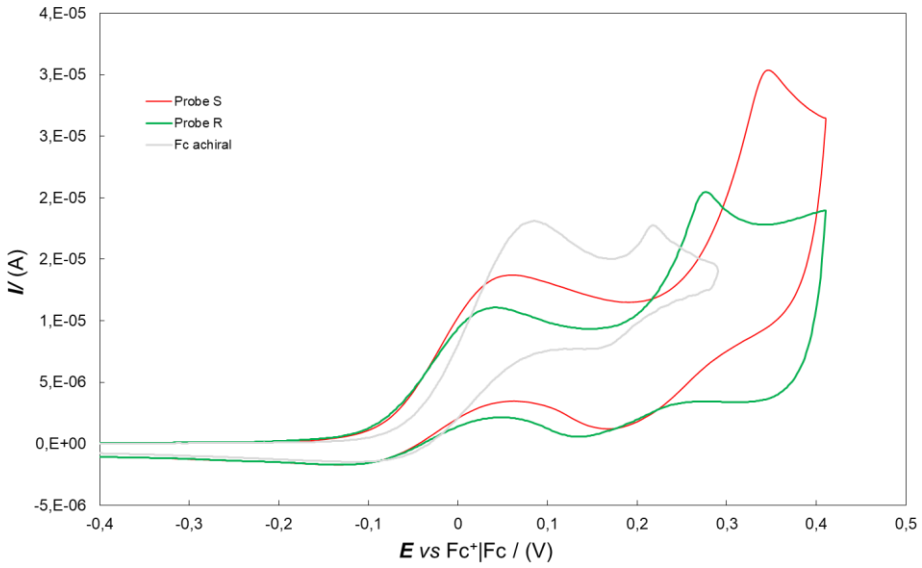

Figure 94: Enantiorecognition tests on enantiopure oligomeric (*S*)-ec-p(BN_2T_4) (deposited form thirty-six cycles, 0.5 mM monomer solution in CH_2Cl_2 + $TBAPF_6$, 200 mV s^{-1} scan rate) in the presence of enantiopure probes *S*- and *R*- *N,N*-dimethyl-1-ferrocenylethylamine ferrocene. Grey line represents the achiral ferrocene recorded on (*S*)-ec-p(BN_2T_4).

7. Inherently chiral spider-like oligothiophenes

Recently the synthesis and large-scale production of materials based on multithiophene structure has attracted considerable attention, especially in the field of diodes, photovoltaic or photoluminescent devices.[70] Furthermore, the possibility to tune the nature of the substituent, the inter-ring connectivity, the molecular symmetry or shape is considered a strong advantage in the different application of these materials. Multi-branched oligothiophene in particularly are peculiar structures due to their 3D conjugated architectures endowed with isotropic charge transport and optical properties; at the same time the present high chemical stability and remarkable solubility in organic non-polar solvents.[71][72][73] Among this class of materials, different structure, as swivel-cruciform[74], star-[75] and X-shaped[76], and dendrimeric[77][78] oligothiophenes have been reported together with their application as sensitive materials for OFETs and photovoltaic devices.

In 2010 the synthesis and the computational investigation of several examples of a class of oligothiophenes (spider-like) was reported.[79] These compounds resulted to be promising materials for applications as active layers in multifunctional organic devices,[80] where fine tuning between charge transport ability, intermolecular interactions and light emission efficiency is crucial.

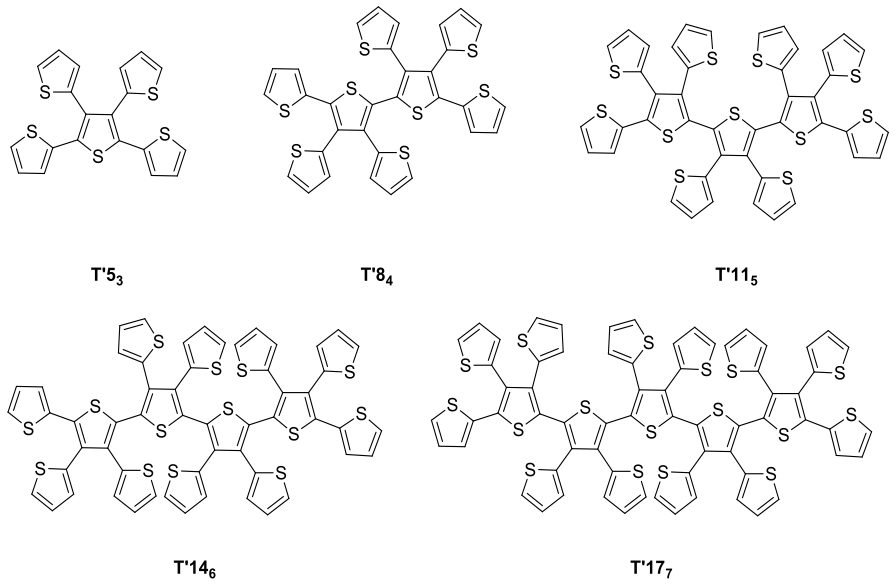

Figure 95: Molecular structure of T'5_3, T'8_4, T'11_5, T'14_6 and T'17_7.

Particularly interesting for the aim of the present research project resulted to be the octathiophene T'8_4 (Figure 95) characterized by a 2,2'-bithiophene core fully functionalized with six thiophene units. The subscript 4 in the nick-name indicates the length of the longest α-conjugated thiophene chain.

A new inherently chiral monomer which is a constitutional isomer of T'8_4, characterized by the same thiophene numbers but with a different 3,3' core, was designed.

The synthesis started from the commercially available 3-bromothiophene which was treated with *n*-BuLi and the resulting anion was submitted to an oxidative coupling in the presence of $CuCl_2$ to give the 3,3'-bithiophene **58** in high yields. The bithiophene was hexabrominated with liquid bromine in CS_2 at reflux. The use of a dangerous solvent like carbon disulfide is mandatory since in other experimental condition it was not possible to perbrominate the atropisomeric scaffold. T8_3 **60** was obtained in moderate yields by a Stille reaction coupling between the hexabromo-3,3'-bithiophene and 2-tributylstannylthiophene in the presence of Pd(0)tetrakis.

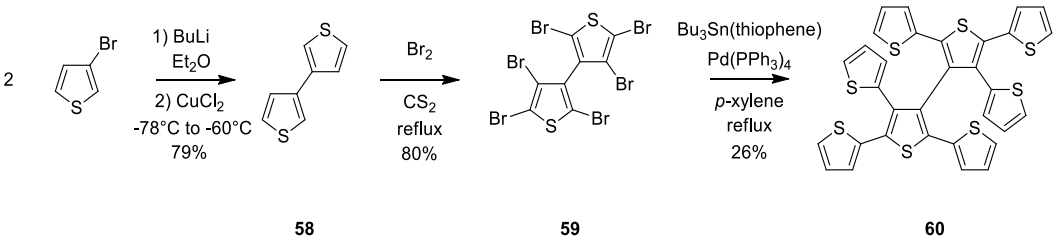

Scheme 22: Synthesis of 2,2',4,4',5,5'-tetra(2-thienyl)-3,3'-bithiophene (T8_3).

DFT calculations, performed by Prof. Rocco Martinazzo of Università degli Studi di Milano, suggested a racemization energy barrier very high (178.74 kJ mol^{-1}), thereby granting the configurational stability of the enantiomers. Furthermore, DFT calculation gave information about the π-electron distribution on the different thiophene rings: the equilibrium geometry of the most stable conformer (depicted in Figure 96 for the *R* enantiomer) exhibits two homotopic α-terthiophene units orthogonal to each other with the three rings coplanar and the 2-thienyl groups in β-position nearly perpendicular to them.

Lastly, calculations revealed that both the HOMO and the HOMO-1 orbitals have sizable amplitude on the α-terthiophene moieties and modest weight on the β-connected units; for this reason, the preferred electrooxidation-electrooligomerization sites resulted to be the four α-positions of the two homotopic α-conjugated fragments and the compound resulted to be suitable for an oxidative electrooligomerization.

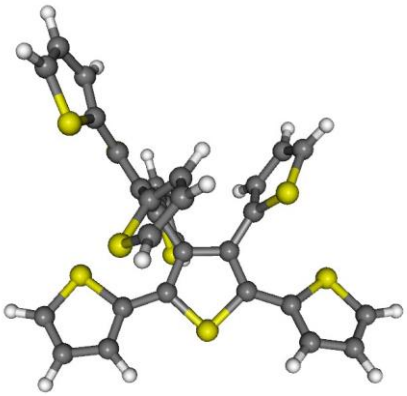

Figure 96: Calculated preferred conformation for (*R*)-$T8_3$.

The redox properties of $T8_3$ were investigated by cyclic voltammetry in different solvents (CH_2Cl_2, ACN and butylmethylimidazolium hexafluophosphate ionic liquid). In ACN and (BMIM)PF_6 both oxidation and reduction peaks can be observed, affording to estimate HOMO–LUMO gaps for the molecule, 2.93 and 2.89 eV respectively. Furthermore, in the anodic window, a two-peak oxidation system is clearly observed in all the solvents: this behaviour can be attributed to the presence of two equivalent redox centers reciprocally interacting in space. Additionally, the absence of symmetrical return peaks is a clear evidence of the formation of electron transfer products arising from a coupling of the radical cations in α-terminal positions.

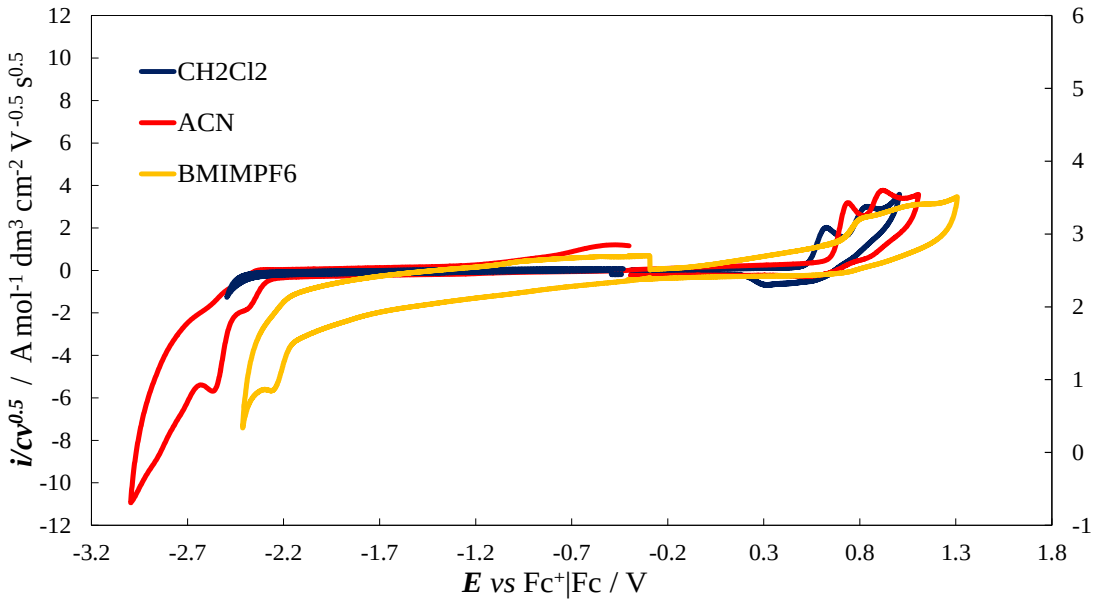

Figure 97: Complete CV patterns of $T8_3$ monomer (0.5 mM). 200 mV s^{-1}scan rate on the GC electrode in different solvents. Blue curve: dichloromethane + 0.1 M $TBAPF_6$; red curve: ACN + 0.1 M $TBAPF_6$; yellow curve: $(BMIM)PF_6$ ionic liquid (x 5).

Due to its intrinsic properties, $T8_3$ underwent to electrochemical oxidation and very regular electroactive films grew (Figure 98) on all supports and in all solvents, and the stability of the oligomeric films was evaluated. Furthermore the electrodeposited films were stable upon subsequent oxidative potential cycling in a monomer-free solution.

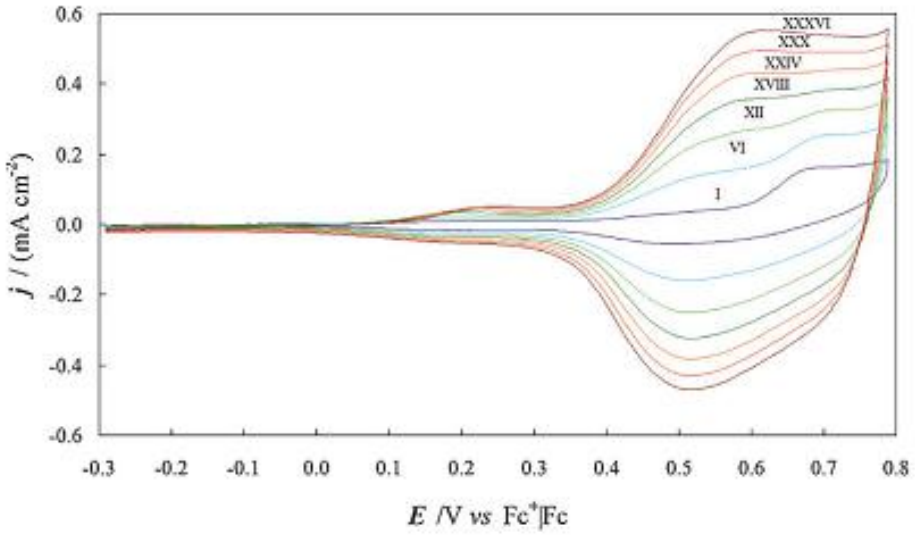

Figure 98: Potentiodynamic electro-oxidation of $T8_3$ on GC electrode. Tthirty-six consecutive cycles, 50 mVs^{-1} scan rate, 10 mM solution of $T8_3$ in CH_2Cl_2 + 0.1 M $TBAPF_6$.

The resolution of racemic $T8_3$ by HPLC on a chiral stationary phase presented some difficulties related to the low-resolution factor (a = 1.11), so that only very low amounts of the enantiopure

dextrorotatory (+)-$T8_3$ first eluted antipode (15 mg) could be obtained, while an 84% enantiomeric purity was the highest value achieved for the more retained levorotatory enantiomer. The configuration assignment to the enantiomers was performed by comparison of the experimental CD curves (Figure 99 B) with that calculated for the (*S*)-antipode, which corresponds to the first eluted dextrorotatory antipode.

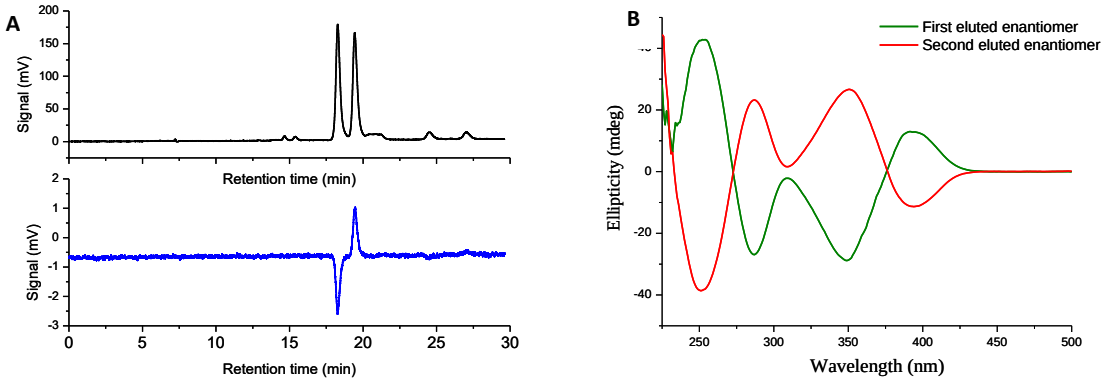

Figure 99: A) Analytical resolution of the racemate of $T8_3$ through HPLC on a chiral stationary phase. CSP: Chiralpak IB-3 250 × 4.6 mm I.D. + Chiralpak IB-3 250 × 4.6 mm I.D., eluent: *n*-hexane : dichloromethane : ethanol 100 : 5 : 0.2, flow rate: 1.0 mL/min, temperature: 25°C, detector: UV (black) and CD (blue) at 350 nm. B) CD spectra of (+)-$T8_3$ (green) and (–)-$T8_3$ (red) in $CHCl_3$ solution.

The enantiorecognition ability of enantiopure oligo-$T8_3$ films was tested with two structurally different probes and two different protocols, previously developed for the oligo-BT_2T_4 films. The enantiopure monomer was electrodeposited on Au screen-printed electrodes (SPE) from a drop of the monomer solution in (BMIM)PF_6 ionic liquid (36 oligomerization potential cycles, $T8_3$ conc. = 12 mM, scan rate = 50 mV s^{-1}).

The first test was performed with (*R*)- and (*S*)-*N,N*-dimethyl-1-ferrocenylethylamine probes, (enantiopure and as racemate), chosen for their electrochemical reversibility and commercial availability (Figure 100 A and B). An impressive and specular discrimination was obtained for the enantiopure probes of the ferrocenylamine on the enantiopure oligo-$T8_3$ electrode surfaces, with a peak separation of ~ 250 mV and, as observed for BT_2T_4, the probe's enantiomer that showed the lower oxidative potential on the (*R*)-film was oxidized at a higher potential on the (*S*)-film and vice versa.

Moreover, enantioselectivity tests were carried out with racemic probe (Figure 100 C): in this case, peak separation was significantly lower (about 150 mV). Finally, for the racemate of the probe, the peak potentials are shifted to more positive potentials with respect to those observed for the pure enantiomers of the probe. This suggests the occurrence of some reciprocal interaction of the two antipodes in the sensing process within the chiral film.

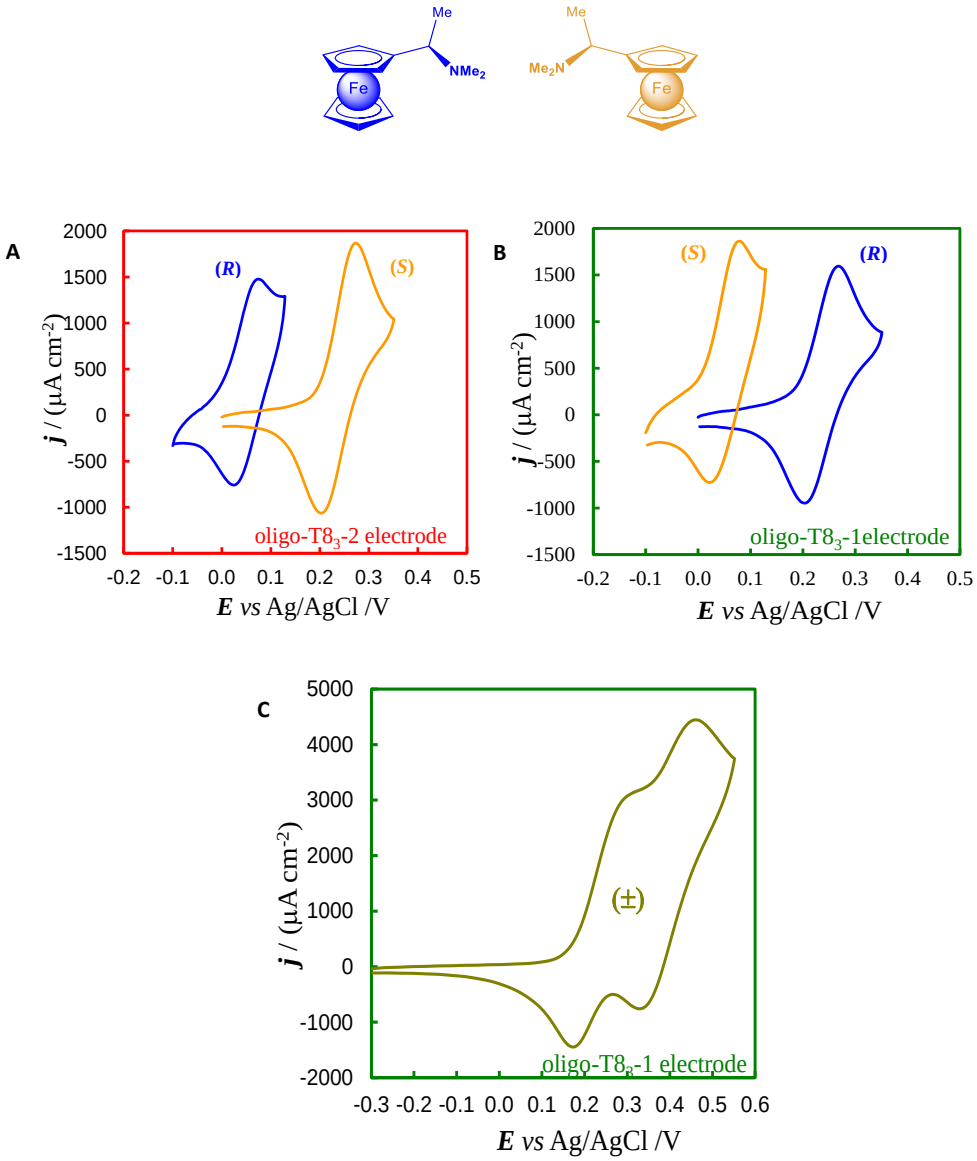

Figure 100: Enantiorecognition tests on $T8_3$: A) Oligo-(+)-(*S*)-$T8_3$ film coated electrode in the presence of enantiopure (*R*)- (blue) and (*S*)-*N,N*-dimethyl-1-ferrocenylethylamine (orange) probes (8 mM). B) Oligo-(–)-(*R*)-$T8_3$ film coated electrode. C) Oligo-(–)-(*R*)-$T8_3$ film coated electrode in the presence of racemic redox probe. 50 mV s^{-1} scan rate.

The second test was performed on enantiopure *L*- and *D*-DOPA (0.016 M) in 0.05 M HCl, using (*R*)-oligo-$T8_3$ film deposited by electrooxidation on the Au SPE. Similarly, to what observed in the first test, a neat enantiodiscrimination was achieved, although with a less pronounced peak separation (60–70 mV) (Figure 101).

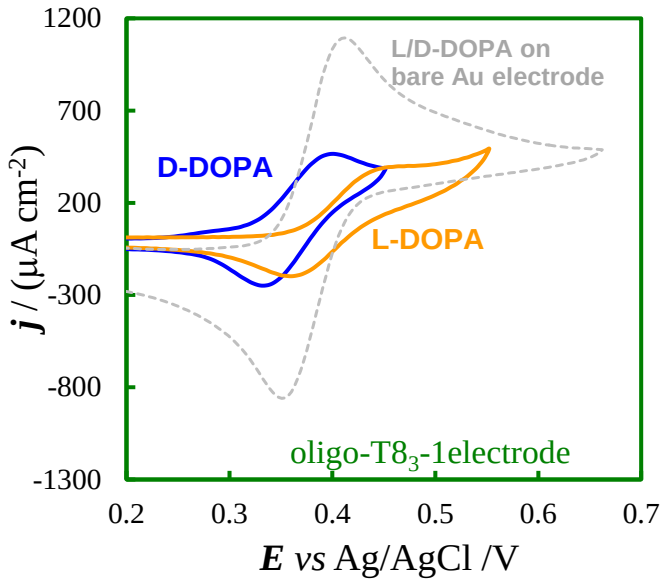

Figure 101: Enantiorecognition tests on enantiopure oligomeric on oligo-(–)-(*R*)-$T8_3$ film coated electrode with *D*-DOPA (blue) and *L*-DOPA (orange) probes (0.016 M). 50 mV s^{-1} scan rate.[79]

Based on the peculiar structural characteristics of $T8_3$, the possibility of using the racemate as co-monomer able to produce a 3D architecture in the construction of the rigid tridimensional framework MIPs[81] capable of selective hosting a tridimensional molecule in tailored cavities was considered.

In the MIP synthesis, a cross-linking and functional monomer is co-polymerized in the presence of a selected template, which is subsequently removed from the resulting MIP, leaving empty molecularly imprinted cavities capable of recognizing the original imprinter (Figure 100).[82]

In collaboration with the group of professor Kutner of Institute of Physical Chemistry Polish Academy of Sciences of Warsaw, a MIP imprinted with the 5'-TATAAA-3'-oligonucleotide was prepared in which $T8_3$ acts as a cross-linking monomer.

For the TATAAA imprinting the bis[2-(5,2'-bithienyl-)]methane functional monomers, reported in Figure 102, bearing thymine and adenine pendant were used.

The possibility of employing the $T8_3$ monomer also as racemate, represents an added value considering that its resolution is a very difficult process.

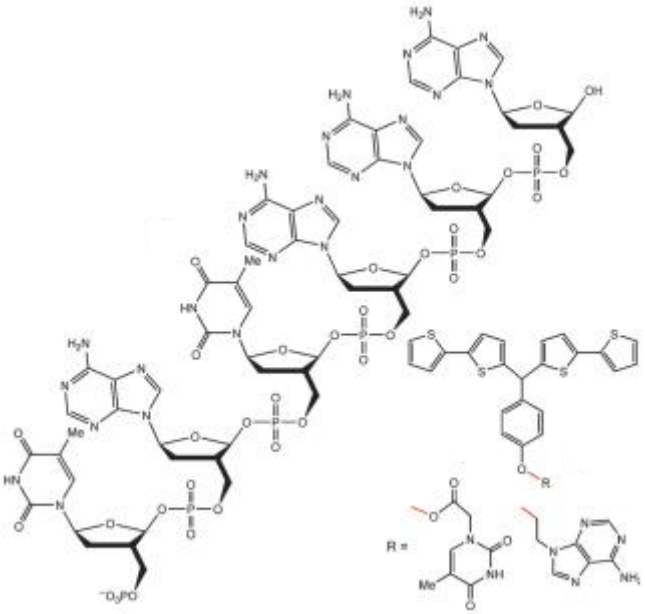

Figure 102: Structural formulas of the templating molecule, 5'-TATAAA-3' and bis[2-(5,2'-bithienyl-)]methane functional co-monomers.

8. Conclusions and Outlook

The present PhD thesis research was focused mainly on the design of new inherently chiral monomers and on their applications as chiral sensors in the fields of OSCs.

Specifically, we focused on new possible application of BT_2T_4, the parent inherently chiral monomer; in particular we investigated its application as donor in bulk-heterojunction solar cells in combination with commonly used acceptors, namely C_{60} and PCBM.

Preliminary results gave interesting indications on the more promising strategies to adopt in the design of these kind of donor materials, even if the measured performances could not be compared with those reported in the specialized literature.

Furthermore, the library of inherent chiral monomers was expanded. New monomers based both on different atropisomeric backbone with respect to 3,3'-bithianaphtene or 2,2'-biindole and different side chain pendants were synthesized and characterized.

In particular, from this investigation the following aspects can be underline:

- The concept of inherent chirality and the application of inherent chiral oligomeric films in the field of chiral sensors can be extended over different atropisomeric cores. 3,3'-Bithianaphthene, 2,2'-biindole, spider-like oligothiophene and 1,1'-binaphthalene showed their potentialities for this application with interesting results.
- Film morphology is essential for obtaining reproducible and remarkable enantiorecognition tests. The presence of nanoporous structure in the oligomeric film leads to the interaction of the chiral probes also with the bare electrode and not only with the chiral film deposited on it. Two peaks (one for the oxidation of the probes on the bare surface and one for the oxidation of the probes on the oligomer surface) were observed, due to the irregularity of the film surface.
- A fine tuning of the monomer is necessary in order to obtain a final material endowed with exhibits appropriate properties. A compromise between monomer solubility, racemate resolution feasibility, processability and film stability must be achieved in order to obtain a racemic material easily resolvable but at the same time able to form stable films under repeated oxidative cycles.
- Considering the same atropisomeric core, i.e. 3,3'-bithianaphthene, the modification of the side chain pendants deeply modify the optical properties. Under this point of view, particularly interesting could be the preparation of chiral optical devices, able to

combine peculiar optical properties with the presence of a stereogenic element like stereogenic axes.

- A possible correlation between dihedral angle and enantiorecognition capability could be observed. Considering the enantioregognition tests carried out on the parent compounds BT_2T_4 (82°), $T8_3$ (109°) and IND_2T_4Me (115°) in the presence of (*R*)-(+)- and (*S*)-(−)-*N,N*-dimethyl-1-ferrocenylethylamine ferrocene as chiral probes, a distance of 200 mV between the oxidation peaks was found for the 3,3'-bithianaphthene derivative, 250 mV for the spider-like derivative and 300 mV for the 2,2'-biindole derivative.

Finally, considering the future evolution of the present research project, the development of additionally methods suitable for the racemate resolution seems to be a foundamental target.

An interesting approach could be the introduction of two carboxyilic groups on the 3,3'-bithianaphtene or the 2,2'-biindole core in order to resolve their racemate through a selective precipitation of diastereoisomeric salts formed with an appropriate chiral base. The structure of three possible new monomers are depicted in Figure 103. In the case of the 2,2'-biindole derivatives the introduction of the carboxylic groups could be performed by *N*-alkylation, or by synthesizing a suitable 2,2'-biindole scaffold starting from the commercially available 4-amino-3-iodobenzoic acid.

On the contrary, the synthesis of the 3,3'-bithianaphthene derivative would result more complicate and it would require the synthesis of an appropriate thianaphthene derivative synthesized *ad hoc*.

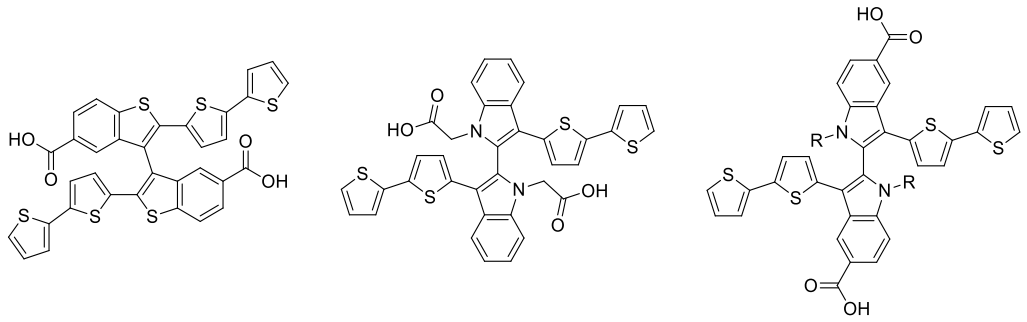

Figure 103: Structural formulas of BT_2T_4 and IND_2T_4 derivatives functionalized with carboxyilic groups, suitable for the resolution of the racemates through classical methods.

The last considered frontier in the synthesis of new inherently chiral monomer is the synthesis of new 2,2'-biindole monomers by exploiting the expertise achieved in the synthesis of side chain pendants.

In particular, the introduction of other substituents, like bis-EDOT pendants appeared to be an interesting target due to the possibility of obtaining soluble derivatives through the introduction of lipophilic chains on the nitrogen atoms.

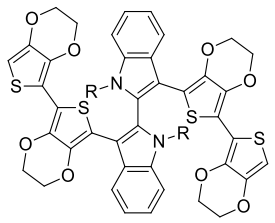

Figure 104: Structural formulas of IND_2E_4.

9. Experimental Section

9.1. General Conditions

All the reactions were carried out in anhydrous conditions in flame-dried glassware with magnetic stirring under nitrogen or argon atmosphere, unless otherwise stated.

The solvents for reactions were distilled over the following drying agents and transferred under nitrogen: $CHCl_3$ (P_2O_5), ACN ($CaCl_2$). Dry Et_2O, THF, toluene, DMF and MeOH (over molecular sieves in bottles with crown cap) were purchased from Sigma Aldrich, Alfa Aesar or Acros Organics and stored under nitrogen.

The reactions were monitored by analytical thin-layer chromatography (TLC) using pre-coated TLC sheets ALUGRAM® Xtra SIL G/UV254 (0.2 mm layer thickness; Macherey-Nagel). Visualization was accomplished by irradiation with a UV lamp (365 nm and/or 254 nm respectively). Gravimetric chromatography was performed using silica gel (particle size 0.63-2.00 mm) as stationary phase, flash column chromatography was performed using silica gel (60 Å, particle size 0.4-0.064 mm) as stationary phase, following the procedure by Still and co-workers.[83]

^{1}H-NMR spectra were recorded on a Bruker AVANCE spectrometer operating at 400.13 MHz or Bruker FT 300 operating at 300.16 MHZ or Bruker AMX 300 operating at 300.16 MHz. Proton chemical shifts are reported in ppm (δ) with the solvent reference relative to tetramethylsilane (TMS) employed as the internal standard ($CDCl_3$ δ = 7.26 ppm; CD_2Cl_2, δ = 5.32 ppm; $[D]_6$DMSO, δ = 2.50 ppm; $[D]_6$acetone, δ = 2.05 ppm). The following abbreviations are used to describe spin multiplicity: s = singlet, d = doublet, t = triplet, q = quartet, m = multiplet, br = broad signal, dd = doublet-doublet, td = triplet-doublet. ^{13}C-NMR spectra were recorded on a Bruker AVANCE spectrometer 400 MHz operating at 100.56 MHz, with complete proton decoupling. Carbon chemical shifts are reported in ppm (δ) relative to TMS with the respective solvent resonance as the internal standard ($CDCl_3$, δ = 77.16 ppm; CD_2Cl_2, δ = 54.00 ppm; $[D]_6$DMSO, δ = 39.51 ppm; $[D]_6$acetone, δ = 29.84 ppm, 206.26 ppm). The coupling constant values are given in Hz.

Melting point were determined on a Stuart Melting Point SMP30 instrument.

Optical rotation values were measured on an automatic polarimeter Jasco P1010 with a 1 dm cell at the sodium D line (λ = 589 nm), interfaced with a Spectra Manager software, 1.53.00 version from Jasco Company.

High resolution mass spectra (HRMS) were performed on a Fourier Transform Ion Cyclotron Resonance (FT-ICR) Mass Spectrometer APEX II & Xmass software (Bruker Daltonics) – 4.7 T Magnet (Magnex) equipped with ESI source, available at CIGA (Centro Interdipartimentale Grandi Apparecchiature) c/o Università degli Studi di Milano.
Low resolution mass spectra (MS) were acquired either on a Thermo-Finnigan LCQ Advantage mass spectrometer (ESI ion source), or on a VG AUTOSPEC M246 spectrometer (EI).

UV-vis spectroscopy measurements were performed with the UV2501 PC UV-vis recording spectrometer of Shimadzu (Kyoto, Japan) operating either in a transmission or reflection mode.

MALDI-TOF mass spectrometric measurements were performed on a Bruker autoflex speed spectrometer. The polymer samples concentration was set to 3 mg mL^{-1}. A poly(ethylene glycol) standard was used for internal calibration (3 mg mL^{-1}). Matrix trans-2-[3-(4-tert-butylphenyl)-2-methyl-2-propenylidene]malononitrile (DCTB, 10 mg mL^{-1}) containing the ionizer sodium trifluoromethanesulfonate was used. The mixed samples were prepared by the dried-droplet method or with a solid-phase method used for non-soluble polymers.[84]

In-situ Spectroelectrochemical Measurements on thin films were conducted using an Autolab PGSTAT101 potentiostat (Metrohm) and a Zeiss UV−vis spectrometer equipped with a MCS621 Vis II spectrometer cassette and a CLH600F lamp in a custom-built three electrode-one compartment quartz cell at room temperature under argon atmosphere. The counter and reference electrode consisted of a Pt wire and an AgCl-coated Ag wire (pseudoreference electrode). Transparent ITO coated float glass slides (≤20 Ω/sq, PGO, Germany) (∼2 × 1 cm^2) were used as the working electrode and for background measurements a non-modified ITO-coated float glass slide was used. Electrolyte solutions (0.1 M NBu_4PF_6/MeCN) were deaerated by argon bubbling before use.

In-situ conductance measurements were performed using an electrolyte gated transistor setup with interdigitated Pt electrodes (distance = 10 µm) as the working electrodes.[85] The CV experiments were performed at room temperature under argon atmosphere using an Autolab PGSTAT101 potentiostat (Metrohm) with a Pt wire as counter electrode and an AgCl coated Ag wire directly immersed into the electrolyte solution as pseudoreference electrode. Additionally, a constant bias of 10 mV was applied between the combs of the interdigitated electrode using a

second potentiostat (DropSens, Spain). Electrolyte solutions (0.1 M NBu_4PF_6/MeCN) were deaerated by argon bubbling before use.

9.1.1. Materials

Commercially available reagents were purchased from commercial suppliers (TCI Chemicals, ACROS, Sigma Aldrich) and used as received: thianaphthene, sodium acetate, potassium acetate, bromine, *n*-BuLi (1.6 M and 2.5 M in *n*-hexane), copper dichloride, 2,2'-bithiophene, tributyltin chloride, $Pd(PPh_3)_4$, 5-tributhyltin-thiophene, 2,5-dibromo-thiophene, magnesium(0), trimethyltin chloride, 1-bromo butane, 1,3-(dppp)$NiCl_2$, 2-bromothiophene, diisopropylamine, trimethylsilyl chloride, 2,3-dibromo-thiophene, 1,2-(dppe)$NiCl_2$, TBAF, EDOT, 3,3'-dibromo-2,2'-bithiophene, (±)-BINAP, potassium *tert*-butoxide, *n*-octyl amine, 3-thiophen-carboxaldehyde, Vitamin B_1, pyridine, copper sulfate pentahydrate, potassium hydroxide, aluminum trichloride, copper(0), quinoline, *n*-hexyl bromide, potassium iodide, benzothiadiazole, TMP, TMSA, triethyl amine, potassium fluoride, copper iodide, trifluoracetic anhydride, potassium carbonate, methyl iodide, ethyl iodide, propyl iodide, (*R*)-phenyl ethanol, (*S*)-phenyl ethanol, sodium hydride, ethyl bromoacetate, *N*-bromosuccinimide, *N*-iodosuccinimide, *n*-hexyl bromide, benzylamine, 2-naphtol, ammonium sulfite monohydrate, ammonia (30%), (*R*)-CSA, (*S*)-CSA, sodium nitrite, urea, mercury(I) bromide, potassium bromide, 3-bromo-thiophene, $Pd_2(DBA)_3$, 2,2'-bithiophene-boronic acid, zinc(0).

9.1.2. Codes and abbreviations used

BINAP: (±)-2,2'-bis(diphenylphosphino)-1,1'-binaphthalene;

1,2-(dppe)$NiCl_2$: [1,2-bis(diphenylphosphino)ethane]-nickel(II)chloride;

1,3-(dppp)$NiCl_2$: [1,3-bis(diphenylphosphino)propane]-nickel(II)chloride;

(*R*)-CSA: (1*R*)-(-)-camphorsulfonyc acid;

(*S*)-CSA: (1*S*)-(+)-camphorsulfonyc acid;

$Pd_2(DBA)_3$: tris(dibenzylideneacetone)-dipalladium(0);

TBAF: tetra *n*-butylammonium fluoride;

TMSA: ethynyltrimethylsilane;

$Pd(PPh_3)_4$: tetrakis(triphenylphosphine)palladium(0) 97%;

$PdCl_2(PPh_3)_2$: bis(triphenylphosphine)palladium(II) dichloride 98%;

TMP: 2,2,6,6-tetramethylpiperidine;

Vitamin B_1: thiamine hydrocloride;

2,2'-bithiophene-boronic acid: 5-(4,4,5,5-Tetramethyl-1,3,2-dioxaborolan-2-yl)-2,2'-bithiophene;

9.2. Synthesis 2,2'-dibromo-3,3'-bithianaphthene, BT_2Br_2 (4)

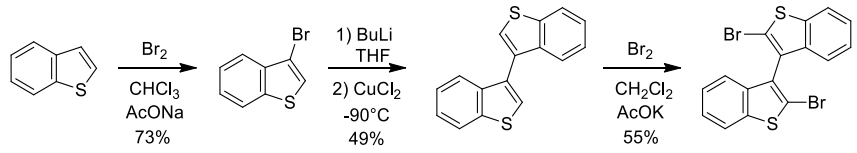

2 3 4

9.2.1. Synthesis of 3-bromothianaphthene (2)

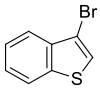

2

A solution of Br_2 (1.07 eq., 32 g, 200 mmol) in $CHCl_3$ (30 mL) was slowly added dropwise to a suspension of thianaphthene (1 eq., 25 g, 186 mmol) and sodium acetate (1.64 eq., 25 g, 305 mmol) in $CHCl_3$ (250 mL) under stirring over a period of 2 hours and keeping the temperature below 20°C. At the end of the addition the obtained orange solution was stirred at 20°C for 30 minutes. Afterwards water (150 mL) was added under stirring keeping the temperature below 20°C. The two phases were separated and the aqueous phase was extracted with CH_2Cl_2. The collected organic phases were washed with water, NaOH solution (1 M), dried over $MgSO_4$, filtered and the solvent was removed under reduced pressure to give an orange oil. The product was purified by distillation in vacuum (17 mm Hg) to afford the desired product **2** as a colorless oil.[86]

Yield: 28.76 g (73%);

B.p.: 140°C (17 mm Hg);

^{1}H NMR ($CDCl_3$, 400 MHz): δ = 7.91-7.79 (m, 2H), 7.56-7.35 (m, 3H).

9.2.2. Synthesis of 3,3'-bithianaphthene (3)

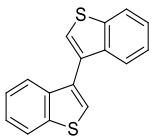

3

A solution of 3-bromothianaphthene (1 eq., 28.76 g, 135 mmol) in dry THF (52 mL) was added dropwise at -90°C to a 2.5 M *n*-BuLi solution (in *n*-hexane) (1.04 eq., 56 mL, 140 mmol) in dry

THF (98 mL). At the end of the addition the solution was stirred for 5 minutes and then anhydrous $CuCl_2$ (1.6 eq., 29 g, 215 mmol) was added. The solution was stirred for one additional hour keeping the temperature at -90°C. Afterwards the temperature was raised to 0°C and 2 M aqueous NH_3 solution (200 mL) was added; the phases were filtered over celite, separated and the aqueous phase was extracted with CH_2Cl_2. The collected organic phases were dried over $MgSO_4$, filtered and the solvent was removed under reduced pressure. The residue obtained was purified by crystallization from isopropanol to afford the desired product **3** as a white solid.[87]

Yield: 4.84 g (49%);

^{1}H NMR ($CDCl_3$, 400 MHz): δ = 7.97 (d, J = 7.5 Hz, 2H), 7.77 (d, J = 7.8 Hz, 2H), 7.58 (s, 2H), 7.41 (q, J = 7.8 Hz, 4H).

9.2.3. Synthesis of 2,2'-dibromo-3,3'-bithianaphthene (4)

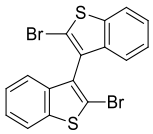

4

A solution of Br_2 (2 eq., 0.77mL, 15 mmol) in CH_2Cl_2 (5 mL) was added to a mixture of 3,3'-bithianaphthene (1 eq., 2.0 g, 7.5 mmol) and potassium acetate (2 eq., 1.5 g, 15 mmol) in CH_2Cl_2 (15 mL) at room temperature and the reaction mixture was then stirred for 24 hours. After that, water was added and the phases were separated, the organic layer was dried over $MgSO_4$, filtered and the solvent was removed under reduced pressure to give a residue which was purified by crystallization from diisopropyl ether to afford the desired product **4** as a white solid.[28]

Yield: 1.7 g (55%);

M.p.: 171°C;

^{1}H NMR ($CDCl_3$, 400 MHz): δ = 7.81 (d, J = 8.0 Hz, 2H), 7.40–7.30 (m, 2H), 7.30–7.20 (m, 4H);

^{13}C NMR ($CDCl_3$, 100 MHz) δ = 140.3, 138.6, 130.5, 125.4, 125.3, 123.4, 122.3, 117.3;

M.S. (EI): 422, 424 (77%), 426 (t, M^+), 344, 342 (d, M^+-Br, 18%), 264 (M^+-2Br, 100%).

9.3. Synthesis of 2,2'-bis(2,2’-bithiophene-5-yl)-3,3'-bithianaphthene, BT_2T_4 (1)

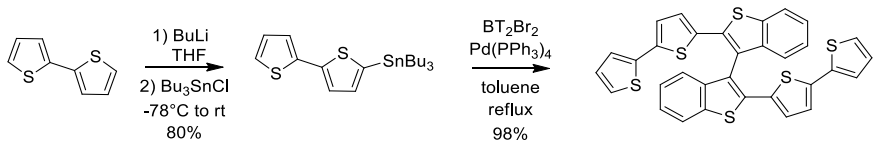

5 1

9.3.1. Synthesis of 5-(tributylstannyl)-2,2’-bithiophene (5)

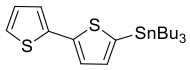

5

A 1.6 M *n*-BuLi solution (in *n*-hexane) (1.1 eq., 1.25 mL, 1.92 mmol) was added to a solution of 2,2’-bithiophene (1 eq., 291 mg, 1.75 mmol) in dry THF (25 mL) over a period of 5 minutes at −78 °C; then the mixture was stirred for 30 min. Tributyltin chloride (1.2 eq., 690 mg, 2.1 mmol) was added, and the mixture was stirred for 40 min at −78 °C and then for 12 hours at room temperature. The mixture was quenched with saturated NH_4Cl solution, the two phases were separated and the aqueous phase was extracted with Et_2O. The collected organic phases were dried over $MgSO_4$ and the solvent was removed under reduced pressure, to afford the desired product **5** as a brown oil that is used without any further purification.[88]

Yield from ^1H NMR: (83%);

^1H-NMR ($CDCl_3$, 300 MHz) δ = 7.28 (d, J = 3.4 Hz, 1H), 7.14–7.17 (m, 1H), 7.05 (d, J = 3.4 Hz, 1H), 7.05 (d, J = 3.4 Hz, 1H), 6.98 (dd, J = 5.5 Hz, J = 3.4 Hz, 1H), 1.56–1.61 (m, 6H), 1.35 (m, 6H), 1.09–1.14 (m, 6H), 0.90 (t, J = 7.0 Hz, 9H).

9.3.2. Synthesis of 2,2'-bis(2,2’-bithiophene-5-yl)-3,3'-bithianaphthene (1)

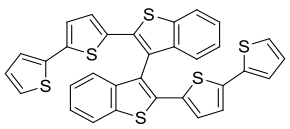

1

5-Tributylstannyl-2,2’-bithiophene (3 eq., 3.27 g, 7.2 mmol) and $Pd(PPh_3)_4$ (0.15 eq., 420 mg, 0.36 mmol) were added under nitrogen atmosphere to a warm stirred solution of 2,2’-dibromo-3,3-bithianaphthene (**4**) (1 eq., 1 g, 2.4 mmol) in dry toluene (40 mL). The mixture was refluxed

for 24 hours, then additional amounts of 5-tributylstannyl-2,2'-bithiophene (**5**) (1.4 eq., 1.1 g, 3.4 mmol) and $Pd(PPh_3)_4$ (0.1 eq., 280 mg, 0.24 mmol) were added. The mixture was refluxed for 4 hours, then the solvent was removed under reduced pressure to give a residue, which was purified by column chromatography (*n*-hexane : CH_2Cl_2 = 6 : 4) to afford the desired product **1** as a yellow solid.[28]

Yield: 1.4 g (98%);

M.p.: 86°C;

^{1}H NMR ($CDCl_3$, 400 MHz): δ = 7.87 (d, J = 8.0 Hz, 2H), 7.38–7.30 (m, 2H), 7.23–7.17 (m, 4H), 7.12 (dd, J = 4.9 Hz, J = 1.0 Hz, 2H), 7.09 (d, J = 4.0 Hz, 2H), 6.98–6.87 (m, 6H);

^{13}C NMR ($CDCl_3$, 100 MHz): δ = 140.4, 138.9, 138.1, 136.8, 136.7, 134.4, 127.7, 127.1, 125.2, 125.0, 124.6, 123.9, 123.7, 122.9, 122.0;

MS (EI): 594 (M^+, 18%), 430 (100%), 330 (95%).

9.4. Synthesis of stereoisomeric mixture BT_2T_4 open-chain dimer (6)

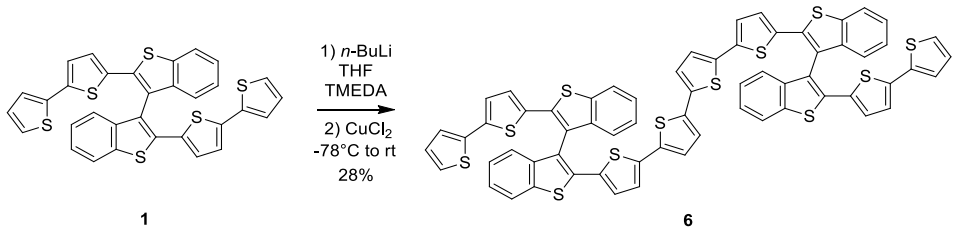

1 **6**

A 1.6 M *n*-BuLi solution (in *n*-hexane) (1.14 eq., 600 µL, 0.96 mmol) was added dropwise under argon atmosphere to a solution of **1** (1 eq., 500 mg, 0.84 mmol) in dry THF (25 mL) and freshly distilled TMEDA (2 eq., 250 µL, 1.68 mmol) under stirring at −78 °C in 30 minutes. Within this time the mixture became dark orange. Then, solid $CuCl_2$ (3 eq., 340 mg, 2.53 mmol) was added and the mixture was allowed to warm up to room temperature and stirred for 20 hours. The solvent was removed under reduced pressure and the residue was dissolved in CH_2Cl_2 and washed with 1 M HCl and water. The organic layer was dried over $MgSO_4$, filtered and then the solvent was removed under reduced pressure. The orange brown solid was purified by column chromatography (THF : *n*-hexane = 4 : 6) to afford the desired product **6** in a stereoisomeric mixture (racemate/mesoform).[34]

Yield: 141.2 mg (28%).

^{1}H NMR (CD_2Cl_2, 500 MHz,): δ = 7.96 (d, *J* = 8.8 Hz, 4H), 7.41 (t, *J* = 7.4 Hz, 4H), 7.28 (t, *J* = 7.4 Hz, 4H), 7.15-7.24 (m, 10H), 7.03-6.92 (m, 10H), 7.29 (d, *J* = 3.8 Hz, 2H).

^{13}C NMR (CD_2Cl_2, 100 MHz): δ = 140.8, 140.7, 139.3, 138.7, 138.7, 137.3, 137.1, 136.9, 136.4, 136.0, 135.0, 134.7, 128.2, 127.7, 127.6, 125.8, 125.7, 125.4, 125.2, 125.1, 124.8, 124.4, 124.1, 124.0, 123.1, 123.0, 122.53.

9.5. Synthesis of BT_2T_4 cyclic tetramer (7)

A solution of **6** (1 eq., 140 mg, 0.118 mmol) in dry chloroform (20 mL) was added dropwise under argon atmosphere into a slurry of $FeCl_3$ (2.5 eq., 90 mg, 0.55 mmol) in dry chloroform (180 mL), under stirring at room temperature over a period of 2 hours. The dark purple mixture was stirred overnight, then the volume of the solvent was reduced to 70 mL by evaporation under reduced pressure and the remaining solution poured into MeOH (150 mL). The mixture became bright orange, the precipitate was recovered by filtration and suspended in MeOH (30 mL), then hydrazine (4 drops) was added. The orange-red solid (130 mg) was recovered by filtration and extracted with THF using a Soxhlet apparatus, affording a soluble residue. The solid was dissolved in CH_2Cl_2 (20 mL), the suspension was filtered and the resulting solution concentrated to 3 mL. *n*-Hexane (7 mL) was added to the solution and the orange solid was collected after centrifugation. This procedure was repeated 6 times to give **7** in a pure state.[34]

Yield: 12.0 mg (17%)

^{1}H NMR (CD_2Cl_2, 400 MHz): δ(ppm) = 8.13 (m, 8H), 7.44 (m, 8H), 7.27 (m, 16H), 7.18 (m, 24H), 7.08 (m, 8H), 6.98 (m, 8H).

9.6. Synthesis of 2,2'-bis(2,2':5',2''-terthiophen-5-yl)-3,3'-bithianaphthene, BT_2T_6 (10)

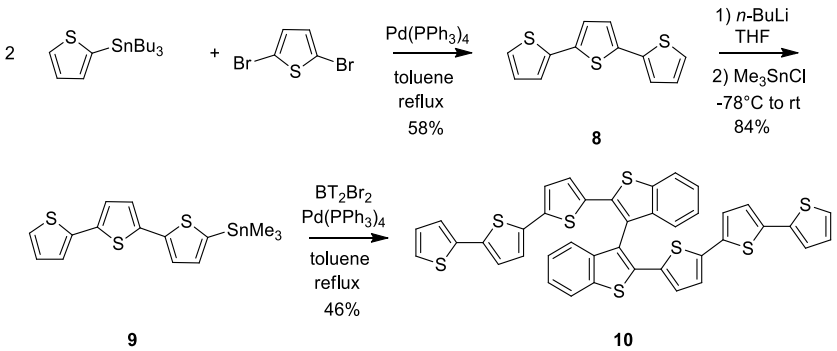

9.6.1. Synthesis of 2,2':5',2''-terthiophene (8)

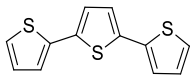

8

5-Tributylstannyl-thiophene (2.1 eq., 5.5 mL, 17.4 mmol) was added dropwise under nitrogen atmosphere to a stirred solution of 2,5-dibromo-thiophene (1 eq., 1 mL, 8.3 mmol), and $Pd(PPh_3)_4$ (0.1 eq., 93 mg, 0.08 mmol) in dry toluene (50 mL). The solution was refluxed under stirring to reflux for 24 hours, then diluted with CH_2Cl_2: the collected organic phases were washed with water, dried over $MgSO_4$, filtered and the solvent was removed under reduced pressure. The residue obtained was purified by flash chromatography (*n*-hexane : CH_2Cl_2 = 8 : 2) to afford the desired product as a yellow solid.[89]

Yield: 1.19 g (58%);

^{1}H-NMR ($CDCl_3$, 400 MHz) δ = 7.16 (d, J = 9.2 Hz, 2H), 7.13 (d, J = 3.6 Hz, 2H), 7.03 (s, 2H), 6.97 (t, J = 4.4 Hz, 2H).

9.6.2. Synthesis of 5-(trimethylstannyl)-2,2':5',2''-terthiophene (9)

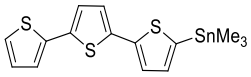

9

A 2.5 M *n*-BuLi solution (in *n*-hexane) (1 eq., 2.4 mL, 6 mmol) was added dropwise to a solution of 2,2':5',2''-terthiophene (1 eq., 1.5 g, 6 mmol) in dry THF (35 mL) over a period of 5 minutes at −78 °C, and the mixture was stirred for 20 minutes. A trimethyltin chloride (1.1 eq., 1.3 g, 6.6 mmol) solution in dry THF (15 mL) was added, and the mixture was stirred for 1 hour at −78 °C and then for 24 hours at room temperature. The mixture was quenched with water; the two phases were separated and the aqueous phase was extracted with CH_2Cl_2. The collected organic phases were dried over $MgSO_4$, filtered and the solvent was removed under reduced pressure, to afford the desired product as a brown oil used without any further purification.[90]

Yield from ^{1}H NMR: (84%);

^{1}H-NMR ($CDCl_3$, 300 MHz) δ = 7.30 (m, 1H), 7.24 (m, 1H), 7.19 (m, 1H), 7.05 (d, J = 3.4 Hz, 1H), 7.12-7.09 (m, 2H), 7.06–7.03 (m, 1H), 0.27 (t, J = 7.0 Hz, 9H).

9.6.3. Synthesis of 2,2'-bis(2,2':5',2''-terthiophen-5-yl)-3,3'-bithianaphthene (10)

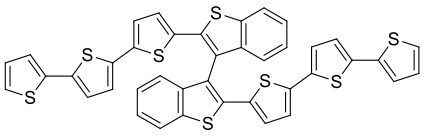

10

5-Trimethylstannyl-2,2':5',2''-terthiophene (2 eq., 4.8 mmol) and $Pd(PPh_3)_4$ (0.05 eq., 260 mg, 0.25 mmol) were added under nitrogen atmosphere to a warm stirred solution of 2,2'-dibromo-3,3-bithianaphthene (1 eq., 980 mg, 2.3 mmol) in dry toluene (45 mL). The mixture was refluxed for 24 hours, then the solvent was removed under reduced pressure to give a residue, which was purified by column chromatography (*n*-hexane : CH_2Cl_2 = 7 : 3) to afford the desired product as an orange solid.

Yield: 800 mg (46%);

M.p.: 194°C;

^{1}H NMR (CD_2Cl_2, 400 MHz): δ = 7.87 (d, J = 8.0 Hz, 2H), 7.45–7.38 (m, 4H), 7.28–7.24 (m, 6H), 7.22 (d, J = 4.9 Hz, 2H), 7.18 (d, J = 4.0 Hz, 2H), 7.06–7.03 (m, 4H), 6.92 (d, J = 4.0 Hz, 2H);

^{13}C NMR ($CDCl_3$, 100 MHz): δ = 140.4, 138.6, 138.2, 137.0, 136.7, 136.6, 135.6, 134.5, 127.9, 127.2, 125.3, 125.1, 124.8, 124.6, 124.3, 123.8, 123.7, 122.9, 122.1;

M.S. (ESI): 758.0.

9.7. Synthesis of 2,2'-bis[3',4'-di-*n*-butyl-(2,2':5',2''-terthiophen)-5-yl]-3,3'-bithianaphthene, BT_2T_6Bu (15)

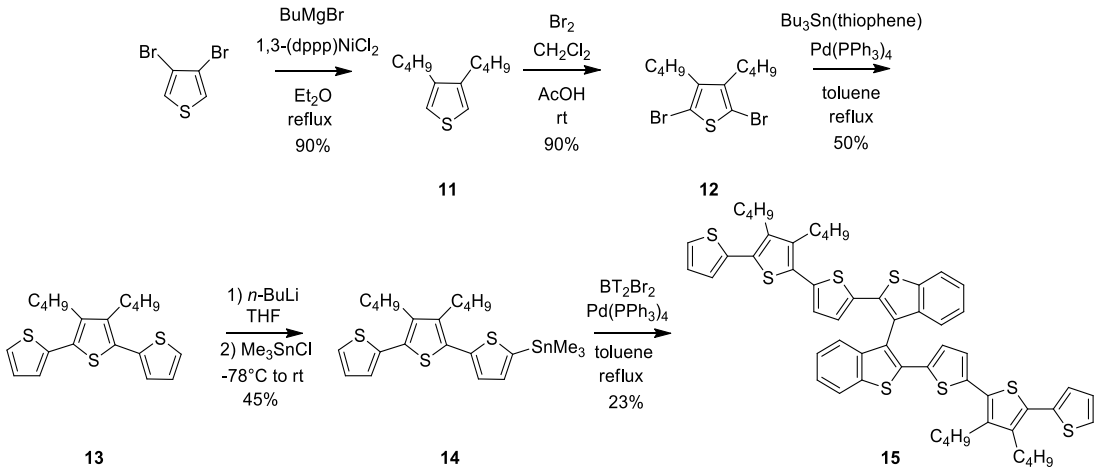

9.7.1. Synthesis of 3,4-di-*n*-butylthiophene (11)

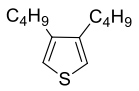

11

1-Bromobutane (4.1 eq., 1.8 mL, 17 mmol) was added dropwise to magnesium turnings (2.87 eq., 281 mg, 12.5 mmol) in dry Et_2O (8 mL) at room temperature, heating gently to improve the magnesium dissolution. The mixture was stirred at room temperature until the disappearance of magnesium and the obtained solution was added dropwise into a solution of 3,4-dibromothiophene (1 eq., 1 g, 4.15 mmol) and 1,3-(dppp)$NiCl_2$ (0.02 eq., 45 mg, 0.08 mmol) in dry Et_2O (15 mL) at 0°C. The mixture was refluxed for 24 hours and then poured into a 10% HCl aqueous solution. The phases were separated and the aqueous layer was extracted with Et_2O. The collected organic phases were washed with water and brine, dried over $MgSO_4$, filtered and the solvent was removed under reduced pressure. The residue obtained was purified by flash chromatography (*n*-hexane) to afford the desired product as a colorless liquid.[91]

Yield: 733 mg (90%);

^{1}H NMR ($CDCl_3$, 400 MHz): δ = 6.89 (s, 2H), 2.53 (t, J = 6.1 Hz, 4H), 1.61 (m, 4H), 1.41 (m, 4H), 0.89 (t, J = 11.3, 6H).

9.7.2. Synthesis of 2,5-dibromo-3,4-di-*n*-butylthiophene (12)

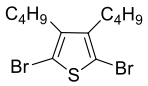

12

A solution of Br_2 (2.3 eq., 0.7 mL, 13.5 mmol) in acetic acid (2 mL) was added dropwise over a period of 30 minutes into a 2:1 ratio solution of 3,4-di-*n*-butylthiophene (1 eq, 1.15 g, 5.25 mmol) in acetic acid (4 mL) and CH_2Cl_2 (2 mL). The red suspension obtained was quenched with saturated $Na_2S_2O_3$ aqueous solution. The phases were separated and the organic solution was dried over $MgSO_4$, filtered and the solvent was removed under reduced pressure. The residue obtained was purified by chromatography (*n*-hexane) to afford the desired product as a colorless liquid.[92]

Yield: 1.67 g (93%);

^{1}H NMR ($CDCl_3$, 400 MHz): δ = 2.53 (m, 4H), 1.59 (m, 4H), 1.40 (m, 4H), 0.92 (t, J = 11.1, 6H

9.7.3. Synthesis of 3',4'-di-*n*-butyl-2,2':5',2''-terthiophene (13)

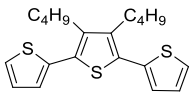

13

$Pd(PPh_3)_4$ (0.1 eq., 427 mg, 0.37 mmol) was added to a solution of 2,5-dibromo-3,4-di-*n*-butylthiophene (1 eq., 1.3 g, 3.67 mmol) and 5-tributylstannyl-thiophene (2.2 eq., 2.5 mL, 8.08 mmol) in dry toluene (40 mL). The reaction mixture was refluxed under stirring for 24 hours, then diluted with CH_2Cl_2. The collected organic phases were washed with water, dried over $MgSO_4$, filtered and the solvent was removed under reduced pressure. The residue obtained was purified by flash chromatography (*n*-hexane : CH_2Cl_2 = 8 : 2) to afford the product as an orange solid.

Yield: 662 mg (50%);

^{1}H-NMR (CD_2Cl_2, 400 MHz) δ = 7.38 (d, J = 6.8 Hz, 2H), 7.18 (br, 2H), 7.12 (d, J = 6.0 Hz, 2H), 2.75 (t, J = 9.6 Hz, 4H), 1.64-1.44 (m, 8H), 0.98 (t, J = 9.8 Hz, 6H).

9.7.4. Synthesis of 5-trimethylstannyl-(3',4'-di-*n*-butyl-(2,2':5',2''-terthiophene)) (14)

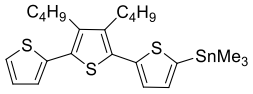

14

A 2.5 M *n*-BuLi solution (in *n*-hexane) (1 eq., 1.1 mL, 2.72 mmol) was added dropwise into a solution of 3',4'-dibutyl-2,2':5',2''-terthiophene (1 eq., 970 mg, 2.72 mmol) in dry THF (20 mL) over a period of 5 minutes at −78 °C; then the mixture was stirred for 20 min. A trimethyltin chloride (1 eq., 550 mg, 2.72 mmol) solution in dry THF (8 mL) was added, and the mixture was stirred for one hour at −78 °C and then for 24 hours at room temperature. The mixture was quenched with water, the two phases were separated and the aqueous phase was extracted with CH_2Cl_2. The collected organic phases were dried over $MgSO_4$, filtered and the solvent was removed under reduced pressure, to afford the desired product as a brown oil used without further purification.

Yield from ^{1}H NMR: (45%);

^{1}H-NMR ($CDCl_3$, 300 MHz) δ = 7.38 (m, 1H), 7.28 (m, 1H), 7.19 (m, 2H), 7.11 (m, 1H), 2.75 (m, 4H), 1.64-1.41 (m, 8H), 0.95 (m, 6H), 0.27 (t, J = 7.0 Hz, 9H).

9.7.5. Synthesis of 2,2'-Bis[3',4'-di-*n*-butyl-(2,2':5',2''-terthiophen)-5-yl]-3,3'-bithianaphthene (15)

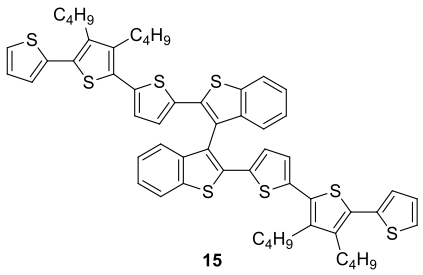

15

$Pd(PPh_3)_4$ (0.1 eq., 45 mg, 0.06 mmol) was added to a solution of 2,2'-dibromo-3,3'-bithianaphthene (1 eq., 254 mg, 0.6 mmol) and 5-trimethylstannyl-(3',4'-di-*n*-butyl-2,2':5',2''-terthiophene) (2 eq., 1.2 mmol) in dry toluene (10 mL). The reaction mixture was refluxed under stirring for 24 hours, then diluted with CH_2Cl_2. The collected organic phases were washed with water, dried over $MgSO_4$, filtered and the solvent was removed under reduced pressure. The obtained residue was purified by flash chromatography (*n*-hexane : CH_2Cl_2 = 8 : 2) to afford the desired product as an orange solid.

Yield: 135 mg (23%);

^{1}H NMR ($CDCl_3$, 400 MHz): δ = 7.95 (d, J = 8.0 Hz, 2H), 7.41 (t, J = 8.0 Hz, 2H), 7.34 (d, J = 5.5 Hz, 2H), 7.30-7.23 (m, 6H), 7.13 (d, J = 4.0 Hz, 2H), 7.08 (t, J = 5.6 Hz, 2H), 7.00 (d, J = 5.8 Hz, 2H), 2.66 (t, J = 9.1 Hz, 4H), 2.52 (t, J = 9.1 Hz, 4H), 1.51-1.41 (m, 12H), 1.24-1.20 (m, 6H), 0.95 (t, J = 9.4 Hz, 6H), 0.86 (t, J = 9.4 Hz, 6H);

^{13}C NMR ($CDCl_3$, 100 MHz): δ = 140.3, 140.1, 138.2, 138.0, 137.1, 135.9, 135.0, 130.0, 129.3, 127.4, 126.7, 125.9, 125.6, 125.4, 125.3, 125.0, 124.6, 122.6, 122.1, 32.7, 27.8, 27.6, 22.9, 22.9, 13.8, 13.6;

M.S. (EI): 594 (M^+, 18%), 430 (100%), 330 (95%).

9.8. Synthesis of 2,2'-Bis(*N*-*n*-octyl-dithieno[3,2-*b*:2',3'-*d*]pyrrol-2-yl)-3,3'-bithianaphthene, BT_2DTP_2 (18)

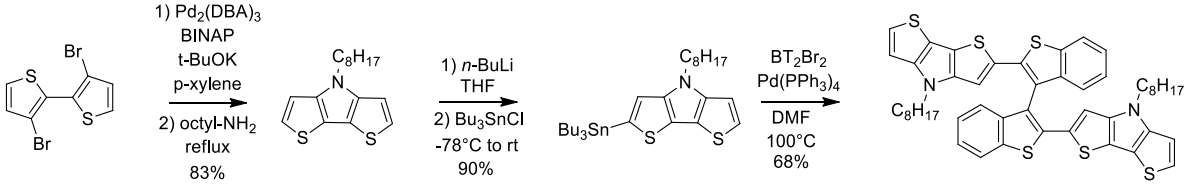

16 17 18

9.8.1. Synthesis of *N*-*n*-octyl-dithieno[3,2-*b*:2',3'-*d*]pyrrole (16)

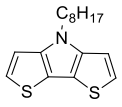

16

3,3'-Dibromo-2,2'-bithiophene (1 eq., 2 g., 6.17 mmol), potassium *tert*-butoxide (3.5 eq., 2.42 g, 21.6 mmol), $Pd(DBA)_3$ (0.1 eq., 568 mg, 0.62 mmol) and BINAP (0.3 eq., 1.15 g, 1.85 mmol) were dissolved in dry *p*-xylene (100 mL) and the solution was stirred under argon atmosphere for 20 minutes at room temperature; then *n*-octylamine (1 eq., 1 mL, 6.17 mmol) was added to the mixture and the reaction mixture was refluxed for 24 hours. Then, the reaction was cooled to room temperature and water was added; the phases were separated and the aqueous phase was extracted with CH_2Cl_2. The collected organic phases were dried with Mg_2SO_4, filtered and the solvent was removed under reduced pressure. The obtained residue was purified by chromatography (*n*-hexane : CH_2Cl_2 9 : 1) to afford the desired product as a yellow oil.[93]

Yield: 1.48 g (83%);

^{1}H NMR ($CDCl_3$, 300 MHz): δ = 7.15 (d, J = 5.4 Hz, 2H), 7.03 (d, J = 5.4 Hz, 2H), 4.22 (t, J = 3.9, 2H), 1.89 (m, 2H), 1.34-1.26 (m, 10 H), 0.90 (t, J = 7.2 Hz, 3H).

9.8.2. Synthesis of 2-trimethylstannyl-*N*-*n*-octyl-dithieno[3,2-*b*:2',3'-*d*]pyrrole (17)

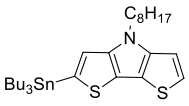

17

n-BuLi (1.6 M in *n*-hexane) (1 eq., 2 mL, 3.33 mmol) was added to a solution of *N*-*n*-octyl-dithieno[3,2-b:2',3'-d]pyrrole (1 eq., 970 mg, 3.33 mmol) in dry THF (30 mL) over a period of 5 minutes at −78 °C, and the mixture was stirred for 20 min. Tributyltin chloride (1.1 eq., 0.9 mL, 3.66 mmol) was added, and the mixture was stirred for 1 hour at −78 °C and then for 24 hours at room temperature. The mixture was quenched with water, the two phases were separated and the aqueous phase was extracted with CH_2Cl_2. The collected organic phases were dried over $MgSO_4$, filtered and the solvent was removed under reduced pressure, to afford the desired product as a brown oil used without further purification.[94]

Yield from ^{1}H NMR: (90%);

^{1}H NMR ($CDCl_3$, 300 MHz): δ = 7.08 (d, J = 5.4 Hz, 1H), 6.97 (m, 3H), 4.19 (t, J = 7.2 Hz, 2H), 1.85 (m, 2H), 1.59 (m, 6H) 1.34 (m, 16H), 1.13 (m, 6H), 0.86 (m, 12H).

9.8.3. Synthesis of 2,2'-bis(*N*-*n*-octyl-dithieno[3,2-*b*:2',3'-*d*]pyrrol-2-yl)-3,3'-bithianaphthene (18)

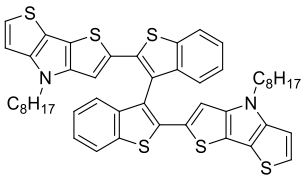

18

A mixture of 2,2'-dibromo-3,3'-bithianaphthene (1 eq., 346 mg, 0.82 mmol), 2-(trimethylstannyl)- *N*-*n*-octyl-dithieno[3,2-*b*:2',3'-*d*]pyrrole (3.5 eq., 1.3 g, 2.86 mmol) and $Pd(PPh_3)_4$ (0.13 eq., 133 mg, 0.11 mmol) in dry DMF (20 mL) was heated until 100°C under argon atmosphere for 5 hours. Then, the reaction was cooled to room temperature and CH_2Cl_2 was added; the organic phase was washed 5 times with water and two times with a 1 M NaOH solution; the organic phases were dried with $MgSO_4$, filtered and the solvent was removed under reduced pressure. The obtained residue was purified by chromatography (*n*-hexane : CH_2Cl_2 = 9 : 1) to afford the desired product as an orange solid.

Yield: 470 mg (68%);

M.p.: 58°C;

^{1}H NMR ($CDCl_3$, 300 MHz): δ = 7.91 (d, J = 7.8 Hz, 2H), 7.38-7.32 (m, 2H), 7.23 (m, 4H), 7.18 (s, 2H), 7.07 (d, J = 5.4 Hz, 2H); 6.88 (d, J = 5.4 Hz, 2H), 4.08 (t, J = 7.2 Hz, 4H), 1.77 (m, 4H), 1.26 (m, 20 H), 0.89 (t, J = 6.9 Hz, 6H);

^{13}C NMR ($CDCl_3$, 100 MHz): δ = 145.4, 144.0, 140.9, 138.5, 137.8, 132.8, 124.9, 124.9, 123.9, 122.7, 121.9, 117.0, 114.7, 110.6, 109.9, 47.3, 31.8, 30.2, 29.7, 29.1, 29.1, 26.9, 22.6, 14.1;

M.S. (EI): 844 (100%).

9.9. Synthesis of 2,2'-bis(4,4'-di-*n*-hexyl-4*H*-cyclopenta[1,2-b:5,4-b']dithiophen-2-yl)-3,3'-bithianaphthene, BT_2CPDT_2 (26)

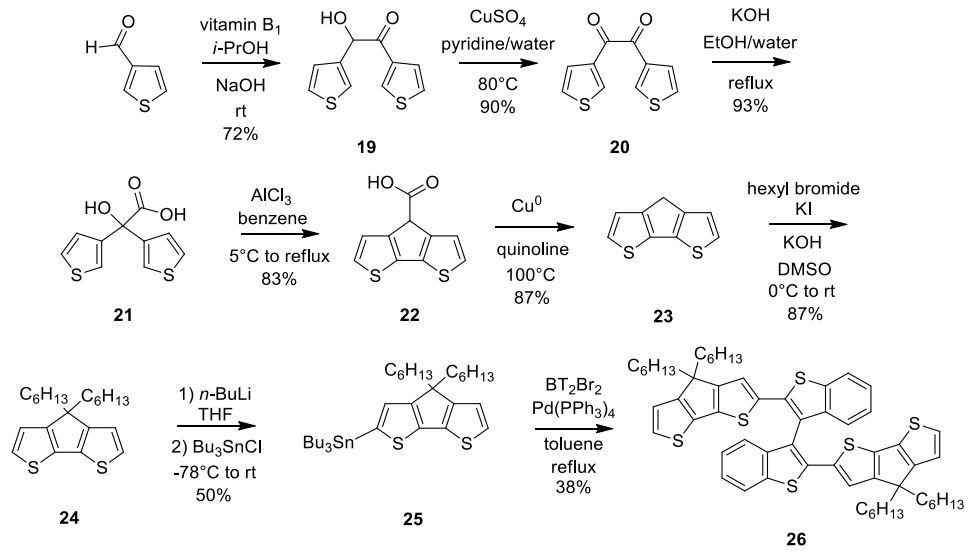

9.9.1. Synthesis of 3-thenoin (19)

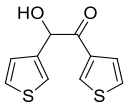

19

A solution of 3-thiophene-carboxaldehyde (1 eq., 38.6 g, 345 mmol) in isopropanol (50 mL) was prepared setting the pH at 7 with ethanoic NaOH solution (1 M), then vitamin B_1 (0.07 eq., 8.6 g, 25 mmol) was added at room temperature under stirring. The pH was monitored during the reaction and adjusted with ethanoic NaOH at 9.1. The reaction mixture was stirred at room temperature for 12 hours, then a second amount of vitamin B_1 (0.03 eq., 4 g, 11.6 mmol) was added keeping the pH at 9.1. The reaction mixture was stirred for 24 hours and the obtained cloudy solution was filtered and a grey precipitate was collected. The solid was dissolved in CH_2Cl_2, the organic phase was washed with water, dried over $MgSO_4$, filtered, and the solvent was removed under reduced pressure. The product was crystallized from isopropanol to afford the desired product as a pale yellow solid.

Yield: 29.6 g (72%);

^{1}H NMR ($CDCl_3$, 400 MHz): δ = 8.07 (d, J = 3.8, 1H), 7.54 (dd, J = 5.2, J = 0.8 Hz, 1H), 7.35 (dd, J = 5.9, J = 1.0 Hz, 1H), 7.12 (m, 2H), 7.03 (dd, J = 4.8, J = 0.4 Hz, 1 H), 5.86 (1H, s), 4.36 (br, 1H).

9.9.2. Synthesis of 3,3'-thienyl (20)

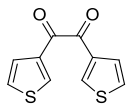

20

3-Thenoin (1 eq., 21.4 g, 95.6 mmol) was added to a solution of $CuSO_4 \cdot 5\ H_2O$ (2.3 eq., 54.4 g, 218 mmol) in water (30 mL) and pyridine (50 mL) preheated at 60°C. The reaction mixture was stirred for 4 hours at 80°C, afterwards it was cooled to room temperature and a 10% with aqueous HCl solution was added until the solution color changed from blue to green. The phases were separated and the aqueous phase was extracted with AcOEt. The collected organic phases were dried over $MgSO_4$, filtered, and the solvent was removed under reduced pressure. The product was recrystallized from isopropanol to afford the desired product as a pale yellow solid.[95]

Yield: 19.1 g (90%);

^{1}H NMR ($CDCl_3$, 400 MHz): δ = 8.36 (d, J = 1.8 Hz, 2H), 7.70 (d, J = 5.4 Hz, 2H), 7.41 −7.39 (m, 2H).

9.9.3. Synthesis of (3,3'-dithienyl)glycolic acid (21)

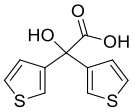

21

3,3'-Thienyl (1eq., 17.2 g, 77 mmol) was diluted in a 90 mL 1:1 solution of KOH (4.4 eq., 13.5 g, 337 mmol) in ethanol/water and stirred under reflux for 10 minutes. The reaction mixture was cooled to 0°C and pH was adjusted to 1 by adding concentrated HCl. Afterwards the ethanol was evaporated and the reaction mixture was diluted with AcOEt. The organic phase was extracted with saturated $NaHCO_3$ solution. The aqueous phase was decolorized with charcoal and HCl (10%) was added to precipitate the product. The white precipitate was filtered and dissolved in diethyl ether. The organic phase was dried over $MgSO_4$, filtered and the solvent was removed under reduced pressure. The raw product was directly used in the next step without any further purification since it was unstable.[95]

Yield: 16.7 g (93%).

^{1}H NMR ($CDCl_3$, 400 MHz): δ = 7.39 (dd, J = 3.1 Hz, J = 1.3 Hz 2H), 7.31 (dd J = 5.4 Hz, J = 3.1 Hz, 2H), 7.17 (dd, J = 5.4 Hz, J = 1.3 Hz, 2H).

9.9.4. Synthesis of *4H*-cyclopenta[1,2-b:5,4-b']dithiophene-4-carboxylic acid (22)

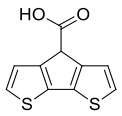

22

Dry $AlCl_3$ (3.1 eq., 15.9 g, 119 mmol) was added to a solution of (3,3'-dithienyl)glycolic acid (1 eq., 9.12 g, 38 mmol) in benzene (200 mL) at 5°C under vigorous stirring. Afterwards the temperature of the reaction mixture was raised to room temperature and the it was stirred under reflux for 1 hour. The reaction mixture was cooled to room temperature and a 5% HCl solution was added. The phases were separated and the aqueous phase was extracted with CH_2Cl_2. The collected organic phases were washed with water and brine; the organic phases were dried over $MgSO_4$, filtered and the solvent was removed under reduced pressure. The product was obtained as a brown solid and was isolated without any further purification.[95]

Yield: 7.3 g (87%);

M.p.: 166°C;

^{1}H NMR ($CDCl_3$, 300 MHz): δ = 7.21 (dd, J = 5.1 Hz, 4H), 4.63 (s, 1H).

9.9.5. Synthesis of *4H*-cyclopenta[1,2-b:5,4-b']dithiophene (23)

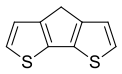

23

A suspension of 4H-cyclopenta[1,2-b:5,4-b']dithiophene-4-carboxylic acid (1 eq., 2.5 g, 6.85 mmol) and Cu(0) powder (0.36 eq, 160 mg, 2.45 mmol) in dry quinoline (16 mL) was heated at 100°C for 2 hours. The reaction mixture was allowed to cool to room temperature and then poured into a 5% HCl solution. The aqueous phase was extracted with diethyl ether. The collected organic phases were washed with water and brine; the organic phases were dried over $MgSO_4$, filtered and the solvent was removed under reduced pressure. The obtained residue was purified by chromatography (*n*-hexane : CH_2Cl_2 = 7 : 3) to afford the desired product as a white solid.[95]

Yield: 1.06 g (87%);

^{1}H NMR ($CDCl_3$, 300 MHz): δ = 7.17 (d, J = 4.8 Hz, 2H), 7.08 (d, J = 4.8 Hz, 2H), 3.53 (s, 2H).

9.9.6. Synthesis of 4,4'-di-*n*-hexyl-4*H*-cyclopenta[1,2-b:5,4-b']dithiophene (24)

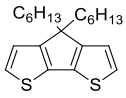

24

A mixture of 4H-cyclopenta[1,2-b:5,4-b']dithiophene (1 eq., 500 mg, 2.81 mmol), hexyl bromide (2.5 eq., 1.16 g, 7.02 mmol) and KI (0.026 eq., 12 mg, 0.075 mmol) in dry DMSO (50 mL) was cooled at 0°C. Then, KOH (3.2 eq., 500 mg, 8.93 mmol) was added in small portions. The reaction mixture was stirred for 24 hours at room temperature, shielded from light. The reaction mixture was then cooled at 0°C, and water (50 mL) was added. The phases were separated and the aqueous layer was extracted with *n*-hexane; the collected organic phases were washed with water and with saturated solution of NH_4Cl. The organic phases were dried over $MgSO_4$, filtered and the solvent was removed under reduced pressure. The obtained residue was purified by chromatography (*n*-hexane) to afford the desired product as a yellow oil.[96]

Yield: 972 mg (87%);

^1H NMR ($CDCl_3$, 300 MHz): δ = 7.14 (d, J = 4.9 Hz, 2H), 6.92 (d, J = 4.9 Hz, 2H), 1.84 (m, 4H), 1.19 (m, 12H), 0.95 (m, 4H), 0.82 (m, 6H).

9.9.7. Synthesis of 2-tributylstanny-4,4'-di-*n*-hexyl-4*H*-cyclopenta[1,2-b:5,4-b']dithiophene (25)

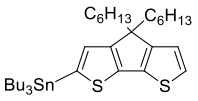

25

A 2.5 M *n*-BuLi solution (in *n*-hexane) (1.1 eq., 0.63 mL, 1.58 mmol) was added dropwise to a solution of 4,4-dihexyl-4H-cyclopenta[1,2-b:5,4-b']dithiophene (1 eq., 500 mg, 1.44 mmol) in dry THF (20 mL) over a period of 5 minutes at −78 °C, then the solution was stirred for 20 min. The reaction temperature was raised up to -30°C and then cooled again at -78°C. Tributyltin chloride (1 eq., 0.39 mL, 1.44 mmol) was added dropwise, and the mixture was allowed to reach room temperature and was kept under stirring for 24 hours at room temperature. The mixture was quenched with water; the phases were separated and the aqueous phase was extracted with CH_2Cl_2. The collected organic phases were dried over $MgSO_4$, filtered and the solvent was

removed under reduced pressure, to afford the desired product as a yellow oil which was used without further purification.

Yield from ^{1}H NMR: (50%);

^{1}H NMR ($CDCl_3$, 300 MHz): δ = 7.13 (dd, J = 10.0 Hz, J = 4.6 Hz, 1H), 6.92 (dd, J = 8.0 Hz, J = 4.6 Hz, 1H), 6.90 (s, 1H), 1.81 (m, 4H), 1.58 (m, 4H), 1.35 (m, 6H), 1.14 (m, 18H), 0.90 (m, 15H), 0.80 (m, 6H).

9.9.8. Synthesis of 2,2'-bis(4,4'-di-*n*-hexyl-4*H*-cyclopenta[1,2-b:5,4-b']dithiophen-2-yl)-3,3'-bithianaphthene (26)

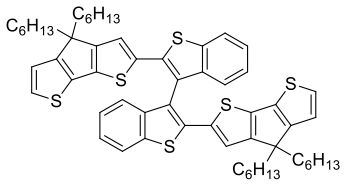

26

A solution of 2-tributylstanny-4,4-dihexyl-4H-cyclopenta[1,2-b:5,4-b']dithiophene (2 eq., 850 mg, 1.34 mmol) in dry toluene (10 mL) was added dropwise to a mixture of 2,2'-dibromo-3,3'-bithianaphthene (1 eq., 264 mg, 0.67 mmol) and $Pd(PPh_3)_4$ (0.05 eq., 39 mg, 0.033 mmol) in dry toluene (5 mL) and the reaction mixture was heated until 100°C under argon atmosphere for 24 hours. After that, the reaction mixture was cooled to room temperature and CH_2Cl_2 was added; the organic phase was washed with water, dried over $MgSO_4$, filtered and the solvent was removed under reduced pressure. The obtained residue was purified by column chromatography (*n*-hexane : CH_2Cl_2 = 9 : 1) to afford the desired product as a yellow solid.

Yield: 240 mg (38%);

M.p.: 55°C;

^{1}H NMR ([D]$_6$acetone, 300 MHz): δ = 7.98 (d, J = 8.0 Hz, 2H), 7.37 (t, J = 8.0 Hz, 2H), 7.28 (d, J = 4.8 Hz, 2H), 7.25 (t, J = 8.0 Hz, 2H), 7.18 (d, J = 8.0 Hz, 2H), 7.12 (s, 2H), 7.28 (d, J = 4.8 Hz, 2H), 1.78 (m, 8H), 1.06 (m, 24H), 0.77 (m, 20H);

^{13}C NMR ($CDCl_3$, 100 MHz): δ = 160.0, 159.2, 142.1, 140.5, 139.4, 137.7, 136.7, 134.1, 128.7, 126.9, 126.3, 125.8, 125.2, 124.2, 123.4, 123.0, 122.5, 54.8, 39.0, 33.1, 31.2, 25.9, 24.1, 15.5;

M.S. (EI): 954.3 (100%).

9.10. Synthesis of 2,2'-bis(2,2':3',2''-terthiophen-5'-yl)-3,3'-bithianaphthene, $BT_2(T_3)_2$ (31)

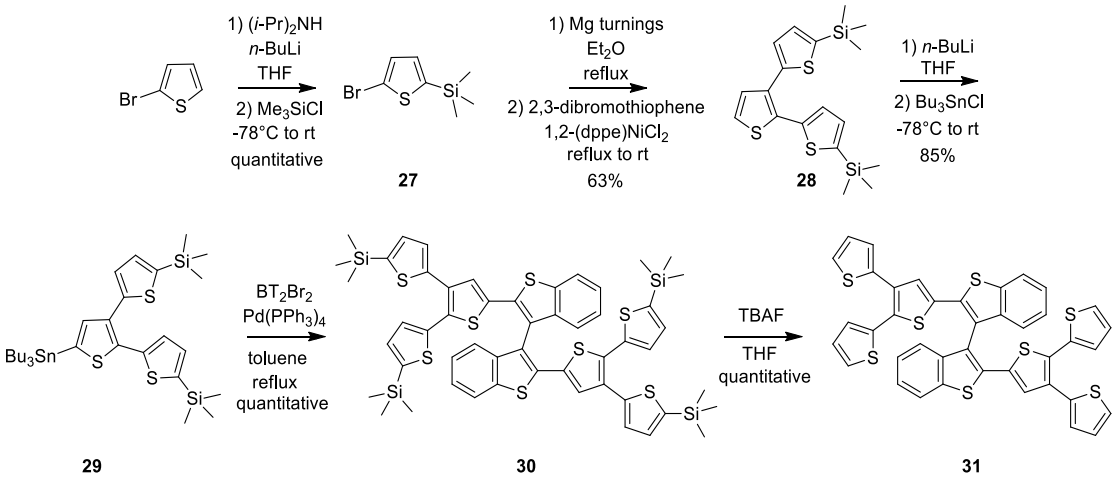

9.10.1. Synthesis of 2-bromo-5-trimethylsilylthiophene (27)

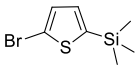

27

A 1.6 M solution of *n*-BuLi (in *n*-hexane) (1.2 eq., 15 mL, 24 mmol) was added dropwise to a solution of diisopropylamine (1.4 eq., 3.92 mL, 28 mmol) in dry THF (40 mL) at -78°C. The reaction mixture was warmed to 0°C for 5 minutes and then cooled again to -78°C. 2-Bromothiophene (1 eq., 1.94 mL, 20 mmol) was added dropwise, then the solution was warmed to 0°C for 5 minutes; then the reaction mixture was cooled at -78°C and trimethylsilyl chloride (1.2 eq., 3.95 mL, 24 mmol) was added in one portion. The solution was allowed to warm to room temperature and stirred for 30 minutes at that temperature then poured into water with HCl (3M) (0.3 mL). The two phases were separated and the aqueous phase was extracted with Et_2O. The collected organic phases were washed with water and Na_2CO_3 saturated solution, dried over $MgSO_4$, filtered and the solvent was removed under reduced pressure. The residue obtained was purified by column flash chromatography (petroleum ether : TEA = 99 : 1) to afford the desired product as a colorless liquid.[97]

Yield: 4.6 g (quantitative);

^{1}H NMR ($CDCl_3$, 300 MHz): δ = 7.11 (d, J = 4.2 Hz, 1H), 7.01 (d, J = 4.2 Hz, 1H), 0.34 (s, 9H).

9.10.2. Synthesis of 2,2':3',2''-terthiophen-5,5''-di(trimethylsilane) (28)

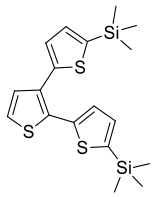

28

A solution of 2-bromo-5-trimethylsilylthiophene (2.75 eq., 1 g, 4.25 mmol) in Et_2O (2 mL) was added dropwise to magnesium turnings (4.11 eq., 155 mg, 6.37 mmol) in dry Et_2O (4.5 mL). After the addition the reaction mixture was refluxed for 2 hours and the solution was then transferred in a flask containing a 2,3-dibromothiophene (1 eq., 374 mg, 1.55 mmol) and 1,2-(dppe)$NiCl_2$ (0.015 eq., 15 mg, 0.023 mmol) solution in dry Et_2O (4.5 mL) at 0°C. The reaction mixture was heated to reflux for 4 hours and then stirred at room temperature for 24 hours. The reaction mixture is poured into ice-water, the two phases were separated and the aqueous phase was extracted with Et_2O. The collected organic phases were washed with water and a Na_2CO_3 saturated solution, dried over $MgSO_4$, filtered and the solvent was removed under reduced pressure. The residue obtained was purified by column flash chromatography (PE = 100) to afford the desired product as a yellow liquid.[98]

Yield: 385 mg (63%);

^{1}H NMR ($CDCl_3$, 300 MHz): δ = 7.29 (d, J = 6.3 Hz, 1H), 7.19 (d, J = 6.3 Hz, 1H), 7.18 (d, J = 4.2 Hz, 1H), 7.16 (d, J = 4.2 Hz, 1H), 7.14 (d, J = 4.2 Hz, 1H), 7.12 (d, J = 4.2 Hz, 1H), 0.34 (s, 9H), 0.33 (s, 9H).

9.10.3. Synthesis of 5'-tributylstannyl-2,2':3',2''-terthiophene-5,5''-di(trimethylsilane) (29)

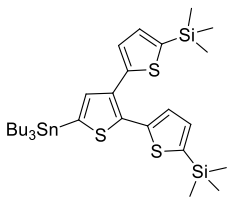

29

A 1.6 M solution of *n*-BuLi (in *n*-hexane) (1.1 eq, 2.88 mL, 4.6 mmol) was added dropwise to a solution of 2,2':3',2''-terthiophene-5,5''-di(trimethylsilane) (1 eq., 1.65 g, 4.19 mmol) in dry THF (10 mL) keeping the temperature of the solution below -72°C. After 30 minutes the reaction mixture was allowed to heat to room temperature and stirred for 15 minutes; then, tributyltin

chloride (1.1 eq., 1.25 mL, 4.6 mmol) was added. The reaction was stirred at room temperature for 24 hours and then was quenched with water. The phases were separated and the aqueous phase was extracted with Et_2O; the collected organic phases were washed with water, dried over $MgSO_4$, filtered and the solvent was removed under reduced pressure to afford the product as an orange oil that was used without any further purification.[99]

Yield from ^1H NMR: (85%);

^1H NMR ($CDCl_3$, 300 MHz): δ = 7.19 (s, 1H), 7.15 (m, 4H), 1.67-1.55 (m, 6H), 1.43-1.34 (m, 6H), 1.27-1.17 (m, 6H), 0.93 (t, J = 6.0 Hz, 9H), 0.34 (s, 9H), 0.33 (s, 9H).

9.10.4. Synthesis of 2,2'-bis(2,2':3',2''-terthiophen-5,5''-di(trimethylsilane))-3,3'-bithianaphthene (30)

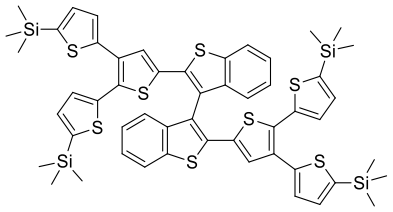

30

$Pd(PPh_3)_4$ (0.1 eq., 116 mg, 0.1 mmol) was added to a mixture of 2,2'-dibromo-3,3'-bithianaphtene (1 eq., 424 mg, 1 mmol) and 5'-tributylstannyl-2,2':3',2''-terthiophene-5,5''-di(trimethylsilane (4 eq., 4 mmol) in dry toluene (20 mL). The solution was heated under stirring to reflux for 24 hours, then diluted with AcOEt; the collected organic phases were washed with water, dried over $MgSO_4$, filtered and the solvent was removed under reduced pressure. The obtained residue was purified by column flash chromatography (petroleum ether : AcOEt = 97.5 : 2.5) to afford the desired product as a yellow solid.

Yield: 1047 mg (quantitative);

^1H NMR ($CDCl_3$, 300 MHz): δ = 7.93 (d, J = 9.6 Hz, 1H), 7.34 (s, 1H), 7.26 (m, 3H), 7.10 (d, J = 3.9 Hz 1H), 7.03 (m, 2H), 6.99 (d, J = 3.9 Hz, 1H), 0.31 (s, 9H), 0.28 (s, 9H).

9.10.5. Synthesis of 2,2'-bis(2,2':3',2''-terthiophen-5’-yl)-3,3'-bithianaphthene (31)

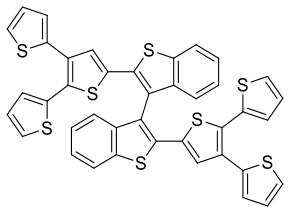

31

A solution of TBAF (1M in THF) (10 eq., 10 mL, 10 mmol) was added to a solution of 2,2'-bis(2,2':3',2''-terthiophene-5,5''-di(trimethylsilane))-3,3'-bithianaphthene (1 eq., 1047 mg, 1 mmol) in THF (25 mL). The reaction mixture was stirred for 2.5 hours and then poured into water (40 mL); the organic layer was separated and the aqueous layers was extracted with AcOEt. The collected organic phases were washed with water, dried over $MgSO_4$, filtered and the solvent was removed under reduced to afford the product as an orange solid. No further purification steps were required.[100]

Yield: 740 mg (quantitative);

M.p.: 230°C;

^{1}H NMR (CD_2Cl_2, 400 MHz): δ = 7.92 (d, J = 9.9 Hz, 2H), 7.42–7.37 (m, 2H), 7.33 (s, 2H), 7.30 (m, 8H), 6.99 (d, J = 3.9 Hz, 4H), 6.95–6.91 (m, 4H);

^{13}C NMR-APT ($CDCl_3$, 100 MHz) δ = 140.3, 138.2, 136.7, 136.5, 134.4, 134.0, 133.6, 131.6, 129.0, 127.8, 127.1, 127.1, 126.9, 126.8, 125.7, 125.4, 125.13 125.1, 123.0, 122.1;

M.S. (ESI): 758.95 (q, M^+), 780.93 (q, M + Na^+).

9.11. Synthesis of 2,2'-bis{bi[2,2’-(3,4-ethylenedioxy)thiophen-5-yl]}-3,3'-bithianaphthene, BT_2E_4 (38)

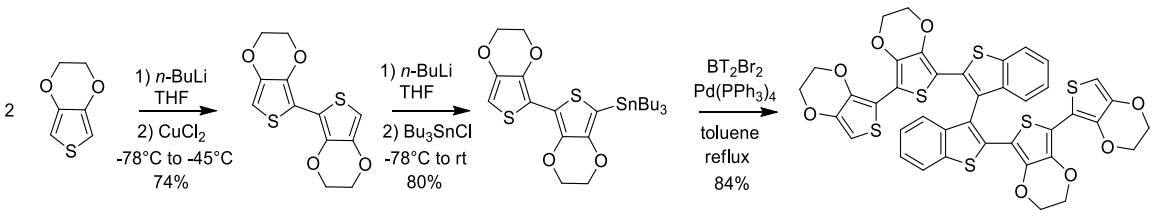

32 33 34

9.11.1. Synthesis of 2,2'-bis(3,4-ethylenedioxythiophene) (32)

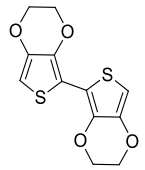

32

A 1.6 M solution of *n*-BuLi (in *n*-hexane) (1.1 eq., 9.67 mL, 15,5 mmol) was added dropwise to a solution of EDOT (1 eq., 2 g, 14.07 mmol) in dry THF (70 mL) cooled at -78°C over a period of 30 minutes: after the addition the reaction mixture was stirred for 45 minutes at -78°C and then $CuCl_2$ (1.1 eq., 2.08 g, 15.5 mmol) was added one pot. The reaction temperature was raised up to -45°C and the solution was stirred at this temperature for 2 hours. The reaction mixture was then poured into water (150 mL) and stirred for 10 minutes. The formation of a green precipitate was observed, which precipitate was filtered and washed with *n*-hexane. The collected solid was dissolved into CH_2Cl_2 and the organic phase was washed with water, dried over $MgSO_4$, filtered and the solvent was removed under reduced pressure. The residue obtained was purified by column flash chromatography (PE : CH_2Cl_2 = 6 : 4) to afford the desired product as a white/greenish solid.[49]

Yield: 1.45 g (74%);

^{1}H NMR ($CDCl_3$, 300 MHz): δ = 6.30 (s, 2H), 4.36 (m, 4H), 4.25 (m, 4H).

9.11.2. Synthesis of 5-tributyltin-2,2'-bis(3,4-ethylenedioxythiophene) (33)

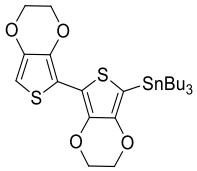

33

A 1.6 M solution of *n*-BuLi (*n*-hexane) (1.1 eq., 3.16 mL, 5,1 mmol) was added dropwise to a solution of 2,2'-bis(3,4-ethylenedioxythiophene) (1 eq., 1.3 g, 4.6 mmol) in dry THF (54 mL) cooled at -80°C, over a period of 25 minutes. The solution was stirred at -78°C for 1 hour and at -60°C for an additional hour. After cooling at -78°C, tributyltin chloride (1.1 eq., 1.37 mL, 5.1 mmol) was added dropwise within 15 minutes. After stirring at -78°C for 30 minutes the reaction mixture was allowed to reach room temperature and was stirred for further 2 hours, the

quenched with aqueous NH_4Cl solution. The phases were separated and the aqueous phase was extracted with AcOEt; the collected organic phases were washed with water, dried over $MgSO_4$, filtered and the solvent was removed under reduced pressure to afford the desired product as a brown oil that was used without any further purification. [49]

Yield from ^1H NMR: (80%);

^1H NMR ($CDCl_3$, 400 MHz): δ = 6.26 (s, 1H), 4.38-4.19 (m, 8H), 1.67-1.52 (m, 6H), 1.44-1.26 (m, 6H), 1.17-1.09 (m, 6H), 0.92 (t, J=7 Hz, 9H).

9.11.3. Synthesis of 2,2'-bis{bi[2,2'-(3,4-ethylenedioxy)thiophen-5-yl]}-3,3'-bithianaphthene (34)

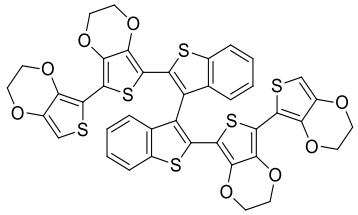

34

$Pd(PPh_3)_4$ (0.09 eq., 108 mg, 0.09 mmol) was added to a mixture of 2,2'-dibromo-3,3'-bithianaphthene (1 eq., 424 mg, 1 mmol) and 5-tributyltin-2,2'-bis(3,4-ethylenedioxythiophene) (3.68 eq., 3.68 mmol) in dry toluene (20 mL). The solution was refluxed under stirring for 24 hours, then diluted with AcOEt; the collected organic phases were washed with water, dried over $MgSO_4$, filtered and the solvent was removed under reduced pressure. The obtained residue was purified by column flash chromatography (petroleum ether : AcOEt = 6 : 4) to afford the desired product as a yellow solid.

Yield: 700 mg (84%);

M.p.: 265°C;

^1H NMR (CD_2Cl_2, 400 MHz): δ = 7.96 (d, J = 9.0 Hz, 2H), 7.40–7.2 (m, 6H), 6.23 (s, 2H), 4.36 (br, 5H), 4.19 (m, 5H);

^{13}C NMR-APT ($CDCl_3$, 100 MHz) δ = 141.1, 140.1, 139.1, 138.8, 137.4, 136.0, 134.9, 124.5, 123.9, 123.7, 122.5, 121.3, 112.1, 109.5, 109.2, 98.0, 64.9, 64.7, 64.5, 64.2;

MS (ESI): 827.00 (q, M^+), 848.99 (q, M + Na^+), 864.96 (q, M + K^+).

9.12. Synthesis of 2,2'-bis{2-[7-(thiophen-2-yl)-2,1,3-benzothiadiazol-4-yl]thiophen-5-yl}-3,3'-bithianaphthene, BT_2BTD_2 (38)

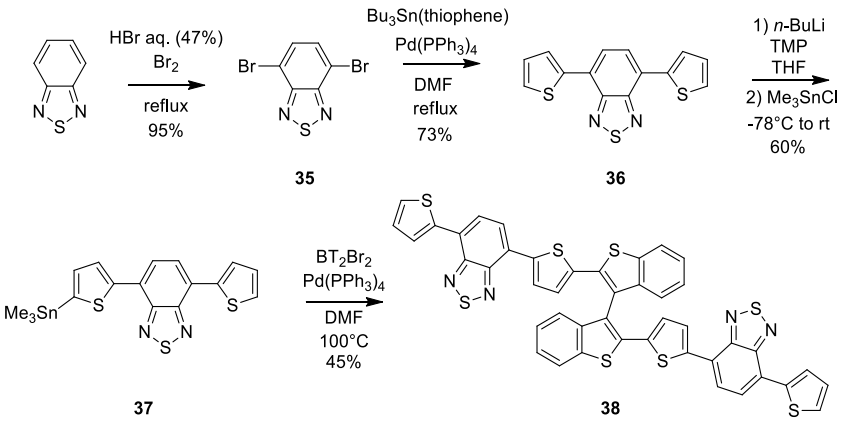

9.12.1. Synthesis of 4,7-dibromobenzo[1,2,5]thiadiazole (35)

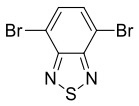

35

Benzothiadiazole (1 eq., 20 g, 147 mmol) was dissolved in aqueous HBr (47%) (150 mL). A solution containing Br_2 (3 eq., 70 g, 0.44 mol) in HBr (100 mL) was added dropwise over a period of 2 hours; after the addition, the solution was refluxed for 6 hours. The mixture was allowed to cool to room temperature and a saturated solution of $NaHSO_3$ was added. The mixture was filtered under vacuum and the collected solid was washed with water. The solid was then triturated with cold Et_2O and dried under vacuum, affording the desired product as a yellow solid.[101]

Yield: 41 g (95%);

^{1}H NMR ($CDCl_3$, 300 MHz): δ = 7.75 (s, 2H).

9.12.2. Synthesis of 4,7-bis(thiophen-2-yl)-2,1,3-benzothiadiazole (36)

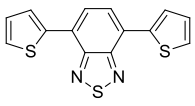

36

$Pd(PPh_3)_4$ (0.1 eq., 1.6 g, 1.4 mmol) was added to a solution of 4,7-dibromobenzo[1,2,5]thiadiazole (1 eq., 4.18 g, 14.22 mmol) and 5-tributylstannyl-thiophene (2.1 eq., 11.1 g, 29.9 mmol) dissolved in dry DMF (96 mL). The solution was refluxed for 5 hours under nitrogen atmosphere. After removing the solvent under reduced pressure, the crude product was washed several times with methanol and used without further purification.[102]

Yield: 3.1 g (73%);

^{1}H NMR ($CDCl_3$, 300 MHz): δ = 8.15 (dd, J = 3.6 Hz, J = 0.9 Hz, 2H), 7.90 (s, 2H), 7.48 (dd, J = 5.1 Hz, J = 0.9 Hz, 2H), 7.24 (dd, J = 5.1 Hz, J = 3.6 Hz, 2H).

9.12.3. Synthesis of 5-trimethylstannyl-4,7-bis(thiophen-2-yl)-2,1,3-benzothiadiazole (37)

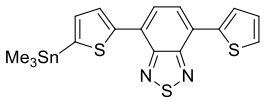

37

A 2M *n*-BuLi solution (in *n*-hexane) (1.2 eq., 0.6 mL, 1.2 mmol) was added to a solution of TMP (1.2 eq., 200 µL, 1.2 mmol) in dry THF (7 mL), at -78°C. After 1 hour stirring at -78°C, a solution of 4,7-bis(thiophen-2-yl)-2,1,3-benzothiadiazole (1 eq., 300 mg, 1 mmol) in dry THF (6 mL) was added one pot. After stirring for 2 hours at -78°C, a solution of trimethyltin chloride (1.3 eq., 259 mg, 1.3 mmol) in dry THF (2 mL) was added and the reaction mixture was allowed to heat to room temperature and stirred for 24 hours. Then the reaction was quenched with water, the two phases were separated and the aqueous phase was extracted with CH_2Cl_2. The collected organic phases were dried over $MgSO_4$, filtered and the solvent was removed under reduced pressure, to afford the desired product as an orange oil used without further purification.[103]

Yield from ^{1}H NMR: (60%);

^{1}H NMR ($CDCl_3$, 300 MHz): δ = 8.26 (d, J = 3.6 Hz, 1H), 8.17 (m, 1H), 7.94 (s, 2H), 7.52 (m, 1H), 7.34 (d, J = 3.6 Hz, 1H), 7.26 (m, 1H), 0.42 (s, 9H).

9.12.4. Synthesis of 2,2'-bis{2-[7-(thiophen-2-yl)-2,1,3-benzothiadiazol-4-yl]thiophen-5-yl}-3,3'-bithianaphthene (38)

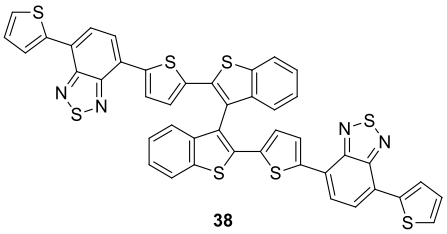

38

A mixture of 2,2'-dibromo-3,3'-bithianaphthene (1 eq., 165 mg, 0.39 mmol), 5-trimethylstannyl-4,7-bis(thiophen-2-yl)-2,1,3-benzothiadiazole (3.5 eq., 632 mg, 1.36 mmol) and $Pd(PPh_3)_4$ (0.14 eq., 63 mg, 0.05 mmol) in dry DMF (10 mL) was heated until 100°C under argon atmosphere for 5 hours. Then, the reaction was cooled to room temperature and CH_2Cl_2 was added; the organic phase was washed 5 times with water and two times with a 1 M NaOH solution. The organic phases were dried with $MgSO_4$, filtered and the solvent was removed under reduced pressure. The obtained residue was purified by chromatography (*n*-hexane : CH_2Cl_2 = 7 : 3) to afford the product as a deep red solid.

Yield: 150 mg (45%);

M.p.: 284°C;

^{1}H NMR (DMSO, 300 MHz): δ = 8.17 (d, J = 8.1 Hz, 2H), 8.05 (d, J = 3.0 2H), 7.92 (m, 4H), 7.73 (m, 4H), 7.46 (t, J = 7.8 Hz, 2H); 7.35-7.30 (m, 2H), 7.23-7.17 (m, 2H).

M.S. (EI): 861 (100%), 862 (65%), 863 (55%).

9.13. Synthesis of 3,3'-bis(2,2'-bithiophen-5-yl)-1*H*,1'*H*-2,2'-biindole (43)

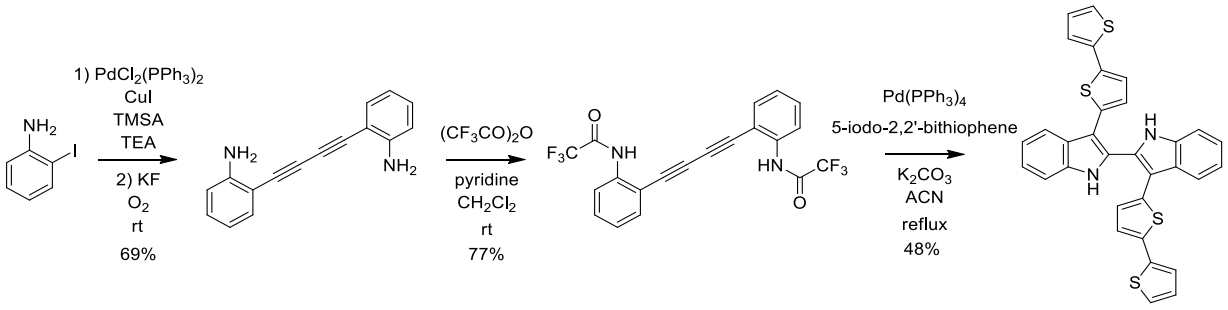

40 41 43

9.13.1. Synthesis of 2[-4-(2-aminophenyl)-1,3-butadienyl]phenylamine (40)

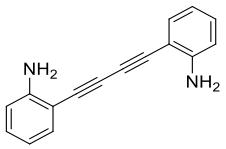

40

2-Iodoaniline (1 eq., 15.3 g, 71.23 mmol), $PdCl_2(PPh_3)_2$ (0.01 eq., 500 mg, 0.71 mmol) and CuI (0.02 eq., 270 mg, 1.42 mmol) were dissolved in dry and degassed TEA (240 mL). TMSA (1.3 eq., 13.1 mL, 92.6 mmol) was added and the reaction mixture was stirred for 2 hours at room temperature under inert atmosphere. KF (2 eq., 8.3 g, 142 mmol) in methanol (160 mL) was added and the reaction mixture was stirred for 24 hours at room temperature in air. The mixture was filtered on celite and the solvents were removed under reduced pressure. The residue obtained was purified by column flash chromatography (*n*-hexane : CH_2Cl_2 = 4 : 6) to afford the desired product as a yellow solid.[104]

Yield: 5.73 g (69%);

^{1}H NMR (CD_2Cl_2, 400 MHz): δ = 7.36 (dd, J = 7.5 Hz, J = 1.2 Hz, 2H), 7.18 (dt, J = 8.7 Hz, J = 1.5, 2H), 6.74 (m, 4H).

9.13.2. Synthesis of 2,2,2-trifluoro-*N*-(2-(4-[2,2,2-trifluoro-acetylamino-phenyl]-buta-1,3-diynyl)-phenyl)-acetamide (41)

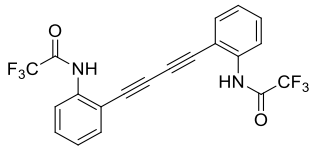

41

Trifluoracetic anhydride (2.1 eq., 5 mL, 36.16 mmol) was slowly added to a solution of 2[-4-(2-aminophenyl)-1,3-butadienyl]phenylamine (1 eq., 4 g, 17.22 mmol) and pyridine (4.16 mL) in CH_2Cl_2 at room temperature. The reaction mixture was stirred at room temperature for 3 hours and then was filtered and the precipitate obtained was dried under vacuum to afford the desired product as a white solid.[104]

Yield: 5.63 g (77%);

^{1}H NMR (DMSO, 400 MHz): δ = 11.39 (s, 2H), 7.74 (d, J = 7.8 Hz, 2H), 7.57 (t, J = 7.8 Hz, 2H), 7.45 (m, 4H).

9.13.3. Synthesis of 5-iodo-2,2'-bithiophene (42)

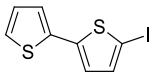

42

2,2'-bithiophene (1 eq., 4.53 g, 27.2 mmol) was dissolved in a 1:1 mixture of $CHCl_3$ and acetic acid (108 mL) and NIS (1.1 eq., 6.74 g, 29.9 mmol) was added one pot. The reaction mixture was shielded from light and was stirred at room temperature for 24 hours. The solution was then filtered and the solvent was removed under reduced pressure. The obtained residue was diluted with CH_2Cl_2 and the solution obtained was washed with saturate $NaHCO_3$ solution and water. The obtained solid was dissolved in a 1:1 mixture of $CHCl_3$ and acetic acid, cooled and the precipitate, corresponding to the 5,5'-diiodo-2,2'-bithiophene, was removed by filtration. The solvents were removed under reduced pressure to afford the desired product as a grey solid. [67]

Yield: 4.43 g (56%);

^{1}H NMR ($CDCl_3$, 400 MHz): δ = 7.24 (dd, J = 4.8 Hz, J = 0.8 Hz, 1H), 7.18 (d, J = 4 Hz, 1H), 7.14 (dd, J = 3.6 Hz, J = 1.2 Hz, 1H), 7.03 (dd, J = 4.8 Hz, J = 3.6 Hz, 1H), 6.87 (d, J = 4.0 Hz, 1H).

9.13.4. Synthesis of 3,3'-bis(2,2'-bithiophen-5-yl)-1*H*,1'*H*-2,2'-biindole (43)

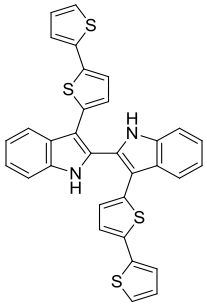

43

5-Iodo-2,2'-bithiophene (4.3 eq., 5.9 g, 20.3 mmol), $Pd(PPh_3)_4$ (0.1 eq., 544 mg, 0.47 mmol) and K_2CO_3 (5 eq., 3.2 g, 23.5 mmol) were added to a stirred solution of 2,2,2-trifluoro-*N*-(2-(4-[2,2,2-trifluoro-acetylamino-phenyl]-buta-1,3-diynyl)-phenyl)-acetamide (1 eq., 1.99 g, 4.7mmol) in dry and degassed ACN (94 mL) under N_2. The reaction mixture was stirred under reflux for 24 hours. The solvent was removed under reduced pressure and the obtained residue was diluted with AcOEt; the organic phase was washed with water. The organic phases were dried over $MgSO_4$, filtered and the solvent was removed under reduced pressure. The obtained residue was

purified by column chromatography (*n*-hexane : CH_2Cl_2 = 4 : 6) to afford the desired product as a yellow/brown solid.

Yield: 1.28 g (45%);

M.p.: 215°C;

^{1}H NMR (DMSO, 400 MHz): δ = 11.95 (s, 2H), 7.99 (d, J = 7.6 Hz, 2H), 7.48 (d, J = 8.0 Hz, 2H), 7.40 (d, J = 4.4 Hz, 2H), 7.29 (t, J = 5.2 Hz, 2H), 7.23 (t, J = 5.2 Hz, 2H), 7.12 (d, J = 3.6 Hz, 2H), 7.09 (d, J = 3.6 Hz, 2H), 7.00 (dd, J = 5.2 Hz, J = 4.0 Hz, 2H), 6.88 (d, J = 4.0 Hz, 2H);

^{13}C NMR (DMSO, 100 MHz): δ = 137.1, 136.8, 136.4, 134.3, 128.7, 126.8, 125.9, 125.3, 124.7, 124.6, 123.7, 123.4, 120.9, 120.0, 112.4, 110.9;

M.S. (EI): 560 (100%).

9.14. *N*-alkylation of IND_2T_4 scaffold

9.14.1. Synthesis of 3,3'-bis(2,2'-bithiophen-5-yl)-1,1'-bismethyl-1*H*,1'*H*-2,2'-biindole, IND_2T_4Me (39a)

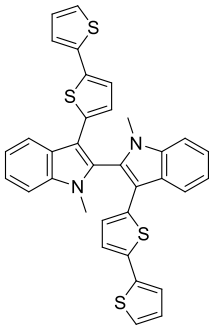

39a

3,3'-Di([2,2'-bithiophen]-5-yl)-1H,1'H-2,2'-biindole (1 eq., 310 mg, 0.55 mmol) was dissolved in dry DMF (3 mL) and the solution was cooled at 0°C. KOH (6.5 eq., 200 mg, 3.56 mmol) was added and the solution was stirred at that temperature for 10 minutes. The reaction mixture was allowed to reach room temperature and then methyl iodide (10 eq., 300 µL, 5.53 mmol) was added one pot. The reaction mixture was stirred at room temperature for 36 hours. The solvent was removed under reduced pressure and the residue was dissolved into CH_2Cl_2; the organic phase was washed with water and brine, then dried over $MgSO_4$, filtered and the solvent was removed under reduced pressure. The obtained residue was purified by column chromatography (*n*-hexane : CH_2Cl_2 = 8 : 2) to afford the desired product as a yellow solid.

Yield: 228 mg (70%);

^{1}H NMR ($CDCl_3$, 400 MHz): δ = 8.19 (d, J = 7.8 Hz, 2H), 7.45-7.32 (m, 6H), 7.14 (d, J = 5.1 Hz, 2H), 7.03 -7.01 (m, 4H), 6.97-6.95 (m, 2H), 6.81 (d, J = 3.9, 2H), 3.48 (s, 6H);

^{13}C NMR ($CDCl_3$, 100 MHz): δ = 137.7, 137.6, 135.8, 135.2, 127.7, 126.9, 125.7, 124.3, 124.2, 123.8, 123.4, 123.2, 120.8, 120.6, 112.9, 110.1, 30.3.

M.S. (EI): 588.1 (100%).

9.14.2. Synthesis of 3,3'-bis(2,2'-bithiophen-5-yl)-1,1'-bisethyl-1*H*,1'*H*-2,2'-biindole, IND_2T_4Et (39b)

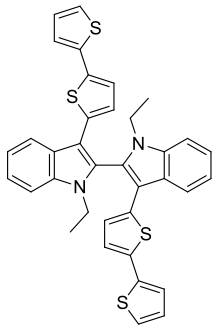

39b

3,3'-Di([2,2'-bithiophen]-5-yl)-1H,1'H-2,2'-biindole (1 eq., 110 mg, 0.20 mmol) was dissolved in dry DMF (2.5 mL) and the solution was cooled at 0°C. KOH (5 eq., 55 mg, 0.98 mmol) was added and the solution was stirred at that temperature for 10 minutes. The reaction mixture was allowed to reach room temperature and then ethyl iodide (10 eq., 200 µL, 1.98 mmol) was added one pot. The reaction mixture was stirred at room temperature for 36 hours. The solvent was removed under reduced pressure and the obtained residue was dissolved into CH_2Cl_2; the organic phase was washed with water and brine then dried over $MgSO_4$, filtered and the solvent was removed under reduced pressure. The obtained residue was purified by column chromatography (*n*-hexane : CH_2Cl_2 = 7 : 3) to afford the desired product as a yellow solid.

Yield: 85 mg (70%);

^{1}H NMR ($CDCl_3$, 400 MHz): δ = 8.24 (d, J = 7.5 Hz, 2H), 7.49-7.34 (m, 6H), 7.14 (d, J = 4.8 Hz, 2H), 7.05 (m, 4H), 6.99 (d, J = 3.9 Hz, 2H), 6.97 (m, 2H), 6.85 (d, J = 3.6 Hz, 2H), 4.02-3.88 (m, 4H), 1.12 (m, 6H);

^{13}C NMR ($CDCl_3$, 100 MHz): δ = 137.7, 136.6, 135.9, 135.2, 127.7, 126.3, 126.0, 124.4, 124.2, 123.8, 123.3, 123.2, 120.7, 120.1, 113.2, 110.4, 39.0, 14.9.

M.S. (EI): 616.1 (100%).

9.14.3. Synthesis of 3,3'-bis(2,2'-bithiophen-5-yl)-1,1'-bis(*n*-propyl)-1*H*,1'*H*-2,2'-biindole, IND_2T_4Pr (39c)

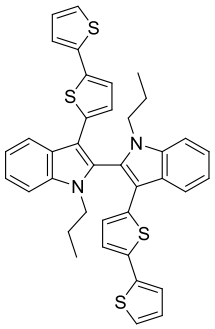

39c

3,3'-Di([2,2'-bithiophen]-5-yl)-1H,1'H-2,2'-biindole (1 eq., 135 mg, 0.24 mmol) was dissolved in dry DMF (3 mL) and the solution was cooled at 0°C. KOH (5 eq., 67 mg, 1.2 mmol) was added and the solution was stirred at that temperature for 10 minutes. The reaction mixture was allowed to reach room temperature and then 1-iodopropane (6 eq., 71 μL, 0.72 mmol) was added one pot. The reaction mixture was stirred at room temperature for 36 hours. The solvent was removed under reduced pressure and the obtained residue was dissolved into CH_2Cl_2; the organic phase was washed with water and brine, then dried over $MgSO_4$, filtered and the solvent was removed under reduced pressure. The obtained residue was purified by column chromatography (*n*-hexane : CH_2Cl_2 = 8 : 2) to afford the desired product as a yellow solid.

Yield: 120 mg (79%);

^{1}H NMR ($CDCl_3$, 400 MHz): δ = 8.21 (d, J = 7.8 Hz, 2H), 7.46-7.31 (m, 6H), 7.14 (d, J = 5.1 Hz, 2H), 7.02-6.94 (m, 4H), 6.82 (d, J = 3.9 Hz, 4H), 3.86-3.73 (m, 4H), 1.37-1.29 (m, 4H), 0.75 (t, J = 7.2 Hz, 6H);

^{13}C NMR ($CDCl_3$, 100 MHz): δ = 137.7, 137.1, 135.9, 135.3, 127.7, 126.5, 125.9, 124.4, 124.2, 123.8, 123.4, 123.2, 120.7, 120.6, 113.3, 110.6, 46.14, 23.0, 11.5.

M.S. (EI): 644.1 (100%).

9.14.4. Synthesis of 3,3'-bis(2,2'-bithiophen-5-yl)-1,1'-bis(*n*-hexyl)-1*H*,1'*H*-2,2'-biindole, IND_2T_4Hex (39d)

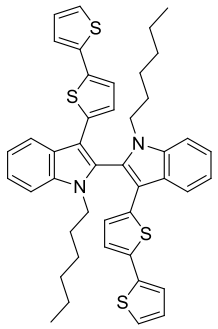

39d

3,3'-Di([2,2'-bithiophen]-5-yl)-1H,1'H-2,2'-biindole (1 eq., 135 mg, 0.24 mmol) was dissolved in dry DMF (3 mL) and the solution was cooled at 0°C. KOH (5 eq., 67 mg, 1.2 mmol) was added and the solution was stirred at that temperature for 10 minutes. The reaction mixture was allowed to reach room temperature and then 1-iodohexane (6 eq., 91 μL, 0.72 mmol) was added one pot. The reaction mixture was stirred at room temperature for 36 hours. The solvent was removed under reduced pressure and the obtained residue was dissolved into CH_2Cl_2; the organic phase was washed with water and brine, then dried over $MgSO_4$, filtered and the solvent was removed under reduced pressure. The obtained residue was purified by column chromatography (*n*-hexane : CH_2Cl_2 = 8 : 2) to afford the desired product as a yellow solid.

Yield: 130 mg (81%);

^{1}H NMR ($CDCl_3$, 400 MHz): δ = 8.21 (d, J = 7.8 Hz, 2H), 7.45-7.33 (m, 6H), 7.14 (d, J = 5.1 Hz, 2H), 7.01-6.94 (m, 4H), 6.82 (d, J = 3.9 Hz, 4H), 3.86-3.73 (m, 8H), 1.37-1.25 (m, 12H), 0.75 (t, J = 7.2 Hz, 6H);

^{13}C NMR ($CDCl_3$, 100 MHz): δ = 137.7, 137.1, 135.9, 135.3, 127.7, 126.5, 125.9, 124.4, 124.2, 123.8, 123.4, 123.2, 120.7, 120.6, 113.3, 110.6, 46.4, 30.3, 28.7, 25.7, 21.35, 11.8.

M.S. (EI): 728.2 (100%).

9.14.5. Synthesis of (*S*)-(1-bromoethyl)benzene (47)

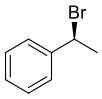

47

Pyridine (5 mL) was added to a stirred solution of (*R*)-1-phenyl ethanol (1 eq., 2 g, 16.4 mmol) in anhydrous pentane (50 mL), and the reaction mixture was stirred at -20 °C. A solution of $POBr_3$ (1.1 eq., 5.1 g, 18 mmol) in dry pentane (30 mL) was added dropwise to the mixture over a period of 45 minutes. After reaction for 15 minutes, the reaction mixture was slowly poured into cold water (150 mL). The phases were separated and the organic layer was washed with a 5% Na_2CO_3 solution, 2 M HCl and brine, then dried over $MgSO_4$, filtered and the solvent was removed under reduced pressure to afford the desired product as a colorless oil.[105]

Yield: 1062 mg (35%);

^{1}H NMR ($CDCl_3$, 400 MHz): δ = 7.47-7.28 (m, 5H), 5.25 (q, J = 6.9 Hz, 1H), 2.05 (d, J = 6.9 Hz, 3H);

$[\alpha]_D^{20}$= -96° (1g/100 mL in CH_2Cl_2);

ee = 86% (*S*).

9.14.6. Synthesis of (*R*)-(1-bromoethyl)benzene (48)

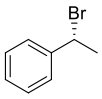

48

Pyridine (5 mL) was added to a stirred solution of (*S*)-1-phenyl ethanol (1 eq., 2 g, 16.4 mmol) in anhydrous pentane (50 mL), and the reaction mixture was stirred at -20 °C. A solution of $POBr_3$ (1.1 eq., 5.1 g, 18 mmol) in dry pentane (30 mL) was added dropwise to the mixture over a period of 45 minutes. After reaction for 15 minutes, the reaction mixture was slowly poured into cold water (150 mL). The phases were separated and the organic layer was washed with a 5% Na_2CO_3 solution, 2 M HCl and brine, then dried over $MgSO_4$, filtered and the solvent was removed under reduced pressure to afford the desired product as a colorless oil.[105]

Yield: 910 mg (30%);

^{1}H NMR ($CDCl_3$, 400 MHz): δ = 7.45-7.27 (m, 5H), 5.23 (q, J = 6.8 Hz, 1H), 2.07 (d, J = 6.8 Hz, 3H);

$[\alpha]_D^{20}$= -91° (1g/100 mL in CH_2Cl_2);

ee = 80% (*R*).

9.14.7. Synthesis of 3,3'-bis(2,2'-bithiophen-5-yl)-1,1'-bis((*R*)-1-phenylethyl)-1*H*,1'*H*-2,2'-biindole, (*R*)-IND$_2$T$_4$Ph (49)

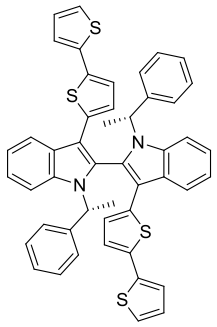

49

3,3'-Di([2,2'-bithiophen]-5-yl)-1H,1'H-2,2'-biindole (1 eq., 300 mg, 0.53 mmol) was dissolved in dry DMF (13 mL) and the solution was cooled at 0°C. KOH (5 eq., 150 mg, 2.67 mmol) was added and the solution was stirred for 15 minutes. The reaction mixture was allowed to reach room temperature and then (*S*)-(1-bromoethyl)benzene (10 eq., 900 mg, 4.89 mmol) was added one pot. The reaction mixture was stirred at room temperature for 36 hours. The solvent was removed under reduced pressure and the obtained residue was dissolved into CH_2Cl_2; the organic phase was washed with water and brine, then dried over $MgSO_4$, filtered and the solvent was removed under reduced pressure. The residue was purified by column chromatography (*n*-hexane : AcOEt = 97 : 3) to afford the desired product as a brown solid. The last fraction eluted was collected, the solvent removed under reduced pressure to give a single diastereoisomer (50 mg, 12%).

Yield: 375 mg (90%);

^{1}H NMR (CD_2Cl_2, 300 MHz): δ = 8.05 (d, J = 7.8 Hz, 2H), 7.25-6.87 (m, 26H), 5.53 (q, J = 7.2 Hz, 2H), 1.96 (d, J = 6.9 Hz, 6H);

^{13}C NMR ($CDCl_3$, 100 MHz): δ = 139.0, 136.5, 135.4, 134,4, 134.2, 127.1, 126.7, 126.3, 126.2, 125.5, 125.6, 124.9, 123.4, 122.9, 122.4, 121.9, 119.6, 119.5, 113.8, 112.5, 53.2, 19.03

MS (EI): 768 (100%);

$[\alpha]_D^{20}$= +694° (0.1 g/100 mL in CH_2Cl_2);

de = 85 %.

9.14.8. Synthesis of 3,3'-bis(2,2'-bithiophen-5-yl)-1,1'-bis((*S*)-1-phenylethyl)-1*H*,1'*H*-2,2'-biindole, (*S*)-IND$_2$T$_4$Ph (50)

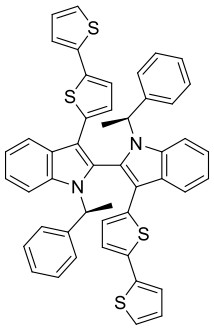

50

3,3'-Di([2,2'-bithiophen]-5-yl)-1H,1'H-2,2'-biindole (1 eq., 250 mg, 0.45 mmol) was dissolved in dry DMF (13 mL) and the solution was cooled at 0°C. KOH (6 eq., 150 mg, 2.67 mmol) was added and the solution was stirred at that temperature for 15 minutes. The reaction mixture was allowed to reach room temperature and then (*R*)-(1-bromoethyl)benzene (10 eq., 760 mg, 4.13 mmol) was added in one fraction. The reaction mixture was stirred at room temperature for 36 hours. The solvent was removed under reduced pressure and the obtained residue was diluted with CH_2Cl_2; the organic phase was washed with water and brine. The organic phase was dried over $MgSO_4$, filtered and the solvent was removed under reduced pressure. The obtained residue was purified by gravimetric chromatography (*n*-hexane : AcOEt = 97 : 3) to afford the desired product as a brown solid. The last fraction eluted was collected, the solvent removed under reduced pressure to give a single diastereoisomer (60 mg, 17%).

Yield: 383 mg (92%);

^{1}H NMR (CD_2Cl_2, 400 MHz): δ = 7.95 (d, J = 8.0 Hz, 2H), 7.17-6.73 (m, 26H), 5.42 (q, J = 6.9 Hz, 2H), 1.82 (d, J = 7.1 Hz, 6H);

^{13}C NMR ($CDCl_3$, 100 MHz): δ = 140.1, 137.6, 136.4, 135.5, 135.2, 128.2, 127.7, 127.4, 127.3, 126.5, 126.3, 126.0, 124.4, 124.0, 123.5, 123.0, 120.6, 120.6, 114.8, 113.6, 54.21, 20.1;

MS (EI): 768 (100%);

$[\alpha]_D^{20}$= -627° (0.1 g/100 mL in CH_2Cl_2);

de = 74 %.

9.15. Synthesis of 2,2'-bis{2-[7-(thiophen-2-yl)-2,1,3-benzothiadiazol-4-yl]thiophen-5-yl}-*N*,*N*'-dihexyl-1*H*,1'*H*-2,2'-biindole), IND_2BTD_2Hex (48)

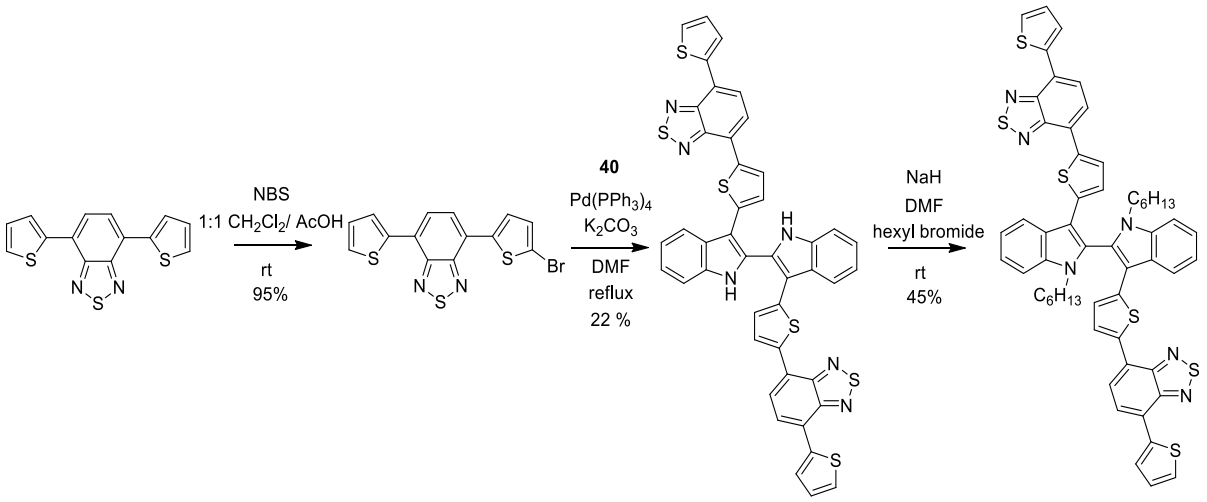

9.15.1. Synthesis of 4-(5-bromothiophen-2-yl)-7-(thiophen-2-yl)benzothiadiazole (44b)

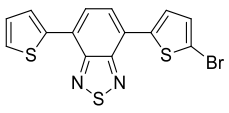

44b

NBS (1.1 eq., 280 mg, 1.6 mmol) was added in small portion over a period of 30 minutes to a stirred solution of 4,7-bis(thiophen-2-yl)benzothiadiazole (1 eq., 440 mg, 1.46 mmol) in CH_2Cl_2/AcOH (1:1, 126 mL), shielding the solution from the light. The reaction mixture was stirred for 24 hours at room temperature and then poured into water. The phases were separated and the organic layer was washed with saturated $NaHCO_3$ solution and brine. The organic phase was dried over $MgSO_4$, filtered and the solvent was removed under reduced pressure to afford the desired product as dark red solid.[106]

Yield: 530 mg (95%);

^{1}H NMR ($CDCl_3$, 400 MHz): δ = 8.13 (d, J = 3.6 Hz, 1H), 7.88-7.79 (m, 3H), 7.47 (d, J = 4.4 Hz, 1H), 7.21 (dd, J = 4.6 Hz, J = 4 Hz, 1H), 7.15 (d, J = 4 Hz, 1H).

9.15.2. Synthesis of 2,2'-bis{2-[7-(thiophen-2-yl)-2,1,3-benzothiadiazol-4-yl]thiophen-5-yl}-1*H*,1'*H*-2,2'-biindole, IND_2BTD_2 (45)

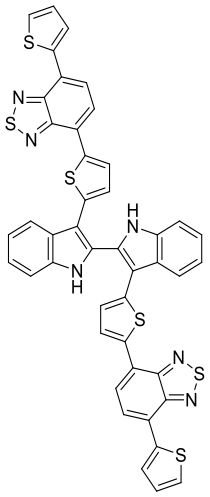

45

4-(5-Bromothiophen-2-yl)-7-(thiophen-2-yl)benzothiadiazole (4 eq., 1.97 g, 5.19 mmol), $Pd(PPh_3)_4$ (0.1 eq., 149 mg, 0.13 mmol) and K_2CO_3 (5 eq., 897 mg, 6.5 mmol) were added to a stirred solution of *N,N'*-(buta-1,3-diyne-1,4-diylbis(2,1-phenylene))bis(2,2,2-trifluoroacetamide) (1 eq., 551 mg, 1.3 mmol) in dry DMF (33 mL) under N_2 atmosphere. The reaction mixture was refluxed under stirring for 24 hours. The solvent was removed under reduced pressure and the residue was diluted with AcOEt; the organic phase was washed with water, dried over $MgSO_4$, filtered and the solvent was removed under reduced pressure. The residue was purified by column chromatography (*n*-hexane : CH_2Cl_2 = 3 : 7) to afford the desired product as a purple solid.

Yield: 170 mg (23%);

M.p.: 268°C;

^{1}H NMR (DMSO, 400 MHz): δ = 12.14 (s, 2H), 8.11 (m, 2H), 8.02 (d, J = 4.0 Hz, 2H), 7.97 (d, J = 7.6 Hz, 2H), 7.85 (d, J = 7.6 Hz, 2H), 7.77 (d, J = 4.8 Hz, 2H), 7.60 (d, J = 8.0 Hz, 2H), 7.39 (t, J = 7.6 Hz, 2H), 7.33 (t, J = 7.6 Hz, 2H), 7.28 (t, J = 4.0 Hz, 2H), 7.03 (d, J = 4.0 Hz, 2H);

^{13}C NMR-APT (DMSO, 100 MHz) δ = 151.5, 151.4, 139.1, 138.4, 128.0, 127.9, 127.8, 127.1, 126.9, 125.8, 125.7, 125.1, 124.5, 124.1, 123.0, 120.5, 119.6, 112.0, 110.4;

M.S. (EI): 828 (100%).

9.15.3. Synthesis of 2,2'-bis{2-[7-(thiophen-2-yl)-2,1,3-benzothiadiazol-4-yl]thiophen-5-yl}-*N*,*N*'-dihexyl-1*H*,1'*H*-2,2'-biindole, IND_2BTD_2Hex (46)

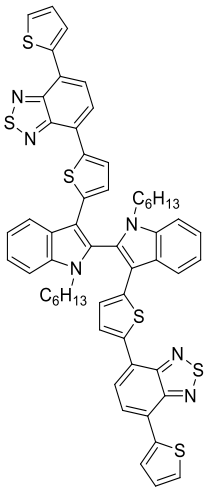

46

NaH (60% in mineral oil) (5 eq., 25 mg, 0.6 mmol) was added under stirring to a solution of 3,3'-bis(5-(7-(thiophen-2-yl)benzo[c][1,2,5]thiadiazol-4-yl)thiophen-2-yl)-1H,1'H-2,2'-biindole (1 eq., 100 mg, 0.12 mmol) in dry DMF (15 mL). After 15 minutes, *n*-hexyl bromide (10 eq., 159 µL, 1.2 mmol) was added one pot and the reaction mixture was stirred for 24 hours. The solvent was removed under reduced pressure and the residue was diluted with CH_2Cl_2; the organic phase was washed with water, was dried over $MgSO_4$, filtered and the solvent was removed under reduced pressure. The residue was purified by column chromatography (*n*-hexane : CH_2Cl_2 = 7 : 3) to afford the desired product as a red solid.

Yield: 50 mg (42%);

^{1}H NMR (CD_2Cl_2, 400 MHz): δ = 8.21 (d, J = 7.6 Hz, 2H), 7.98 (d, J = 3.2 Hz, 2H), 7.91 (d, J = 4.0 Hz, 2H), 7.71 (d, J = 7.6 Hz, 2H), 7.62 (d, J = 7.6 Hz, 2H), 7.42 (d, J = 8.0 Hz, 2H), 7.36-7.26 (m, 6H), 7.10 (dd, J = 5.2 Hz, J = 3.6 Hz, 2H), 6.98 (d, J = 3.6 Hz, 2H), 3.89 (m, 2H), 3.74 (m, 2H), 1.50 (m, 4H), 1.21 (m, 4H), 0.98 (m, 8H), 0.54 (t, J = 6.4 Hz, 6H);

^{13}C NMR-APT ($CDCl_3$, 100 MHz) δ = 151.5, 151.4, 138.5, 137.5, 136.2, 136.1, 126.9, 126.1, 124.8, 123.9, 123.9, 122.3, 119.8, 112.5, 109.7, 43.6, 30.3, 28.7, 25.7, 21.3, 12.8;

M.S. (EI): 996.2 (100%).

9.16. Synthesis of 2,2'-bis(2,2'-bithiophen-5-yl)-1,1'-binaphthalene, BN_2T_4 (55)

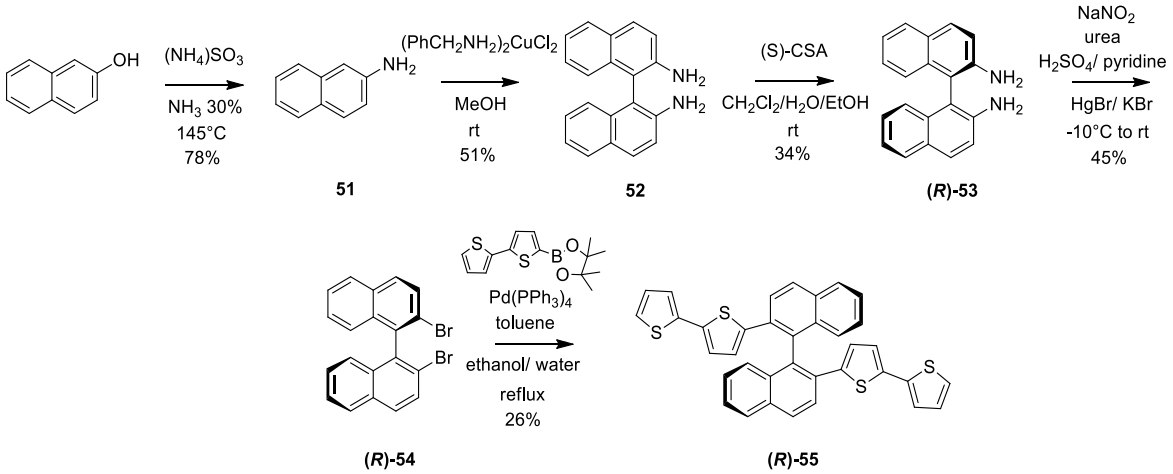

9.16.1. Synthesis of $CuCl_2$(benzylamine)$_2$ (57)

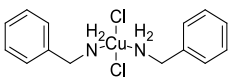

57

Benzylamine (2 eq., 42.86 g, 0.4 mol) was added to a methanol solution (270 mL) of $CuCl_2 \cdot 2\ H_2O$ (1 eq, 34.09 g, 0.2 mol) under stirring at room temperature. Immediately a green precipitate was formed and the mixture was stirred for 30 minutes at room temperature. The precipitate was filtered, washed with methanol and dried under vacuum.[107]

Yield: 63 g (89.6%);

IR (KBr): 3323 cm^{-1} = (NH_2), 3024 cm^{-1} = (Ar-H), 1562 cm^{-1} = (NH_2), 1494 cm^{-1}= $(C=C)_{ar}$, 1454 cm^{-1}= (CH_2), 752 cm^{-1} = (Ar-H), 697 cm^{-1}= $(C=C)_{ar}$

9.16.2. Synthesis of 2-naphthylnamine (51)

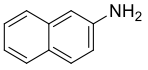

51

2-Naphtol (1 eq., 11.53 g, 80 mmol) and ammonium sulfite monohydrate (2 eq., 24.46 g, 160 mmol) were added to a steel autoclave and suspended in ammonium hydroxide solution (30%)

(112 mL); the solution was heated for 12 hours at 145°C. The reaction was then diluted with 1 M NaOH solution and extracted with CH_2Cl_2; the organic phases were dried with $MgSO_4$, filtered and the solvent was removed under reduced pressure. The obtained product was purified by column chromatography (CH_2Cl_2 : *n*-hexane = 7 : 3) to afford the desired product as a brown solid.[108]

Yield: 9 g (78%);

^{1}H NMR ($CDCl_3$, 300 MHz): δ 7.71 (d, J = 10 Hz, 2H), 7.68 (d, J = 10.3 Hz, 2H), 7.62 (d, J = 9.0 Hz, 2H), 7.37 (dt, J = 7.7 Hz, J = 1.3 Hz, 2H), 7.25 (dt, J = 7.7 Hz, J = 1.3 Hz, 2H), 7.02 (d, J = 2.7 Hz, 2H), 6.97 (dd, J = 9.3 Hz, J = 2.3 Hz, 2H), 3.87 (bs, 4H).

9.16.3. Synthesis of 1,1'-binaphthyl-2,2'-diamine (52)

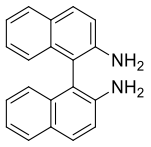

52

A methanol solution of 2-naphthylamine (1 eq., 716 mg, 5.0 mmol) was added to a methanol suspension of $CuCl_2$(benzylamine)$_2$ (2 eq., 3.487 g, 10 mmol) under stirring at room temperature. The reaction mixture was stirred at room temperature for 2 hours, then the solvent was removed under reduced pressure to give a brown residue, which was acidified with concentrated HCl (25 mL). The reaction mixture was stirred at room temperature for 10 minutes, then concentrated NH_4OH (75 ml) was added and the reaction mixture was stirred for 5 minutes and then diluted with water (125 mL). The resulting suspension was filtered to give the crude product.

The residue was purified by column chromatography (CH_2Cl_2: *n*-hexane = 7 : 3) to afford the desired product as a brown solid.[107]

Yield: 359 mg (51%);

^{1}H NMR ($CDCl_3$, 300 MHz): δ 7.71 (d, J = 10 Hz, 2H), 7.68 (d, J = 10.3 Hz, 2H), 7.62 (d, J = 9.0 Hz, 2H), 7.37 (dt, J = 7.7 Hz, J = 1.3 Hz, 2H), 7.25 (dt, J = 7.7 Hz, J = 1.3 Hz, 2H), 7.02 (d, J = 2.7 Hz, 2H), 6.97 (dd, J = 9.3 Hz, J = 2.3 Hz, 2H), 3.87 (bs, 4H).

9.16.4. Resolution of 1,1'-binaphthyl-2,2'-diamine with (*S*)-CSA ((*R*)-53)

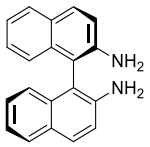

(*R*)-53

A solution of (*S*)-CSA (1 eq., 4.8 g, 20.63 mmol) in EtOH (5.78 mL) and water (3 mL) was added to a solution of 1,1'-binaphthyl-2,2'-diamine (1 eq., 5.87 g 20.63 mmol) in CH_2Cl_2 (76 mL), under slow stirring under inert atmosphere over a period of 10 minutes. After 3 minutes under very slow stirring the solution was kept still and shielded by light for 24 hours. The obtained precipitate was filtered, washed with CH_2Cl_2, collected and suspended in AcOEt. A 20% NaOH solution was added and the two phases were stirred for 1 hour. The phases were separated, dried over $MgSO_4$, filtered and the solvent was removed under reduced pressure to afford the desired product as a brown solid.

Yield: 2 g (34%);

$[\alpha]_D^{20}$= +151° (0.5 g / 100 mL in pyridine);

ee = 98 % (*R*).

The organic phase collected from the filtration were treated with a 20% NaOH solution was added and the two phases were stirred for 1 hour. The phases were separated, dried over $MgSO_4$, filtered and the solvent was removed under reduced pressure to afford the unprecipitated material.

9.16.5. Resolution of (*S*)-(-)-1,1'-binaphthyl-2,2'-diamine with (*R*)-CSA ((*S*)-53)

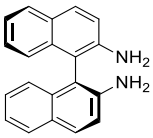

(*S*)-53

A solution of (*R*)-CSA (1 eq., 3.2 g, 13.78 mmol) in EtOH (3.86 mL) and water (2 mL) was added to a solution of 1,1'-binaphthyl-2,2'-diamine (1 eq., 3.92 g 13.78 mmol) in CH_2Cl_2 (51 mL), under slow stirring under inert atmosphere over a period of 10 minutes. After 3 minutes under very slow stirring the solution is kept still and shielded by light for 24 hours. The obtained precipitate was filtered, washed with CH_2Cl_2, collected and suspended in AcOEt. A 20% NaOH solution was added and the two phases were stirred for 1 hour. The phases were separated, the organic phases were dried over $MgSO_4$, filtered and the solvent was removed under reduced pressure.

Yield: 1.6 g (42%);

$[\alpha]_D^{20}$= - 153° (0.5 g / 100 mL in pyridine);

ee = 99 % (*S*).

The organic phase collected from the filtration were treated with a 20% NaOH solution was added and the two phases were stirred for 1 hour. The phases were separated, dried over $MgSO_4$, filtered and the solvent was removed under reduced pressure to afford the unprecipitated material.

9.16.6. Synthesis of (*R*)-(+)-1,1'-binaphthyl-2,2'-dibromide ((*R*)-54)

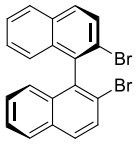

(*R*)-54

Concentrated H_2SO_4 (68 mL) was cooled to -10°C and $NaNO_2$ (5 eq., 2.1 g, 30 mmol) was slowly added under stirring. After the addition, the solution was allowed to come at room temperature until the $NaNO_2$ was dissolved then it was cooled between -5 and -10 °C.

A solution of (*R*)-1,1'-binaphthyl-2,2'-diamine (1 eq., 1.7 g, 5.98 mmol) in pyridine (14.6 mL) previously prepared was added dropwise to the solution, paying attention to keeping the temperature below -5 °C. The resulting dark solution was stirred for an additional hour. Small chunks of ice were slowly added to the stirring mixture, keeping the temperature below -5 °C. Addition of ice was continued until no rise in temperature was observed. An ice-cooled mixture of urea (5 eq., 1.8 g, 30 mmol) in water (44 mL) was then added dropwise, maintaining the temperature below -5 °C; the addition evolved persistent foam. When the addition was complete, the solution is stirred for 30 minutes.

A cold solution of mercuric bromine (2.8 eq., 6.03 g, 16.74 mmol) and KBr (8.5 eq., 6.05 g, 51 mmol) in water (40 mL) was then added to the reaction mixture, causing the immediate formation of a light brown precipitate that was collected by filtration.

The brown residue was grinded with KBr (10 eq, 7.14 g, 60 mmol) until a fine, intimate mixture was obtained. This mixture was dried in a round bottom flask under vacuum and heated at 95 °C (0.1 torr) for 2 h. The resulting residue was dissolved and extracted with CH_2Cl_2, the organic phase was washed with aqueous sodium bisulfite, dried over $MgSO_4$, filtered and the solvent

was removed under reduced pressure. The residue was purified by column chromatography (*n*-hexane : CH_2Cl_2 = 9 : 1) to afford the desired product as a yellow solid.[109]

Yield: 1.12 g (45%);

^{1}H NMR ($CDCl_3$, 300 MHz): δ = 7.95 (d, J = 9.0 Hz, 2H), 7.89 (d, J = 9.6 Hz, 2H), 7.53 (d, J = 10.0 Hz, 2H), 7.52 (dd, J = 7.7 Hz, J = 1.3 Hz, 2H), 7.33 (dd, J = 7.7 Hz, J = 1.6 Hz, 2H), 7.11 (d, J = 9 Hz, 2H);

$[\alpha]_D^{20}$= + 67.5° (1 g / 100 mL in CH_2Cl_2);

ee = 96 % (*R*).

9.16.7. Synthesis of (*S*)-(-)-1,1'-binaphthyl-2,2'-dibromide ((*S*)-54)

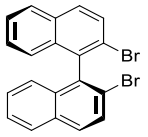

(*S*)-54

Concentrated H_2SO_4 (64 mL) was cooled to -10°C and $NaNO_2$ (5 eq., 1.94 mg, 28.13 mmol) was slowly added under stirring. After the addition, the solution was allowed to come at room temperature until the $NaNO_2$ was dissolved, then it was cooled between -5 and -10 °C.

A solution of (*S*)-1,1'-binaphthyl-2,2'-diamine (1 eq., 1.6 g, 5.63 mmol) in pyridine (14 mL) previously prepared was added dropwise to the solution, paying attention to keeping the temperature below -5 °C. The resulting dark solution was stirred for an additional hour. Small chunks of ice were slowly added to the stirring mixture, keeping the temperature below -5 °C. Addition of ice was continued until no rise in temperature was observed. An ice-cooled mixture of urea (5 eq., 16.9 g, 28.13 mmol) in water (42 mL) was then added dropwise, maintaining the temperature below -5 °C; the addition evolved persistent foam. When the addition was complete, the solution was stirred for 30 minutes.

A cold solution of mercuric bromine (2.8 eq., 5.68 g, 15.76 mmol) and KBr (8.5 eq., 5.7 g, 47.8 mmol) in water (5 mL) was then added to the reaction mixture, causing the immediate formation of a light brown precipitate that was collected by filtration.

The obtained brown residue was grinded with KBr (10 eq, 6.7 g, 56.3 mmol) until a fine, intimate mixture was obtained. This mixture was dried in a round bottom flask under vacuum and heated at 95 °C (0.1 torr) for 2 h. The resulting residue was dissolved and extracted with CH_2Cl_2, the organic phase was washed with aqueous sodium bisulfite, dried over $MgSO_4$, filtered and the solvent was removed under reduced pressure. The residue was purified by column chromatography (*n*-hexane : CH_2Cl_2 = 9 : 1) to afford the desired product as a yellow solid.[109]

Yield: 1.4 g (60%);

^{1}H NMR ($CDCl_3$, 400 MHz): δ = 7.94 (d, J = 9.0 Hz, 2H), 7.89 (d, J = 9.6 Hz, 2H), 7.53 (d, J = 10.0 Hz, 2H), 7.52 (dd, J = 7.7 Hz, J = 1.3 Hz, 2H), 7.33 (dd, J = 7.7 Hz, J = 1.6 Hz, 2H), 7.11 (d, J = 9 Hz, 2H);

$[\alpha]_D^{20}$= -34° (1 g / 100 mL in pyridine);

ee = 98.5 % (*S*).

9.16.8. Synthesis of (*R*)-2,2'-bis(2,2'-bithiophen-5-yl)-1,1'-binaphthalene, (*R*)-BN_2T_4 ((*R*)-55)

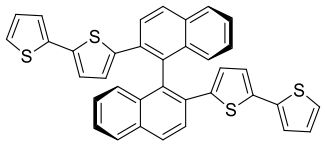

(*R*)-55

A mixture of (*R*)-(-)-1,1'-binaphthyl-2,2'-dibromide (1 eq., 182 mg, 0.44 mmol), 22-([2,2'-bithiophen]-5-yl)-4,4,5,5-tetramethyl-1,3,2-dioxaborolane (2.5 eq., 323 mg, 1.1 mmol), $Pd(PPh_3)_4$ (0.1 eq., 51 mg, 0.044 mmol) and Na_2CO_3 (3.5 eq., 164 mg, 1.55 mmol) in a degassed mixture of dry toluene (18 mL), ethanol (6 mL) and water (6 mL) was refluxed under argon atmosphere for 24 hours. Then, the reaction was cooled at room temperature and AcOEt was added; the organic phase was washed with water, dried with $MgSO_4$, filtered and the solvent was removed under reduced pressure. The residue was purified by column chromatography (*n*-hexane : CH_2Cl_2 = 9 : 1) to afford the desired product as a yellow solid.

Yield: 67 mg (26%);

^{1}H NMR ($CDCl_3$, 400 MHz): δ = 8.05 (d, J = 8.7 Hz, 2H), 7.93 (d, J = 8.4 Hz, 2H), 7.89 (d, J = 8.7 Hz, 2H), 7.46 (ddd, J = 8.1 Hz, J = 6.3 Hz, J = 1.8 Hz, 2H), 7.27-7.11 (m, 4H), 7.12 (dd, J = 4.2 Hz, J = 2.4, 2H) 6.92 (dd, J = 5.4 Hz, J = 3.6 Hz, 2 H) 6.91 (s, 2H), 6.79 (d, J = 3.9 Hz, 2H), 6.58 (d, J = 3.9 Hz, 2H);

^{13}C NMR ($CDCl_3$, 100 MHz) δ = 141.6, 137.8, 137.4, 134.0, 133.0, 132.8, 132.3, 128.9, 128.0, 127.6, 127.1, 127.0, 126.9, 126.6, 126.2, 124.1, 123.4, 123.3;

$[\alpha]_D^{20}$= +207° (0.1 g/100 mL in CH_2Cl_2)

ee = 96%

M.S. (ESI): 582 (100%), 584 (42%).

9.16.9. Synthesis of (*S*)-2,2'-bis(2,2'-bithiophen-5-yl)-1,1'-binaphthalene, (*S*)-BN_2T_4 ((*S*)-55)

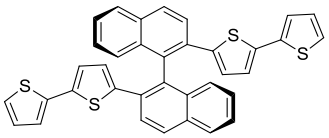

(*S*)-55

A mixture of (*S*)-(-)-1,1'-binaphthyl-2,2'-dibromide (1 eq., 226 mg, 0.55 mmol), 2-([2,2'-bithiophen]-5-yl)-4,4,5,5-tetramethyl-1,3,2-dioxaborolane (2.5 eq., 400 mg, 1.36 mmol), $Pd(PPh_3)_4$ (0.1 eq., 63 mg, 0.05 mmol) and Na_2CO_3 (3.5 eq., 204 mg, 1.93 mmol) in a degassed mixture of dry toluene (22 mL), ethanol (7.5 mL) and water (7.5 mL) was refluxed under argon atmosphere for 24 hours. Then, the reaction was cooled at room temperature and AcOEt was added; the organic phase was washed with water, dried with $MgSO_4$, filtered and the solvent was removed under reduced pressure. The residue was purified by column chromatography (*n*-hexane : CH_2Cl_2 = 9 : 1) to afford the desired product as a yellow solid.

Yield: 87 mg (27%);

^{1}H NMR ($CDCl_3$, 400 MHz): δ = 8.05 (d, J = 8.7 Hz, 2H), 7.93 (d, J = 8.4 Hz, 2H), 7.89 (d, J = 8.7 Hz, 2H), 7.46 (ddd, J = 8.1 Hz, J = 6.3 Hz, J = 1.8 Hz, 2H), 7.27-7.11 (m, 4H), 7.12 (dd, J = 4.2 Hz, J = 2.4, 2H) 6.92 (dd, J = 5.4 Hz, J = 3.6 Hz, 2 H) 6.91 (s, 2H), 6.79 (d, J = 3.9 Hz, 2H), 6.58 (d, J = 3.9 Hz, 2H);

^{13}C NMR ($CDCl_3$, 100 MHz) δ = 141.6, 137.8, 137.4, 134.0, 133.0, 132.8, 132.3, 128.9, 128.0, 127.6, 127.1, 127.0, 126.9, 126.6, 126.2, 124.1, 123.4, 123.3;

$[\alpha]_D^{20}$= -206° (0.1 g/100 mL in CH_2Cl_2)

ee = 98%

M.S. (ESI): 582 (100%), 584 (42%).

9.17. Synthesis of 2,2',4,4',5,5'-tetra(2-thienyl)-3,3'-bithiophene, $T8_3$ (60)

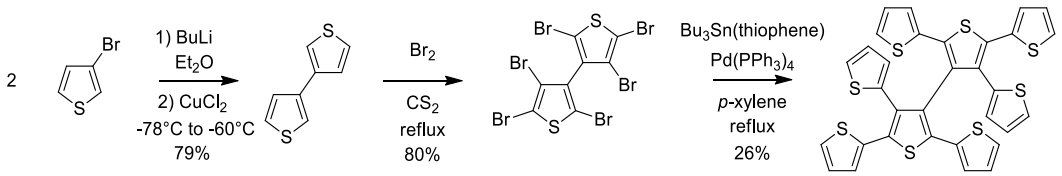

58 **59** **60**

9.17.1. Synthesis of 3,3'-bithiophene (58)

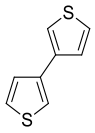

58

3-Bromothiophene (1 eq., 10 g, 61 mmol) was dissolved in anhydrous diethyl ether (50 mL). The solution was cooled at -78 °C. A 2.5 M solution of *n*-BuLi (in *n*-hexane) (1.1 eq., 26.8 mL, 67 mol) was added dropwise to the mixture over a period of 20 minutes. The reaction was stirred for 10 minutes at -78 °C and 20 minutes at -60 °C. Then $CuCl_2$ (1.1 eq., 8.7 g, 67 mol) was added in one portion at -60 °C. The reaction was kept at -60 °C for 1 hour and warmed to room temperature and stirred for 24 hours at room temperature. The reaction mixture was quenched with water (30 mL). The phases were separated and the organic layer was dried over $MgSO_4$, filtered and the solvent was removed under reduced pressure. The residue was purified by column chromatography (*n*-hexane) to afford the desired product as a white solid.[110]

Yield: 4 g (79%);

^{1}H NMR ($CDCl_3$, 300 MHz): δ = 7.40-7.37 (m, 2H), 7.36-7.34 (m, 4H).

9.17.2. Synthesis of hexabromo-3,3'-bithiophene (59)

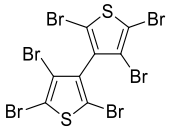

59

Liquid Br_2 (32 eq., 5.0 mL, 96 mmol) was added dropwise to a solution of 3,3'-bithiophene (1 eq., 500 mg, 3.0 mmol) in dry CS_2 (15 mL) and the solution was heated to reflux for 36 h. A saturated solution of $Na_2S_2O_5$ in water was added portion-wise to the mixture until the brown color completely disappeared. The crude product, separated as a brown-colored solid, was repeatedly treated with hot ethanol to remove all soluble impurities.[111]

Yield: 1.56 g (80%);

M.p. 180–183 °C;

M.S. (EI) = 640 [M^+].

9.17.3. Synthesis of 2,2',4,4',5,5'-tetra(2-thienyl)-3,3'-bithiophene (60)

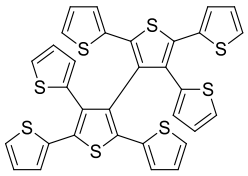

60

A mixture of hexabromo-3,3'-bithiophene (1 eq., 0.50 g, 0.8 mmol), 2-(tributylstannyl) thiophene (8 eq., 2.4 g, 6.4 mmol) and $Pd(PPh_3)_4$ (0.2 eq., 0.185 g, 0.16 mmol) in *p*-xylene (25 mL), was refluxed under nitrogen atmosphere for 20 h. The reaction mixture was filtered on a silica gel cake to remove the catalyst, the solvent was removed under reduced pressure and the crude residue was purified by column chromatography (*n*-hexane : CH_2Cl_2 = 8 : 2) to afford the desired product as a pale yellow solid.[111]

Yield: 150 mg (26%);

M.p.: 120–125 °C;

^{1}H NMR ($CDCl_3$, 400 MHz): δ = 7.24 (dd, J = 5.1 Hz, J = 1.2 Hz, 2H), 7.17 (dd, J = 5.1 Hz, J = 1.1 Hz, 2H), 7.16 (dd, J = 5.1 Hz, J = 1.0 Hz, 2H), 7.13 (dd, J = 3.7 Hz, J = 1.1 Hz, 2H), 7.06 (dd, J = 3.7 Hz, J =

1.1 Hz, 2H), 6.95 (dd, J = 5.1 Hz, J = 3.7 Hz, 2H), 6.92 (dd, J1 = 5.1 Hz, J = 3.7 Hz, 2H), 6.87 (dd, J = 5.1 Hz, J = 3.5 Hz, 2H), 6.56 (dd, J = 3.5 Hz, J = 1.1 Hz, 2H);

^{13}C NMR ($CDCl_3$, 100 MHz) δ = 135.7, 135.6, 135.0, 134.9, 133.3, 132.6, 131.9, 128.9, 127.0, 126.9, 126.8, 126.6, 126.2, 126.1, 126.0, 125.1;

M.S. (EI): 658 [M^+].

9.18. General procedure of monomers oxidation

A solution of the monomer (1 eq., 0.2 mmol) in dry $CHCl_3$ (50 mL) was added dropwise under N_2 atmosphere into a slurry of $FeCl_3$ (5 eq., 1 mmol) in dry chloroform (200 mL), under stirring at room temperature over a period of 2-5 hours. The dark mixture obtained was stirred for 24 hours at room temperature, then the volume of the solvent was reduced to 50 mL by evaporation under reduced pressure and the remaining solution was poured into MeOH (150 mL); then few drops of hydrazine hydrate were added and the solution turns orange-red. The obtained precipitate was recovered by filtration and then extracted with THF using soxhlet apparatus affording a soluble residue composed by oligomers.

10. References

[1] http://www.luc.edu/faculty/spavko1/minerals/quartz/qa4.htm;

[2] https://en.wikipedia.org/wiki/Neptunea_despecta;

[3] Organic Chemistry, Solomons & Fryhle, 8th edition;

[4] Avrin, J.S.; *Symmetry*, **2012**, *4*, 39-115;

[5] Benincori, T.; Marchesi, A. et al.; *Chemistry - A European Journal*, **2009**, *15*, 86-93;

[6] Lange's Handbook of Chemistry, James G. Speight, 16th edition;

[7] Smith, S.W.; *Toxicol. Sci.*, **2009**, *110*, 4-30;

[8] Pochettino, A.; *Acad. Lincei Rend.* **1906**, *15*, 355;

[9] Shirakawa, H; Louis, E. J.; MacDiarmid, A. G. et al.; *Chem. Commun.*, **1977**, 578-580;

[10] Peierl, R. E.; *Quantum Theory of Solids* **1956**, Oxford Univeristy press, London;

[11] Roncali, J.; *Macromol. Rapid Commun.* **2007**, *28*, 1761-1775;

[12] Heeger, A.; *Chem. Soc. Rev.* **2010**, *39*, 2354-2371;

[13] Bredas, J. L.; *J. Chem. Phys.* **1985**, *82*, 3808;

[14] Yu, G.; Gao, J. at al.; *Science* **1995**, *270*, 1789-1791;

[15] Kane-Maguire, L.A; Wallace, G.G.; *Chem. Soc. Rev.*, **2010**, *39*, 2545-2576;

[16] Watanabe, K., Suda, K.et al.; *Chem. Mater.,* **2012**, *24*, 1011-1024;

[17] Janssen, R.A.J.; Langeveld-Voss, B.M.W. et al. *J. Molecular Structure*, **2000,** *521*, 285-301;

[18] Pleus, S. and Schwientek M.; *Synthetic Metals*, **1998**, *95*, 233-238;

[19] Wienk, M.M.; Kroon, J.M. et al.; *Angew. Chem. Int. Ed.*, **2003**, *42*, 3371-3375;

[20] Torsi, L; Farinola, G.M. et al.; *Nature Materials*, **2008**, *7*, 412-417;

[21] Dong, L.; Lu, B. et al.; *J. Pol. Chem. A,* **2015***, 53,* 2238-2251;

[22] Muskal, N.; Turyan, I. et al.; *J. Am. Chem. Soc*., **1995**, *117*, 1147-1148;

[23] Nakanishi, T.; Matsunaga, M. et al.; *J. Am. Chem. Soc*., **2006**, *128*, 13322-13323;

[24] Han, Q.; Chen, Q. et al.; *Electroanalysis*, **2012**, *24*, 332-337;

[25] Nie, R; Bo. X. et al.; *Electrochemistry communications*, **2013**, *27*, 112-115;

[26] Wattanakit, C; Kuhn, A. et al.; *Nature Comm*., **2014**, *5*, 3325-3332;

[27] Yutthalekha, T.; Kuhn, A. et al; *Nature Comm*., **2016**, 7, 12678-12685;

[28] Sannicolò, F.; Rizzo, S. et al.; *Electrochimica Acta*, **2010**, *55* (27), 8352-8364;

[29] Sannicolò, F.; Arnaboldi, S. et al.; *Angew. Chem. Int. Ed*., **2014**, *53*, 2623-2627;

[30] Sannicolò, F.; Mussini, P.R. et al.; *Chem. Eur. J.*, **2014**, *20*, 15298-15302;

[31] Arnaboldi, S.; Benincori, T. et al.; *Chem. Sci.*, **2015**, *6*, 1706–1711;

[32] Arnaboldi, S.; Benincori, T. et al.; *Anal. Bioanal. Chem*., **2016**, *408*, 5243-7254;

[33] Mena-Osteritz, E. and Bäuerle, P.; *Adv. Mater*., **2006**, *18*, 447-451;

[34] Quartapelle Procopio, E., Benincori, T., Appoloni, G. et al.; A family of solution-processable macrocyclic and open-chain oligothiophenes with atropoisomeric scaffolds: structural and electronic features for potential energy applications; *New Journal of Chemistry*, **2017**, *41*, 10009-10019;

[35] Sanchez-Carnerero, E.M.; Agarrabeitia, A.R. et al.; *Chem. Eur. J*., **2015**, *21*, 13488-13500;

[36] Kumar, J.; Kawai, T. et al.; *Chem.Commun*., **2017**, *53*, 1269—1272;

[37] Longhi, G.; Abbate, S. et al.; *J. Phys. Chem. C*, **2014**, *118*, 16019-16027;

[38] Rybakiewicz, R., Glowacki, E.D. et al.; *Chemistry - A European Journal*, **2017**, *23*, 2839-2851;

[39] Busireddy, M.R.; Mantena, V.N.R. et al.; *Organic Electronics*, **2016**, *37*, 312-325;

[40] Domínguez, R.; Schulz, G.L. et al.; *Dyes and Pigments*, **2017**, *143*, 112-122;

[41] Tomar, M.; Ashar, A.Z. et al.; *Journal of Polymer Research*, 23, **2016**, 1-10;

[42] Harada, N.; Nakanishi, K. et al; "Comprehensive Chiroptical Spectroscopy", Volume Two **2012**, Wiley, Hoboken, NJ, Chapter 4, 115-166;

[43] Scheuble, M.; Goll, M. et al.; *Macromol. Rapid Commun*. **2015**, *36*, 115−137;

[44] Richter, T.; Ludwigs, S. et al.; *Macromolecules,* **2012**, *45*, 5782−5788;

[45] Scheuble, M.; Ludwigs, S. et al.; *Polym. Chem*., **2014**, *5*, 6824–6833;

[46] Kirchmeyer, S.; Reuter, K. *J. Mater. Chem.* **2005**, *15*, 2077-2088;

[47] Heywang, G.; Jonas, F.; *Adv. Mater.*, **1992**, *4*, 117;

[48] Groenendaal, L.; Zotti, G. et al.; *Adv. Mater*., **2003**, 15, 855–879;

[49] Abdo, N. I.; Ku, J. et al.; *J. Mater. Chem. A,* **2013**, *1*, 10306-10317;

[50] Meerholz, K. and Heinze, J.; *Electrochimica Acta*, **1996**, *41*, 1839-1854;

[51] Perepichka, I. F. and Perepichka, D. F.; *Handbook of Thiophene-based Materials: Applications in Organic Electronics and Photonics.*; John Wiley & Sons Ltd. **2009**;

[52] Plieth, W.; Wilson, S. et al.; *Pure & Appl. Chem*., **1998**, *70*, 1395-1414;

[53] Skotheim, T.A.; Reynolds, J. R. et al.; *Conjugated polymers: Theory, Synthesis, Properties, and Characterization*; CRC Press Taylor & Francis Group; **2007**;

[54] Schiavon, G.; Sitran, S. et al.; *Synthetic Metals*, **1989**, *32*, 209-217;

[55] Ofer, D.; Crooks, R. M. et al*.; J. Am. Chem. Soc.*., **1990**, *112*, 7869-7879;

[56] Link, S.; Scheuble, M.; Ludwigs, S. et al.; *Langmuir,* **2013**, *29*, 15463 −15473;

[57] Neto, B.; Lapis, A. et al.; *Eur. J. Org. Chem.,* **2013**, 228–255;

[58] Ledwon, P.; Thomson, N. et al.; *RSC Adv*., **2015**, *5*, 77303–77315;

[59] Mo, H.; Radke, K. R. et al.; *Phys. Chem. Chem. Phys*., **2010**, *12*, 14585-14595;

[60] Barlow, S.; Odom, S. A. et al.; *J. Phys. Chem*., **2010**, *114*, 14397-14407;

[61] Cansu-Ergun, E: G.; Akbayrak, M. et al.; *J. Electrochem. Soc*., **2016**, *163*, G153-G158;

[62] Li, J. C.; Kim, S. J. et al.; *Macromol. Res*., **2009**, *17*, 356-360;

[63] Abbiati, G.; Arcadi, A. el al.; *Tetrahedron*, **2006**, *62*, 3033-3039;

[64] Larock, R. C.; Yum, E. K. et al.; *J. Am. Chem. Soc*., **1991**, *113*, 6689-6690;

[65] Glaser. C; *Ber. Dtsch. Chem. Ges.*, vol. 2, nº 1, **1869**, 422-424;

[66] Rizzo, S.; Menta, S. et al.; *J. of Chromatography A*, **2014**, *1363*, 128–136;

[67] Boas, U.; Dhanabalan, A. et al.; *Synlett.*, **2001**, *5*, 634-636;

[68] Amatore, C.; Le Duc, G. et al.; *Chem. Eur. J.*, **2013**, *19*, 10082-10093;

[69] Lennox A. J. J. and Lloyd-Jones G. C.; *Angew. Chem. Int. Ed*., **2013**, *52*, 7362-7370;

[70] Perepichka, I.F., Perepicka D.F. (Eds.), Handbook of Thiophene-based materials. Application in Organic Electronics and Photonics. Wiley, Chichester, **2009**;

[71] Ma, C. Q.; Fondrona, M. et al.; *Adv. Funct. Mater*., **2008**, *18*, 3323 – 3331;

[72] Richter, T. V.; Ludwigs, S. et al.; *Macromol. Rapid Commun*., **2009**, *30*, 1323-1327;

[73] Richter, T. V.; Bühler, C.; Ludwigs, S.*; J. Am. Chem. Soc*., **2012**, *134*, 43–46;

[74] Bilge, A.; Zen, A. et al.; *J. Mater. Chem*., **2006**, *16*, 3177-3182;

[75] Nicolas, Y.; Blanchard, P. et al.; *Org. Lett*., **2004**, *6*, 273-276;

[76] Sun, B. X.; Liu, Y. Et al.; *Funct. Mater.,* **2006**, *16*, 917-925;

[77] Ma, C.; Mena-Osteriz, E. et al.; *Angew. Chem.,* **2007**, *119*, 1709-1713;

[78] Xia, C.; Fan, X. et al.; *Org. Lett*., **2002**, 4, 2067-2070;

[79] Benincori, T.; Capaccio, M. et al.; *Chem. Eur. J*., **2008**, *14*, 459-471;

[80] Muccini, M.; *Nature Mater*. **2006**, *5*, 605-613;

[81] Grate, J. W. and Frye, G. C.; *Sensors Update*, *Vol. 2*, Wiley-VCH, Weinheim, **1996**, pp. 10-20;

[82] Huynh, T.; Wojnarowicz, A. et al.; *Biosens. Bioelectron*., **2015**, *70*, 153 -160.

[83] Still, W. C.; Kahn, M. et al.; *J. Org. Chem.* **1978**, *43*, 2923 - 2925;

[84] Skelton, R.; Dubois, F. et al.; *Anal. Chem.* **2000**, *72*, 1707-1710;

[85] Link, S.; Richter, T.; Ludwigs, S. et al.; *J. Phys. Chem. B* **2010**, *114*, 10703-10708;

[86] Yamamoto, T.; Ogawa, S. et al.; *Tetrahedron*, **2004**, *45*, 3221-3230;

[87] Kauffmann, T.; Muke, B. et al.; *Angewandte*, **1975**, *87*, 746-747;

[88] Kitagawa, T.; Matsubara, H. et al.; *Molecules*, **2014**, *19* (9), 15298-15312;

[89] Crisp, G. T.; *Synthetic Comm*., **1989**, *19*, 307-316;

[90] Hui-Jun, Y.; Jong-Man, P. et al; *J. of Nanoscience and Nanotechnology*, **2014**, *14*, 5942-5946;

[91] Aya, Y.; Akihiro, N. et al.; *Research on Chemical Intermediates*, **2014**, *40*, 2381-2389;

[92] Andrei, H.; Robert, M. M. et al.; *J. Am. Chem. Soc.*, **2007**, *129*, 8310-8319;

[93] Koeckelberghs, G.; De Cremer, L. et al.; *Tetrahedron*, **2005**, *61*, 687-691;

[94] Yuancheng, Q.; Xing, L. et al.; *RSC Advances*, **2015**, *5*, 2147-2154;

[95] Lange, A., Krueger, H. et al.; *J. Pol. Chem. A*, **2012**, *50*, 1622-1635;

[96] Coppo, P.; Cupertino, D. C. et al.; *Macromolecules*, **2003**, *36*, 2705–2711;

[97] Zhang, W., Meng NG, G. et al.; *J. Pol. Chem. A*, **2011**, *49*, 1865-1873;

[98] Mishra, A.; Ma, C.-Q. et al.; *Chem. Eur. J.*, **2009**, *15*, 13521-13534;

[99] Wang, S-A.; Hung, W-Y. et al.; *Org. electronics*, **2012**, *13*, 1576-1582;

[100] Ma, C-Q.; Mena-Osteritz, E. et al.; *Chem. Eur. J.*, **2012**, *18*, 12880-12901;

[101] DaSilveira Neto, B. A.; Lopes A. et al.; *Tetrahedron*, **2005**, *61*, 10975-10982;

[102] Lee, J-F; Hsu, S. L-C et al., *J. Pol. Chem. A*, **2011**, *49*, 4618-4625;

[103] Lin-Feng, Y.; Cong-Wu, G.; *Polymer*, **2015**, *59*, 57-66;

[104] Balamurugan, R.; Naveen, N. et al.; *Aust. J. Chem*., **2011**, *64*, 567-575;

[105] Chen, W.; L. Tang, J. et al.; *Angew. Chem. Int. Ed.,* **2010**, *49*, 5278;

[106] Jeum-Jong, K.; Hyunbong, C et al.; *J. Mater. Chem*., **2008**, *18*, 5223-5229;

[107] Zi, G.; Xiang, L. et al.; *Appl. Organometal. Chem*., **2007**, *21*, 177–182;

[108] Cañete, A.; Meléndrez M. X. et al.; *Syn. Comm*., **2001**, *31*, 2143-2148;

[109] Brown, K. J.; Berry, M. S. et al; *J. Org. Chem.*, **1985**, *50* (22), 4345–4349;

[110] R. Satapathy, Y. H. Wu, H. C. Lin, *Org. Lett.,* **2012**, 14, 2564-2567;

[111] Sannicolò, F.; Mussini, P. R. et al.; *Chem. Eur. J*., **2016**, *2*, 10839-10847;

11. Appendix – Towards a new low band donor-acceptor copolymer

11.1. Introduction

During the period spent in the prof. Ludwigs' group we moved our attention from inherent chirality to the synthesis of a new donor-acceptor copolymer, exploiting the expertise of the Institut für PolymerChemie (IPOC), was planned.

Donor/acceptor polymer (D-A) structure, based on a blend of two types of conjugated polymers acting as an electron donor and electron acceptor, have recently attracted considerable attention for the preparation of solar cells because they have numerous potential advantages over conventional polymer/fullerene blend solar cells.[1]

The most widely studied bulk-heterojunction organic solar cells (BHJ) structure in which a conjugated polymer is intimately mixed with a low-molecular-weight fullerene derivative[2]: D-A polymers, compared to fullerene-based structure, allow a flexible molecular design of both the components (and not only for the donor, as in BHJ solar cells), tuning the optical, morphological and electronic properties of materials. Furthermore, polymer/polymer blends can harvest a larger fraction of solar light and all-polymer blends yield superior thin-film formation properties, including flexibility and mechanical robustness.[3]

Unfortunately, the majority of these D-A polymer/polymer have exhibited significantly lower electron mobility (μ_e) than the fullerene derivatives, resulting in lower charge generation efficiency. For this reason, significant efforts have been made towards enhancing the power conversion efficiencies (PCEs) of polymer/polymer blend solar cells, trying to achieve and develop low-bandgap polymer acceptors with both high μ_e and high electron affinity.

The D:A blend ratio is an important parameter with regard to the fabrication of polymer/polymer blend solar cells. Ito and co-workers[4] have investigated the effect of the D:A ratio on the photovoltaic performance of polymer/polymer blend solar cells based on an amorphous donor PTQ1 and a semi crystalline acceptor P(NDI2OD-T2) (Figure A 1) proving that photovoltaic parameters depend strongly on the D:A ratio.

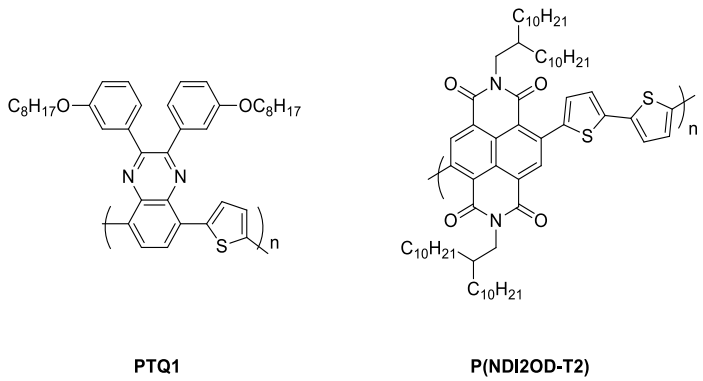

PTQ1 **P(NDI2OD-T2)**

Figure A 1: Chemical structures of PTQ1 and P(NDI2OD-T2).

Regioregular poly(3-hexylthiophene) (P3HT) and 2,2';3,2"-terthiophene (3T) are two of the most widely used donor polymers in the polymer/polymer BHJ solar cells because of their excellent hole mobility owing to the π–π interchain stacking in crystals. On the other hand, benzothiadiazole derivate are well-known to be suitable electron acceptors structure. Finally, EDOT is a well-known building block for the preparation of oligomers and polymers and, as previously reported in this thesis it possesses a remarkable conductivity, it is relatively stable in its oxidized form, and above all, it is endowed with a quite low redox potential and a moderate band gap, properties strongly required for the preparation of a D-A polymer.

It was reported by Ludwigs and co-worker[5] that the use of a branched monomer unit like 3T leads to the formation of 3D oligothiophene networks, in particular in the presence of EDOT as co-monomer. EDOT was found to be able to tune the properties of the material: it was introduced not only on the 3T structure (leading to a $3TE_3$ monomer) but also it was used as co-monomer during electropolymerization processes in different 3T:EDOT ratio. The architectures resulting from the analysis were found to be interesting for electrochemical devices where ions flow in and out of the structure is required. The project to investigate further copolymerization of 3T with other interesting co-monomers (e.g., for the preparation of low-bandgap polymers) arises from the results obtained in this field.

11.2. Results and discussion

2,2':3',2''-Terthiophene (3T) and 4,7-bis(3,4-diethylenedioythiophene)benzo[*c*][1,2,5]thiadiazole (BTDE) (Figure A 2) were selected for the preparation of a D-A copolymer.

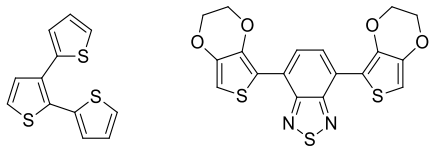

Figure A 2: 2,2′:3′,2′′-Terthiophene (3T) and 4,7-bis(3,4-diethylenedioythiophene)benzo[*c*][1,2,5]thiadiazole (BTDE).

BTDE was synthesized according to a Stille protocol by reaction between 4,7-dibromobenzothiadiazole and the 2-tributylstannyl-3,4-ethylenedioxythiophene. The latter was obtained, in turn, by treatment with *n*-BuLi and the generated anion was reacted with tributyltin chloride to give the desired product.

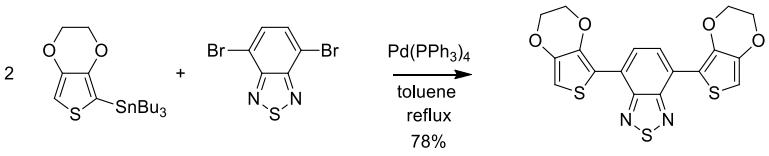

Scheme A 1: Synthesis of BTDE.

Both the monomers have characteristics suitable to undergo chemical or electrochemical oxidation. Scheme A 2 represents the conditions applied in order to promote the formation of the two homopolymers and the copolymer.

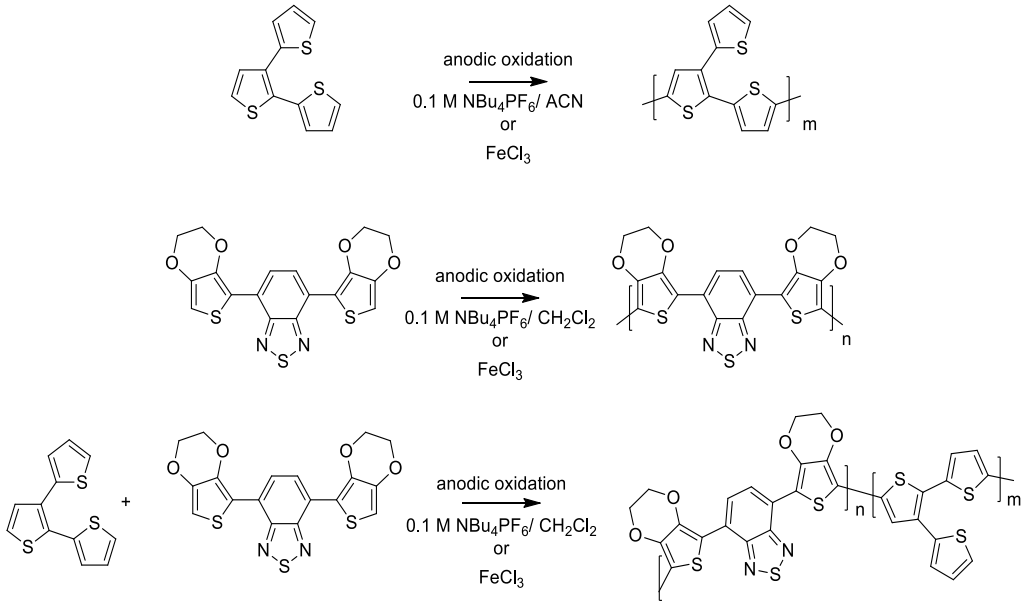

Scheme A 2: Formation of homopolymers and copolymer by anodic oxidation processes from monomer 3T, BTDE or a mixture of 3T and BTDE.

It must be considered that, for the direct electrochemical copolymerization of two different monomers, the oxidation potentials of the two co-monomer species must be very similar.[6] Preliminary cyclic voltammetric measurements on ITO electrodes in 0.1 M tetrabutylammonium hexafluorophosphate (NBu_4PF_6)/CH_2Cl_2 or acetonitrile, however, showed that the oxidation potentials are very different, being specifically E_{ox} (vs Fc/Fc^+) of BTDE (-0.55 V on ITO) and 3T (+0.4 V on ITO) ($\Delta E_{ox} \cong 1$ V). The possibility of a major tendency to homopolymerization compared to copolymerization must be considered.

For this reason, preliminary tests aimed to prove the possible copolymerization were carried out. Chemical oxidation mediated by $FeCl_3$ was carried out on a 1:1 mixture of 3T and BTDE in a chloroform diluted solution under Ar atmosphere. The oxidized black material was treated with hydrazine hydrate in order to reduce the material, filtered and extracted with THF through a soxhlet apparatus. The resulted oligomeric mixture was analyzed by MALDI mass analysis: the spectrum is depicted in Figure A 3 A while the complete peaks analysis is reported in Table A 1. The trend observed was, mainly, a strong tendency of 3T to homopolymerize to give a mixture of oligomers of different length (up to seven units). The formation of copolymers was observed and a different number of 3T units were found but containing just one BTDE unit. On the other hand, BTDE showed a lower tendency to polymerize both with itself and with 3T. However, the small amounts of BTDE polymers isolated after the soxhlet extraction could be attribute to the low solubility of the monomer itself.

However, the possibility to chemically copolymerize the two monomers seems to be attainable but, in order to complete the mass characterization, a second MALDI analysis was carried out from the material electrodeposited on electrode surfaces. The copolymeric films of ec-p(BTDE-co-3T)-[1:1], deposited on ITO electrodes in CH_2Cl_2 containing 0.1 M NBu_4PF_6 as supporting electrolyte were physically removed from the electrodes and treated according to the procedure reported by Skelton and co-workers[7]: that is a solid-phase method used for analyzing non-soluble polymers and it requires to grind in a mortar appropriate quantity of matrix, ionizer and sample and mashing the obtained mixture directly on the polished steel target through a spatula.

This technique, compared to the usually used dried-droplet method, leads to spectra less resolved and with higher background noise (as is possible to observe from Figure A 3 B) but it is necessary for compounds not enough soluble to be dissolved and deposited as drop on the target.

A different behaviour (summarized in Figure A 3 B and in Table A 1) was found from the analysis of the ec-p(BTDE-co-3T)-[1:1]: a less strong tendency of 3T homopolymerization and a much wider range of BTDE-3T copolymers were observed. This behaviour confirmed the results of chemical oxidation: 3T and BTDE can indeed copolymerize (chemically and electrochemically) despite the huge difference between their oxidative potential. The low amount of the BTDE-3T copolymer found in the ch-p(BTDE-co-3T)-[1:1] analysis must be related to the low solubility of the oligomers with higher molecular weight and, especially, higher number of BTDE units in their structure.

After demonstrating the reliability of the copolymerization between 3T and BTDE, an electrochemical characterization of the homopolymers and of the copolymer was carried out.

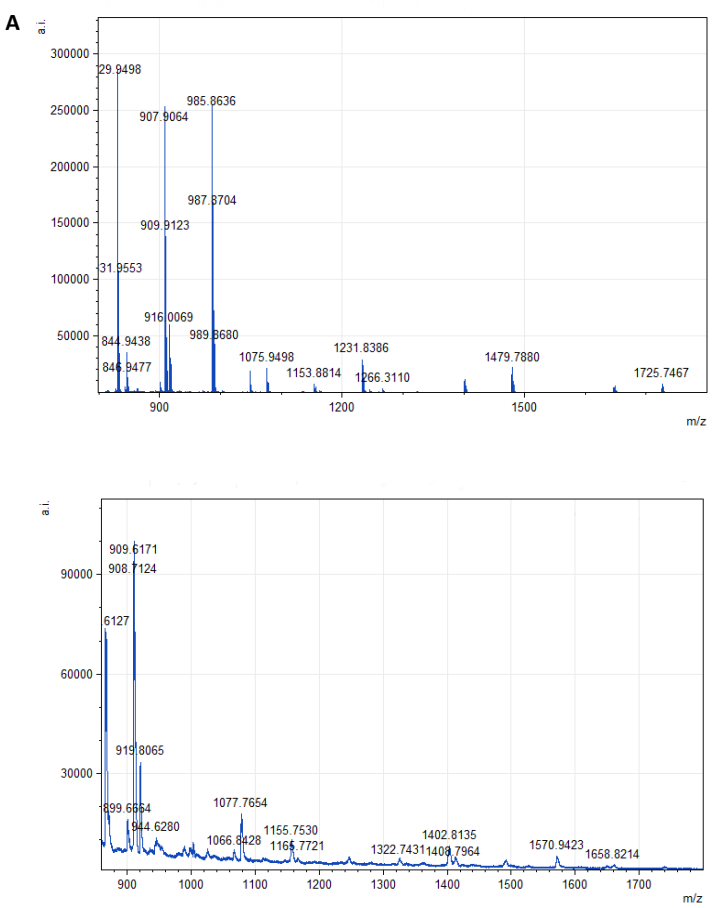

Figure A 3: A) MALDI spectrum of ch-p(BTDE-co-3T)-[1:1], sample prepared by the dried-droplet method. B) MALDI spectrum of ec-p(BTDE-co-3T)-[1:1], sample prepared with solid-phase method.

	ch-p(BTDE-co-3T)-[1:1]				ec-p(BTDE-co-3T)-[1:1]			
BTDE : 3T	***m/z***	***calc.***	***int***	***r.int.***	***m/z***	***calc.***	***int***	***r.int.***
2 : 0	829.950	829.98	276506.418	100.000			-	
1 : 2	907.906	907.92	233900.877	84.591	908.712	907.92	81931.375	93.480
0 : 4	985.864	985.87	248470.634	89.861			-	
2 : 1	1075.950	1075.94	20582.846	7.444	1076.832	1075.94	10540.636	12.026
1 : 3	1153.881	1153.89	6986.097	2.527	1154.836	1153.89	4308.048	4.915
0 : 5	1231.839	1231.83	28749.198	10.397			-	
3 : 0			-		1244.875	1243.96	1559.731	1.780
2 : 2			-		1322.743	1321.9	971.720	1.109
1 : 4	1399.844	1399.85	9565.625	3.459	1398.871	1399.85	876.195	1.000
0 : 6	1477.797	1477.79	14839.250	5.367			-	
3 : 1			-		1488.216	1489.92	915.041	1.044
2 : 3			-		1570.942	1567.87	3337.563	3.808
1 : 5			-		1658.821	1645.81	798.235	0.911
0 : 7	1723.730	1724.76	3085.145	1.116			-	

Table A 1: MALDI spectrum peak analysis of ch-p(BTDE-co-3T)-[1:1]. Sample prepared by the dried-droplet method. MALDI spectrum peak analysis of ec-p(BTDE-co-3T)-[1:1]. Sample prepared with solid-phase method.

Thin homopolymeric films of ec-p(3T) and ec-p(BTDE) were electrodeposited on Au and on ITO in acetonitrile or CH_2Cl_2, respectively, containing 0.1 M NBu_4PF_6 as supporting electrolyte. A copolymeric film of ec-p(BTDE-co-3T)-[1:1] (obtained from 1 mM solution of 3T and 1 mM of BTDE in CH_2Cl_2) and a double-layer of the two homopolymeric film deposited on the same electrode (ec-p(BTDE-dl-3T)) were prepared. The cyclic voltammograms recorded from homopolymeric or copolymeric films deposited on ITO electrodes, together with the related Vis/NIR spectra recorded during the forward scan in the p-doping process, are reported in Figure A 4. The analysis carried out on a double layer of BTDE and 3T must be considered in order to confirm with a different method the actual copolymerization and rules out the possibility of the formation of different layers of homopolymers on the electrode surface instead of a real copolymer.

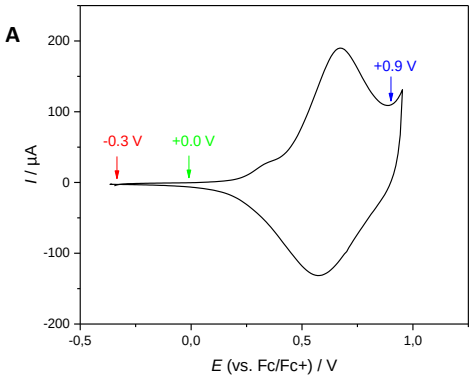
A
-0.3 V
+0.0 V
+0.9 V
I / µA
E (vs. Fc/Fc+) / V

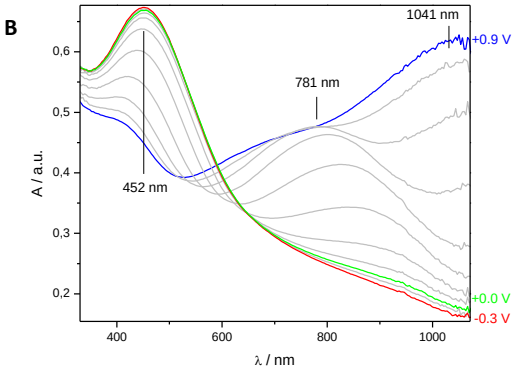
B
1041 nm
+0.9 V
781 nm
452 nm
+0.0 V
-0.3 V
A / a.u.
λ / nm

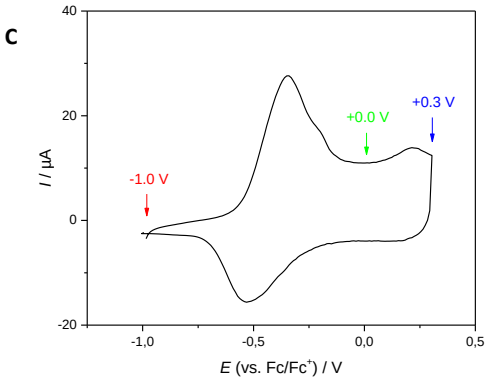
C
-1.0 V
+0.0 V
+0.3 V
I / µA
E (vs. Fc/Fc+) / V

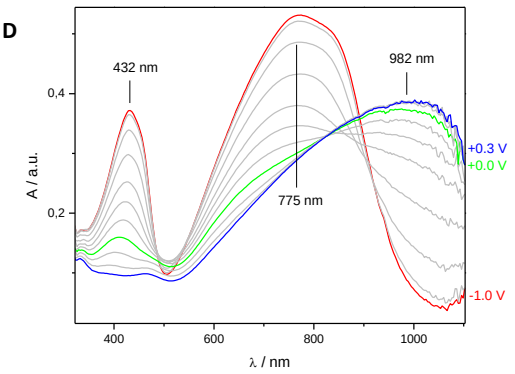
D
432 nm
982 nm
775 nm
+0.3 V
+0.0 V
-1.0 V
A / a.u.
λ / nm

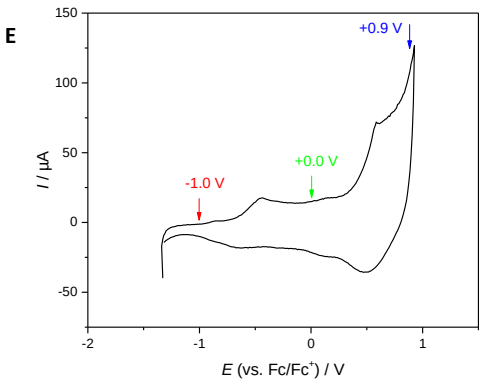
E
+0.9 V
-1.0 V
+0.0 V
I / µA
E (vs. Fc/Fc+) / V

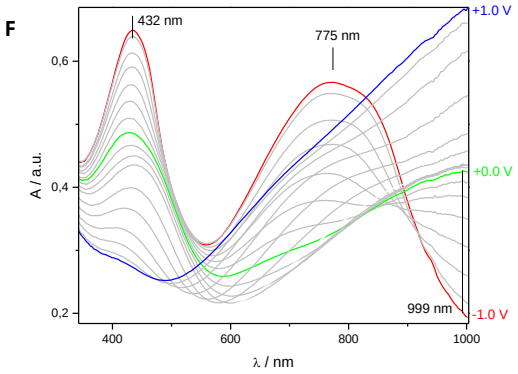
F
432 nm
775 nm
+1.0 V
+0.0 V
999 nm
-1.0 V
A / a.u.
λ / nm

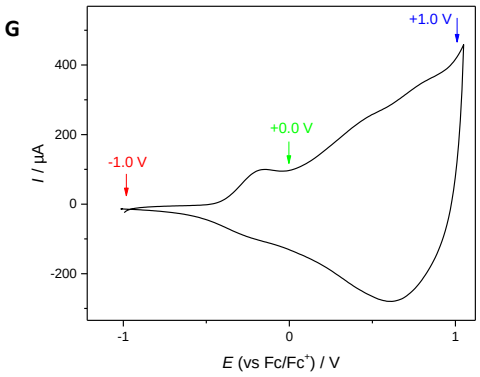
G
+1.0 V
+0.0 V
-1.0 V
I / µA
E (vs Fc/Fc+) / V

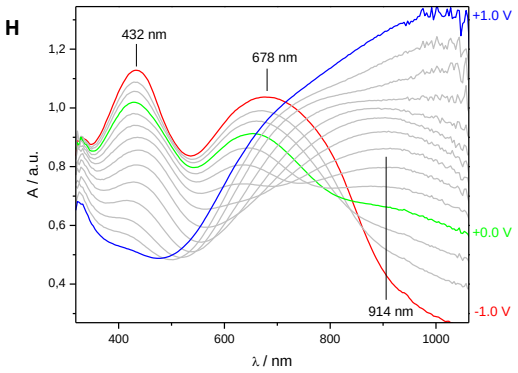
H
432 nm
678 nm
+1.0 V
+0.0 V
914 nm
-1.0 V
A / a.u.
λ / nm

Figure A 4: *In-situ* spectroelectrochemistry of homo- and co-polymers) (deposited on ITO electrodes from five cycles, 1 mM monomer solution in CAN or CH_2Cl_2 + $TBAFPF_6$, 50 mV s^{-1} scan rate), ACN + 0.1 M $TBAPF_6$ solution, 20 mV s^{-1} scan rate. Cyclovoltammograms of: A) ec-p(3T) C) ec-p(BTDE) E) ec-p(BTDE-dl-3T)-[1:1] G) ec-p(BTDE-co-3T). Vis/NIR spectra recorded during the forward scan (oxidation) in the p-doping process of: B) ec-p(3T) D) ec-p(BTDE) F) ec-p(BTDE-dl-3T)-[1:1] H) ec-p(BTDE-co-3T). Neutral (red line) and dication species (blue line) are highlighted together with the Vis/NIR absorption of the four polymers al 0.0 V (green line).

The two homopolymers were compared to the copolymer and to the double layer. ec-p(3T) (Figure A 4 A and B) showed an oxidative potential (E_{onset}^{ox}) of +0.40 V and a neutral absorbance profile characterized by the presence of a strong band at 452 nm. This band, during the stepwise increase of the anodic potential, decreased in intensity meanwhile the increasing presence of a transient radical cation absorption band (λ_{max} = 781 nm), overwhelmed by the band characteristic for the dication (λ_{max} = 1041 nm) when a further anodic potential was applied. Due to its oxidative potential, P(3T) results to be in its neutral state at 0.0 V.

Ec-p(BTDE) (Figure A 4 C and D) showed an oxidative potential (E_{onset}^{ox}) of -0.55 V and a neutral absorbance profile characterized by the presence of two strong bands at 432 nm and 775 nm, respectively. These bands, during the stepwise increase of the anodic potential decreased simultaneously in intensity and meanwhile the radical cation absorption band (λ_{max} = 982 nm) appeared. Due to its oxidative potential, P(BTDE) results to be present as a radical cation at 0.0 V.

Ec-p(BTDE-dl-3T) (Figure A 4 E and F) was constituted by a double layer of BTDE and 3T (because of solubility issues only two layers, BTDE first and 3T last) were deposited on ITO electrode surface. The behavior of the double layer both in cyclic voltammograms and in spectroelectrochemical analysis, resulted to be the perfect superimposition of the 3T and BTDE profiles. In particular, the CV profile resulted to be very similar to that observed for the single components and both the oxidative potentials were present in the voltammogram. Secondly, the Vis/NIR spectra of the neutral species showed two strong bands at 432 nm and 775 nm like BTDE but, during a stepwise increase of the anodic potential, the two bands decrease in a different ratio: at an oxidative potential of 0.0 V the band corresponding to λ_{max} = 775 nm resulted to be absent while the band at λ_{max} = 432 nm was still present. This result can be attributable to the simultaneous presence of two species, namely the radical cation BTDE and the neutral 3T.

A totally different behaviour was observed for ec-p(BTDE-co-3T) (Figure A 4 G and H). Cyclic voltammetry showed a first oxidation peak at -0.40 V, remarkably higher that that observed for c-p(BTDE) but strongly lower than that relative of ec-p(3T). An even more interesting behaviour could be observed from spectroelectrochemical data: the neutral copolymer ec-p(BTDE-co-3T) showed two intense bands at 432 nm and 678 nm while, if the first matches perfectly with that

of the homopolymers and of the double layer, the second one resulted to be blue-shifted of 100 nm. Furthermore, differently from what was found for the double layer ec-p(BTDE-dl-3T): for the copolymer it was possible to observe a simultaneously decrease of the two bands above-mentioned that were still present at an anodic potential of 0.0 V, proving that the radical cation, although inchoate, was not the predominant species.
These electrochemical analyses allowed to state that, despite the difference in oxidative potential, not only electro copolymerization between 3T and BTDE can be performed but also the resulting material possess new and interesting properties.

Furthermore, *in-situ* conductance measurements (Figure A 5) demonstrated some different features between the copolymer and the two homopolymers. Unfortunately, in order to estimate the absolute conductance, the value of conductance must be related with the exact amount of material deposited on the interdigitated electrode surface and, in this case, this operation was not possible. For that reason, the only information that was possible to extrapolate was the range of conductance of the different polymers. Under this point of view, ec-p(BTDE-co-3T) resulted to have a conductive window from -0.25 V while ec-p(BTDE) from -0.5 and ec-p(3T) from +0.5 V. It was so possible to state that a tuning in the 3T:BTDE ratio leads to a tuning of the conductive characteristics of the material.

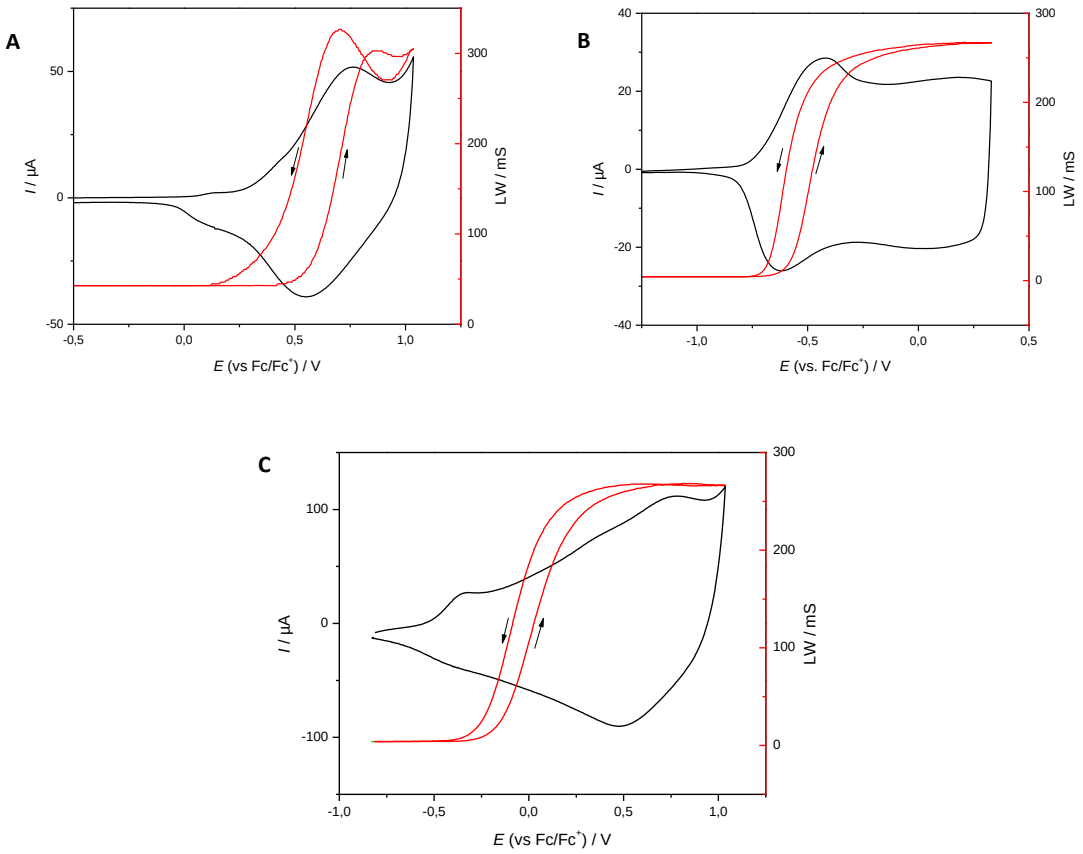

Figure A 5: *In-situ* Conductance analysis of A) ec-p(3T) B) ec-p(BTDE) and C) ec-p(BTDE-co-3T)-[1:1] (deposited on 10 µm interdigitated Pt electrode, 1 mM monomer solution in CH_2Cl_2 + $TBAFPF_6$, 50 mV s^{-1} scan rate) ACN + 0.1 M $TBAPF_6$ solution, 20 mV s^{-1} scan rate.

To prove the influence of stoichiometry, different co-monomer 3T:BTDE ratios, from [5:1] to [1:5], were investigated. As for the experiments described above, the copolymeric films were electrodeposited on Au and on ITO electrodes in CH_2Cl_2 containing NBu_4PF_6 (c = 0.1 M) as supporting electrolyte. The final overall concentration of each solution used for the electrodepositions was setted at 2 mM.

The films were analyzed by Vis/NIR spectroelectrochemical analysis (for ITO electrodes, data reported in Table A 2) and by cyclic voltammetry (for Au electrodes, data reported in Table A 3).

polymer	λ/nm (eV) neutral state		radical cation	E^{ox}_{onset}/V (HOMO/eV)	E^{red}_{onset}/V (LUMO/eV)	Electrochemical band gap/eV
ec-p(BTDE)	432	767	1001	-0.55 (-4.25)	-1.60 (-3.20)	1.05
ec-p(BTDE-co-3T)-[5:1]	436	728	1034	-0.64 (-4.16)	-1.58 (-3.22)	0.94
ec-p(BTDE-co-3T)-[3:1]	436	724	1034	-0.63 (-4.17)	-1.60 (-3.20)	0.93
ec-p BTDE-co-3T)-[2:1]	422	701	1047	-0.60 (-4.20)	-1.55 (-3.25)	0.95
ec-p(BTDE-co-3T)-[1:1]	432	678	975	-0.40 (-4.40)	-1.60 (-3.20)	1.20
ec-p(BTDE-co-3T)-[1:2]	422	630	975	-0.33 (-4.47)	-1.56 (-3.24)	1.23
ec-p(BTDE-co-3T)-[1:3]	429	631	995	-0.14 (-4.66)	-1.56 (-3.24)	1.42
ec-p(BTDE-co-3T)-[1:5]	432	627	955	-0.11 (-4.69)	-1.56 (-3.24)	1.45
ec-p(3T)	452	-	1041	0.40 (-5.20)	-1.91 (-2.89)	2.31

Table A 2: Absorption and electrochemical characteristics of electrochemically deposited copolymers ec-p(BTDE-co-3T)-[5:1], [3:1], [2:1], [1:1], [1:2], [1:3] and [1:5], and homopolymers ec-p(BTDE) and ec-p(3T) derived from *in-situ* spectroelectrochemical experiments on ITO electrodes.

polymer	E^{ox}_{onset}/V (HOMO/eV)	E^{red}_{onset}/V (LUMO/eV)	Electrochemical band gap/eV
ec-p(BTDE)	-0.66 (-4.14)	-1.73 (-3.07)	1.07
ec-p(BTDE-co-3T)-[5:1]	-0.75 (-4.05)	-1.63 (-3.17)	0.88
ec-p(BTDE-co-3T)-[3:1]	-0.74 (-4.06)	-1.64 (-3.16)	0.86
ec-p(BTDE-co-3T)-[2:1]	-0.73 (-4.07)	-1.60 (-3.20)	0.91
ec-p(BTDE-co-3T)-[1:1]	-0.53 (-4.27)	-1.67 (-3.13)	1.14
ec-p(BTDE-co-3T)-[1:2]	-0.38 (-4.42)	-1.59 (-3.21)	1.21
ec-p(BTDE-co-3T)-[1:3]	-0.06 (-4.74)	-1.72 (-3.08)	1.66
ec-p(BTDE-co-3T)-[1:5]	0.01 (-4.81)	-1.72 (-3.08)	1.71
ec-p(3T)	0.46 (-5.26)	-1.99 (-2.81)	2.45

Table A 3: Electrochemical characteristics of electrochemically deposited copolymers ec-p(BTDE-co-3T)-[5:1], [3:1], [2:1], [1:1], [1:2], [1:3] and [1:5], and homopolymers ec-p(BTDE) and ec-p(3T) derived from cyclic voltammetric experiments on Au electrodes.

The electrochemical band gap (EBG) measured for the homopolymeric films resulted to be 1.05 eV and 1.07 eV respectively on ITO and Au for ec-p(BTDE) and 2.31 eV and 2.45 eV for ec-p(3T). As expected, in most cases the EBG for the copolymers resulted to be intermediate between those values: the copolymers obtained by electrooxidizing BTDE and 3T in [1:1], [1:2], [1:3], and [1:5] ratio showed this behaviour.

However, copolymers prepared with a ratio of BTDE higher than 3T (ec-p(BTDE-co-3T)-[5:1], -[3:1] and -[2:1]) showed a EBG lower that the expected values: the measured band gap values resulted to be lower even compare to the BTDE homopolymer. Those values of electrochemical energy band gap, for films deposited and ITO and Au, are also plotted and showed in Figure A 6.

A plausible explanation of this phenomenon is to assume a peculiar geometry or stacking or structure of the materials that results to be optimize at certain BTDE:3T ratio; from the optimized structure, the band gap lowering could arise. Anyhow, this theoretical explanation

must be proved by theoretical DFT calculation, in order to give an unambiguous explanation of the collected data.

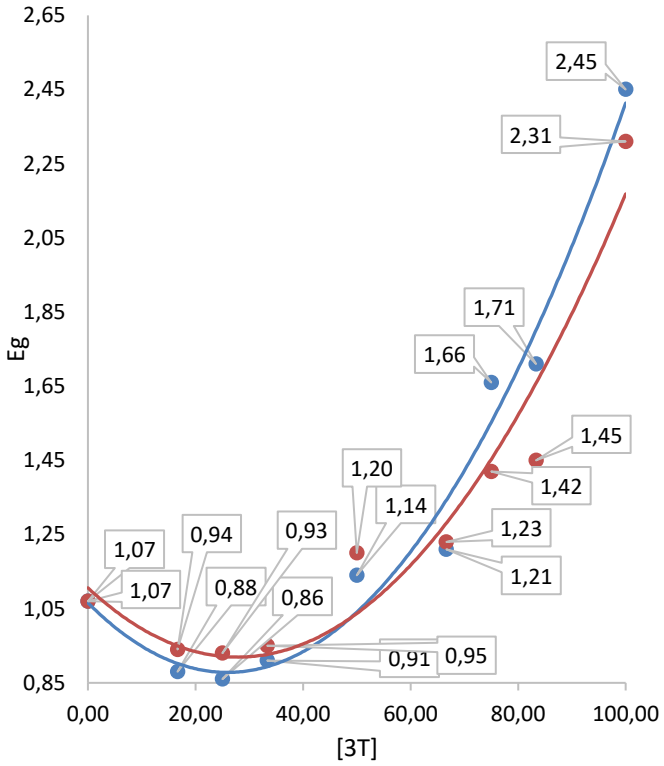

Figure A 6: Electrochemical band gap vs. [BTDE:3T] ratio derived from experiments on Au (blue) and ITO (red) electrodes.

In Figure A 7 the normalized absorbances of the neutral copolymer are depicted. The UV/vis profiles show two remarkable trends, one expected, the other unforeseen.

As previously mentioned, on one hand, 3T has an absorption band in its neutral form at 452 nm while, on the other hand, BTDE and its copolymers show two strong absorption bands, the first around 430 nm, while the second one around 775 nm (for ec-p(BDTE)), band that shifts to 678 nm (for ec-p(BTDE-co-3T)-[1:1]).

An expected phenomenon is a difference in intensity for the two bands as the BTDE:3T ratio is modified: the more blue-shifted band, indeed, resulted to be the superimposition of the bands of both the monomers while, the other one is related only to the presence of BTDE units in the copolymer. For that reason, as the BTDE:3T ratio decreases a parallel decrease of intensity of the red-shifted band is observed.

At the same time, an unexpected phenomenon was observed analyzing the maximum absorption wavelength of the red-shifted band: a continuous hypsochromic shift was observed as the amount of BTDE in the polymeric film decreases.

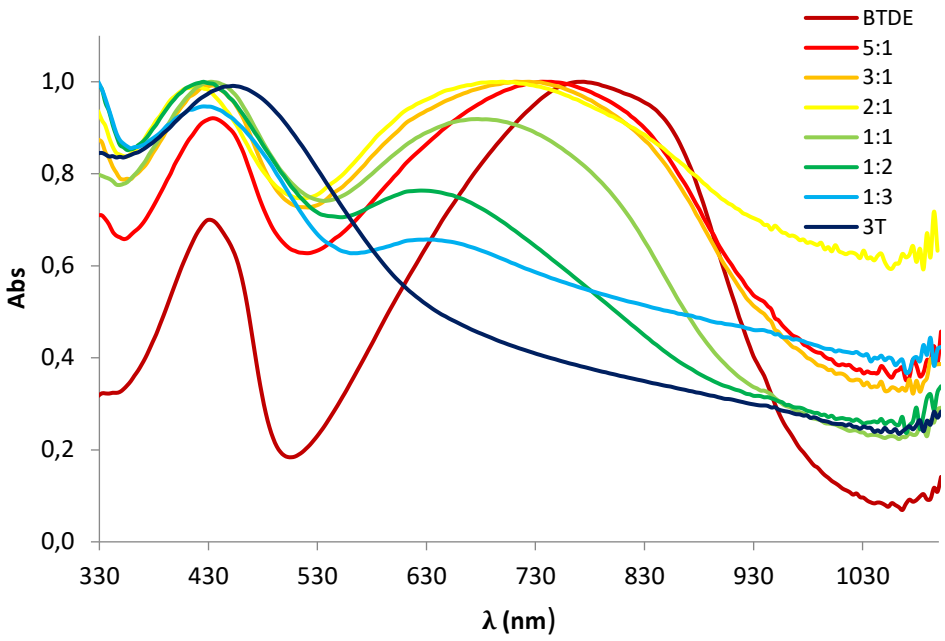

Figure A 7: UV/vis spectrum of the neutral species of electrochemically deposited copolymers ec-p(BTDE-co-3T)-[5:1], [3:1], [2:1], [1:1], [1:2], [1:3] and [1:5], and homopolymers ec-p(BTDE) and ec-p(3T). The absorbances are normalized.

In conclusions, the BTDE:3T copolymer seems to be a highly appealing donor-acceptor copolymer: the material was obtained despite the remarkable difference between the oxidation potential of the two monomers. Furthermore, the properties of the copolymers resulted to be extremely tunable: the band gap, for example, can be set in a range between 0.9 to 1.7 V as is possible to set the conductive window of the material. Additionally, it is interesting to underline how easy was to modify the absorbance profile of the copolymeric material only by adjusting wisely the ratio between the two copolymer units.

11.3. Experimental section

11.3.1. Materials and methods

All chemicals and solvents were purchased from Sigma-Aldrich, TCI Chemicals, Alfa-Aesar or Acros Organics. Solvents were at least HPLC grade and were used as received except otherwise noted. NBu_4PF_6 (TCI) was stored in a desiccator over blue gel. Acetonitrile (Alfa Aesar, supergradient HPLC grade (far-UV), 99.9+%) and dichloromethane (Acros Organics, 99.9% analytical grade) were stored under argon atmosphere and over activated neutral Al_2O_3 or were dried over activated Al_2O_3 before use. All reactions were carried out under argon atmosphere unless otherwise noted.

The NMR spectra were recorded on a Bruker AC 300 spectrometer. Chemical shifts are given in ppm and the coupling constants are given in Hz; s=singlet, ddd=double double doublet, m=multiplet.

MALDI-TOF mass spectrometric measurements were performed on a Bruker autoflex speed spectrometer. The polymer samples concentration was set to 3 mg mL^{-1}. A poly(ethylene glycol) standard was used for internal calibration (3 mg mL^{-1}). Matrix trans-2-[3-(4-tert-butylphenyl)-2-methyl-2-propenylidene]malononitrile (DCTB, 10 mg mL^{-1}) containing the ionizer sodium trifluoromethanesulfonate was used. The polymer samples were mixed in a 1:2 ratio with the DCTB matrix. The mixed samples were prepared by the dried-droplet method (1 µL of the mixed solution was allowed to dry on a polished steel target) or with a solid-phase method used for non-soluble polymers (grinding in a mortar appropriate quantity of matrix, ionizer and sample and mashing the mixture on a polished steel target through a spatula)[7].

11.3.2. Synthesis

2, 2': 3', 2''-terthiophene (3T)[8], benzo[*c*][1,2,5]thiadiazole[9] and 4,7-dibromobenzo[*c*][1,2,5] thiadiazole[9] were synthesize based on literature and are not reported.

2-tributylstannyl-3,4-ethylenedioxythiophene: A 2.5 M solution of *n*-BuLi (1.1 eq., 1.55 mL, 3.86 mmol,) in *n*-hexane was slowly added to a solution of 3,4-ethylenedioxythiophene (1 eq., 500 mg, 3.52 mmol) and *N,N,N',N'*-tetramethylethylenediamine (TMEDA) (1.1 eq., 0.58 mL, 3.86 mmol) in anhydrous diethyl ether (14 mL) under argon atmosphere at room temperature. The mixture was stirred at room temperature for 10 minutes and then refluxed for 30 minutes. The reaction mixture was then cooled at -78°C and tributyltin chloride (1 eq., 1.37 mL, 3.52 mmol) was slowly added over 1 hour. The reaction was stirred at -78°C for 30 minutes, then warmed up to room temperature and stirred for 3 h. The reaction mixture was then quenched with saturated NaCl solution; the aqueous layer was extracted with diethyl ether, dried over $MgSO_4$ and filtered. The solvent was removed under reduced pressure and the TMEDA was removed by vacuum distillation to produce a pale-yellow oil that was used without any further purification (72% yield). ^{1}H NMR (300 MHz, $CDCl_3$) δ = 6.60 (1 H, s), δ = 4.18 (4 H, m), δ = 1.59 (6 H, m), δ = 1.35 (6 H, m), δ = 1.12 (6 H, m), δ = 0.92 (9 H, m).

4,7-Bis(3,4-diethylenedioythiophene)benzo[*c*][1,2,5]thiadiazole (BTDE): A mixture of 4,7-dibromobenzothiadiazole (1 eq., 310 mg, 1.06 mmol), 2-tributylstannyl-3,4-ethylenedioxythiopene (2.5 eq., 1.14 g, 2,64 mmol), 99% $Pd(PPh_3)_4$ (0.05 eq., 61 mg, 0.05 mmol)

and toluene (10 mL) was refluxed under nitrogen atmosphere for 6 hours. The reaction mixture was cooled to room temperature, the solvent was removed under reduced pressure and the crude residue was purified by column chromatography using a 7:3 mixture of CH_2Cl_2 and *n*-hexane. Combined final fractions gave BTDE as a deep red solid by removal of the solvent (343 mg, 78% yield). ^{1}H NMR (300 MHz, $CDCl_3$) δ = 8.41 (2 H, s), δ = 6.59 (2 H, s), δ = 4.42 (4 H, ddd, *J* = 2.4 Hz, *J* = 1.8 Hz, *J* = 1.5 Hz), δ = 4.34 (4 H, ddd, *J* = 2.4 Hz, *J* = 1.8 Hz, *J* = 1.5 Hz).

11.3.3. Chemical copolymerization of ec-p(BTDE-co-3T)-[1:1]

$FeCl_3$ (5 eq., 213 mg, 1.31 mmol) was added one pot to a stirred solution of 3T (1 eq., 65 mg, 0.26 mmol) and BTDE (1 eq., 109 mg, 0.26 mmol) in dry chloroform (120 mL) under argon atmosphere. The mixture was stirred at room temperature for 16 h; the solvent was removed under reduced pressure and then methanol (60 mL) and hydrate hydrazine (1 mL) were added to the obtained black residue to give a red solution. The mixture was stirred for 10 minutes and filtered. The solid residue was washed with methanol (3x10 mL) and diethyl ether (3x10 mL). The solid residue was collected and transferred into a cellulose extraction thimble; the thimble was insert into a soxhlet assembly and the extraction was performed using 120 mL of THF heating for 36 h the whole assembly to obtain an orange solution. The solvent was removed under reduced pressure to give the final polymer (98 mg, 56% yield).

11.3.4. Electrochemical Experiments

All electrochemical experiments were performed with an Autolab PGSTAT101 potentiostat (Metrohm, Germany) in a three-electrode glass cell at room temperature under argon atmosphere using the NOVA software (version 1.10). The counter electrode was a Pt plate. The reference electrode consisted of an AgCl-coated silver wire (pseudoreference electrode) directly immersed into the electrolyte. As working electrodes, gold-coated Si wafers (50 nm Au layer with a 5 nm Cr layer between the Si wafer and the Au layer) or ITO (Indium-Tin Oxide)-coated glass (≤20 Ω/sq, PGO, Germany) slides were used (~2 × 1 cm^2). The gold working electrodes were fabricated by physical vapor deposition of Cr and Au on rotating Si wafers. The gold-coated Si wafers and the ITO substrates were thoroughly washed with water, isopropanol and acetone prior to use. Additionally, the ITO electrodes were treated with oxygen plasma for 10 min before measurements. NBu_4PF_6 was used every time as electrolyte at a concentration of 0.1 M in HPLC

grade dichloromethane or acetonitrile. Electrolyte solutions were deaerated by argon bubbling before use. All potentials are rescaled to the formal potential of the redox couple Fc/Fc^+ (internal standard).[10] To avoid charge-trapping effects during cyclic voltammetric experiments, the oxidation and reduction cycles were performed separately.

Electropolymerization of homopolymer ec-p(BTDE) on gold or ITO was performed under potentiostatic control for 200 s using a 1 mM solution of BTDE in 0.1 M NBu_4PF_6/DCM at 0.5-0.6 V vs Fc/Fc^+. After deposition, the oxidized films were directly reduced to the neutral form by applying a potential between −1.3 and −1.4 V (vs Fc/Fc^+) for 200 s. Finally, the deposited films were washed with MeCN.

Electropolymerization of homopolymer ec-p(3T) on gold or ITO was performed under potentiostatic control for 200 s using a 1 mM solution of 3T in 0.1 M NBu_4PF_6/MeCN at 1.1-1.2 V vs Fc/Fc^+. After deposition, the oxidized films were directly reduced to the neutral form by applying a potential between −1.3 and −1.4 V (vs Fc/Fc^+) for 200 s. Finally, the deposited films were washed with MeCN.

Electropolymerization of copolymer ec-p(BTDE-co-3T)-[5:1] -[3:1] -[2:1] -[1:1] -[1:2] -[1:3] -[1:5] on gold or ITO was performed under potentiostatic control for 200 s using an overall concentration of 2 mM solution of 3T and BTDE in 0.1M NBu_4PF_6/DCM at 1.1-1.2 V vs Fc/Fc^+. After deposition, the oxidized films were directly reduced to the neutral form by applying a potential between −1.3 and −1.4 V (vs Fc/Fc^+) for 200 s. Finally, the deposited films were washed with MeCN.

Electropolymerization of blend polymer ec-(double layer) on gold or ITO was performed under potentiostatic control for 200 s depositing two homopolymer layers; two consecutive potentiostatic polymerization (first 1 mM solution of BTDE in 0.1M NBu_4PF_6/DCM at 0.5-0.6 V vs Fc/Fc^+ then 1 mM solution of 3T in 0.1M NBu_4PF_6/MeCN at 1.1-1.2 V vs Fc/Fc^+). After each deposition, the oxidized films were directly reduced to the neutral form by applying a potential between −1.3 and −1.4 V (vs Fc/Fc^+) for 200 s. After each reduction, the deposited films were washed with MeCN.

11.3.5. *In-Situ* Spectroelectrochemical Measurements

Spectroelectrochemical experiments on thin films were conducted using an Autolab PGSTAT101 potentiostat (Metrohm) and a Zeiss UV–vis spectrometer equipped with a MCS621 Vis II spectrometer cassette (mean spectral pixel pitch: 3.2 nm) and a CLH600F lamp in a custom-built

three electrode-one compartment quartz cell at room temperature under argon atmosphere. The counter and reference electrode consisted of a Pt wire and an AgCl-coated Ag wire (pseudoreference electrode) directly immersed into the electrolyte solution, respectively. Transparent ITO coated float glass slides (≤20 Ω/sq, PGO, Germany) (~2 × 1 cm^2) were used as the working electrode and for background measurements a non-modified ITO-coated float glass slide was used. The absorption spectra of the polymer films were recorded in transmission mode. All voltammograms were recorded with a scan rate of 20 mV s^{-1} with step potentials of 50 mV. At every potential step a UV−vis absorption spectrum was recorded. Electrolyte solutions (0.1 M NBu_4PF_6/MeCN) were deaerated by argon bubbling before use.

11.3.6. *In-Situ* Conductance Measurements

ISC measurements were performed using an electrolyte gated transistor setup with interdigitated Pt electrodes (distance = 10 µm) as working electrodes.[11] The CV experiments were performed at room temperature under argon atmosphere using an Autolab PGSTAT101 potentiostat (Metrohm) with a Pt wire as counter electrode and an AgCl coated Ag wire directly immersed into the electrolyte solution as pseudoreference electrode. Additionally, a constant bias of 10 mV was applied between the combs of the interdigitated electrode using a second potentiostat (DropSens, Spain). The conductance of the polymers on the microarray electrode was calculated from the measured current between the two interdigitated Pt electrodes according to Ohm's law (U = R·I; G = 1/R). Electrolyte solutions (0.1 M NBu_4PF_6/acetonitrile) were deaerated by argon bubbling before use.

11.4. References

[1] Benten, H.; Mori, D. et al.; J. *Mater. Chem. A*, **2016**, *4*, 5340–5365;

[2] Dennler, G.; Scharber, M. C. and Brabec, C. J.; *Adv. Mater*., **2009**, *21*, 1323-1338;

[3] Kim, T.; Kim, J. H. et al.; *Nat. Commun*., **2015**, *6*, 8547-8553;

[4] Mori, D.; Ito, S. et al.; *Adv. Energy Mater.,* **2014**, *4*, 1301006;

[5] Link, S.; Scheuble, M. et al.; *Langmuir,* **2013**, *29*, 15463 −15473;

[6] Huang, H.; Pickup, P. G.; *Chem. Mater*., **1998**, *10*, 2212 −2216;

[7] Skelton, R.; Dubois, F; Zenobi, R; *Anal. Chem.,* **2000**, *72*, 1707-1710;

[8] Richter, T. V.; Link, S. et al.; *Macromol. Rapid Comm*., **2009**, *30*, 1323-1327;

[9] DaSilveira Neto, B. A.; San'Ana Lopes, A. et al.; *Tetrahedron*, **2005**, *61*, 10975-10982;

[10] Gritzner, G.; Kůta, J.; *Pure Appl. Chem.,* **1984**, *56*, 461 −466;

[11] Link, S.; Richter, T. et al.; *J. Phys. Chem. B,* **2010**, *114*, 10703 −10708:

12. Unofficial acknowledgement

Beh, eccoci ancora alla fine. La fine di una tesi, di un ciclo e di un percorso. Tesi, ciclo e percorso sofferti e lunghi, non esenti da gioie ma anche pieni di difficoltà. Tutto ciò ovviamente non è semplicemente farina del mio sacco e molte persone meritano di essere ringraziate per quel che hanno fatto per me. Non tanto per la realizzazione del presente lavoro di tesi, che si spera possa essere giudicato come interessante e ben fatto e che come detto non sarei stato in grado di realizzare da solo, quanto per me come uomo. Persone che mi hanno aiutato a crescere e a diventare quello che sono oggi, che spero possano essere fiere di quel che sono e sono diventato. Per semplicità forse è meglio listarle, alcune in ordine di importanza, altre no, giudicate voi se vi è stata resa giustizia (dalle parole, non dalla classifica):

- Beh, Tiziana, ovviamente. Tiziana che in questi tre anni mi ha seguito e guidato in argomenti a me sconosciuti. Voglio ringraziarti soprattutto perché mi hai dato una possibilità. La possibilità di intraprendere ciò che desideravo, la possibilità di andare via (via all'estero, via di casa, indipendentemente via, solamente via). Ho potuto crescere come chimico, imparando cose nuove (magari anche ad usare la celite), ho potuto fare l'esame di stato, migliorare in inglese, visitare un paese straniero, seguire studenti e insegnare loro qualcosa. Ho potuto crescere come uomo, imparando a ragionare di più, a relazionarmi con persone che ne sanno di più e altre che ne sanno di meno, cercando di trattare tutti con rispetto e pazienza. A te il ringraziamento più grande per ciò che hai fatto e che mi hai lasciato fare. Grazie
- Ai vari tutor che mi hanno aiutato insieme a Tiziana: il prof, Sannicolò che già mi conosceva e che spero possa aver convinto delle mie ipotetiche doti e potenzialità. Monica, per avermi fatto conoscere Tiziana e per avermi consigliato quando ne avevo bisogno. La chance datami da Tiziana è anche merito tuo. Tutti gli altri, docenti e non, che mi hanno saputo consigliare e guidare in alcuni momenti. Grazie
- Alla mia famiglia, mia madre Catia alla quale mi ispiro per la sete di conoscenza, mio padre Silvio dal quale spero di ereditare la perseveranza e la cocciutaggine nel fare le cose con i sacri crismi, mia sorella Delia che sa farmi arrabbiare ma che mi abbraccia ogni volta che torno a casa per il week end. Mia nonna Eda che, fino che ha potuto, c'è sempre stata e che spero di aver reso fiera di tutto quel che ho fatto in 27 anni. Mia zia Franca che, anche se ci vediamo raramente, so sempre essere presente e che condivide

con mia madre una passione per le lettere e la cultura. Non solo supporto economico o psicologico ma modelli. Forse dopo 28 anni si può anche ammettere. Grazie

- Ai chimici che mi sono stati vicini e che mi hanno insegnato qualcosa. A Sofia, per quello che è stata, non per quello che è. A Serena, che si è dimostrata, oltre che una chimica eccellente, una persona paziente e capace di ascoltare, sicuro non ce l'avrei fatta senza di te. A Biagio per quel che ancora fa quando ascolta e consiglia e perché prova che la chimica unisce. Ai colleghi di unimi, uninsubria, Stoccarda, se ci siamo dedicati un minuto e ancora mi ricordate, magari con affetto, se ci siamo scambiati qualcosa (magari più di una info). A studenti e studentesse con i quali ho condiviso un consiglio (dato o ricevuto) un momento (di riso o di fatica). Grazie
- Ai non chimici, amici miei (qui se mi leggete sicuro ci sarà lotta). A Veronica che nonostante i mille anni passati mi ascolta, mi calma, mi sta accanto e mi vuole bene. Ad Andre, Gio e Pally, compagni di vita, custodi di segreti e condivisori di momenti, di chimica non capite nulla ma il supporto che date è fondamentale. Grazie
- Genericamente a te che leggi e che non sei stato menzionato. Se mi hai aiutato, consigliato, ascoltato, se mi hai voluto bene e hai fatto il tifo per me, se mi pensi e per te non sono solo una persona a caso, beh, scusa la dimenticanza. Grazie

Ora, al termine di questo percorso, forse posso pensare di essere arrivato alla fine. Forse un punto fermo può essere messo. Finisce un ciclo ma un altro deve necessariamente cominciare. Per me che scrivo e per te che leggi, è importante ricordare che bisogna sempre andare avanti, mai fermarsi, mai perdere tempo. Riflettere, certamente, ponderare i propri passi, ma subito mettersi in marcia, anelare a raggiungere sempre qualcosa di più in alto, dimostrare agli altri e a sé stessi ciò di cui siamo capaci. E che non bisogna sprecare il poco tempo che abbiamo, "Don't waste your time looking back, you are not going that way".